Multifunctional role of the iron-regulated protein HupB in *Mycobacterium tuberculosis*

A thesis

Submitted for the degree of

Doctor of Philosophy

By

Mitali Choudhury

Regd. No. 10LAPH10

Department of Animal Biology

School of Life Sciences

University of Hyderabad

Hyderabad - 500 046

India

November 2016

University of Hyderabad

(Central University established in 1974 by an Act of Parliament)

Hyderabad - 500046, India

CERTIFICATE

This is to certify that Ms. Mitali Choudhury has carried out the research work embodied in the present thesis under my supervision and guidance for a full period prescribed under the Ph.D. Ordinance of this University. We recommend her thesis entitled "**Multifunctional role of the iron-regulated protein HupB in *Mycobacterium tuberculosis***" for submission for the award of the degree of Doctor of Philosophy in Animal Sciences of this University.

Prof. Manjula Sritharan

Ph.D. Supervisor _____

Head

Department of Animal Biology _____

Dean

School of Life Sciences _____

University of Hyderabad

(Central University established in 1974 by an Act of Parliament)

Hyderabad - 500046, India

DECLARATION

I hereby declare that the work embodied in this thesis entitled "**Multifunctional role of the iron-regulated protein HupB in *Mycobacterium tuberculosis***" is the result of the investigation carried out by me in the Department of Animal Biology, School of Life Sciences, University of Hyderabad, Hyderabad and has not been submitted to any other University for the award of any degree or diploma.

Mitali Choudhury

Research scholar

Prof. Manjula Sritharan

Ph.D. Supervisor

Acknowledgements

I would like to express my deepest gratitude and sincere appreciation to my supervisor Prof. Manjula Sritharan for her unwavering patience, instruction, guidance and support. At many stages in the course of my graduate studies I benefited from her advice, particularly so when exploring new ideas. Her positive outlook and confidence in my research inspired me and elevated my confidence. She has given me every opportunity to grow and develop in my academic endeavours and has pushed me to better myself. Her approach to supervision has allowed me to become a confident and independent scientist. Her careful editing contributed enormously to the production of this thesis.

I am thankful to Prof. Appa Rao Podile and Dr. K. Arun Kumar for their guidance during Doctoral Committee meetings.

I am thankful to Prof. P. Jagan Mohan Rao, Head, Department of Animal Biology and the former Heads, Prof. B. Senthilkumaran and Prof. Manjula Sritharan for allowing me to use departmental facilities.

I am thankful to Prof. P. Reddanna, Dean, School of Life Sciences and former Deans Prof. R. P. Sharma, Prof. Aparna Dutta Gupta and Prof. M. Ramanadham for allowing me to use the school facilities.

I am grateful to Dr. K. Subhakar, Dr. Ramulu and the nurses at the Government General Chest Hospital (A.P) for their help in blood collection.

I am thankful to Dr. Sanjeev Khosla from CDFD for allowing me to use his lab facilities and Mr. Imtiyaz in his assistance in ChIP assay.

I am grateful to Dr. N. Prakash Prabhu and Mr. Tejaswi for helping me in biophysical studies.

I am thankful to Mr. Tushar for his guidance in biochemical analysis of lipids.

I also thank all the faculty members of School of Life Sciences for their valuable discussions and suggestions.

I thank all my lab members Dr. Veena, Dr. Suneel, Dr. Satya Deo Pandey, Dr. Subha, Naveen, Reetika, Kemelia and Chandram for all their help and support in the lab.

I wish to thank all my friends from School of Life Sciences for their constant support and encouragement.

I take this opportunity to thank all non-teaching staff of Department of Animal Biology for their help in all the administrative work.

I sincerely thank UGC for funding during my doctoral studies.

I thank DRDO, DRDE, DBT–NIAB, UGC - SAP and DBT - CREBB for providing financial support to lab and for the infrastructural facility of the school.

I would specially like to thank Subha, Sahil, Tejaswi, Gouri and Reetika for making this journey beautiful.

I wish to thank my friends Saranya, Sonakshi, Siuli, Jitu and Subas for their unconditional support and for believing in me when I ceased to do so.

Above and beyond all, my heartfelt gratitude to my parents, Mr. Janaki Prasad Choudhury and Mrs. Jyotsnarani Choudhury, my sister Sonali and my brother-in-law Ankit for their unflagging support, patience, understanding and encouragement in every possible way. Special thanks to my nephew Aarush for making me cheerful and filling me with positivity.

MITALI CHOUDHURY

TABLE OF CONTENTS

LIST OF ABBREVIATIONS

ADC	Albumin-dextrose-catalase
AG	Arabinogalactan
ATP	Adenosine triphosphate
ATT	Anti-tubercular Therapy
BCG	Bacille Calmette Guérin
Bp	Base pair
ChIP	Chromatin immunoprecipitation
CMb	Carboxymycobactin
DAT	Diacyl trehalose
DOTS	Directly observed treatment, short-course
EMSA	Electrophoretic mobility shift assay
EPTB	Extrapulmonary tuberculosis
FBS	Fetal bovine serum
Fe-CMb	Ferri-carboxymycobactin
Fe-Mb	Ferri-mycobactin
Fur	Ferric uptake regulator
H	Hour
HI	High iron
HIV	Human immunodeficiency virus
H_2O_2	Hydrogen peroxide
INH	Isonicotinic acid hydrazide (Isoniazid)
IREP	Iron-regulated envelope protein
IdeR	Iron-dependant regulator
kDa	kilo Dalton
KO	Knock out
LI	Low iron
mAGP	Mycolyl-arabinogalactan-peptidoglycan
Mb	Mycobactin
MDR	Multi-drug resistant
MEGA	Molecular Evolutionary Genetic Analysis
µM	Micromolar
mg	Milligram
mL	Milliliter
mM	Millimolar

NCBI	National Center for Biotechnology Information
Nm	Nanometer
OADC	Oleate-albumin-dextrose-catalase
OD	Optical density
o/n	Overnight
PAGE	Polyacrylamide gel electrophoresis
PAT	Penta-acyl trehalose
PBS	Phosphate buffered saline
PCR	Polymerase chain reaction
PDIM	Phthiocerol dimycocerosate
PG	Peptidoglycan
PTB	Pulmonary tuberculosis
RNTCP	Revised National TB Control Programme
SD	Standard deviation
SDS	Sodium dodecyl sulphate
SL-1	Sulfolipid-1
TB	Tuberculosis
TBS	Tris-buffered saline
TLC	Thin-layer chromatography
TMB	Tetramethyl benzidine
WHO	World Health Organization
WT	Wild type

Abstract

Mycobacterium tuberculosis, the causative agent of tuberculosis is one of the most successful pathogens that has adapted to the hostile environment of the human host. When the pathogen gains entry, the innate immune response of the host initially aims to control the pathogen, followed by the triggering of the cell-mediated immune response that involves several components of the host immune system and the production of cytokines and chemokines. If however, the pathogen adapts itself to the hostile environment and overcomes the efforts of the host, it establishes itself and causes disease. There are several reports on host-pathogen interactions that involve nutrient acquisition, oxidative stress and the immune response in response to the bacterial antigens. The successful adaptation of the pathogen to the mammalian host has made tuberculosis a disease of great public concern today. The latency of the mycobacterium, when it is able to persist within the human host in a dormant state with the potential to be activated and cause disease has contributed significantly to the vain efforts of man to contain the pathogen, as the currently available anti-tubercular drugs cannot target latent bacilli.

An important micronutrient needed for the successful growth and survival of the pathogen is iron. Upon entry into the human host, the pathogen faces iron-limiting conditions because of 'iron withholding', an important facet of host innate immunity that lowers the availability of iron by a process termed 'nutritional immunity'. The pathogen, like all mycobacteria has adapted to iron deprivation by elaboration of two siderophores, the intracellular mycobactin (Mb) and extracellular carboxymycobactin (CMb). It lacks the biosynthetic machinery for the synthesis of exochelin, the major extracellular siderophore secreted by non-pathogenic mycobacteria. The CMb / Mb-based siderophore machinery is essential for the pathogen, a disruption of which is lethal, as specific knock out mutants, unable to express the siderophores do not survive inside macrophages and in experimental animals.

Efforts to identify cell surface proteins as potential receptors for the siderophores in *M. tuberculosis* have not been successful. In the non-pathogenic *Mycobacterium smegmatis*, a 29 kDa iron-regulated envelope

proteins (IREP) was first demonstrated as the ferri-exochelin receptor. In *M. tuberculosis*, the IrtAB protein, localised in the cytoplasmic membrane is established as an ABC transporter that mediates the internalisation of iron, a process shown to be essential for the survival of the pathogen *in vivo.* Our lab identified HupB as a 28 kDa protein in the cell wall fractions of *M. tuberculosis* under conditions of iron limitation when it produced high levels of Mb and CMb. While our initial interest was to study its role as a receptor for ferri-carboxymycobactin (Fe-CMb), we unravelled its role as a positive transcriptional regulator of mycobactin biosynthesis. This was made possible by the generation of a *hupB* knock out mutant that did not express HupB.

Transcriptional profiling of the mutant strain by microarray analysis led us to re-visit the possibility of exploring additional roles of HupB. Several genes associated with iron transport and lipid metabolism were down-regulated in the mutant strain. HupB binds ferric iron and preliminary studies showed it can bind to ferri-siderophores. As these observations showed its possible role in iron transport, *in silico* and experimental approaches were made to establish HupB as an iron transporter. Additionally, its role in the biosynthesis of different lipids were studied and the findings were correlated with changes in the colony morphology of the mutant strain as cell envelope lipids contribute to the cell integrity and susceptibility to drugs.

HupB is essential for the *in vivo* survival of the pathogen and it is expressed in tuberculosis (TB) patients. A strong negative correlation of the serum iron status with the circulating antibodies against the protein was reported from our lab. This finding is of significance in EPTB patients, which not only reflects the potential of the protein as a diagnostic marker but also establishes the basis of the protein as an adherence factor. The diagnostic potential of the protein was probed using serum samples from both pulmonary and extrapulmonary TB patients and evaluated using different antigenic fractions of the protein. In addition, as high levels of antibodies were observed, the role of the protein in triggering a strong humoral response by way of shifting the response to Th2 type was analysed.

Findings from our study here in *M. tuberculosis* and reports on the homologous protein in other mycobacteria lead us to conclude that HupB is a ‘moonlighting’ protein with multiple roles.

CHAPTER 1

REVIEW OF LITERATURE

1.1 Introduction

Tuberculosis is an ancient disease and one of the major causes of human affliction. In 1882 Robert Koch discovered *Mycobacterium tuberculosis* as the causative agent of tuberculosis for which he was awarded the Nobel Prize in 1905. The generic name Mycobacterium was given due to its mould-like growth in liquid medium (Lehman & Neumann, 1896). Despite the use of potent anti-tubercular drugs, the pathogen has not been eradicated and due to various factors has become a major concern globally. In 1993, due to the worldwide high death rate and morbidity, tuberculosis was declared as a global emergency by World Health Organisation (WHO). The genus Mycobacterium consists of more than 100 species which belong to the family Mycobacteriaceae. Due to high level of genetic relatedness, 0.01-0.03% synonymous nucleotide variation (Gutacker *et al.*, 2002; Hughes *et al.*, 2002) *M. tuberculosis*, *M. africanum*, *M. bovis*, *M. canetti, M. microti*, *M. pinnipedii* and *M. caprae* are grouped under *Mycobacterium tuberculosis* complex (MTBC). *Mycobacterium bovis* infects cattle and causes bovine TB. Mycobacteria, other than *M. tuberculosis,* causing clinical disease are known by various names - non tuberculous mycobacteria (NTM), mycobacteria other than tuberculosis (MOTT) and atypical mycobacteria. NTM infections can also occur throughout the body (Johnson & Odell, 2014), more common are pulmonary infections caused by *M. avium, M. kansasii* and *M. abscessus*, lymphadenitis and skin & soft tissue infections (Chan & Iseman, 2013). Mycobacteria that are not normally associated with human tuberculosis but can cause disease in immuno-compromised individuals such as HIV-infected individuals are called opportunistic pathogens. They include *M. avium-intracellulare* complex (Girard *et al.*, 2005) and *M. kansasii* (Canueto-Quintero *et al.*, 2003).

1.2. Mycobacteria

1.2.1. General features

Mycobacteria are aerobic, obligate intracellular, non-motile, non-capsulated, non-spore forming bacilli. Although mycobacteria are aerobic, some of them, for example *M. bovis* are microaerophilic and grow better at lower oxygen tensions. The 4.41 Mb genome has a high G+C content (61-71%) with approximately

4000 ORFs, 10% of which is dedicated to lipid metabolism (Cole *et al.*, 1998). These Gram-positive rods are unable to stain by the conventional Gram stain due to the lipid-rich cell wall. Mycobacteria stain pink with basic dyes such as carbol fuchsin that cannot be decolorized with acid-alcohol (95% ethanol and 3% hydrochloric acid). This unique property termed as 'acid-fastness' is the basis of the Ziehl-Neelsen staining technique for the identification of mycobacteria. Mycobacteria mostly require simple substrates for growth such as ammonia or amino acids as nitrogen sources and glycerol as a carbon source in the presence of mineral salts.

1.2.2. Classification

Taxonomically, mycobacteria belong to the Genus Mycobacterium, family Mycobacteriaceae belonging to the Order Actinomycetales that include diverse bacteria. Mycobacteria and other allied taxa are distinguished by their ability to synthesize mycolic acids. Mycobacteria can be classified based on their growth rates and pigment production. On the basis of generation time, they are classified as rapid growers (generation time of 3 - 4 h) which include *M. smegmatis, M. neoaurum*, *M. kansasii*, *M. fortuitum* and slow growers (generation time of 20 - 24 h) which include pathogenic mycobacteria *M. tuberculosis, M. bovis*, *M. africanum, M. leprae.* On the basis of pigment production (Runyon classification, 1959), mycobacteria are classified as:

a) Scotochromogens that include mycobacteria producing yellow pigment in the dark (*M. scrofulaceum, M. gordonae*).
b) Photochromogens that produce an orange pigment in the presence of light (*M. kansasii, M. marinum*).
c) Achromogens that do not produce any pigment (*M. avium, M. intracellulare, M. ulcerans*).

1.2.3. Mycobacterial cell envelope

Mycobacterial cell envelope is complex and intricately designed. It accounts for ~40% of the cell dry mass of the bacteria compared to less than 5% in other Gram-positive bacteria and only 10% in Gram-negative bacteria (Goren & Brennan, 1979) but this percentage is dependent on the species / isolate and the growth conditions. The native structure of the mycobacterial cell envelope as shown in Fig. 1.1 has been elucidated recently by cryo-electron microscopy of vitreous section (CEMOVIS) of mycobacteria and cryo-electron microscopy

(cryoEM) of whole mount mycobacteria (Hoffmann *et al.*, 2008; Sani *et al.*, 2010; Zuber *et al.*, 2008).

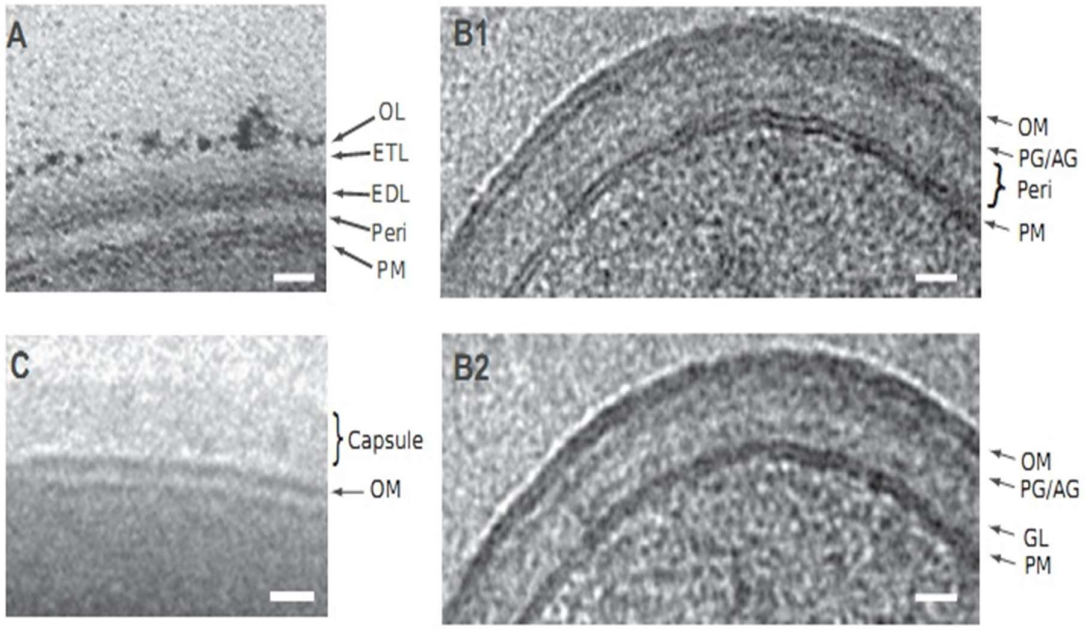

Fig. 1.1. TEM micrographs of mycobacteria. The plasma membrane and the outer membrane elucidated by conventional preparation (Panel A) and CEMOVIS (Panel B) are shown. The plasma membrane and the outer membrane bilayer are clearly visible in B1, whereas the granular layer and the peptidoglycan / arabinogalactan layers are clearer in B2. Panel C shows the whole cell cryoEM demonstrating the native capsule. Abbreviations: ETL, electron-transparent layer; EDL, electron-dense layer; OL, outer layer; GL, granular layer; Peri, periplasm; OM, outer membrane; PM, plasma membrane; PG, peptidoglycan; AG, arabinogalactan. Panel A and B are adapted from Zuber *et al.,* 2008 and C is adapted from Sani *et al.,* 2010.

The mycobacterial cell envelope comprises of many complex sugars and lipids of exceptional structure (Fig. 1.2). First, the presence of very long chain (C_{70}-C_{90}) fatty acids called mycolic acids; second, the unusual organization of these lipids into a Gram-negative-like outer membrane (mycomembrane) in these Gram-positive bacteria and the presence of pore-forming proteins in the mycomembrane and third, the covalent linkage of mycolic acids, arabinogalactan and peptidoglycan to form the cell wall skeleton (CWS). In slow-growing pathogenic mycobacterial species, this giant structure is surrounded by a capsular layer composed mainly of polysaccharides, primarily

a glycogen-like glucan. The CWS is separated from the plasma membrane by a periplasmic space which is approximately 20 nm thick and contains a granular layer, possibly representing membrane proteins.

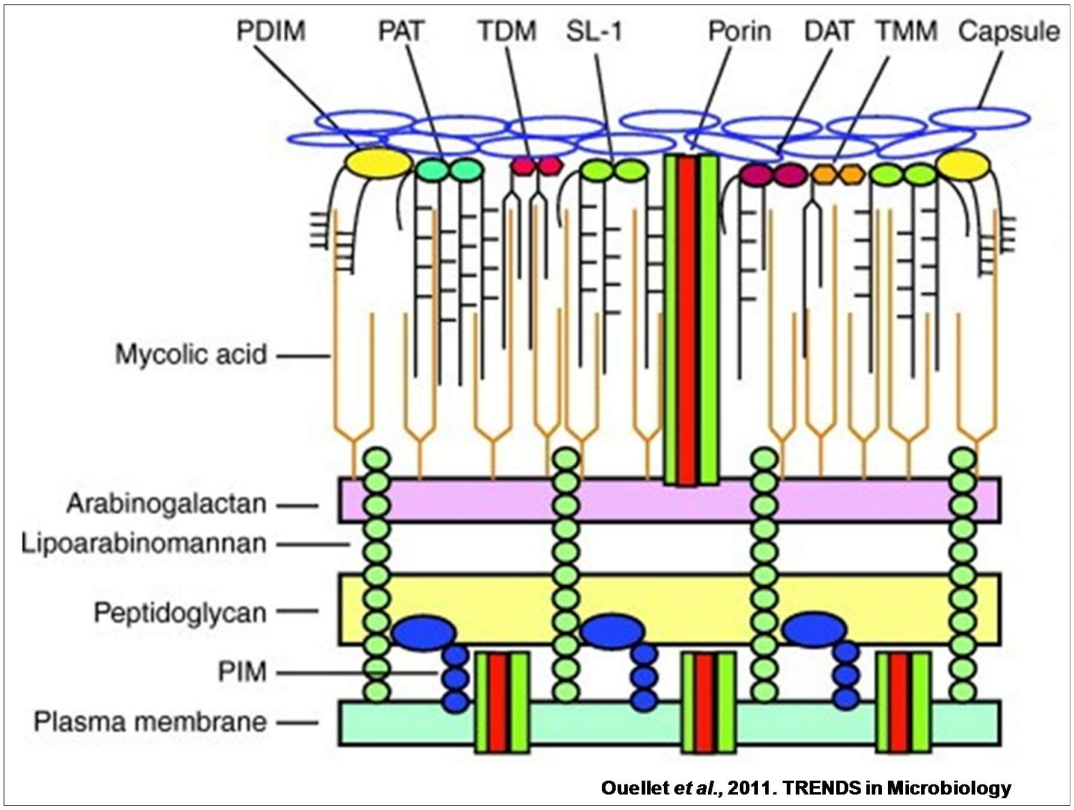

Fig. 1.2. Schematic representation of the cell envelope of *M. tuberculosis.* The cell envelope of *M. tuberculosis* cells consists of a plasma membrane, a cell wall composed of covalently linked mycolic acids, arabinogalactan and peptidoglycan and non-covalently linked lipids and proteins and a capsule consisting of polysaccharides, proteins and lipids. Abbreviations: PIM, phosphatidylinositol mannoside; PDIM, phthiocerol dimycocerosate; DAT, diacyltrehalose; PAT, penta-acyltrehalose; SL-1, sulfolipid-1; TMM, trehalose monomycolate; TDM, trehalose dimycolate.

1.2.3.1. Plasma membrane

The ultra-thin sections of the mycobacterial cell envelope revealed that the plasma membrane is similar to other biological plasma membranes (Zuber *et al.*, 2008) both in chemical composition and metabolic functions. As far as lipid composition of the plasma membranes is concerned, no obvious difference was found between those of rapid- and slow-growing *Mycobacterium* species examined. Polar lipids, mainly phospholipids, in association with proteins

assemble into a lipid bilayer (Minnikin, 1982). Palmitic ($C_{16:0}$), octadecenoic ($C_{18:1}$) and 10-methyloctadecanoic (or tuberculostearic acid) are the major fatty acid constituents of the isolated plasma membranes. The main phospholipids of the plasma membrane are phosphatidylinositol mannosides (PIM), phosphatidylglycerol (PG), cardiolipin and phosphatidylethanolamine (PE) while phosphatidylinositol (PI) occurs in small amounts. Lipoarabinomannan (LAM) is composed of a phosphatidylinositol group (Hunter & Brennan, 1990) covalently linked to arabinomannan. The non-covalently linked glycophospholipids [phosphatidyl-myo-inositol mannosides (PIMs) and their more related glycosylated end products, lipomannan (LM) and lipoarabinomannan (LAM)] are abundant in the inner (interspersed within the mAGP framework) and outer membranes of all *Mycobacterium* species (Gilleron *et al.*, 2008; Ortalo-Magne *et al.*, 1996; Pitarque *et al.*, 2008).

1.2.3.2. Cell wall skeleton

The intricate cell wall is the hallmark of mycobacteria which defines the shape of the mycobacterial cell owing to its rigidity. It consists of a covalently linked cell wall skeleton (CWS), an abundant variety of wall-associated lipids and a few polypeptides. The CWS consists of the material remaining after removal of all non-covalently bound wall-associated substances such as soluble proteins, lipids and glycans (Daffé, 2008). It is a giant macromolecule surrounding the entire cell and chemically composed of three covalently linked constituents: peptidoglycan, arabinogalactan and mycolates known as mycolyl-arabinogalactan-peptidoglycan (mAGP) complex.

Peptidoglycan

Peptidoglycan (PG) present in both Gram-negative and Gram-positive bacilli provides shape, rigidity and osmotic stability (Schleifer & Kandler, 1972). Although the backbone of PG is typically made up of N-acetylglucosamine (GlcNAc) and N-acetylmuramic acid (MurNAc) linked via β(1→4) linkages, mycobacterial PGs possess one notable structural modification: MurNAc is oxidized to N-glycolylmuramic acid (MurNGlyc) (Mahapatra *et al.*, 2005; Raymond *et al.*, 2005). This modification increases the overall strength of PG by providing sites for hydrogen bonding and also decreases the susceptibility to lysozyme (Brennan & Nikaido, 1995; Raymond *et al.*, 2005). Tetrapeptide side

chains of PG consist of L-alanyl–D-isoglutaminyl–meso-diaminopimelyl–D-alanine (L-Ala–D-Glu–A2pm–D-Ala) with the Glu being further amidated. These are attached to the muramyl components of the backbone that become cross-linked to provide a mesh-like structure. Another unique feature of mycobacterial PG is that it provides the site for AG attachment.

Arabinogalactan

The PG is covalently linked to the galactan chain through the C-6 of its muramyl residues via a diglycosylphosphoryl bridge, L-Rha*p*-GlcNAc-1-phosphate. Mycobacterial arabinogalactan (AG) comprises of D-galactofuranoses (Gal*f*) and D-arabinofuranoses (Ara*f*), which are extremely rare in nature. AG has a few defined structural motifs rather than repeating units as seen in all other bacterial polysaccharides. The non-reducing end of the arabinan consists of a branched hexa-arabino-furanosyl structure [βAra*f*- (1→2)-αAra*f*] 2-3,5-αAra*f*-(1→5)-αAra*f* and the back-bone of AG chain consists of 5-linked αAra residues punctuated with 3,5-αAra*f* branching. The galactan consists of alternating 5- and 6-linked β-D-galactofuranose (Gal*f*) units and the arabinan chain is attached to the galactan core through C-5 of some of the 6-linked Gal*f* units (Jankute *et al.*, 2015). The link between the arabinan and the galactan is not yet defined. In *M. tuberculosis*, mycolyl units were shown to cluster in groups of four and occupy only about two-thirds of the available attachment sites on the terminal hexa-arabinoside motif (McNeil *et al.*, 1991).

Mycolic acids

Mycolic acids are long chain α-alkyl, β-hydroxy fatty acids ($C_{70\text{-}90}$). The term “mycolic acid” was given by Stodola *et al.* (1938) to designate the principal ether-soluble fraction of the wax isolated from *M. tuberculosis* (Stodola *et al.*, 1938). They form an integral component of the mAGP complex or found as free lipids esterified to trehalose or glucose in the cell wall. Three distinct types are found (Fig. 1.3): α-mycolic acids are abundantly present (>70%) and exist in the cis-cyclopropane configuration whereas the methoxy mycolic acids and keto mycolic acids are the minor components (10 to 15%) and contain cyclopropane rings in either a cis- or trans-configuration with an adjacent methyl branch (Jankute *et al.*, 2015; Takayama *et al.*, 2005).

They have been shown to modulate cell wall fluidity and permeability, protect mycobacteria against chemical compounds or stress, play a role in

pathogenicity and persistence, and have diverse immunological functions (Kremer & Besra, 2005; Liu *et al.*, 1996). They also contribute to drug tolerance owing to the ability of *M. tuberculosis* to form biofilms (Ojha *et al.*, 2005; Ojha *et al.*, 2010; Sambandan *et al.*, 2013). The cyclopropane rings in mycolic acids of *M. tuberculosis* contribute to the structural integrity of the cell wall complex (George *et al.*, 1995) and protect the bacillus from oxidative stress (Yuan *et al.*, 1995). Mycobacteria have unique mycolic acid patterns. Using approaches such as thin-layer chromatography (TLC), gas-liquid chromatography (GLC) and high-performance liquid chromatography (HPLC), mycobacterial species are identified based on their mycolic acid patterns (Tortoli, 2003).

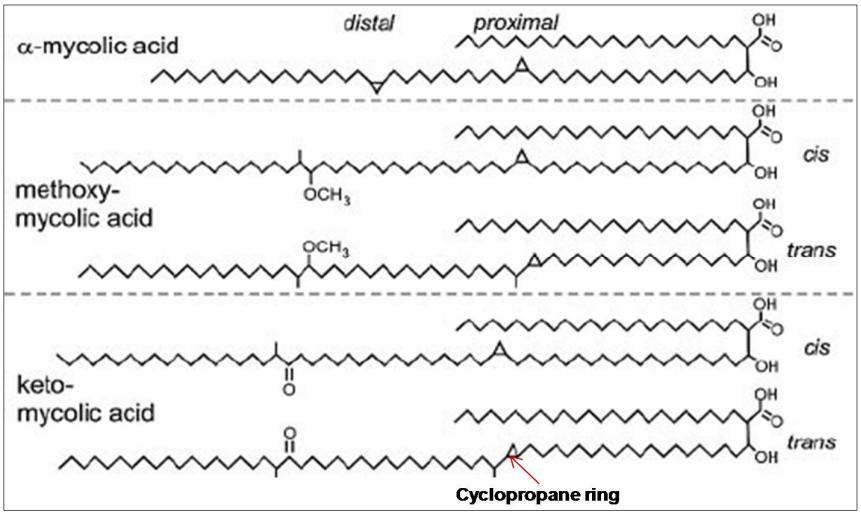

Fig. 1.3. Chemical structures of mycolic acids from *M. tuberculosis*. There are five forms of mycolic acids in *M. tuberculosis.* The cyclopropane rings in α-mycolic acid have cis configuration whereas either cis or trans configuration is present on the proximal ring of both methoxy- and keto-mycolic acids. Adapted from Takayama *et al.,* 2005.

1.2.3.3. Capsule

The capsule, an outer layer of the mycobacterial envelope consisting of a mixture of polysaccharide, protein and lipid can be always seen around intracellular mycobacterial pathogens but not around non-pathogenic mycobacteria or pathogenic mycobacteria grown *in vitro* in standard conditions (Frehel *et al.*, 1986; Ryter *et al.*, 1983). Lipids such as PIM and PE are present in very small amounts on the (capsular) surface of all the mycobacterial species

examined (Ortalo-Magne *et al.*, 1996). The main components of the outermost capsular layer of slow-growing mycobacterial species (e.g. *M. tuberculosis* and *M. kansasii*) are polysaccharides whereas the major components in rapid growers (e.g. *M. phlei* and *M. smegmatis*) are proteins (Lemassu *et al.*, 1996; Ortalo-Magne *et al.*, 1995). They consist mainly of a glucan, an arabinomannan and a mannan. Small amounts of other, still uncharacterized oligo- and polysaccharides are also present. The outermost part of the mycobacterial cell envelope contains only a tiny amount of lipid (2-3% of the surface-exposed material), and progressive removal of the capsular material shows that most of the lipids are in the inner rather than the outer part of the capsule (Ortalo-Magne *et al.*, 1996). Some of the species- and type-specific lipids and glycolipids, e.g. phthiocerol dimycocerosates (PDIM), phenolic glycolipid (PGL) and glycopeptidolipid (GPL), can be found on the surface of the capsule.

1.2.3.4. Solvent extractable lipids in the mycobacterial cell wall

A variety of lipids are found interspersed in the mAGP complex. Some of these lipids are common to all mycobacteria, for example trehalose dimycolates (TDMs) while others like phthiocerol dimycocerosates (PDIM), sulfolipids (SLs), phenolic glycolipid (PGL), glycopeptidolipids (GPLs) and lipooligosaccharides (LOSs) are species / strain-specific. The possibility of a correlation between the lipids of *M. tuberculosis* and TB pathogenesis led to the identification of TDM, SL and PDIM and derivatives as factors that can likely modulate the immune response (Bloch, 1950; Daffé & Draper, 1997). Structures of the above mentioned lipids are depicted in Fig. 1.4.

a) Trehalose-based lipids

In mycobacteria, trehalose (α-D-glucopyranosyl-α-D-glucopyranoside), is found either in the cytosol as free forms or in the cell wall as acylated forms (esterified to various fatty-acyl groups). It plays the role of a carrier molecule. Based on the esterifications, acylated trehaloses are grouped as:

- Mycolyl trehaloses - trehalose monomycolate (TMM) and trehalose dimycolate (TDM)
- Sulfated acyl-trehaloses - Sulfolipids (SLs)
- Methyl-branched acyl trehaloses - Di-acyl (DAT), Tri-acyl (TAT) and Penta-acyl (PAT)

Trehalose dimycolate

Trehalose-6-6'-dimycolate (TDM), also known as 'cord factor' is the most abundant lipid produced by virulent *M. tuberculosis*, responsible for the characteristic serpentine morphology (Noll & Block, 1953; Noll *et al.*, 1956). TMM, the precursor of TDM is found intracellularly as well as extracellularly. It is the mediator in the transport of mycolates across the membrane (Belisle *et al.*, 1997).

TDM essentially recruits cells for granuloma formation, apotosis and regulates production of nitric oxide and cytokines conducive for antibody production (Hunter *et al.*, 2006; Lima *et al.*, 2001; Perez *et al.*, 2000). Loss of TDM leads to reduced viability and loss of virulence.

Methyl-branched acyl trehaloses

Methyl-branched acyl trehaloses carry various methyl branched acyl chains such as mycosanoic acids in diacyl trehaloses (DATs) and mycolipenic acids in triacyl trehaloses and pentaacyl trehaloses (PATs). These molecules, being amphiphillic, interact with the mycolic acid core and the capsule layer (Minnikin *et al.*, 2002). DATs are non-covalently linked to the peptidoglycan in the outer layer of the mycobacterial cell wall (Ortalo-Magne *et al.*, 1996).

Mycolipenic acids are potent inhibitors of leukocyte migration *in vitro* (Husseini & Elberg, 1952). Antibodies against DATs and TATs are detected with very high specificity and sensitivity (Muñoz *et al.*, 1997). DATs also inhibit the proliferation of murine T cells *in vitro* (Saavedra *et al.*, 2001). They play an important role in capsule attachment and their absence leads to cell aggregation (Dubey *et al.*, 2002).

Sulfolipids (SL)

Sulfolipids are found in virulent mycobacterial strains (Middlebrook *et al.*, 1959). They are composed of sulfated trehalose esters, acylated with three to four fatty acyl groups which consist of one short chain saturated fatty acid (e.g. palmitic acid or stearic acid) and different long chain multi-methyl branched fatty acids (e.g., phthioceranic acid and hydroxyphthioceranic acids). The most abundant SL in mycobacterial cell wall is SL-1 which is a 2,3,6,6'-tetraacyl 2' sulfate (Goren *et al.*, 1976).

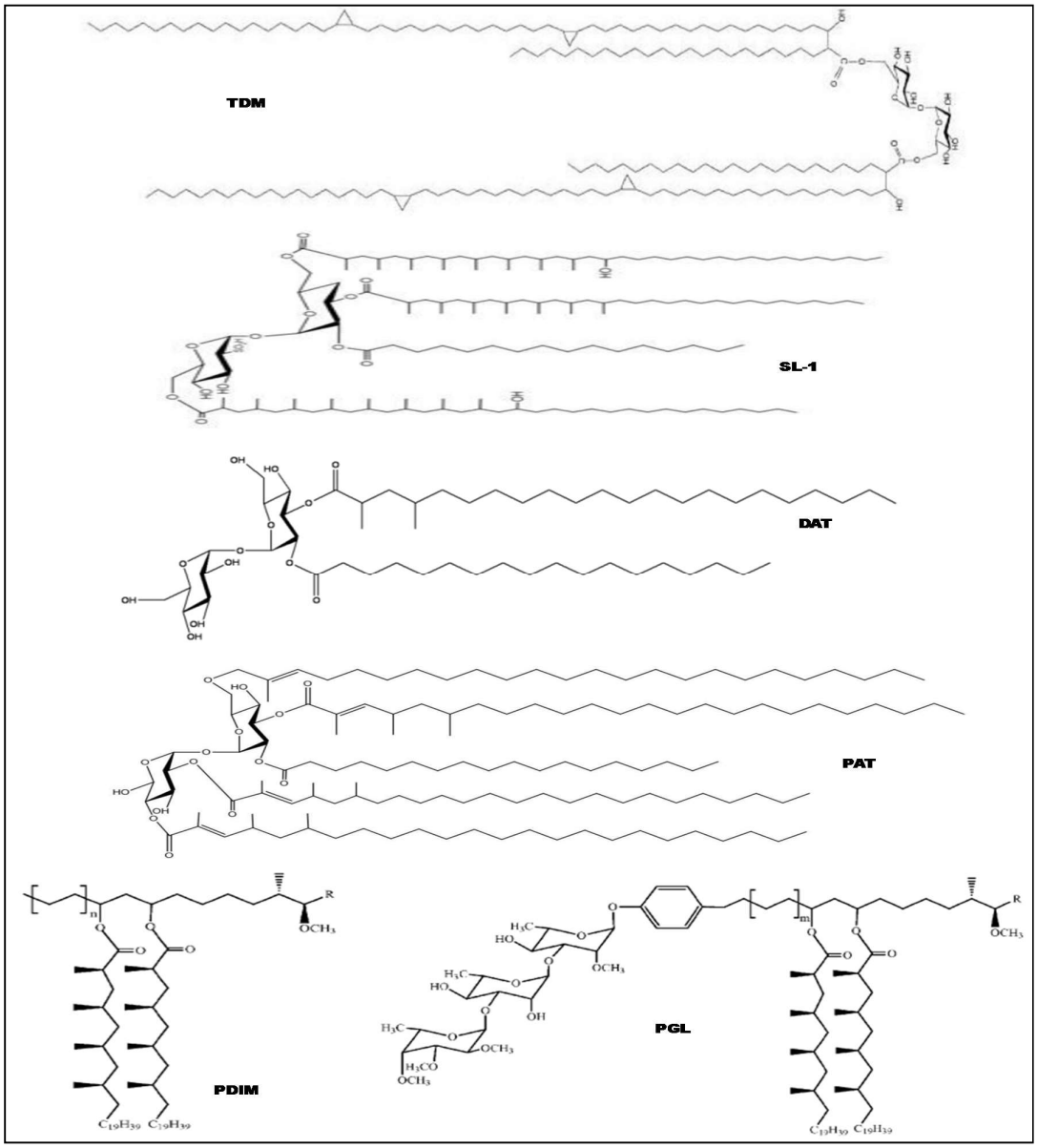

Fig. 1.4. Structures of surface exposed lipids from *M. tuberculosis*. In trehalose dimycolate (TDM), the trehalose sugar which is a disaccharide is esterified to two mycolic acid residues. In sulfolipid-1 (SL-1), trehalose is sulfated at the 2'-position and esterified with palmitic acid and the multimethyl-branched phthioceranic and hydroxyphthioceranic acids. In diacyl trehalose (DAT), trehalose is esterified with palmitic acid and the multimethyl-branched mycosanoic acid. In penta-acyl trehalose (PAT), trehalose is esterified with palmitic acid and the multimethyl-branched mycolipenic acids. In phthiocerol dimycocerosates (PDIM), the long-chain β-diol (phthiocerol moiety) is esterified with two mycocerosic acids; n = 10–11; R = $-CH_2-CH_3$ or $-CH_3$. The lipid core of phenolic glycolipid (PGL) is composed of phenolphthiocerol esterified by mycocerosic acids; m = 7–8; R = $-CH_2-CH_3$ or $-CH_3$.

SLs block the release of TNF-α from macrophages thereby inhibiting the formation of granuloma. It also prevents phagosome-lysosome fusion, inhibits mitochondrial oxidative phosphorylation and modulates oxidative response by regulating cytokine secretion (Jackson *et al.*, 2007). Both *in vivo* and *in vitro* studies show that SLs play a significant role in persistence and pathogenicity of *M. tuberculosis* (Rousseau *et al.*, 2003). SL_{1278} was found to be an immunostimulant in human tuberculosis patients (Gilleron *et al.*, 2004).

b) Phthiocerol dimycocerosate (PDIMs) and Phenolic glycolipids (PGL)

PDIMs are composed of a long chain phthiocerol or phthiodiolone esterified with two multimethyl-branched long-chain mycocerosic acids (Minnikin *et al.*, 2002) whereas in PGLs, the hydroxyl group of the phenol moiety is glycosylated by species-specific mono-, tri- or tetra-saccharide units (Daffé *et al.*, 1987). PGLs are found in pathogenic mycobacterial strains such as members of the *M. tuberculosis* complex, especially *M. canettii*, *M. leprae, M. kansasii, M. marinum, M.gastri*, and *M. ulcerans* (Daffé *et al.*, 1987).

PDIMs are essential for successful infection as their loss results in attenuation of *M. tuberculosis* in mice lungs (Cox *et al.*, 1999). PDIM provides protection against reactive nitrogen intermediates (Rousseau *et al.*, 2004), arrests acidification of phagosome and alters the host cell membranes (Simeone *et al.*, 2007). PGL-1 from *M. leprae* has been used for serodiagnosis of leprosy and TB (Gaylord *et al.*, 1987). PGLs inhibit the release of pro-inflammatory chemokines during infection (Reed *et al.*, 2004).

1.3. Tuberculosis

1.3.1. Epidemiology

TB is airborne and contagious. It affects millions of people each year and ranks alongside the human immunodeficiency virus (HIV) as a leading cause of death worldwide. According to the year 2015 report of World Health Organization (WHO, 2015), in 2014 there were an estimated 9.6 million new TB cases (5.4 million among men, 3.2 million among women and 1.0 million among children) and 1.5 million deaths of which approximately 890,000 were men, 480,000 were women and 140,000 were children (Fig. 1.5). TB and HIV co-infection occurs when people have both HIV infection, and also either latent or active TB disease. Globally there was an estimated 1.2 million new HIV-positive TB cases

(12% of all TB cases) and 0.4 million deaths. Almost three-quarters of HIV-positive TB cases were in the African Region. Drug-resistant TB is a major threat to controlling the disease and is acquired either due to inadequate TB treatment or due to direct transmission of drug-resistant TB from one person to another. There were approximately 480,000 new cases of MDR-TB and about 190,000 deaths from MDR-TB worldwide. Most of the estimated number of cases in 2014 occurred in South-East Asia and Western Pacific regions (58%) and the African Region (28%) while smaller proportions of cases occurred in the Eastern Mediterranean Region (8%), the European Region (3%) and the Region of the Americas (3%) (WHO, 2015).

India with 23% of the global total of new cases stands top amongst the 22 high burden countries (HBCs). An estimated incidence figure of 2.2 million cases of TB was in India out of a global incidence of 9.6 million. The estimated TB mortality was 240,000 deaths. The incidence of HIV-positive TB cases was 120,000 cases where the mortality was estimated to be 38,000 deaths. In India, MDR-TB levels are about 3% in new cases and around 12-17% in retreatment cases. Most of the national TB statistics for India are collected by the government Revised National Tuberculosis Control Programme (RNTCP) which was started in 1997 and which was then expanded across the country. The aim of the programme is to decrease mortality and morbidity due to this disease and reduce transmission of infection until TB ceases to be a major public health problem in India.

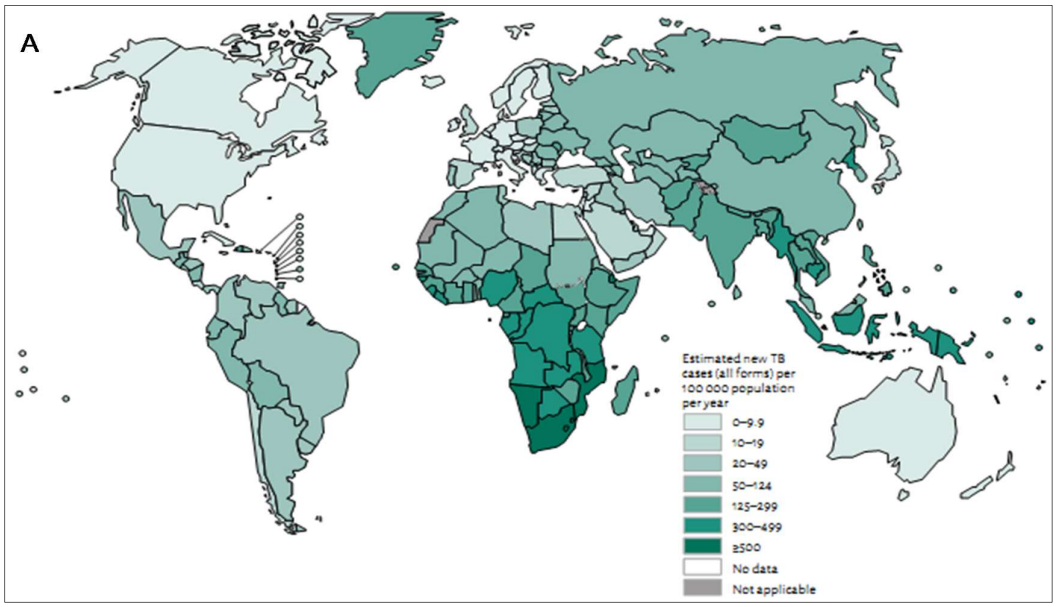

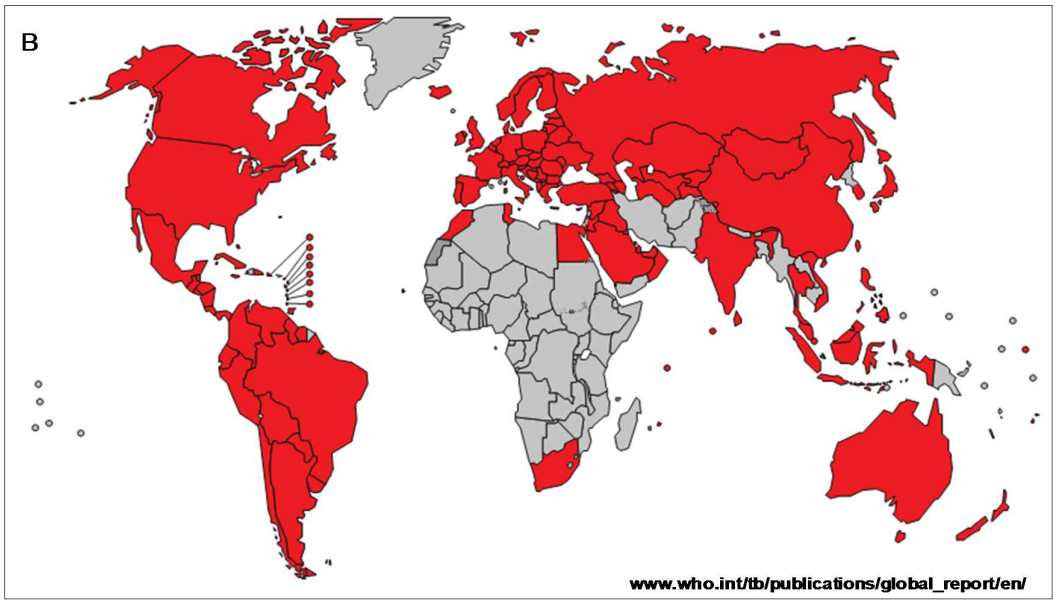

Fig.1.5. Estimated incidence rate and mortality rate of TB. Panel A shows the number of incident TB cases relative to population size (the incidence rate) varies widely among countries. Incidence rates are falling globally after peak in 2004, but only at the rate of <1% per year (WHO, 2015). Panel B shows countries (in red) for which TB mortality is estimated using measurements from vital registration systems and / or mortality surveys.

1.3.2. Control measures

Control measures for tuberculosis include timely diagnosis, anti-TB treatment, check on the emergence of drug-resistant forms of *M. tuberculosis* and preventive measures by vaccination.

1.3.2.1. Diagnosis

Diagnosis of TB involves clinical examination of the patient and investigations including chest X-ray for identifying the granuloma formation, sputum smear testing for acid-fast bacilli (AFB) done in three consecutive days, tuberculin skin test (Mantoux test) and culture. Both Mantoux test and AFB smear test have drawbacks such as non-specificity, less sensitivity and false positivity. A false positive result could be due to non-tuberculous mycobacteria or previous administration of BCG vaccine. The 'gold standard' for diagnosis is culture confirmation. However, it takes 4-6 weeks to get the confirmation using the conventional growth in Lowenstein-Jensen medium owing to the long generation time of *M. tuberculosis*. Currently, a number of culture confirmation systems that can monitor growth parameters using defined sensor systems are

available, such as the BACTEC system (Becton Dickinson, NJ, USA) (Rohner *et al.*, 1997). The radiometric BACTEC 460 system uses ^{14}C-palmitic acid and growth is determined by quantifying released $^{14}CO_2$. The non-radiometric MB / BacT Mycobacteria Detection System and the BacT / ALERT Microbial Detection Systems utilize a colorimetric sensor and reflected light to monitor the presence and production of carbon dioxide (CO_2) dissolved in the culture medium (Thorpe *et al.*, 1990) while the BACTEC MGIT 960 System utilises a fluorescent compound sensitive to the presence of oxygen dissolved in the Middlebrook 7H9 broth (Tortoli *et al.*, 1999). However these systems are economically not viable, especially for developing countries. Other diagnostic tests include PCR amplification of the insertion element IS*6110* (Torrea *et al.*, 2005) and assays that are based on cell-mediated immune response such as QuantiFERON-TB Gold (Mori *et al.*, 2004) and T SPOT-TB assays (Soysal & Bakir, 2011). The immune response is recorded by measuring the stimulation indices and / or production of IFN-γ in response to mycobacterial proteins such as ESAT-6. Line probe assay (LiPA) is used for the detection of rifampicin-resistant TB among culture and clinical isolates (Morgan *et al.*, 2005). MTB / RIF is a recently developed automated molecular test, which provides sensitive detection of TB and rifampicin resistance, directly from untreated sputum in less than 2 hours with minimal hands-on time (Boehme *et al.*, 2010).

Diagnosis of extrapulmonary TB (EPTB) is challenging as most forms of EPTB are paucibacillary and have variable clinical presentations. Most reliable method includes invasive procedures such as bronchoscopy and biopsy. Other techniques such as Nucleic acid amplification tests (NAAT), BACTEC system, MTB / RIF and culture.

1.3.2.2. Anti-TB treatment

Chemotherapy can cure tuberculosis in 95% of patients with active pulmonary TB (Spigelman & Gillespie, 2006). The global TB control strategy of the World Health Organization (WHO) involves a short term strategy known as Directly Observed Treatment Short-course (DOTS). The program provides free of cost, quality anti-tubercular drugs across the country through the numerous primary health centres and the growing numbers of the private-sector DOTS-providers. The treatment strategy involves two phases; first, intensive phase where three or more drugs (isoniazid, pyrazinamide, rifampicin and streptomycin) are used

for two months, aimed at killing the actively growing bacteria and second, maintenance phase in which usually isoniazid and rifampicin are used for 4-7 months to remove any residual bacilli and prevent disease recurrence and development of drug-resistant organisms. The other drugs used are known as second-tier antibiotics that includes streptomycin, kanamycin, amikacin, aminoglycosides, capreomycin, cycloserine, ethionamide, PAS, thioamides, prothionamide and fluoroquinolones such as gatifloxacin, levofloxacin and moxifloxacin.

Mode of action of front-line drugs

(a) Isoniazid (INH) or isonicotinic acid enters the pathogen as a pro-drug and is activated by the catalase-peroxidase (KatG) expressed by the pathogen. The peroxidase activity of KatG is necessary to activate INH to the active drug in the bacterial cell (Zhang *et al.*, 1992) that blocks mycolic acid biosynthesis, thereby disrupting the cell wall synthesis.

(b) Rifampicin (RIF) is extremely effective against *M. tuberculosis*, (MIC 0.1-0.2 pg / mL) and its rapid bactericidal activity in combination with the other front-line drugs helped to shorten the course of treatment against drug-susceptible infections (Heifets, 1994; Mitchison, 1985). Rifampicin binds to the β-subunit of DNA-dependent RNA polymerase and blocks transcription, thereby killing the organism.

(c) Pyrazinamide (PZA), a nicotinamide analog, targets an enzyme involved in fatty-acid synthesis and is responsible for killing persistent tubercle bacilli in the initial intensive phase of chemotherapy (Somoskovi *et al.*, 2001). Pyrazinamide is a pro-drug, which is converted to its active form, pyrazinoic acid by the pyrazinamidase elaborated by the pathogen. The activity of PZA is highly specific for *M. tuberculosis*, as it has no effect on other mycobacteria.

(d) Ethambutol (ETH) is a front-line drug used in combination with other drugs and is specific to mycobacteria. It inhibits arabinosyl transferase used for the synthesis of arabinogalactan involved in cell wall biosynthesis (Takayama & Kilburn, 1989). The inhibition of arabinogalactan biosynthesis by ethambutol accounts for the accumulation of mycolic acids and their trehalose esters and affects the permeability of cell wall.

(e) Streptomycin (STM), an aminocyclitol glycoside, is an alternative front-line anti-tubercular drug recommended by the WHO that interacts with the 16S rRNA and S12 ribosomal protein (Finken *et al.*, 1993), resulting in the misreading of the mRNA and inhibition of protein synthesis.

1.3.2.3. Vaccine: BCG as vaccine

Mycobacterium bovis bacillus Calmette-Guerin (BCG) is the first vaccine for TB developed by Albert Calmette and Camille Guerin of Pasteur Institute. The first oral administration of BCG was in 1921, and since then many clinical trials in different parts of the world have evaluated the efficacy of BCG in preventing disease. The efficacy of BCG vaccination in preventing adult pulmonary tuberculosis was found to be low, as concluded from the extensive 10-year follow-up trial in Chingleput (Tamil Nadu, India) (Tuberculosis Prevention Trial, 1979). It was found that BCG conferred efficient protection against childhood miliary TB and TB meningitis in contrast to adult pulmonary TB (Trunz *et al.*, 2006). Re-vaccination with BCG during adolescence in a population vaccinated with BCG at birth does not improve protective efficacy as shown in large, randomized controlled trial in Brazil (Rodrigues *et al.*, 2005). All the new vaccines in development are focused on inducing a strong and durable cellular immune response, as cellular immunity is necessary for protection against tuberculosis. To enhance the efficiency of BCG vaccination, efforts are being made to develop a better recombinant BCG and a subunit boosting vaccine that can be administered after BCG vaccination.

1.4. Pathogenesis of TB

1.4.1. Sequence of events

Tuberculosis is a disease that is transmitted by aerosolized droplets containing infectious *M. tuberculosis.* The inhaled bacilli lodge in the terminal air spaces of the lung where they enter and are engulfed by macrophages. In an immune-competent individual, the bacilli are killed by the macrophages, with the mycobacterial antigenic determinants sensitising the T lymphocytes. When the macrophages fail to counter the bacilli, they infect new alveolar macrophages and replicate within them. The onset of host immune response controls the bacterial replication and dissemination. There is interplay between the

macrophages and T lymphocytes that is mediated by cytokines and chemokines.

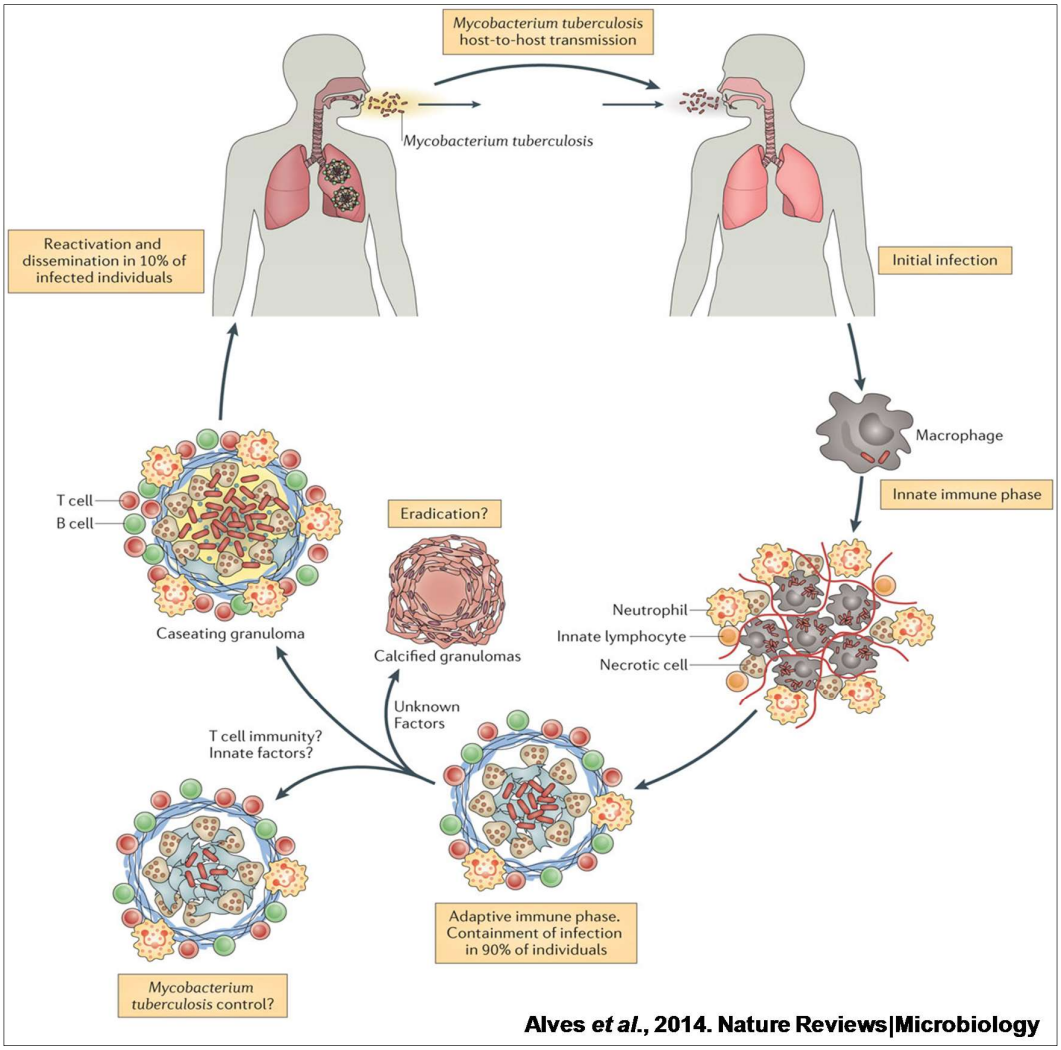

Fig. 1.6. Sequence of events upon entry of the pathogen into the mammalian host. Inhalation of the aerosol droplets containing bacteria marks the initiation of infection. The innate immune response recruits the inflammatory cells to the lung. The recruitment of T cells, B cells, activated macrophages and other leukocytes leads to the establishment of granulomas, which can contain *M. tuberculosis*. Most infected individuals remain clinically asymptomatic known as the 'latent state'. A small percentage of these people, upon immuno-suppression, eventually progress and develop active disease, which can lead to the release of *M. tuberculosis* from granulomas. When individuals with active tuberculosis (TB) cough, they can generate infectious droplets that transmit the infection.

If a Th1 response is produced, it results in the production of pro-inflammatory cytokines like IFN-γ. The host attempts to control the pathogen with granuloma formation by the differentiation of macrophages into 'epithelioid' cells surrounded by lymphocytes (Ehlers & Hölscher, 2005). This solid necrotic mass (granuloma) is thought to deprive oxygen to the pathogen and may over time, became sclerotic and even calcified, commonly resulting in containment or death of *M. tuberculosis* (Mack *et al.*, 2009). Primary granulomatous lesion in the lung and the dependent enlarged hilar lymph node is collectively called as 'Ghon complex' (Mack *et al.*, 2009). The strength of the host cellular immune system decides whether an infection is arrested here or progresses to the next stage. Here, the pathogen as latent bacilli can persist throughout a person's life in an asymptomatic state and the only clinical evidence of *M. tuberculosis* infection during latency is delayed type hypersensitivity against mycobacterial antigens, demonstrated by a tuberculin skin test (Glickman & Jacobs, 2001). A small percentage of these people (between 5 and 10%) will eventually progress and develop active disease upon immunosuppression. The granuloma becomes liquefied and uncontrolled replication of the pathogen results in their spread within the lungs (active pulmonary TB) and even other tissues via lymphatic system and the blood (miliary or extrapulmonary TB). This sequence of events is depicted in Fig. 1.6.

1.4.2. Infection *vs* disease development

The bacterium faces adverse conditions after its internalization by the alveolar macrophages. Macrophage activation leads to phagosomal maturation and production of antimicrobial molecules such as reactive nitrogen intermediates (RNI) and reactive oxygen intermediates (ROI), toxic peptides, oxygenated lipids, lysosomal enzymes and fatty acids (Fenton & Vermeulen, 1996; Nathan & Shiloh, 2000). TNF-α induces apoptosis in response to mycobacterial infection while IFN-γ kills and clears the mycobacteria. Despite the fact that these phagocytes are usually very effective in internalizing and clearing most of the bacteria, *M. tuberculosis* has evolved several mechanisms to circumvent the hostile environment of the macrophage, its primary host cell. The ability of the population of viable *M. tuberculosis* to survive and evade the host immune surveillance (Boshoff & Barry, 2005) has been attributed to many factors:

interference in immune signalling pathways subverting the local immune response, phenotypic tolerance of immune-mediated effectors by the induction of stress regulons, metabolic alteration or quiescence, detoxification or damage repair mechanisms and the ability to adjust metabolic processes to varying nutrient availability (Stewart *et al.*, 2003).

1.4.3. Cell-mediated immune response and cytokine expression in tuberculosis

The T cell-mediated acquired immune response to infection with *M. tuberculosis* is a complex event involving a variety of T cell subsets that manifest themselves in numerous functions, including protection, delayed-type hypersensitivity, cytolysis and the establishment of a state of memory immunity. These functions are dependent on the secretion of an array of cytokines by the monocytes, macrophages, granulocytes and natural killer cells in containing or destroying the bacilli. Cytokines are small, non-structural proteins with molecular weights of up to 40 kDa without a consistent amino sequence motif or three-dimensional structure. They act as a link between the innate and adaptive immune system with the objective of promoting a powerful immune response against pathogens. Cytokines promoting inflammation are called pro-inflammatory cytokines whereas cytokines which block the signal cascade are called anti-inflammatory cytokines. Chemokines attract circulating immune cells by chemotaxis so that they accumulate around the source of chemokine production. The outcome of an infection depends on the sum of various factors influencing each other (Fig. 1.7). Disturbances of the balance of this highly complex and intricate network of cytokines and effector cells by genetic, environmental or microbial elements might have harmful consequences (Westendorp *et al.*, 1997).

In the case of infection with *M. tuberculosis,* the macrophages get activated and start secreting cytokines stimulating the complex interacting machinery of the host immune system. The inflammatory response is essential for granuloma formation and long term survival of *M. tuberculosis* (Sasindran & Torrelles, 2011). The various cytokines modulating host immune response during *M. tuberculosis* infection are discussed here.

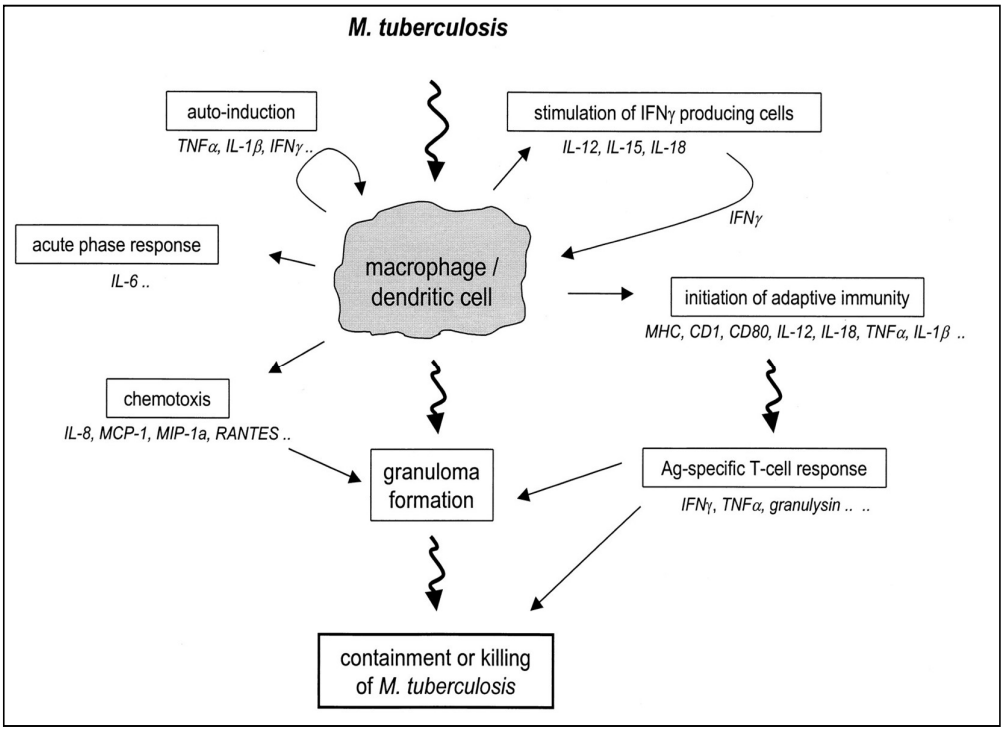

Fig. 1.7. Inflammatory response of phagocytic cells upon activation with *M. tuberculosis*. The recognition of *M. tuberculosis* by macrophages and dendritic cells leads to an inflammatory response by the production of cytokines which may either result in the early killing of the bacteria or containment of infection. Adapted from Van Crevel *et al.,* 2002.

1.4.3.1. Pro-inflammatory cytokines

Tumor necrosis factor-alpha (TNF-α): TNF-α, a prototype pro-inflammatory cytokine is produced by monocytes, macrophages and dendritic cells when stimulated with mycobacteria or mycobacterial products. It plays a key role in granuloma formation, induces macrophage activation and has immunoregulatory properties (Van Crevel *et al.*, 2002). TNF-α activated macrophages release chemokines which attract additional immune cells to the infection site (Algood *et al.*, 2004). TNF-α induces apoptosis that helps in confining intracellular pathogens and clearing some infections (Keane *et al.*, 1997). TNF-α, if left unregulated may cause tissue damage and necrosis making the balance of TNF-α production imperative. The anti-inflammatory cytokine IL-10 helps in maintaining the levels of TNF-α (Byrd, 1997). TNF-α knockout mice fail to induce granuloma formation and are unable to limit bacterial dissemination leading to death (Saunders & Cooper, 2000).

Interferon-gamma (IFN-γ): IFN-γ is secreted by T lymphocytes (type 1 helper T cells and cytotoxic T cells) and natural killer (NK) cells and is responsible for the activation of macrophages which in turn produce inflammatory cytokines. IFN-γ promotes the monocyte fusion and plays an important role in the multinucleated giant cell formation in the tuberculosis granulomas (Möst *et al.*, 1990). Patients with defects in IFN-γ receptors are highly susceptible towards mycobacterial infections and have a higher risk of recurrence of infection (Ottenhoff *et al.*, 2002). IFN-γ knockout mice are particularly susceptible to *M. tuberculosis* (Flynn *et al.*, 1993). It has been shown that the macrophage-activating cytokines IFN-γ and TNF-α are important for the initial control of tuberculosis (Cooper *et al.*, 1993; Flynn *et al.*, 1993).

Interleukin-1 beta (IL-1β): IL-1β is mainly produced by monocytes / macrophages (Ward *et al.*, 2010) and dendritic cells (Michelini-Norris *et al.*, 1992) after the recognition of mycobacterial lipoproteins which are potent activators of the TLR2 (Aliprantis *et al.*, 2000). TLR activation leads to an increased production of the precursor molecule pro-IL-1β which co-localizes in the cytosol with pro-caspase-1 (Andrei *et al.*, 1999). A protein complex termed 'IL-1β inflammasome' converts the inactive procaspase-1 into active caspase-1 that activates IL-1β which promotes phagosome maturation (Martinon *et al.*, 2002). An IL-1α and -1β double KO mice displayed an increased mycobacterial outgrowth and also defective granuloma formation after infection with *M. tuberculosis* (Juffermans *et al.*, 2000; Yamada *et al.*, 2000).

Interleukin-12 (IL-12): IL-12, produced mainly by monocytes and macrophages, plays a pivotal role in host defence against *M. tuberculosis* (Fulton *et al.*, 1996; Ladel *et al.*, 1997). In tuberculosis, IL-12 has been detected in lung infiltrates, in pleurisy, in granulomas and in lymphadenitis (Van Crevel *et al.*, 2002). IL-12 has a regulatory role connecting both the innate and adaptive immune response to mycobacteria. It exercises its protective effects mostly through the induction of IFN-γ (Cooper *et al.*, 1997). Patients with mutations in the genes encoding IL-12p40 and IL-12R display a reduced capacity to produce IFN-γ (Ottenhoff *et al.*, 1998).

Interleukin-18 (IL-18) : IL-18, produced by macrophages is an IFN-γ inducing factor, having similarity to IL-1β and works synergistically with IL-12 (O'Neill & Greene, 1998). IL-18 induces the production of other pro-inflammatory

cytokines, chemokines and transcription factors (Netea *et al.*, 2000; Puren *et al.*, 1998). *Mycobacterium tuberculosis*-mediated production of IL-18 by peripheral blood mononuclear cells is reduced in tuberculosis patients, and this reduction may be responsible for reduced IFN-γ production (Vankayalapati *et al.*, 2000).

Interleukin-6 (IL-6): IL-6 has both pro- and anti-inflammatory properties and is produced early during mycobacterial infection by the macrophages and helper T cells (Hoheisel *et al.*, 1998; Law *et al.*, 1996). A deficient IFN-γ production in the early stages of immune response was seen in IL-6-deficient mice that increased the susceptibility to *M. tuberculosis* infection (Saunders *et al.*, 2000). IL-6 has been shown to inhibit the production of TNF-α and IL-1β (Schindler *et al.*, 1990) and stimulates *in vitro* growth of *M. avium* (Shiratsuchi *et al.*, 1991).

Interleukin-8 (IL-8): IL-8 is a chemokine mainly secreted by granulomas infiltrated by neutrophils, macrophages infected with *M. tuberculosis* and other cells with TLR involved in the unspecific immune response. Its primary function is to attract circulating leukocytes to invade inflammated tissues (Broaddus *et al.*, 1992). The IL-8 production is negatively regulated by IL-1β and TNF-α (Zhang *et al.*, 1995b). The importance of IL-8 for bacterial containment was seen when it was totally blocked in rabbits whereupon the granuloma formation was inhibited (Larsen *et al.*, 1995).

1.4.3.2. Anti-inflammatory cytokines

Interleukin-10 (IL-10): The anti-inflammatory cytokine IL-10 is released by macrophages, type 2 helper T cells, B cells, neutrophils, eosinophils, and mast cells (Gerosa *et al.*, 1999; Hickman *et al.*, 2002; Shaw *et al.*, 2000). The secretion is promoted mostly by IL-12 and IL-6 (Saraiva & O'Garra, 2010). As an antagonist to pro-inflammatory cytokines IL-10 alleviates the process of inflammation in monocytes by limiting the IL-8, IFN-γ, TNF-α and granulocyte-macrophage colony-stimulating factor (GM-CSF) production (de Waal Malefyt *et al.*, 1991) that includes limiting the production of reactive oxygen intermediates (ROIs) and reactive nitrogen intermediates (RNIs) (Gazzinelli *et al.*, 1992) in macrophages. IL-10 prevents an over-reaction of the inflammation promoting factors, counteracts cell damage, leads to a balance between the pro- and anti-inflammatory factors and is therefore essential for the outcome of disease. IL-10

could effectively suppress the immune response as higher levels of IL-10 was produced in anergic patients even after treatment (Smith, 2003).

Transforming growth factor-beta (TGFβ): TGFβ produced by monocytes and dendritic cells at the site of disease (Toossi *et al.*, 1995) counteracts protective immunity in tuberculosis. TGFβ suppresses cell-mediated immune response in two ways: first by antagonizing antigen presentation, pro-inflammatory cytokine production and cellular activation in macrophages and second by inhibiting proliferation and IFN-γ production in T cells (Toossi & Ellner, 1998). TGFβ selectively induces production of IL-10 and together they suppress IFN-γ production (Othieno *et al.*, 1999).

Interleukin-4 (IL-4): IL-4 is secreted by both type 2 helper T cells and cytotoxic T cells (van Crevel *et al.*, 2000) and suppresses IFN-γ production and macrophage activation (Appelberg *et al.*, 1992; Powrie & Coffman, 1993). Increased production of IL-4 lead to disease progression and reactivation of latent infection in *M. tuberculosis* infected mice (Howard & Zwilling, 1999b).

1.4.4. Adaptation to the environment in the human host

The growth and survival of the pathogen within the macrophages is determined by its ability not only to overcome the oxidative stress and the immune response but also its ability to acquire nutrients from the host. There is increasing evidence that the pathogen preferentially utilises lipids as a carbon source (Keating *et al.*, 2005). Among the micronutrients, iron plays an important role in the metabolism of the pathogen. The iron acquisition machinery is the main focus of this study and is discussed in detail below.

1.5. Acquisition of iron

1.5.1. Role of iron

Iron, a divalent cation is a double-edged sword as it is essential for the survival of an organism but in excess it can prove lethal. It is the second most abundant metal after aluminium and the fourth most abundant element in the earth's crust. It is an requisite micronutrient for all bacteria with few exceptions; lactobacilli which have a cobalt-containing reductase (Sritharan, 2000) and *Borrelia burgdorferi* which have manganese in their metal-requiring enzymes (Posey & Gherardini, 2000). Iron is important for mycobacteria including *M. tuberculosis* as it is involved in vital cellular functions, electron transport, DNA

replication, haem biosynthesis, amino acid biosynthesis and pyrimidine biogenesis (De Voss *et al.*, 1999; Sritharan, 2000). It acts as a co-factor for at least 40 different enzymes encoded in the *M. tuberculosis* genome (Cole *et al.*, 1998) such as oxygenases, superoxide dismutases, hydroxylases and ribonucleotide reductases. The ability of atomic iron to oscillate between two oxidation states: ferrous (Fe^{2+}) and ferric (Fe^{3+}) with the oxidation-reduction potential for the Fe^{2+} / Fe^{3+} couple varying between +300 mV to –500 mV, enables it to serve as a catalyst in biological redox reactions.

The redox potential of iron also generates cellular toxicity under conditions of iron overload. Reactive oxygen intermediates are generated during the course of normal cellular homeostasis. In the presence of such reactive oxygen species, iron can catalyze the Fenton reaction to generate hydroxyl radicals that damage lipids, DNA, and protein. It is therefore critical to maintain optimal levels of iron.

Availability of iron is indispensable for the growth of the pathogen but it faces iron limitation *in vivo*. Poor availability of iron is due to the insolubility of ferric iron (Fe^{3+}) under aerobic, aqueous and neutral pH conditions and existence as insoluble ferric hydroxides and oxyhydroxides. The solubility of the predominant form of iron, $Fe(OH)_2^+$, is $1.4x10^{-9}$ M at pH 7 (Chipperfield & Ratledge, 2000) which is considerably lower than the requirements for bacterial growth (10^{-7} M). Another limiting factor is the withholding of the iron (~99.9%) by the host proteins such as transferrin (in blood circulation), lactoferrin (in leukocytes and mucosal secretions) and ferritin (in liver) (Bullen *et al.*, 1999; Ratledge & Dover, 2000; Sritharan, 2000), a process termed as ‘nutritional immunity’ (Kochan, 1977). These host mechanisms usually keep free iron below the level required for bacterial growth and are regulated by the hormone hepcidin which orchestrates an innate immune response to further reduce available iron and to slow or stop growth of bacterial pathogens (Drakesmith & Prentice, 2012).

1.5.2. Adaptation of mycobacteria to iron limitation: elaboration of the siderophore-mediated iron acquisition machinery

Mycobacteria are able to evade the nutritional immunity by the elaboration of the siderophore-mediated iron acquisition machinery (De Voss *et al.*, 1999; Sritharan, 2000). Siderophores are low molecular weight (500-1000 Da) Fe^{3+}-specific high affinity molecules with binding affinity constant Ks ranging from 10^{22} to 10^{50} and can remove iron from the insoluble $Fe(OH)_3$ and from host-iron binding compounds, but not from heme proteins. Mycobacteria produce two types of siderophores: mycobactin (Mb) produced by all mycobacteria are cell-associated and carboxymycobactin (CMb) and exochelin secreted by pathogenic and non-pathogenic mycobacteria respectively chelates iron from immediate environment that is taken up by these organisms.

1.5.2.1. Mycobactins

Mycobactin was first identified in 1949 *in M. phlei* (Francis *et al.*, 1949) and the structures of several mycobactins were elucidated by Alan Snow and his group (Snow, 1970). Mycobactins are essential for growth within macrophages (De Voss *et al.*, 2000) and have high affinity for Fe^{3+} (~10^{30}) with low binding to Fe^{2+} (Ratledge, 2004). Few mycobacterial strains such as *M. paratuberculosis* and some strains of *M. avium* do not produce mycobactin under iron-limiting conditions. Mycobactins belong to the mixed ligand type siderophores (Fig. 1.8) and have a core nucleus that consists of a 2-hydroxyphenyloxazoline moiety linked via an amide bond to an acylated ε-N-hydroxylysine residue. This lysine is, in turn, esterified at the α-carboxyl with a β-hydroxy acid that forms an amide link with a second ε-N-hydroxylysine which has cyclised to give a seven-membered lactam. Within this core, a methyl group may or may not be present at the 6^{th} position of phenolic ring (R_1) and / or at the 5' position of the oxazoline (R_2). Presence of both types of oxazoline has been reported in *M. tuberculosis* (Gobin *et al.*, 1995a). Alkyl substituents of the hydroxyl acid (R_3 and R_4) and the acyl moiety R_5 are highly variable in different species of mycobacteria (Snow, 1970) and can be used as chemotaxonomic markers for identifying mycobacteria (Hall & Ratledge, 1984; Sritharan, 2000). Fe^{3+} is chelated by the two hydroxamic acids of the ε-N-hydroxylysines, the nitrogen of the oxazoline ring, and the phenolate oxygen atom.

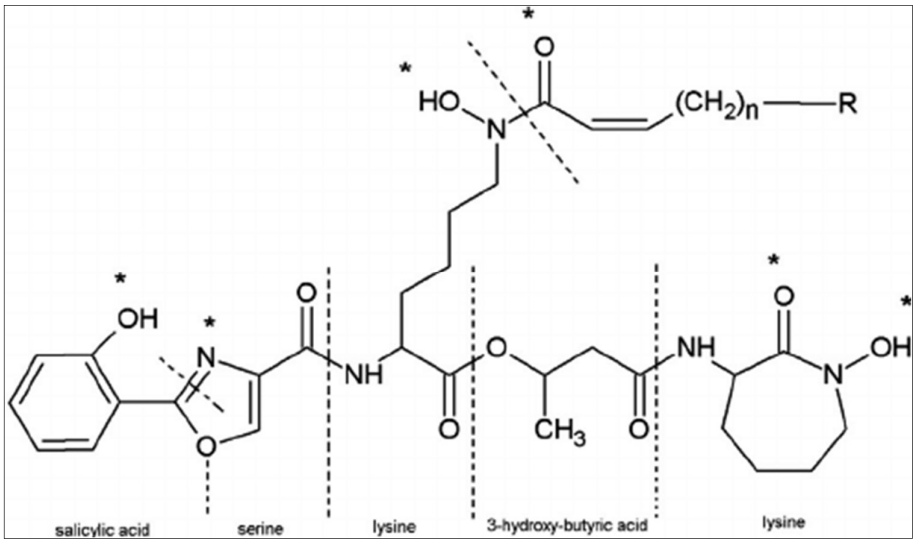

Fig. 1.8. The general structure of mycobactin from *M. tuberculosis*. The structure consists of 5 amino acids including one salicylic acid, one serine, two lysines, and one 3-hydroxybutyric acid. A long alkyl chain extends from the side chain of the middle lysine residue where the length of the R-group may vary amongst the mycobacteria species. The asterisk (*) indicates the chelating group for the ferric ion binding. Adapted from (Fang *et al.*, 2015).

1.5.2.2. Carboxymycobactins

Carboxymycobactins are the extracellular siderophore expressed mainly by pathogenic mycobacteria (Ratledge, 2004) but they have also been detected in small quantities in the non-pathogen *M. smegmatis* (Ratledge & Ewing, 1996). Carboxymycobactin and mycobactin share a common core nucleus but differ in the length of the alkyl substitution. Carboxymycobactin lack the long alkyl chain at R5, the substituents are acyl chains with a terminal carboxylic acid group or its methyl ester form rendering it more hydrophilic (De Voss *et al.*, 1999).

1.5.2.3. Exochelins

Exochelins are water-soluble, peptide siderophores produced by non-pathogenic mycobacteria and well characterized in *M. smegmatis* and *M. neoaurum* (Sharman *et al.*, 1995a; Sharman *et al.*, 1995b). They are small peptides (5-10 aa) consisting of D-amino acids, predominantly ornithine and do not contain conventional peptide bonds (Ratledge & Dover, 2000). The exochelin MS from *M. smegmatis* is a formylated pentapeptide derived from three molecules of δ-N-hydroxyornithine, β-alanine and threonine. Exochelin

MN from *M. neoaurum* is a hexapeptide with two δ-N-hydroxyornithines, one ornithine, two β-alanine residues and one β-hydroxyhistidine. The coordination center with Fe^{3+} is hexa-dendate; it is held in an octahedral structure involving the three-hydroxamic acid groups donated by ornithine.

1.5.3. Iron-regulated envelope proteins (IREPs) / iron-regulated membrane proteins (IRMPs)

1.5.3.1. 29 kDA IREP in *M. smegmatis*

In mycobacteria IREPs were first demonstrated in *M. smegmatis* (Hall *et al.*, 1987) grown under low iron condition (0.02 µg Fe / mL). The receptor for ferri-exochelin was found to be a 29 kDa IREP and its specificity as a receptor was substantiated by inhibiting the uptake of ferri-exochelin using antibodies against the 29 kDa protein (Dover & Ratledge, 1996; Hall *et al.*, 1987). Similarly, a 21 kDa IREP was shown to be co-ordinately regulated with the siderophores mycobactin and exochelin MN in *M. neoaurum* (Sritharan & Ratledge, 1989). Several other IREPs were identified in other mycobacterial species such as *M. avium* and *M. leprae*, both under *in vitro* and *in vivo* conditions. IREPs of 180, 29, 21 and 14 kDa were identified in *M. avium* isolated from infected C57 black mice, while the 21 kDa IREP was shown in the cell wall fraction of *M. leprae* obtained from infected armadillo liver (Sritharan & Ratledge, 1990; Sritharan, 2000). The role of the 21 kDa IREP of *M. leprae* in iron acquisition as a possible receptor of ferri-exochelin MN is worth exploring as *M. leprae* can take up only ferri-exochelin MN (Hall *et al.*, 1983) and not ferri-siderophores from other mycobacteria.

1.5.3.2. IrtAB transporter in *M. tuberculosis*

The synthesis and regulation of *M. tuberculosis* siderophores have been well studied but the molecules involved in transport of iron into this pathogen remain unknown. There are several reports about iron-regulated proteins (Calder & Horwitz, 1998; Wong *et al.*, 1999) and further experimentation is required to establish their role in iron acquisition. The first proteins identified to be involved in iron acquisition in the membrane of *M. tuberculosis* were IrtAB encoded by *irtA* (Rv1348) and *irtB* (Rv1349) (Rodriguez & Smith, 2006). IrtA and IrtB have the motifs typical of ABC transporters, composed of four structural domains; two

membrane-spanning domains and two cytoplasmic domains containing the ATP binding cassette (Braibant *et al.*, 2000). Amino acid sequence analysis of IrtA and IrtB showed 34% identity that spans the transmembrane and carboxy-terminal domains. IrtA has an N-terminal extension of 272 amino acids referred to as IrtA-NTD that is not present in IrtB. The IrtA-NTD has been shown to bind FAD and hypothesized to function as a flavin (FAD)-dependant reductase (Ryndak *et al.*, 2010a). The role of IrtAB as an iron transporter that mediated the internalization of iron using ferri-carboxymycobactin as the source of iron was established using *irtAB* KO mutant strain of *M. tuberculosis* (Ryndak *et al.*, 2010a) while the presence of FAD in the amino terminus implicated its role in catalysing the reduction of Fe^{3+} to Fe^{2+}. The failure of the *irtAB* KO strain to survive inside human macrophages and in experimental mice emphasizes the *in vivo* significance of this transporter.

1.5.3.3. Iron-regulated proteins in *M. tuberculosis*

Iron-regulated proteins were reported in *M. tuberculosis* grown under high and low iron conditions (Calder & Horwitz, 1998). Irp15, 24 and 29 (based on their approximate molecular mass in kDa) were abundant in cells grown under high iron while Irp10, 13, 23, and 28 were expressed in low iron organisms. Irp10 and Mta72 with striking homology to metal transporting P-type ATPases were predicted to function as a two-component metal transport system in *M. tuberculosis*. At least 27 proteins were identified using 2D gel electrophoresis and MALDI-MS whose expression was regulated by iron. 15 proteins were up-regulated and 12 proteins were down-regulated under low iron conditions. Fur and aconitase homologs, up-regulated under high iron condition suggests the possibility that these proteins function as transcriptional regulators in *M. tuberculosis* as in other bacteria. The up-regulated proteins under low iron condition were homologs of GTP-dependent phosphoenol pyruvate carboxykinase (PEPCK) and oxidoreductases.

1.5.3.4. HupB: 28 kDa IREP in *M. tuberculosis*

Studies in our lab (Yeruva *et al.*, 2006), identified an IREP of 28 kDa in the cell wall of low iron (0.02 µg Fe / mL) grown *M. tuberculosis*. The expression of this 28 kDa IREP increased with decrease in iron concentration, with maximal

expression in 0.02 µg Fe / mL in the medium of growth. It was co-ordinately expressed with the siderophores mycobactin and carboxymycobactin and was characterized by protein sequencing as HupB. HupB, encoded by the *hupB* gene (Rv2986c) was first reported in *M. tuberculosis* as a histone-like protein (HLP) (Prabhakar *et al.*, 1998). The protein is 214 amino acid long, the N-terminal region of 90 amino acids are homologous to the *E. coli* histone-like DNA-binding HU class of nucleoid proteins and the C-terminal region is rich in basic amino acids arginine and lysine giving the protein a high pI value of 12.5. HupB referred to by several synonyms is implicated with varying functions. In *M. leprae*, in which it is conserved despite severe genome reduction (Cole *et al.*, 2001), is called as laminin-binding protein (LBP) and is thought to play a role in adhesion (Shimoji *et al.*, 1999; Soares de Lima *et al.*, 2005). It also participates in chromosomal organization *in vivo*, where it possibly plays an architectural role (Kumar *et al.*, 2010) and helps in recombination (Sharadamma *et al.*, 2011). Binding of HupB is reported at the AT rich region of chromosomal DNA, which may occur at the regulatory regions of ORFs and the *oriC* region of *M. tuberculosis* (Kumar *et al.*, 2010). Referred to as MDP1 (Mycobacterial DNA-binding protein 1), it was demonstrated to play a role in cell wall biogenesis (Katsube *et al.*, 2007). It has been demonstrated to belong to the ferritin superfamily proteins and plays a role in iron homeostasis by storing iron; one molecule of MDP1 was shown to capture upto 81 iron (Fe^{3+}) atoms (Takatsuka *et al.*, 2011). Same study also reported the ferroxidase activity of the protein that converts Fe^{2+} to Fe^{3+}.

HupB is expressed *in vivo*. Anti-HupB antibodies are seen in patients with inflammatory bowel disease and Crohn's disease (Cohavy *et al.*, 1999b) and TB patients (Yeruva *et al.*, 2006). A strong negative correlation of anti-HupB antibodies with serum iron levels in TB patients was observed when compared to household contacts and healthy controls (Sivakolundu *et al.*, 2013) where the patients presented low serum iron and high ferritin values. The level of anti-HupB antibodies was interestingly high in extrapulmonary TB patients, higher than that seen in pulmonary TB patients.

1.5.4. Iron as a regulatory signal: role of IdeR

Intracellular iron regulates the expression of the components of the iron-acquisition machinery in several bacterial systems, with the best studied in *E. coli* (Griffiths & Chart, 1999). Iron operates in association with a regulator protein, which is identified as Fur protein in a majority of Gram-negative bacteria and the DtxR and its homologue in Gram-positive bacteria. From the genome sequence of *M. tuberculosis* four regulators, two belonging to the Fur family (FurA and FurB) and two belonging to DtxR family (IdeR and SirR) were identified.

1.5.4.1. Iron dependent Regulator (IdeR)

IdeR is the key regulator of siderophore biosynthesis (*mbt* operon) in *M. tuberculosis* and *M. smegmatis*. It is an iron-responsive DNA-binding protein of the DtxR family (Schmitt *et al.*, 1995) and is present in pathogenic as well as non-pathogenic mycobacteria. IdeR is a 230 amino acids protein sharing 59% overall amino acid identity with DtxR from *C. diphtheriae* with 78% similarity in the N-terminal 140 amino acid region. The N-terminal region (1-73 residues) contains a helix-turn-helix motif that binds DNA. The dimerisation domain (74-120 residues) bears the two metal-binding sites and a third domain in the carboxy terminal (151-230 residues) is free and has a SH3-like fold suggesting a possible interaction with other proteins. The preferred metal ion for binding is Fe^{2+} although other divalent metal ions such as Mn^{2+}, Zn^{2+}, Co^{2+}, Ni^{2+} and Mg^{2+} can bind, but at higher concentrations. In the absence of metal ions, the SH3 domain prevents the formation of the stable dimer by binding to residues 125-139, called the tether region. Four monomers of IdeR form two functional dimers and metal binding activates the protein's DNA binding ability by causing conformational changes in the DNA binding domain (Pohl *et al.*, 1999) The SH3 domain leaves the tether region when the metal binding sites are occupied by the IdeR-Fe^{2+} complex which can then bind DNA strongly (Feese *et al.*, 2001).

In mycobacteria, IdeR functions as a pleiotropic regulator (Li *et al.*, 2013); it acts as a negative regulator repressing the synthesis of the iron acquisition genes in *M. smegmatis* (Dussurget *et al.*, 1999) and *M. tuberculosis* (Gold *et al.*, 2001) and positively regulates the synthesis of iron storage genes *bfrA* and *bfrB* (Gold *et al.*, 2001) and the oxidative stress defence genes (Rodriguez *et al.*, 2002) in *M. tuberculosis*.

ideR is an essential gene in *M. tuberculosis* (Rodriguez *et al.*, 2002) in contrast to *M. smegmatis* where inactivation of *ideR* resulted in iron-independent production of siderophores and salicylic acid (Adilakshmi *et al.*, 2000; Dussurget *et al.*, 1996). IdeR functions in maintaining iron homeostasis and virulence as a conditional *ideR* mutant of *M. tuberculosis* failed to survive in macrophages and experimental mice (Pandey & Rodriguez, 2013).

1.5.4.2. FurA, FurB and SirR

Though studies with *ideR* mutants confirmed the role of IdeR in iron homeostasis, it is not the sole iron regulator (Dussurget *et al.*, 1999). FurA is an additional iron regulator and studies in *M. tuberculosis* and *M. smegmatis* showed that FurA negatively regulates the expression of catalase-peroxidase encoded by *katG*, thereby playing a role in oxidative stress (Pym *et al.*, 2001; Zahrt *et al.*, 2001). FurB acts as a Zinc uptake regulator (Zur) in *M. tuberculosis* and it is co-transcribed with its upstream gene (Rv2358), which encodes another zinc-dependent regulator. SirR (Rv2788), annotated as an iron-dependent regulator belonging to the DtxR family in the *M. tuberculosis* genome is yet to be characterized as an iron regulator.

1.5.5. Biosynthesis of mycobactin

Mycobacterium tuberculosis produces mycobactins via a polyketide synthase / non-ribosomal peptide synthetase (NRPs) pathway encoded by *mbt* genes in two loci, namely *mbt-1* (Quadri *et al.*, 1998) and *mbt-2* (Krithika *et al.*, 2006) loci. The *mbt-1* cluster spanning 24 kilo bases of the *M. tuberculosis* genome consists of ten genes *mbtA-J* and the *mbt-2* cluster consists of four genes *mbtK-N*. *mbt-1* cluster contains the components necessary for synthesizing the core structure of mycobactin and *mbt-2* cluster is involved in the incorporation of lipophilic aliphatic side chain onto the mycobactin backbone (Fig. 1.9). The functionality of eight of the genes in the *mbt-1* cluster was established by systematic mutational approach in *M. smegmatis* (Chavadi *et al.*, 2011).

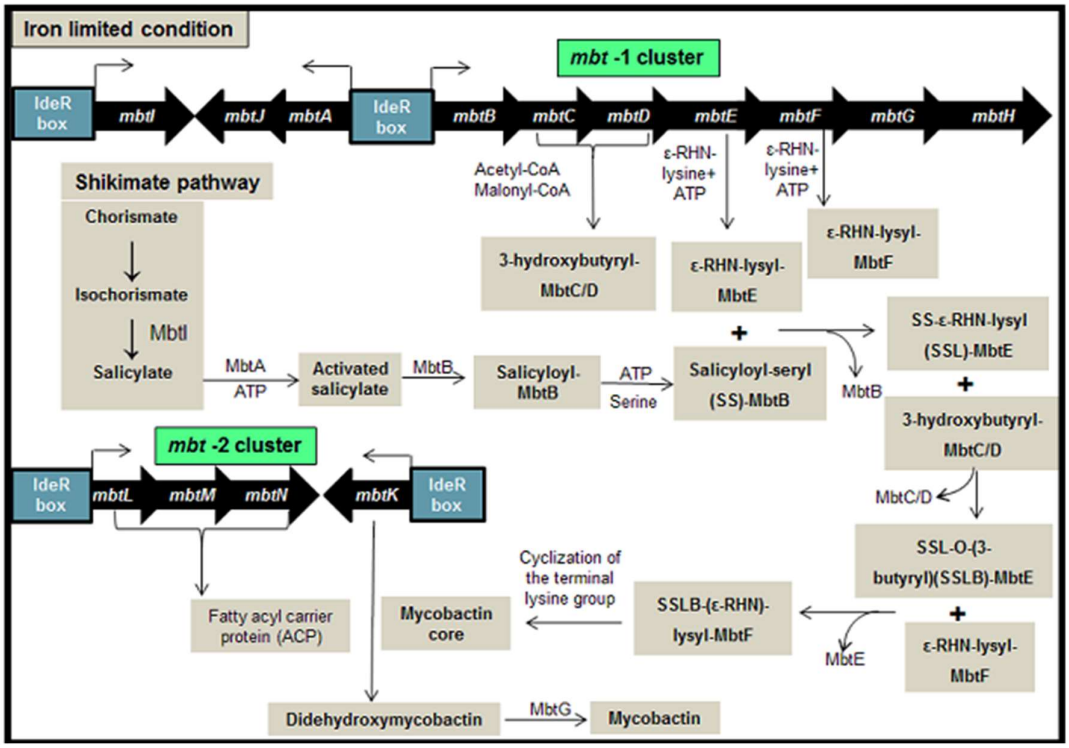

Fig. 1.9. Proposed scheme for the biosynthesis of mycobactin of *M. tuberculosis* (adapted from Quadri *et al.*, 1998 and *Krithika et al.,* 2006). The *mbt*-1 cluster synthesizes the mycobactin core from chorismate. All reactions after formation of salicylic acid involve the attachment of the intermediates to various carrier proteins: MbtB, MbtE, MbtC/D and MbtF. The intermediate SSLB-(ε-RHN)-lysyl-MbtF, must undergo cyclization of the terminal lysine group. The product of *mbt*-2 cluster synthesizes fatty acyl-ACP intermediates, which are transferred to the mycobactin core to produce didehydroxymycobactin by MbtK. MbtL acts as an acyl carrier protein. The final hydroxylation is carried out by MbtG to generate mycobactin. All the reactions are shown during the conditions of iron limitation when the complete machinery is active.

In the biosynthesis of mycobactin, salicylate is synthesized from isochorismic acid by MbtI while MbtG mediates hydroxylation of lysine giving N6- hydroxyl-lysine. Salicylate is activated as its acyl adenylate by MbtA and is then covalently attached to a phosphopantetheine prosthetic group of MbtB. MbtB is a NRP which activates serine by condensing it with the salicylate moiety. MbtC and MbtD are polyketide synthases that help to produce the required β-hydroxybutyrate. Two other NRPs MbtE and MbtF, have the appropriate activation, condensation, and peptide carrier domains for donation of the two lysine-derived moieties of mycobactin. A terminal domain of MbtF,

which acts as either an epimerization domain or as a thioesterase, is responsible for releasing the mycobactin from the enzyme by lactamization of the terminal hydroxyl-lysine residue. The biological role of MbtH and MbtJ has not been assigned clearly (De Voss *et al.*, 1999). The core mycobactin is acylated by a long chain fatty acyl group which is formed by MbtL, MbtM and MbtN of the *mbt-2* cluster. The MbtK protein has exclusive specificity to acylate at the ε-amino position. This protein acylated the δ-position of ornithine and also catalyzed transfer of acyl chains onto two ornithine residues (Card *et al.*, 2005; Krithika *et al.*, 2006) to yield mycobactin.

Regulation of siderophore biosynthesis by IdeR and HupB

When sufficient iron is present, the IdeR-Fe^{2+} complex is formed that binds specifically to a 19 bp consensus sequence called the 'iron box or IdeR box' (5'-TTAGGTTAGGCTAACCTAA-3') in the *mbtB* promoter DNA (located at -32 position from the predicted start point of *mbtB*) that blocks the transcription of the first gene in the biosynthetic pathway of mycobactin (Gold *et al.*, 2001). When the intracellular concentration of iron becomes low, transcription initiation requires binding of HupB to a 10 bp sequence (5'-CACTAAAATT-3') called the HupB box, located immediately upstream of the IdeR box (-40 bp from the transcriptional start point) although IdeR-Fe^{2+} complex is absent (Pandey *et al.*, 2014b; Sritharan, 2016). HupB box has also been identified in the promoter region of *hupB* showing that HupB regulated its own synthesis (Pandey *et al.*, 2014a). The concentration of iron thus determines activation or repression of the *mbt* machinery (Fig. 1.10). Electrophoretic mobility shift assays revealed that IdeR required high concentration of iron (≥ 200 μM Fe) to bind the *mbtB* promoter while HupB required ≤ 25 μM Fe. It has been shown that at ≥ 200 μM Fe *M. tuberculosis* fails to produce both HupB and the two siderophores whereas HupB was expressed much before the siderophores when the iron levels were lowered. Thus, under low iron conditions, IdeR-Fe^{2+} complex fails to form rendering the IdeR box empty and HupB occupies the HupB box promoting the transcription of *mbtB*.

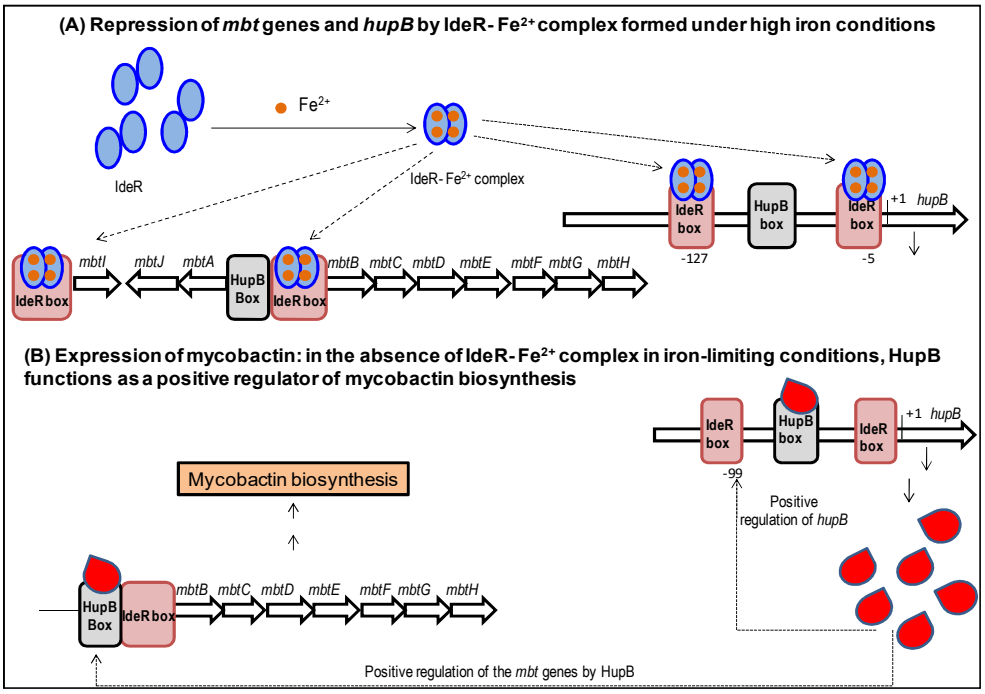

Fig. 1.10. Transcriptional regulation of mycobactin biosynthesis-a schematic model. Panel (A) shows the repression of the *mbt* genes and *hupB* by IdeR-Fe^{2+} complex. In the presence of iron, IdeR forms a stable dimeric IdeR-Fe^{2+} complex with two iron atoms in each of the monomeric units. This complex binds to the IdeR box / iron box in the promoter DNA of the *mbt* genes and blocks their transcription. IdeR-Fe^{2+} complex also binds to the two IdeR boxes in the *hupB* promoter region (positions -5 and -127) repressing the transcription of *hupB*. Panel (B) shows the sequence of events under iron-limiting conditions leading to expression of mycobactin. Adapted from Sritharan, 2016.

1.5.6. Storage of iron

Although iron is essential, excess free iron is potentially toxic for the cells because it catalyzes the production of reactive oxygen radicals by a Fenton reaction, leading to oxidative damage. Under conditions of iron sufficiency, *M. tuberculosis* represses iron acquisition and induces iron storage, suggesting an important role for iron storage proteins in iron homeostasis. *Mycobacterium tuberculosis* synthesizes two iron storage proteins, a ferritin (BfrB; Rv3841) and a bacterioferritin (BfrA; Rv1876). Bacterioferritin, located within the cytoplasm donates iron to all the newly synthesized iron-requiring proteins of the mycobacterial cell (Ratledge, 2004). It was first identified in *M. paratuberculosis* (Brooks *et al.*, 1991) and then in *M. leprae* (Pessolani *et al.*, 1994). The crystal

structures of *M. tuberculosis* bacterioferritin (Gupta *et al.*, 2009) and ferritin (Khare *et al.*, 2011) show the highly conserved architecture of the ferritin superfamily of a cage-like hollow shell (aggregation) formed by 24 monomers with the characteristic fold of a four-helical bundle containing the ferroxidase catalytic center and in bacterioferritin, a heme group in each subunit pair interface. These aggregates can bind 600 - 2,400 iron atoms per molecule.

A double KO mutant of *M. tuberculosis,* H37Rv*ΔbfrAΔbfrB* had significantly reduced growth, was vulnerable to oxidative stress, was attenuated for growth in human macrophages and the reduced bacillary load in the lung and spleen of infected guinea pigs was suggestive of the importance of these proteins in pathogenesis (Reddy *et al.*, 2012). When individual knock out mutants of *bfrA* and *bfrB* in *M. tuberculosis* were studied for their role in iron homeostasis and virulence, it was found *ΔbfrB* mutant suffers from iron-mediated toxicity, is highly susceptible to oxidative stress and killing by antibiotics and is unable to persist in mice (Pandey & Rodriguez, 2012). The *ΔbfrA* mutant did not show any such phenotype.

The IdeR-Fe^{2+} complex binds to the tandem iron boxes, contacts the RNA polymerase and initiates transcription. In case of *bfrA,* it binds to tandem operator sites located 100 bp upstream of the *bfrA* transcriptional start point (TSP) while in *bfrB*, it binds to a double iron box located 106 bp upstream of the TSP (Rodriguez & Smith, 2003). Iron availability is therefore dependent on the IdeR-mediated regulation of expression of bacterioferritin and ferritin. Recently it was shown that under low iron conditions *bfrB* expression is repressed by the presence of a histone-like DNA-binding protein Lsr2. In the presence of iron, IdeR-Fe^{2+} complex is formed that binds to the four IdeR boxes that displaces Lsr2 thereby relieving *bfrB* repression (Kurthkoti *et al.*, 2015).

1.5.7. Transport of iron

1.5.7.1. Export of siderophores

The iron-regulated outer membrane proteins MmpL4, MmpL5 and the associating MmpS4, MmpS5, with the help of specific knock out mutants, were first shown to export siderophores carboxymycobactin and mycobactin across the cytoplasmic membrane (Wells *et al.*, 2013). While MmpS5 interacted only with MmpL5, MmpS4 interacted with both MmpL4 and MmpL5. The double KO

mutant *ΔmmpS4/S5* failed to recycle the exogenously added siderophores although it was able to take up the ferri-siderophores and utilize the iron. Accumulation of desferri-siderophores lead to toxicity and growth inhibition (Jones *et al.*, 2014). These outer membrane proteins are very crucial for iron acquisition and virulence of *M. tuberculosis*.

1.5.7.2. Uptake of iron in mycobacteria

Uptake of ferri-exochelin

Uptake of ferri-exochelin has been well studied in *M. smegmatis* (Ratledge, 2004). It involves the complete transfer of the molecule along with the metal ligand (Stephenson & Ratledge, 1979). After solubilisation of Fe^{3+} by the extracellular exochelin, the ferri-exochelin is recognized by the 29 kDa receptor (Hall *et al.*, 1987). It is then taken up by the FxuD protein and then transferred through the cytoplasmic membrane proteins FxuA, FxuB and FxuC which share amino acid sequence homology with FepG, FepC and FepD and which are involved in the uptake of ferri-enterochelin in *E. coli* (Ratledge, 2004). The release of iron involves reduction of Fe^{3+} to Fe^{2+} involving an appropriate reductase (a non-specific NAD(P)H-dependent siderophore reductase). The exochelin, after releasing its iron into the cytoplasm, is transferred back into the extracellular environment of the cells using a specific exiting protein, ExiT (Zhu *et al.*, 1998) that operates in conjunction with other proteins and involves the input of energy (Pavelka, 2000).

Uptake of ferri-carboxymycobactin

The siderophore-mediated iron uptake by *M. tuberculosis* has been extensively reviewed recently (Sritharan, 2016). The pathogen synthesizes siderophores when faced with low iron conditions which are exported across the membrane by membrane transport proteins MmpL4/MmpS4 and MmpL5/MmpS5 (Wells *et al.*, 2013). The extracellular desferri-CMb chelates Fe^{3+} from insoluble or protein-bound iron forming ferri-CMb which then interacts with a yet unknown cell envelope protein. While it was shown that iron from Fe-CMb is transferred to the Mb located within the cell envelope (Gobin & Horwitz, 1996a), conclusive proof of this process is presented in this study. The ABC transporters IrtAB present on the cytoplasmic membrane mediates the internalization of iron,

possibly from the Fe-Mb by reduction of Fe^{3+} to Fe^{2+} catalysed by the FAD-dependant reductase associated with IrtA (Ryndak *et al.*, 2010b). The proposed model for uptake of ferri-CMb from the information available till date is depicted in Fig. 1.11.

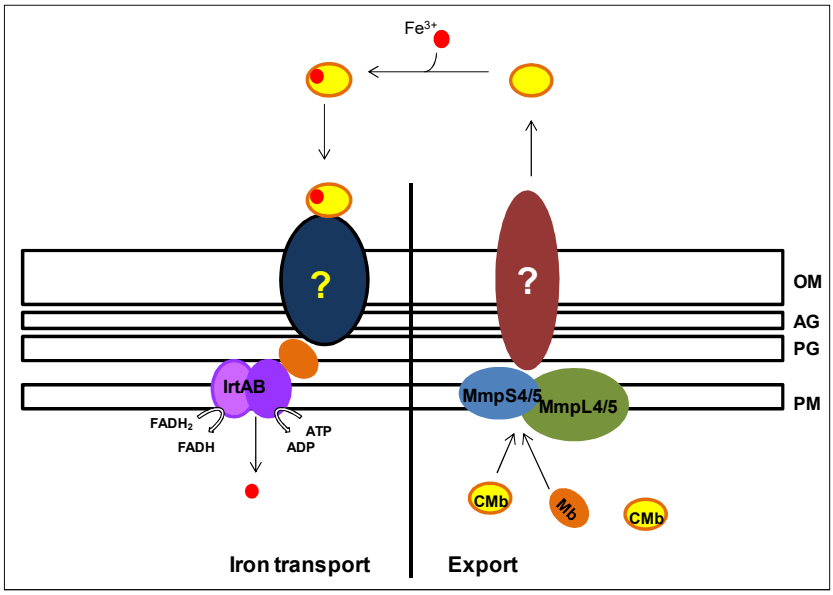

Fig. 1.11. Proposed model for the transport of iron in *M. tuberculosis*. Desferri-carboxymycobactin produced by *M. tuberculosis* upon iron limitation is exported to the outside, process facilitated by the MmpL4 & MmpS4 and MmpL5 & MmpS5 proteins (Jones *et al.*, 2014). It chelates Fe^{3+} present as insoluble or protein-bound iron and forms ferri-carboxymycobactin. The protein present on the cell envelope responsible for the transfer of iron to mycobactin is yet unknown (blue oval). The IrtAB present on the plasma membrane transports the Fe^{3+} into the cytoplasm after reducing it to Fe^{2+} utilising the reductase activity of the bound NAD (Ryndak *et al.*, 2010a).

ESX-3 mediated iron acquisition

Mycobacteria have several paralogous type VII secretion systems, ESX-1 through ESX-5. ESX-1 and ESX-5 are involved in virulence; they both affect the cell-to-cell migration of pathogenic mycobacteria (Abdallah *et al.*, 2007) and conjugation in the non-pathogen *M. smegmatis* (Coros *et al.*, 2008). The best characterized is ESX-1 and its deletion is one of the main causes of *M. bovis* BCG attenuation. In *M. tuberculosis*, ESX-3 is essential for growth *in vitro* and has been shown to be involved in the mycobactin-mediated iron acquisition pathway, but not the exochelin pathway in *M. smegmatis* (Siegrist *et al.*, 2009;

Siegrist *et al.*, 2014). In *M. tuberculosis* the expression of the ESX-3 gene cluster is regulated by the zinc uptake repressor (Zur) and by the iron-dependent transcriptional repressor (IdeR) (Serafini *et al.*, 2009). It has been hypothesized that ESX-3 either encodes or is essential for the functioning of a novel metal uptake / surface permeabilization system. This can function along with the siderophores mycobactin and carboxymycobactin in iron uptake in *M. tuberculosis* or can even function as the main iron uptake system as in *M. leprae* (Serafini *et al.*, 2009).

1.6. Oxidative stress

1.6.1. Environment within macrophages

Mycobacterium tuberculosis survives a hostile environment within the host. Such an environment is formed due to the production of reactive oxygen intermediates (ROI) and nitrogen intermediates (RNI) by macrophages and is an important mechanism of inhibition of mycobacterial proliferation *in vivo* (MacMicking *et al.*, 1997; Ng *et al.*, 2004). Macrophages produce ROI and RNI via NADPH oxidase (NOX2/gp91phox) and inducible nitric oxide synthase (iNOS / NOS2) (Ehrt & Schnappinger, 2009). The mechanism of action includes generation of redox stress and bacterial killing by damaging biomolecules like DNA, proteins and lipids. Damage mediated by these compounds leads to a general inhibition in cellular metabolism by altering processes associated with proton-dependent active transport, oxygen utilization and oxidative phosphorylation (Zahrt & Deretic, 2002). Failure in ROI and RNI generation renders the host sensitive to *M. tuberculosis* infection (MacMicking *et al.*, 1997). The importance of ROI in controlling *M. tuberculosis* infection in humans came from the observation that children with defective oxidative burst mechanisms are highly susceptible to TB and develop severe complications from BCG vaccination (Lee *et al.*, 2008). ROI partially control the *M. tuberculosis* pathogen early in the infection process before the onset of specific immunity as was observed in Phox-deficient mice (Cooper *et al.*, 2000) while RNI is important to control the pathogen; iNOS deficient mice are highly susceptible to *M. tuberculosis* infection (Yang *et al.*, 2009) (Yang et al., 2009). The presence of nitric oxide (NO) within human granulomas could contribute to host resistance since *in vitro* experiments demonstrate direct RNI-mediated bacteriostatic

(Firmani & Riley, 2002; Voskuil *et al.*, 2003) and bactericidal activity (Nathan, 2002).

1.6.2. Oxidative stress defence enzymes

Despite these redox-based bactericidal stresses, *M. tuberculosis* can persist for decades in a non-replicative state *in vivo* suggesting an efficient role of *M. tuberculosis* oxidative stress defence enzymes such as catalase-peroxidase (KatG), superoxide dismutases (SODs) and alkyl hydroperoxidase (AhpC) involved in resistance to oxidative or nitrosative stress and mycobacterial persistence (Bartos *et al.*, 2004; Manca *et al.*, 1999). Mycobacterial KatG are bifunctional enzymes possessing both catalase and peroxidase activities in the same protein molecule. Different isoforms unique to each mycobacterial species are present. They are classified into three types: T (typical), M (manganese-dependent) and A (atypical) catalases. T catalases (KatG) are grouped in the hydroperoxidase I (HPI) family of catalases and they are inducible by H_2O_2 and are heat-labile. M catalases (KatE) belonging to the HPII type catalase family are heat-stable (inactivated at temperatures of about 50°C) and are constitutively expressed. *Mycobacterium avium* and *M. intracellulare* express unique or atypical catalases (A type) that are identical to the KatE family but are inactivated only at high temperatures (Wayne & Diaz, 1988). *Mycobacterium tuberculosis* expresses only KatG (Wayne & Diaz, 1982). The crystal structure of KatG reveals it is homodimeric or homotetrameric with subunits of ~80 kDa or ~40 kDa respectively (Bertrand *et al.*, 2004). KatG activates the front-line anti-tubercular drug isoniazid (INH) by converting the pro-drug INH to the reactive drug that targets InhA required for the synthesis of mycolic acid, an important component of the cell wall (Lei *et al.*, 2000). Catalytic activity of KatG is associated with the N-terminal domain which contains a heme-binding motif. KatG with missense mutations in N-terminal domain resulted in the production of catalase-peroxidase with strongly reduced enzyme activity (Heym *et al.*, 1993). It was identified as a virulence determinant (Middlebrook, 1954) as it is required to counter the oxidative stress within the macrophages.

Superoxide dismutases (SODs) catalyze the conversion of superoxide ions to hydrogen peroxide. SODs differ in their requirement for the metal ion co-factor. The predominant SODs in *M. tuberculosis* are the Fe-containing SodA

(Kusunose *et al.*, 1976) and Cu / Zn-containing SodC (Dussurget *et al.*, 2001). The *sodA* mutant of *M. tuberculosis* was more susceptible to killing by H_2O_2 (Edwards *et al.*, 2001) whereas the *sodC* inactivated *M. tuberculosis* was unable to survive in IFN-γ activated murine peritoneal macrophages (Piddington *et al.*, 2001) but could survive in murine bone marrow-derived macrophages (Dussurget *et al.*, 2001).

AhpC, an orthologue of bacterial alkyl hydroperoxidases catalyses the reduction of peroxides and peroxynitrites with the help of its NADH-dependent peroxidase and peroxynitrites reductase activity (Guimarães *et al.*, 2005). Overexpression of AhpC in INH-resistant strains of *M. tuberculosis* harbouring inactivated *katG* gene shows that AhpC compensates for the loss of KatG (Sherman & Mdluli, 1996).

1.6.3. Regulation of oxidative stress

Oxidative stress response in several bacteria is regulated by OxyR, a tetrameric protein. In *E. coli* and *S. typhymurium*, OxyR is required to induce the expression of KatG and AhpC (Åslund *et al.*, 1999; Christman *et al.*, 1989) but in *M. tuberculosis*, OxyR is absent as *oxyR* is a pseudogene (Deretic *et al.*, 1995). This silencing would results in the lowered expression of *ahpC*, indicating the presence of other regulatory systems that respond to the oxidative stress (Springer *et al.*, 2001).

Fur proteins regulate genes induced by oxidative stress including the genes encoding the superoxide dismutases, catalase and peroxidase, alkyl hydroperoxidase, 8-hydroxyguanine endonuclease and the SoxRS and OxyR regulators (Rodriguez & Smith, 2003). IdeR is thought to influence both KatG and SodA as the ideR mutant of *M. tuberculosis* was more sensitive to hydrogen peroxide and superoxide (Rodriguez *et al.*, 2002). The role of IdeR as a positive regulator of the oxidative stress response agrees with the up-regulation of *ideR* detected in *M. tuberculosis*-infected macrophages (Hobson *et al.*, 2002).

1.6.4. Iron and oxidative stress

Catalase-peroxidase (KatG) has four heme-containing porphyrin groups, the synthesis of which requires iron and the FurA protein. The *furA-katG* is expressed as an operon with FurA autoregulating its own expression by binding

to a unique sequence upstream of the *furA* gene (Sala *et al.*, 2003) called *pfurA* and has been reported in *M. tuberculosis, M. smegmatis* and *M. bovis* BCG (Milano *et al.*, 2001). *pfurA* is negatively controlled by the mycobacterial FurA protein, which binds upstream of the *furA* gene and in turn auto regulates its own expression. In high iron conditions, the pathogen can elaborate high levels of KatG that can counter the free radicals generated within the macrophage. The influence of limiting iron levels on the expression of the catalase-peroxidases in *M. tuberculosis* and in several other mycobacterial species was studied (Yeruva *et al.*, 2005). It was observed that iron-replete organisms expressed 10-13 fold higher catalase and peroxidase activity; the latter dramatically reduced to negligible levels upon iron limitation. The effect of the loss of peroxidase activity on INH activation was analysed that demonstrated that activation of INH was attributed to the peroxidase activity and loss of the latter resulted in the failure to activate INH. Using microplate alamar blue assay (MABA), it was shown that low iron organisms were not killed by INH and only high iron organisms were susceptible to the drug (Sritharan *et al.*, 2006).

1.7. An overview of the basis for the objectives in this study

As detailed earlier, HupB was characterised a transcriptional regulator of mycobactin biosynthesis in *M. tuberculosis*. This was made possible by the generation of a *hupB*-deleted mutant strain of the pathogen by homologous recombination (Pandey *et al.*, 2014b). Transcriptional profiling of the WT and the mutant strains grown in iron-replete and iron-limited conditions by microarray analysis identified not only the *mbt* genes, but several other genes, whose expressions were influenced by HupB protein and / or iron levels. Of interest was the influence of HupB on genes involved in iron acquisition, specifically on the export of siderophores such as *mmpL4, mmpS4, mmpL5* and *mmpS5* and uptake of iron such as *irtA* and *irtB*, were influenced both by iron and HupB. A down-regulation of >1.5-fold was observed in the low iron mutant versus the low iron WT. The *esx-3* operon which has been known to be involved in mycobactin-mediated iron uptake was also influenced by iron and HupB where all the genes *eccA3* – *eccE3* (Rv0282 – Rv0292) were down-regulated (>1.5-fold) in the mutant.

In addition, the transcript levels of several genes associated with lipid biosynthesis were found to be altered. These genes were influenced by HupB and not by iron levels. The genes involved in the FASI (*fas*) and FASII (*fabD, acpM, kasA, kasB, accD6, inhA, pks13* and *fabD32*) systems for the biosynthesis of mycolic acids were down-regulated (>1.0-fold) in the mutant. Similarly, genes involved in the biosynthesis of SL-1 (*pks2, papA1* and *mmpL8*), PDIM (*fadD26, fadD28* and *drrC*) and DAT & PAT (*papA3, pks4, chp2* and *mmpL10*) were also down-regulated (>1.0-fold) in the low iron mutant versus low iron WT.

Finally, of remarkable clinical significance is the analysis of the diagnostic potential of HupB, particularly in extrapulmonary TB (EPTB) as our earlier work showed the correlation of the host iron status and expression of HupB as evaluated by the titre of circulating anti-HupB antibodies (Sivakolundu *et al.*, 2013; Yeruva *et al.*, 2006). The presence of anti-HupB antibodies in Crohn's disease (Cohavy *et al.*, 1999a) and in TB patients, particularly EPTB cases led us to study the potential of HupB as a marker of the disease and also study the immunological basis for the high levels of antibodies in TB patients, specifically the cytokine profile in response to stimulation of host cells with HupB.

Objectives of the study

The focus of the study was to understand the role of HupB in *M. tuberculosis* under the following objectives

a) Characterization of the *hupB* KO mutant *M.tb.ΔhupB*

b) Establishment of HupB as an iron transporter

c) Influence of HupB in lipid metabolism

d) HupB-mediated cell-mediated and humoral immune response studies in TB patients

CHAPTER 2

MATERIALS AND METHODS

2.1. Chemicals and Reagents

Bacterial grade media components were purchased from HiMedia (Mumbai, India). Routine analytical reagents and solvents were from Qualigens (Qualigens Fine Chemicals Pvt. Ltd., India). Fine chemicals (all molecular biology grade) were from Sigma Aldrich Pvt. Ltd. (MO, USA). Culture media Middlebrook 7H9 / 7H10 / 7H11, were from Difco (MD, USA), supplements OADC / ADC from Becton and Dickinson (BD) (MD, USA), Lowenstein-Jensen base from HiMedia (Mumbai, India) and iron-free chemicals from Puratronic Alfa AESAR (Massachusetts, United States). All molecular biology chemicals were from Thermo Fisher Scientific Corporation (MA, USA). Media for cell culture were from Life Technologies (CA, USA). Ni-Sepharose resin was from GE Healthcare (Little Chalfont, United Kingdom). TLC Silica gel 60 F_{254} plates, nitrocellulose membrane and syringe filters were from Merck (NJ, USA). Anti-IgG antibodies were obtained from Bangalore Genei (India). Oligonucleotide primers were synthesized from Biosquare Technologies (India). $^{55}FeCl_3$ was from American Radiolabeled Chemicals (MO, USA).

2.2. Growth and maintenance of mycobacterial strains

2.2.1. Mycobacterial strains: *Mycobacterium tuberculosis* H37Rv (*M.tb.*H37Rv; ATCC 27294) and *M. tuberculosis ΔhupB* (*M.tb.ΔhupB;* lab collection from previous study).

2.2.2. Growth in enrichment media

2.2.2.1. Lowenstein-Jensen (LJ) medium

5.8 g LJ base (HiMedia, India), 2 mL glycerol and 1.8 mL of Tween-80 were dissolved in 90 mL of double-distilled water and autoclaved at 121°C, 15 lbs/sq. inch pressure for 20 min. 100 mL of egg white (3 eggs) were homogenized in a sterile 500 mL conical flask with glass beads by shaking vigorously to form a uniform homogenate. Egg homogenate and 1 mL of 2% malachite green solution were added into the autoclaved LJ base medium and mixed thoroughly. The medium was filtered and 8 mL was aliquoted into 30 mL McCartney bottles. The slants were subjected to inspissation at 80°C for 90 min each for three successive days.

Inoculation: 100 µL of liquid culture was dropped onto the slant, allowed to be absorbed into the LJ media and incubated at 37°C for 2-3 weeks. After colonies appear the slants were stored at 4°C for 2-3 months.

2.2.2.2. Middlebrook 7H9 liquid medium

0.47 g of 7H9 Middlebrook base (Difco, MD, USA), 0.1 g of Bactocasitone (Difco) and 0.2 mL of glycerol was dissolved in 90 mL of double-distilled water in a 250 mL conical flask and autoclaved at 121°C, 15 lbs/sq. inch pressure for 20 min. The media was cooled and filtered (0.2 µm filter) and 10 mL of ADC enrichment (Becton and Dickinson, MD, USA) was added under aseptic conditions, stirred well and stored at 4°C.

Inoculation: A colony from LJ slant was picked or 100 µL from glycerol stock were inoculated in 7H9 liquid medium and allowed to grow at 37°C and 150 rpm in a shaker.

2.2.2.3. Middlebrook 7H11 agar medium

2.1 g of 7H11 Middlebrook base (Difco) and 0.5 mL of glycerol was added to 90 mL of double-distilled water in a 250 mL conical flask and autoclaved at 121°C, 15 lbs/sq. inch pressure for 20 min. 10 mL of OADC enrichment (Becton and Dickinson) was added under aseptic conditions after the media cooled to 50-55°C and stirred well. Middlebrook 7H11 agar with different carbon sources were prepared using either 0.2 mL glycerol or 0.442 g sodium pyruvate (Sigma) and autoclaved.

Inoculation: The mycobacterial cultures were spread on the 7H11 plates and incubated at 37°C for 3-4 weeks till the appearance of colonies. The plates were stored at 4°C after growth by sealing them with parafilm.

2.3. Growth of mycobacteria under iron-regulated conditions

2.3.1. Preparation of glassware

All glassware were made iron free by soaking in 2% methanolic KOH o/n followed by washing with double-distilled water and soaking o/n in 8 N HNO_3. Subsequent washings were done with glass double-distilled water.

2.3.2. Preparation of Proskauer and Beck (P & B) medium

5 g of L-asparagine and 5 g of potassium dihydrogen orthophosphate were dissolved in 900 mL of glass double-distilled water. 20 mL glycerol was added, the pH adjusted to 6.8 with 10 N NaOH and the volume was made up to 1 L. 6 g alumina was added and autoclaved at 121°C, 15 lbs / sq. inch pressure for 20 min. The medium was cooled and filtered using Whatman grade 541 filter to remove the alumina. After filtration, the medium was aliquoted as 100 mL

volume in 250 mL conical flasks and re-autoclaved at 121°C, 15 lbs/sq. inch pressure for 20 min. For iron-regulated growth on solid medium, 1 g noble agar was added to 100 mL of the filtered medium before re-autoclaving.

2.3.3. Preparation of salt solution

567.75 mg $ZnSO_4.XH_2O$, 137.8 mg $MnSO_4.XH_2O$ and 20.5 g $MgSO_4.7H_2O$ were dissolved in 200 mL glass double-distilled water in a 500 mL iron-free volumetric flask. The volume was made up to 500 mL; 10 mL was aliquoted into McCartney bottles and autoclaved.

2.3.4 Preparation of stock solutions of iron

497.8 mg of $FeSO_4.7H_2O$ (Merck) was dissolved in 5 mL of 1 N H_2SO_4 in a 100 mL volumetric flask. 50 mL of glass double-distilled water was added for complete dissolution and heated for 10 min. The solution was made up to 100 mL with glass double-distilled water. This stock contains 1 mg Fe / mL.

Preparation of high iron solution (800 µg Fe / mL): 80 mL of the above stock solution was made up to 100 mL with 0.01 N H_2SO_4 in a 100 mL volumetric flask. This was pipetted as 10 mL aliquots in McCartney bottles and autoclaved. 1 mL of the solution added to 99 mL of culture medium gives a final concentration of 8.0 µg Fe / mL.

Preparation of low iron solution (2.0 µg Fe / mL): 0.25 mL of high iron solution was made up to 100 mL with 0.01 N H_2SO_4 in a 100 mL volumetric flask, aliquoted as 10 mL in McCartney bottles and autoclaved. 1 mL of the solution added to 99 mL of culture medium gives a final concentration of 0.02 µg Fe / mL.

2.3.5. Growth in P & B medium

For iron-regulated growth, 100 mL of P & B medium was supplemented with 1 mL of salt solution (16.8 mM Mg^{2+}, 5.01 µM Mn^{2+} and 17 µM Zn^{2+}) and 8 µg Fe / mL (144 µM Fe) for high iron medium and 0.02 µg Fe / mL (0.36 µM Fe) for low iron medium. The cells from Middlebrook 7H9 medium were transferred to a tube with glass beads, vortexed and re-suspended to McFarland# 4 with P & B medium with no iron. 1 mL of this cell suspension was added to high and low iron flasks. The organisms were maintained at 37°C with shaking at 150 rpm for 14 days.

2.3.6. Extraction and assay of carboxymycobactin and mycobactin

The siderophores carboxymycobactin (CMb) and mycobactin (Mb) were extracted from the culture filtrate (Gobin *et al.*, 1995b) and cell pellet (Ratledge & Ewing, 1996) respectively after harvesting the culture at 6000 rpm for 15 min.

2.3.6.1. Carboxmycobactin: 1 mL of saturated aqueous ferric chloride solution was added to the culture filtrate, vortexed and incubated for 30 min. This was centrifuged at 6000 rpm for 15 min and one and half volume of chloroform was added to the collected supernatant. The ferri-carboxymycobactin (Fe-CMb) extracted into the chloroform layer was washed three times with water and dried. 1 mL ethanol was added to dissolve the CMb and $OD_{450\ nm}$ was taken in a spectrophotometer (UV-1800 Spectrophotometer, Shimadzu, Kyoto, Japan) using ethanol as blank. The concentration of Fe-CMb was calculated using extinction coefficient $A^{1\%}_{450\ nm} = 48$ and expressed as mg / g cell dry weight.

2.3.6.2. Mycobactin: 10 mL of ethanol was added to the cell pellet and incubated o/n. This was centrifuged at 6000 rpm for 15 min and 1 mL of saturated ferric chloride in ethanol was added to the supernatant and incubated for 30 min. Equal volume of chloroform was added and the ferri-mycobactin (Fe-Mb) extracted into chloroform was washed three times with water and dried. The Mb was dissolved in 1 mL ethanol and $OD_{450\ nm}$ was noted. The concentration of Fe-Mb was calculated using extinction coefficient $A^{1\%}_{450\ nm} = 43$ and expressed as mg / g cell dry weight.

2.4. Analysis of mycobacterial proteins

Reagents

a) Wash buffer: 10 mM Tris-HCl, pH 7.8
b) Pre-condensation of Triton X-114 (Bordier, 1981): 1 mL of Triton X-114 was mixed with 500 mL of 10 mM Tris-HCl pH 7.4 containing 150 mM NaCl. It was kept o/n at 4°C for complete dissolution and the clear solution was incubated for 1 h at 37°C. Condensation of detergent occurred and mixture separated into aqueous and detergent phases. The aqueous phase was discarded and replaced by the same volume of above buffer. Condensation was repeated thrice and stored at 4°C.
c) Solubilising buffer: 2.5 mL stacking gel buffer pH 6.8, 6% SDS and 7.5 mL double-distilled water.

2.4.1. Preparation of cell wall and cell membrane

The organisms were grown in high (144 µM Fe) and low (0.36 µM Fe) iron P & B media for 14 days at 37°C and 150 rpm. The cultures were harvested, cell pellets washed and re-suspended in 6 mL of wash buffer. The cells were sonicated for 20 min at 30 s pulse with 30 s interval, amplitude 40 Hz, at probe temperature of 4°C in Vibra Cell Sonicator (Sonics, CT, USA). The cell sonicate was centrifuged at 6,000 rpm at 4°C for 15 min to remove the cell debris and the supernatant was subjected to centrifugation at 18,000 rpm for 40 min at 4°C to pellet the cell wall. The resulting supernatant was then centrifuged at 45,000 rpm for 2 h 30 min at 4°C to pellet the cell membrane. The cell wall and cell membrane pellets were washed twice with 1mL of wash buffer. The pellets were solubilised (Sinha *et al.*, 2002) by adding an appropriate volume of 5% pre-condensed Triton X-114 and incubating at 4°C o/n. The detergent and aqueous phases were separated by incubating in 37°C water bath for 1 h followed by centrifuging at 3000 rpm for 15 min at room temperature. The left-over pellet was again extracted with 5% pre-condensed Triton X-114 and the aqueous and the detergent phases were separated as described previously. After three suitable washes of both aqueous and the detergent phases, the proteins were precipitated by adding 5 volumes of chilled acetone and left o/n at -20°C. The precipitated proteins were centrifuged at 12,000 rpm for 20 min and pellet was re-suspended in 2 mL of chilled acetone and again centrifuged at 12,000 rpm for 10 min. The pellet was dried and dissolved in a minimal amount (50-100 µL) of solubilising buffer and subjected to SDS-PAGE on a 5-20% gradient gel.

2.4.2. Estimation of protein concentration by Bicinchoninic acid (BCA) method

Protein estimation was done using Bicinchoninic acid (BCA) protein assay kit (Sigma) as per manufacturer's instructions. Standard curve was prepared using known concentrations of BSA (200-1000 µg / mL). Appropriate volumes of BSA and 5 µL of test protein samples were added to the microplate and the total volume was made to 25 µL with double-distilled water. 200 µL of BCA reagent (196 µL of BCA + 4 µL of 4% (w/v) $CuSO_4 .5H_2O$) was added to each well and the plate was incubated for 30 min at 37°C. The colour developed was

measured at 570 nm using an ELISA reader (Model 680XR; Bio-Rad, CA, USA). The concentration of protein in the test sample was interpolated from the BSA standard curve.

2.4.3. Separation of proteins by sodium dodecyl sulphate polyacrylamide gel electrophoresis (SDS-PAGE) (Laemmli, 1970)

Reagents

a) Acrylamide and N, N'-bisacrylamide mix (30:0.8): Dissolved 30 g of acrylamide and 0.8 g of bisacrylamide in 60 mL of double-distilled water, filtered and volume made up to 100 mL
b) Resolving gel buffer: Tris-HCl (1.5 M, pH 8.8) with 0.4% SDS
c) Stacking gel buffer: Tris-HCl (0.5 M, pH 6.8) with 0.4% SDS
d) Ammonium per sulphate (APS): 10% APS solution in double-distilled water was prepared fresh before use
e) Tetramethylethylenediamine (TEMED): Directly used as per the volume mentioned
f) Sample buffer (2X): 0.125 M Tris-HCl, pH 6.8 containing 4% SDS, 20% glycerol and 0.002% bromophenol blue
g) Running buffer: Tris-glycine buffer (25 mM Tris, 250 mM glycine and 0.1% SDS), pH 8.8
h) 0.25% Coomassie staining solution: 0.25 g Coomassie Brilliant Blue was dissolved in a small volume of methanol. It was then made up to 100 mL using methanol: glacial acetic acid: water (5:2:5)
i) Destaining solution: Methanol: glacial acetic acid: water (1:1:8)

Gradient gel: The 5-20% resolving gel was prepared using the recipe given in Table 2.1 and allowed to polymerize for 40 min. The stacking gel (Table 2.2) was poured over it after positioning the comb. 60 µg of total protein was mixed with 2X sample buffer (1:1 v/v), boiled for 10 min, centrifuged at 13,000 rpm for 10 min to remove any insoluble material and the clear supernatant was loaded onto the gel (Hoefer electrophoresis unit, Amersham Pharmacia Biotech AB, CA, USA). Electrophoresis was carried out initially at 90 V till the bromophenol blue dye entered the resolving gel and then at 200-250 V maintaining a constant current of 25 mA per plate. Gel was allowed to run till the dye completely migrated off the gel followed by an additional run for 30 min for

optimal resolution. The gel was stained with Coomassie Blue for 1-3 h and then destained o/n.

Mini gel: The 10% resolving gel was prepared (Table 2.1), allowed to polymerize and stacking gel was poured after placing the comb. Samples were prepared in a similar manner as above using 30 µg total protein. The clear supernatant were loaded onto the gel (Broviga electrophoresis unit, Balaji Scientific Services, Chennai, India) and electrophoresis was carried out at a constant current and initial voltage of 70 V and then at 100 V. Gel was run till the dye migrated off the gel.

Table 2.1 Composition of resolving gel

Ingredients	Volume (mL)		
	Gradient gel		10%
	5%	20%	
Acrylamide : bisacrylamide	2.75	10.6	10.6
Resolving gel buffer	4.0	4.0	8.0
Double distilled water	9.3	1.4	13.4
Ammonium per sulphate	0.08	0.08	0.16
TEMED	0.008	0.008	0.008

Table 2.2 Composition of stacking gel

Ingredients	Volume (mL)
Acrylamide : bisacrylamide	1.5
Stacking gel buffer	2.5
Double distilled water	6.0
Ammonium per sulphate	0.03
TEMED	0.01

2.4.4. Western blot analysis

Reagents

a) Transblot buffer (10X): 250 mM Tris and 1.3 M glycine in 400 mL of double-distilled water. Working solution was prepared by mixing 200 mL 10X stock solution, 400 mL methanol and 1.4 L double-distilled water.

b) Tris-buffered saline (TBS): 50 mM Tris-HCl pH 8.0 containing 150 mM NaCl

c) TBST: TBS containing 0.05% Tween 20.

d) Ponceau S stain: Ponceau S, trichloroacetic acid and sulfosalicylic acid were mixed in 2:30:30 (w/v) ratio and the final volume was made up to 100 mL with double-distilled water. One part of stock solution was diluted with 9 parts of deionized water to make a working solution.

Electrophoretic transfer of protein onto nitrocellulose membrane (Towbin *et al.*, 1979)

Proteins separated by SDS-PAGE were electrophoretically transferred onto nitrocellulose membrane at 30 V and constant current o/n or 60 V for 2½ h using 1X transblot buffer in Broviga transfer apparatus (Balaji Scientific Services, India).

Development of blot

After the transfer, the membrane was removed and stained with Ponceau S stain to visualize the transferred proteins. The membrane was blocked for 2 h using 5% non-fat milk solution (NFM) dissolved in TBS. The membrane was washed thrice with TBST and incubated o/n with primary antibody diluted in TBS (1:2500) containing 1% NFM at 4°C. The membrane was washed 4 times with TBST and incubated with appropriate enzyme-conjugated secondary antibody at room temperature for 1½ h. Then, the blot was washed thoroughly with TBST. A ready-to-use 5-bromo-4-chloro-3-indolyl phosphate nitroblue tetrazolium solution (BCIP-NBT; Sigma) was used as the substrate when alkaline phosphatase (ALP)-conjugated secondary antibodies was used; when peroxidase-conjugated secondary antibodies was used, DAB (diaminobenzidine)-H_2O_2 (10 mg DAB in 15 mL TBS with 0.08% H_2O_2) was used as the substrate.

2.5. Cloning and expression of recombinant mycobacterial proteins

2.5.1. Bacterial strains and plasmids

pET22b (+) plasmid (Novagen, Madison, USA) was used for cloning and expression of recombinant mycobacterial proteins. *E. coli* DH5α was used for high-efficiency transformation to increase copy number of the cloned plasmid and *E. coli* BL21 (DE3) (Novagen) was used as expression host.

2.5.2. Preparation of Luria-Bertani (LB) media

1 g tryptone, 0.5 g yeast extract and 1 g NaCl were dissolved in 90 mL of double-distilled water, pH was adjusted to 7.2 and volume was made up to 100 mL. It was autoclaved at 121°C, 15 lbs / sq. inch pressure for 20 min and stored at room temperature. For preparing solid medium, 1.5 g of bacteriological agar was added to the above ingredients before autoclaving.

2.5.3. Isolation of genomic DNA from *M. tuberculosis* H37Rv

Reagents

a) Tris-Cl (1M): Dissolved 121.1 g of Tris base in 800 mL of double-distilled water, adding 42 mL of concentrated HCl, pH adjusted to 8.0 and made up to 1L with double-distilled water and autoclaved
b) 0.5 M EDTA (Ethylene diamine tetraacetic acid): Added 186.1 g of disodium EDTA.$2H_2O$ to 800 mL of double-distilled water, stirred vigorously on a magnetic stirrer and the pH was adjusted to 8.0 with NaOH (~20 g of NaOH pellets). The volume was made up to 1 L with double-distilled water and autoclaved. EDTA does not dissolve into solution until the pH of the solution reached to ~8.0
c) TE buffer, pH 8.0 (10 mM Tris-HCl and 1 mM EDTA): Added 1 mL of 1 M Tris-HCl buffer and 0.2 mL of 0.5 M EDTA and made volume up to 100 mL with double-distilled water
d) Lysozyme: 10 mg / mL in double-distilled water. Stored in -20°C
e) Proteinase K: 10 mg / mL in double-distilled water. Stored in -20°C
f) 10% SDS: 10 g SDS in 100 mL double-distilled water
g) 5 M NaCl: 29.2 g NaCl in 100 mL double-distilled water
h) Cetyl trimethylammonium bromide (CTAB) / NaCl (10% CTAB in 0.73 M NaCl): 4.1 g NaCl dissolved in 80 mL double-distilled water. Added 10 g CTAB and dissolved by heating to 65°C. Volume adjusted to 100 mL with double-distilled water
i) Phenol: Chloroform: Isoamyl alcohol (25:24:1). Store at room temperature

Genomic DNA from *M. tuberculosis* was isolated as per published protocol (van Soolingen *et al.*, 1994). Two loopful of mycobacterial cells were washed thrice with TE buffer and re-suspended into 400 µL of the same buffer.

Organisms were heat killed at 80°C for 1 h. The cells were treated with 50 µL lysozyme for 1 h at 37°C. The solution was then treated with 5 µL of Proteinase K and 70 µL 10% SDS and incubated at 65°C for 10 min. 100 µL of 5 M NaCl and 100 µL CTAB / NaCl was added; the mixture was vortexed till the liquid turned milky white and then incubated at 65°C for 10 min. The sample was allowed to cool to room temperature and to this an equal volume of phenol: chloroform: isoamyl alchohol was added and kept for 20 min at room temperature. The sample was centrifuged at 13,000 rpm for 15 min. The upper aqueous phase was separated and DNA was precipitated by adding 0.6 volumes of isopropanol and kept in -20°C for 30 min. The DNA pellet obtained after centrifugation at 13,000 rpm for 15 min was washed with cold 70% ethanol, air dried and dissolved in an appropriate volume of sterile milliQ water and stored at 4°C. The concentration and purity of DNA was determined spectrophotometrically by measuring the absorbance at 260 nm and 280 nm.

2.5.4. Agarose gel electrophoresis

Reagents

a) Tris-acetate-EDTA (TAE) buffer: 4.84 g Tris, 1.14 mL glacial acetic acid and 20 mL 0.5 M EDTA in a final volume of 1 L of double-distilled water. The pH was adjusted to 8.0
b) Ethidium bromide: 1 mg / mL in double-distilled water

Genomic DNA and PCR amplified products were subjected to electrophoretic separation using 0.8% and 1% agarose gels respectively. The agarose was added to TAE buffer, dissolved by heating and after addition of ethidium bromide (0.1 µg / mL) poured on trough and allowed to set. The DNA samples were prepared by adding 6X gel loading buffer and loaded onto the gel. The DNA size standards loaded onto gel included 1 µL of 1 kb ladder. Electrophoresis was carried out in a horizontal agarose gel unit (Balaji Scientific Services, India) at 100 V for approximately 1-1.5 h. After electrophoresis, the DNA fragments were visualized in an UV trans-illuminator (UVP GelDoc, Cambridge, UK).

2.5.5. Cloning of full length *hupB* and its fragments (Sambrook *et al.*, 1989)

Full length *hupB* and the three *hupB* fragments, namely *hupB*- F1 (aa 1-71), *hupB*-F2 (aa 63-161) and *hupB*-F3 (aa 164-214) were cloned into pET22b (+) vector.

2.5.5.1. PCR amplification

The reaction mix, containing 200 µM dNTP mix, 0.5 U Taq DNA polymerase (Fermentas, Thermo Scientific, Pittsburgh PA, USA), 10 pmoles of the respective primers (Table 2.3) and 100 ng of *M. tuberculosis* genomic DNA in a total volume of 20 µL was subjected to PCR in Master cycler (Eppendorf, CA, USA) using the following program: initial denaturation for 5 min at 95ºC, 30 cycles of amplification for 4 min at 68ºC (annealing and extension) and denaturation for 1 min at 95ºC, followed by a final extension for 10 min at 72ºC. The PCR products were subjected to agarose gel electrophoresis using 1% gel.

Table 2.3 List of primers for cloning

Gene	Primer sequence	Amplicon size	Restriction enzyme
hupB	For: 5'- CCCGGATCCGATGAACAAAGCAGAGCTCA-3'	645	*Bam*HI
	Rev: 5'-CCCAAGCTTTTTGCGACCCCGCCGAG-3'		*Hin*dIII
hupB-F1	For: 5'-GCGTGGATCCCATGAACAAAGC-3'	213	*Bam*HI
	Rev: 5'-CCGCAAGCTTCACCTTTACTGTC-3'		*Hin*dIII
hupB-F2	For: 5'-GTTGGATCCACCGCGTACCG-3'	297	*Bam*HI
	Rev: 5'-CAGTAAGCTTCGTGGCCTTGAC-3'		*Hin*dIII
hupB-F3	For: 5'-CAATGGATCCACCCGCCAAGAA-3'	153	*Bam*HI
	Rev: 5'-GAAGAAGCTTTTTGCGACCCCG-3'		*Hin*dIII

2.5.5.2. Restriction digestion

1 µg of pET22b (+) plasmid DNA and 1 µg of full length *hupB, hupB-F1, hupB-F2* and *hupB*-F3 amplicons were individually subjected to double digestion with 10 units each of *Bam*HI and *Hin*dIII in a reaction mixture of 50 µL and incubated at 37°C o/n. After heat inactivation at 65°C for 10 min, they were purified using clean-up kit (Invitrogen) as per manufacturer's instructions.

2.5.5.3. Ligation

Ligation was done using vector and insert DNA in molar ratio of 1:3 using the following formula.

$$\text{Concentration of the insert (ng)} = \left[\frac{\text{ng of vector x Size of the insert (bp)}}{\text{Size of the vector (bp)}}\right] \text{x } 3$$

The ligation reaction mixture in a volume of 20 µL contained appropriate volumes of vector DNA, 2 µL of 10X ligase buffer, 1 µL of T4 DNA ligase (5 U / µL) and made up to 20 µL with sterile double-distilled water. This was incubated at 16°C o/n, heat inactivated at 65°C for 10 min and stored at -80°C till used. 25 ng of ligation mixture was taken to transform *E. coli* DH5α.

2.5.5.4. Transformation

Single colony of *E. coli* DH5α was inoculated in 5 mL of LB medium under aseptic conditions and incubated o/n at 37°C in an orbital shaker. 1 mL of the culture was used to inoculate 100 mL of LB medium and incubated till $OD_{600\ nm}$ reached 0.4. The cells were then harvested by centrifugation at 7000 rpm for 15 min at 4°C. The cell pellet was re-suspended in 20 mL of sterile, ice-cold 100 mM $CaCl_2$ and incubated in ice for 30 min. The cell suspension was centrifuged as before and the competent cells were finally re-suspended in 2 mL of ice-cold 100 mM $CaCl_2$ and placed on ice.

5 µL of ligation mixture was added to 100 µL of competent cells, mixed gently and incubated on ice for about 30 min. The cells were then subjected to heat shock at 42°C in a water bath for 90 sec and immediately chilled on ice. 800 µL of warm (37°C) LB medium was added to each tube, incubated with shaking at 37°C for 1 h, then plated on LB agar plates supplemented with ampicillin (50 µg / mL). The plates were incubated at 37°C o/n.

2.5.5.5. Screening of transformants

Plasmid DNA preparation (Birnboim & Doly, 1979)

Reagents

a) Solution I: 50 mM glucose in 25 mM Tris-HCl pH 8.0 containing 10 mM EDTA. Adjusted pH to 8.0 with 1 N HCl and stored at 4°C
b) Solution II: 0.2 N NaOH solution containing 1.5% SDS

c) Solution III: 60 mL of 5 M potassium acetate, 11.5 mL of glacial acetic acid and 28.5 mL of double-distilled water. The resulting solution is 3 M with respect to potassium and 5 M with respect to acetate. Stored at 4°C

A single colony was inoculated into 5 mL of LB medium supplemented with ampicillin (50 µg / mL) and incubated o/n with shaking at 37°C. 1.5 mL of the culture was centrifuged for 10 min at 13,000 rpm at 4°C, supernatant was discarded and the cell pellet was re-suspended in 100 µL of Solution I by vortexing and incubated on ice for 5 min. 200 µL of freshly prepared Solution II was added, mixed well and incubated on ice for 5 min. The solution was neutralized by adding 150 µL of ice-cold Solution III, mixed by gentle inversion five times and after incubation in ice for 5 min it was centrifuged at 13,000 rpm for 10 min at 4°C. The supernatant was carefully transferred to a fresh tube and DNase-free RNase was added to a final concentration of 10 µg / mL and incubated at 37°C for 30 min. The plasmid DNA was extracted into the aqueous phase by the addition of equal volume of phenol: chloroform (1:1; v/v) followed by centrifugation at 13,000 rpm for 10 min. The plasmid DNA was precipitated with 2 volumes of isopropanol at room temperature for 10 min and centrifuged at 13,000 rpm for 15 min. The pellet was washed with 70% ethanol, air-dried and dissolved in 20 µL of TE buffer and stored at -20°C.

Screening and selection of recombinant clones

Six transformed colonies were picked and inoculated into 5 mL of LB medium containing ampicillin (50 µg / mL) and incubated o/n at 37°C with shaking. Plasmids were isolated as described above, subjected to restriction digestion o/n at 37°C with *Bam*HI and *Hin*dIII and analysed by agarose gel electrophoresis. A positive clone was confirmed by DNA sequencing of the purified recombinant plasmid (Xcelris Labs Ltd., Ahmedabad, India). Sequence data was analysed with ChromasPro (Version 2.4, Technelysium Pty. Ltd., Australia).

2.5.6. Expression and purification of rHupB

2.5.6.1. Full length rHupB: Expression studies were performed after re-transformation of the recombinant plasmids into *E. coli* BL21 (DE3) (Novagen). Log phase cultures ($OD_{600\ nm}$ = 0.4) were induced with 0.1 mM IPTG (Hi Media Laboratories, Mumbai, India) for 15 h at 18°C. The cells were harvested,

washed twice with 20 mM phosphate buffer pH 7.4, sonicated for 10 min (40 Hz amplitude, 5 s on / 5 s off) in Vibra Cell Sonicator (Sonics), centrifuged at 12,000 rpm for 10 min and both supernatant and pellet were analysed by SDS-PAGE on a 10% gel (Laemmli, 1970). The supernatant containing the soluble protein was subjected to purification by affinity chromatography.

Reagents

a) 0.2 M phosphate buffer, pH 7.4: Prepared 0.2 M NaH_2PO_4 (stock A; 3.12 g in 100 mL double-distilled water) and 0.2 M Na_2HPO_4 (stock B; 2.84 g in 100 mL double-distilled water). Mixed 19 mL of A and 81 mL of B and made up to 200 mL
b) 5 M NaCl – 29.22 g of NaCl dissolved in 100 mL double-distilled water
c) 5 M imidazole – 8.51 g imidazole dissolved in 25 mL double-distilled water
d) Binding buffer: 20 mM sodium phosphate, 0.5 M NaCl, 20 mM imidazole
e) Wash buffer 1: 20 mM sodium phosphate, 0.5 M NaCl, 50 mM imidazole
f) Wash buffer 2: 20 mM sodium phosphate, 0.5 M NaCl, 100 mM imidazole
g) Elution buffer: 20 mM sodium phosphate, 0.5 M NaCl, 200 mM imidazole

The supernatant was loaded on a Ni-Sepharose column (GE Healthcare, India) that was pre-incubated with binding buffer. The column was washed twice with wash buffers 1 & 2 to remove unbound proteins and rHupB was eluted with elution buffer (collected as 1 mL aliquots). The purified protein was confirmed by immunoblotting with both commercial His-probe Antibody H-3, a mouse monoclonal IgG_1 (Santa Cruz Biotechnology, Texas, USA; 1:1000 dilution) and with rabbit anti-HupB antibody available in the lab (1:2500 dilution). The purified protein was concentrated using the Amicon Ultra-15 Centrifugal Filter Unit of 10 kDa cut-off (Millipore Corporation, Billerica, MA, USA). Protein was dialysed with 20 mM phosphate buffer (pH 7.4) and 50 mM NaCl.

2.5.6.2. HupB fragments HupB-F1, HupB-F2 and HupB-F3: The respective clones for the three fragments were confirmed by sequencing and re-transformed into *E. coli* BL21 (DE3) cells for expression studies. Log phase cultures ($OD_{600\ nm}$ = 0.5) were induced with 1 mM IPTG for 3 h at 37°C. The cells were harvested, washed twice with 10 mM Tris-HCl (pH 7.8) and sonicated for 10 min (40 Hz amplitude, 5 s on / 5 s off). The pellet and

supernatant were separated by centrifugation at 12,000 rpm for 10 min and analysed by Tris-Tricine electrophoresis on a 10% gel (Schägger & Von Jagow, 1987) as mentioned in Section 2.5.7.3. Purification was done by affinity chromatography.

Reagents

(i) Purification of rHupB-F3

a) Binding buffer, pH 7.8: 10 mM Tris-HCl, 0.5 M NaCl, 5 mM imidazole
b) Elution buffer, pH 7.8: 10 mM Tris-HCl, 0.5 M NaCl, 100 mM imidazole

(ii) Purification of rHupB-F1 and rHupB-F2

a) Solubilising buffer, pH 8.0: 20 mM Tris-HCl, 0.5 M NaCl, 5 mM imidazole, 8 M urea
b) Binding buffer, pH 8.0: 10 mM Tris-HCl, 0.5 M NaCl, 5 mM imidazole, 8 M urea
c) Elution buffer, pH 8.0: 10 mM Tris-HCl, 0.5 M NaCl, 100 mM imidazole, 8 M urea

Soluble rHupB-F3 was purified by loading the supernatant onto a Ni-Sepharose column (GE Healthcare, India) that was pre-incubated with binding buffer, washed to remove unbound proteins and eluted with elution buffer. Recombinant HupB-F1 and HupB-F2 obtained as inclusion bodies were first dissolved in solubilising buffer for 1 h at room temperature and then subjected to affinity chromatography as done for HupB-F3, except that 8 M urea was included in the buffers. The purity of these proteins, by virtue of their low molecular weight was confirmed by Tris-Tricine electrophoresis. Immunodetection was done as mentioned in Section 2.5.7.1.

2.5.6.3. Tris-Tricine gel electrophoresis for the detection of the recombinant HupB fragments (Schägger & Von Jagow, 1987)

Reagents

a) Acrylamide: bisacrylamide mix (49.5:3): 48 g of acrylamide and 1.5 g of bisacrylamide were dissolved in 50 mL of double-distilled water and made up to 100 mL
b) Gel buffer (for both stacking and resolving gel) - 3 M Tris and 0.3% SDS, pH 8.5
c) Running buffer-
    i) Anode buffer - 0.2 M Tris-HCl, pH 8.9

ii) Cathode buffer - 0.1 M Tris-HCl, 0.1 M Tricine and 0.1% SDS, pH 8.0

Table 2.4 Preparation of 10% gel for Tris-Tricine gel electrophoresis

	Volume (mL)	
Composition	**Resolving gel**	**Stacking gel**
Acrylamide: bisacrylamide	6.1	1.0
Gel buffer	10.0	3.1
Glycerol	3.17	-
Double distilled water	10.8	8.4
10% Ammonium per sulphate	0.1	0.1
TEMED	0.01	0.01

The 10% resolving gel was prepared using the recipe as given in Table 2.4 and allowed to polymerize for 40 min. The stacking gel was poured over it and the comb was appropriately positioned. 30 µg of total protein was mixed with equal volume of 2X sample buffer, boiled for 10 min, centrifuged for 10 min at 13,000 rpm and the supernatant was loaded onto gel. Electrophoresis was carried out at 30V initially till the bromophenol blue tracking dye entered the resolving gel and then at 150V till the dye reached the bottom of the glass plates.

2.6. Characterization of the *hupB* KO mutant strain

2.6.1. Complementation of the *M.tb.ΔhupB* KO mutant with *hupB*

A *hupB* KO mutant was generated in a previous study (Pandey *et al.*, 2014b). The mutant was complemented with the full length *hupB* cloned into the shuttle vector pSM96. It was done as follows: the full length 645 bp *hupB* was amplified from *M.tb*.H37Rv chromosomal DNA using the respective forward (5'-ACGGGATCCATGAACAAAGCAGAGCTC-3'; *Bam*HI) and reverse (5'-GATCTGCAGCTATTTGCGACCCCGCCG-3'; *Pst*I) primers. PCR was done with an initial denaturation at 95°C for 5 min followed by 30 cycles consisting of 1 min at 95°C and 3 min at 68°C followed by 5 min of extension at 72°C. The purified DNA fragment was cloned into pSM96 and then transformed into *E. coli* DH5α. After screening and confirmation of the clones by double digestion with *Bam*HI and *Pst*I and sequencing, the recombinant plasmid pMS101 was electroporated into *M.tb.ΔhupB* mutant. The *M.tb.ΔhupB* mutant was grown in Middlebrook 7H9 media supplemented with 10% ADC and 250 µg hygromycin till it reaches an $OD_{600\ nm}$ = 0.6. The cells were harvested, washed thrice in 1/50

volume of cold 10% glycerol and re-suspended in 1 mL of 10% glycerol. 400 µL of the mycobacterial cell suspension was taken in the electroporation cuvettes, added 1 µg of pMS101 and subjected to electroporation at 2.5 kV (Electroporator 2510, Eppendorf, NY, USA). 10 mL Middlebrook 7H9 media was added to the cell suspension and incubated at 37ºC o/n without shaking to allow the cells to recover. The cells were harvested and the pellet was re-suspended in 1 mL Middlebrook 7H9 medium. The cell suspension was plated onto Middlebrook 7H11 agar plates supplemented with 25 µg / mL kanamycin for selection of complemented strain. The complemented strains were verified by PCR and by immunoblotting with anti-HupB antibodies.

2.6.2. Growth characteristics

2.6.2.1. Solid medium: Cultures were grown in Middlebrook 7H9 media supplemented with ADC, washed, re-suspended and serially diluted in PBS containing 0.05% Tween 80. 10 µL samples of each 10-fold dilution were spotted in four spots adjacently onto Middlebrook 7H11 agar plates using 0.5% glycerol or 40 mM pyruvate as carbon source along with OADC. Control plates were made without any carbon source except OADC and incubated for four weeks at 37°C. Antibiotics, 250 µg / mL hygromycin and 25 µg / mL kanamycin were included as required.

2.6.2.2. High and low iron liquid P & B medium: The three mycobacterial strains *M.tb.*H37Rv, *M.tb.ΔhupB* and *M.tb.ΔhupB* / pMS101 were grown under iron-regulated conditions as mentioned in Section 2.3.5 with the addition of 250 µg / mL hygromycin for KO strain and 25 µg / mL kanamycin for the *hupB*-complemented strain.

2.6.3. Expression of mycobactin and carboxymycobactin

2.6.3.1. Assay of siderophore levels: The mycobacterial strains were grown under iron-regulated conditions and the siderophores were assayed as mentioned in Section 2.3.6.

2.6.3.2. Assay of transcript levels of *mbtA* and *mbtB*

Reagents

a) GTC solution: 294.5 g of GTC (Sigma) was dissolved o/n in 200 mL autoclaved milliQ water. 2.5 g sodium NL sarcosin (Sigma), 3.5 mL β-mercaptoethanol (Sigma), 12.5 mL 1 M sodium citrate pH 7.0 and 5.0 mL Tween 80 were added to GTC solution and made up to 500 mL

b) 3 M sodium acetate pH 5.2: 40.81 g sodium acetate.$3H_2O$ was dissolved in 80 mL autoclaved milliQ water. The pH was adjusted to 5.2 with glacial acetic acid and volume made up to 100 mL with milliQ water and autoclaved
c) 1 M citric acid: 1.92 g citric acid in 10 mL autoclaved milliQ water
d) 1 M sodium citrate pH 7.0: Dissolved 29.41 g sodium citrate in 80 mL milliQ water, adjusted pH to 7.0 using 1 M citric acid and made up to 100mL with milliQ water

Total RNA from the strains were isolated as follows: 100 mL of *M.tb*.H37Rv, *M.tb.ΔhupB* and *M.tb.ΔhupB* / pMS101 strains grown in high and low iron media were harvested on the tenth day after the addition of 60 mL guanidine thiocyanate solution (GTC) to each culture. The cell pellet was re-suspended in 1 mL of Trizol reagent (Invitrogen, CA, USA) and subjected to ribolysis (ZR Bashing Bead Lysis Tubes, Zymo Research, CA, USA). 400 µL of chloroform was added, centrifuged, the aqueous phase was transferred into a new tube and RNA was precipitated by the addition of 0.1 volume of 3 M sodium acetate and 0.8 volumes of isopropanol and kept at -20°C o/n. The tubes were centrifuged at 13,000 rpm, 4°C for 30 min. The RNA pellet was washed with 70% ethanol, dried at room temperature, dissolved in 100 µL of RNase-free water and purified using the RNeasy mini kit (Qiagen, Hilden, Germany). The contaminating genomic DNA was removed using TURBO DNA-free kit (Ambion, Texas, USA). The concentration of the RNA was determined using the NanoDrop Spectrophotometer ND-1000 (NanoDrop Technologies, DE, USA) and an aliquot was analysed for the integrity of 16S and 23S RNA by agarose gel electrophoresis.

qRT-PCR analysis of *mbtA* and *mbtB* were done using 1 µg of the total RNA that was first converted to cDNA using the SuperScript III First-Strand Synthesis System for RT-PCR (Invitrogen, CA, USA) according to the manufacturer's instructions. A suitable dilution of the cDNA was used as the template for the amplification of the *mbtA* and *mbtB* genes and 16S rRNA (internal control) using the primer sets given in Table 2.5. The reaction mixture, consisting of 4 µL of 1:10 dilution cDNA, 5 pmol of each primer and 5 µL of 2X SYBR Green (Applied Biosystems, Warrington, UK) in a total volume of 10 µL was subjected to amplification in the ABI 7500 Fast Sequence Detection

System (Applied Biosystems, CA, USA) using the following program: 95°C for 5 min followed by 40 cycles at 95°C for 15 sec and 60°C for 1 min. The difference in gene expression, expressed as fold-change, was calculated using the $2^{-\Delta\Delta CT}$ method.

Table 2.5 List of primers for *mbtA, mbtB* and 16S rRNA

Gene	Primer sequence
mbtA	For: 5'-TTCCGGCACTGGCCAAACTG-3'
	Rev: 5'-TCTAGCTTGGACCCGCCAAC-3'
mbtB	For: 5'-TGACGCTGTTCGGCCATTGC-3'
	Rev: AAGCCCACAGTGCACGTACC-3'
16S rRNA	For: 5'-GTGGACTACCAGGGTATCTAATCCT-3'
	Rev: GGGTCTCTGGGCAGTAACTG-3'

2.6.3.3. Chromatin immunoprecipitation (ChIP) assay for validation of HupB-regulated genes: DNA enrichment of *hupB*, *mbtA* and *mbtB*

Reagents

a) Lysis buffer: 50 mM Tris-HCl pH 8.0, 140 mM NaCl, 1 mM EDTA pH 8.0, 1% Triton X-100, 0.1% Sodium deoxycholate, 0.1% SDS and freshly prepared protease inhibitors
b) Radio-immunoprecipitation assay (RIPA) Buffer: 50 mM Tris-HCl pH 8.0, 150 mM NaCl, 2 mM EDTA pH 8.0, 1% NP-40, 0.5% Sodium deoxycholate, 0.1% SDS and freshly prepared protease inhibitors
c) Wash Buffer: 20 mM Tris-HCl pH 8.0, 150 mM NaCl, 2 mM EDTA pH 8.0, 1% Triton X-100, 0.1% SDS
d) Final wash buffer: 20 mM Tris-HCl pH 8.0, 500 mM NaCl, 2 mM EDTA pH 8.0, 1% NP-40, 0.1% SDS
e) Elution buffer: 100 mM $NaHCO_3$, 1% SDS
f) Proteinase K: 20 mg / mL in double-distilled water and stored at -20°C

*M.tb.*H37Rv and *M.tb.ΔhupB* were grown under iron-regulated conditions till $OD_{600\ nm}$ = 0.6. For ChIP assay, the protocol from Abcam (http://www.abcam.com/ps/pdf/protocols/x_chip_protocol.pdf) was followed. Briefly, formaldehyde was added dropwise to the culture to a final concentration of 0.75% and kept at room temperature for 10 min at 150 rpm. Glycine was then added to a final concentration of 125 mM and incubated with shaking for 5 min at room temperature. The cells were harvested at 2000 rpm for 15 min and

washed twice with 10 mL cold 1X PBS. The supernatant was carefully aspirated and the pellet was re-suspended to get 1 x 10^7 cells / 300 µL lysis buffer. The cells were sonicated (Bioruptor Plus, Diagenode, NJ, USA) for 20 min, centrifuged for 1 min at 4°C and 13,000 rpm and the supernatant transferred to a new tube. The DNA in the supernatant was quantified. For obtaining INPUT DNA concentration, 10% of the desired concentration of each sample was kept separately. 70 µg of each sample was taken in triplicate (out of which one would be used as beads only control) and diluted 1:10 with RIPA buffer. 30 µg of anti-HupB antibody (i.e., 3 µL) was added to the tubes except the beads only control and incubated with rotation at 4°C for 5 h. 20 µL of protein A/G beads (Protein A/G PLUS-Agarose, Santa Cruz Biotechnology, Texas, USA) was added to all samples and immunoprecipitated o/n with rotation at 4°C. The protein A/G beads were centrifuged for 1 min at 2000 rpm and the supernatant removed. The beads were washed three times with 1 mL wash buffer and finally once with 1 mL final wash buffer. 150 µL of elution buffer was added to the protein A/G beads, incubated with rotation at 30°C for 15 min and then centrifuged to elute the DNA. Reverse cross-linking of the protein and DNA was done by adding 5 µL of Proteinase K (20 mg / mL) for 5 h at 65°C. The DNA was extracted with phenol: chloroform (1:1; v/v), ethanol precipitated in presence of 10 µL glycogen (5 mg / mL) and taken up in 50 µL nuclease-free water. The samples were stored in -80°C till further use.

In silico analysis was done to find the *hupB*-box in the upstream regions of the genes whose transcript levels were altered in microarray (multiple sequence alignment; Clustal Omega). Using primers designed for the upstream region (Table 2.6), the genes were amplified in a 10 µL reaction mixture containing 1 µL extracted DNA, 5 pmol of each primer and 5 µL of 2X SYBR Green (Applied Biosystems, Warrington, UK). Real time PCR was done in the ABI 7500 Fast Sequence Detection System (Applied Biosystems, CA, USA) using the following program: 95°C for 5 min followed by 40 cycles at 95°C for 15 sec and 60°C for 1 min. The ChIP-qPCR data was analysed using the Percent Input Method where both the background levels and the input chromatin in the ChIP are normalized. Negative controls, the genes that are not altered by HupB were also taken to demonstrate the specificity of ChIP assay (Table 2.7).

Table 2.6 List of primers for genes regulated by HupB

Upstream region of the gene	Primer sequence
hupB	For: 5'-AAACCAGTGGTCCTCGTTTG-3'
	Rev: 5'-AACCGGTCGTTGGCTCAGTG-3'
mbtA	For: 5'-CGTAGCATGCACCACAAACC-3'
	Rev: 5'-GCATGTGGGCTCCTTAACAG-3'
mbtB	For: 5'-CGTAGCATGCACCACAAACC-3'
	Rev: 5'-GCATGTGGGCTCCTTAACAG-3'

Table 2.7. List of primers for genes not influenced by HupB

Upstream region of the gene	Primer sequence
rpoB	For: 5'-CGTTGCGCTGGCTACTTCCT-3'
	Rev: 5'-TCGGCCGGCGAACGATCTGT-3'
leuD	For: 5'-GACGTCCAACCGCAACTTCG-3'
	Rev: 5'-TGGACAGTGTGCCGCGAACC-3'
mutT1	For: 5'-GCTGATGGAACGGCACCGCA-3'
	Rev: 5'-ACTCCTGCAGGTCAATTCGG-3'
aroA	For: 5'-TGCCACGTTGTAGCTCGTCT-3'
	Rev: 5'-TGTCGTGGGTACCAGGCACC-3'

2.6.4. Growth of *M.tb.ΔhupB* strain in macrophages

2.6.4.1. Preparation of RPMI media

RPMI medium was prepared by dissolving the contents of one bottle of RPMI 1640 (with glutamine and without $NaHCO_3$; Sigma) in 800 mL milliQ water, added 2 g $NaHCO_3$ (Sigma), adjusted pH to 7.0 with 1 N HCl and the volume made up to 1 L. The medium was filter sterilized using 0.2 µm filter. Fetal bovine serum (FBS; 10% final concentration), penicillin (100 units / mL) and streptomycin (100 µg / mL) were added just before use. This is referred to as complete RPMI medium.

2.6.4.2. Infection of macrophage cell line with mycobacteria

Mouse peritoneal macrophage cell line RAW 264.7 was maintained in RPMI 1640 medium supplemented with 10% fetal bovine serum (Gibco, NY, USA) at 37°C in a carbon dioxide incubator with 5% CO_2. After the formation of the monolayer, the cells were released with 0.25% trypsin-EDTA (Gibco, NY, USA) and washed with phosphate-buffered saline (10 mM phosphate, 137 mM NaCl, 2.7 mM KCl; pH 7.4).

1×10^6 cells were seeded per well into 6-well plates (Corning, NY, USA) and allowed to adhere o/n. Mid-log-phase *M.tb.*H37Rv, *M.tb.*Δ*hupB* and *M.tb.*Δ*hupB* / pMS101 mycobacterial strains grown under high and low iron conditions were harvested, washed, re-suspended in RPMI medium and vortexed for 2 min with 3-mm glass beads to break up clumps. The bacterial suspension was then diluted with RPMI to get an $OD_{600\ nm}$ = 0.15 (equivalent to 3 X 10^8 cells). This was further diluted with RPMI till $OD_{600\ nm}$ = 0.06 which is equivalent to 1 X 10^7 cells / mL. 10^7 cells were added to the RAW cells to achieve a multiplicity of infection (MOI) of 10:1 (10 bacteria to 1 RAW cell). After 4 h, the infected cells were washed twice with warm RPMI to remove all non-phagocytosed mycobacteria. 1 mL of RPMI-1640 medium with 10 µg / mL gentamicin (HiMedia, Mumbai, India) was added and incubated for 2 h. The cells were washed twice with PBS buffer and then maintained in complete RPMI as required.

2.6.4.3. Tests for monitoring growth of phagocytosed mycobacteria

Phagocytosed mycobacteria were released from the macrophages and assay of growth was carried out at 4 h (for determining infectivity) and on days 0, 1, 2, 3, 5 and 7 for monitoring growth inside the macrophages. The macrophage monolayers were washed with PBS, lysed with 500 µL 0.06% SDS in Middlebrook 7H9 medium, the released bacteria were pelleted and re-suspended in 100 µL medium. The number of organisms were evaluated by ATP assay, qRT-PCR and by determining CFU. Two separate experiments were done with each performed under identical conditions in duplicate.

a) **Determination of CFU:** 20 µL of the cell suspension was plated on Middlebrook 7H11 agar plates with hygromycin and kanamycin added for the growth of *M.tb.ΔhupB* and *hupB*-complemented strains respectively. After 3 weeks, the bacterial colonies on plates were counted.
b) **ATP assay:** This was done with the luminescence-based kit BacTiter-Glo™ Microbial Cell Viability Assay (Promega) as per manufacturer's instructions. Briefly, the lyophilized BacTiter-Glo substrate was reconstituted with BacTiter-Glo buffer after equilibrating them to room temperature. 100 µL of this BacTiter-Glo reagent was added to 100 µL of the recovered bacteria in an opaque walled 96-well plate, the contents mixed in an orbital shaker and incubated for 5 min. Control wells

containing medium without cells were prepared to obtain a value for background luminescence The luminescence was reported as relative light units (RLU) with the GloMax® 96 Microplate Luminometer (Promega) (Lewin *et al.*, 2008).

c) **qRT-PCR:** The recovered bacteria were quantified by qRT-PCR. Genomic DNA from the recovered bacteria was extracted based on published protocols (Goelz *et al.*, 1985). The pellet was re-suspended in 100 µL of 7H9 media and 200 µL TE9 buffer [500 mm Tris pH 9, 20 mM EDTA, 10 mM NaCl, 1% SDS and 2 mg / mL Proteinase K] was added. The mixture was incubated at 58ºC for 60 min and then at 97ºC for 30 min. The DNA was extracted with phenol: chloroform (1:1; v/v), precipitated with ethanol and the dried pellet re-suspended in 25 µL of sterile milliQ water. The reaction mixture for qRT-PCR contained 4 µL of the extracted DNA, 5 pmol of the 16S rRNA forward and reverse primers and 5 µL of 2X SYBR Green (Applied Biosystems, Warrington, UK). The PCR program used was same as mentioned in Section 2.6.3.2. From a standard curve generated with known concentrations of genomic DNA from *M.tb.*H37Rv, the test values obtained in qRT-PCR were used to quantify DNA that reflected the bacterial growth.

2.6.5. Oxidative stress studies in macrophages infected with *M.tb.ΔhupB*

2.6.5.1. Determination of reactive oxygen species (ROS) levels

24 h post infection the plates were washed with PBS, the cells were scraped from the plates and transferred into microcentrifuge tubes. The cells were again washed and re-suspended in 100 µL PBS. 10 µM of the dye H_2DCFDA (2',7'-dichlorodihydrofluorescein diacetate) was added and kept at room temperature for 30 min. The tubes were centrifuged at 13,000 rpm for 5 min and the supernatant was discarded. Then the cells were washed twice with 500 µL PBS to remove excess dye, re-suspended in 100 µL PBS and transferred to a 96-well optical-bottom plate (Nunc, cat# 165305). The fluorescence of the bound dye was measured by the emitted light at 530 nm upon excitation at 488 nm (TECAN Infinite M200 Microplate Reader; Männedorf, Switzerland).

2.6.5.2. Transcript levels of *NOX1, NOXA1* and *NOS2* in macrophages

The cells were collected 24 h post infection, total RNA was isolated and cDNA was synthesized as mentioned in Section 2.6.3.2. qRT-PCR was carried out with gene-specific primers (Table 2.8) using β-actin as internal control.

Table 2.8 List of primers for *NOX1, NOXA1* and *NOS2*

Gene	Primer sequence
NOX1	For: 5'-GGTTGGGGCTGAACATTTTTC-3'
	Rev: 5'-TCGACACACAGGAATCAGGAT-3'
NOXA1	For: 5'-ACGCGAAGACTGGGACTCT-3'
	Rev: 5'-AGCCCCTGTTAAAGTACATCCTA-3'
NOS2	For: 5'-GTTCTCAGCCCAACAATACAAGA-3'
	Rev: 5'-GTGGACGGGTCGATGTCAC-3'
β-actin	For: 5'-GGCTGTATTCCCCTCCATCG-3'
	Rev: 5'-CCAGTTGGTAACAATGCCATGT-3'

2.6.5.3. Transcript levels of the mycobacterial *sodA, ahpC* and *katG*

The same cDNA was used for qRT-PCR with gene-specific primers (Table 2.9) using 16S rRNA as internal control.

Table 2.9 List of primers for *sodA*, *ahpC* and *katG*

Gene	Primer sequence
sodA	For: 5'-CGCCAAGGAAGATCACTCAG-3'
	Rev: 5'-TAGGCGACAGGTTCTTCCAC-3'
ahpC	For: 5'-ACCATTGGCGATCAATTCCC-3'
	Rev: 5'-GTGTTCGTCACTGGTGATAG-3'
katG	For: 5'-AGGCTGGCAATCTCGGCTTC-3'
	Rev: 5'-CCCGTTGCGAGATACCTTGG-3'

2.6.5.4. ChIP analysis: HupB interaction with the promoter DNA of *sodA* and *ahpC*

ChIP was done as detailed earlier (section 2.6.3.3). qRT-PCR was carried out with sequence specific primers (Table 2.10) of the upstream regions of the genes following chromatin immunoprecipitation.

Table 2.10 List of primers for oxidative stress genes regulated by HupB

Upstream region of the gene	Primer sequence
sodA	For: 5'-CATGGAGCAGGGTTGACTTG-3'
	Rev: 5'-CCACGGCATTCCTTCCTTCG-3'
ahpC	For: 5'-TTGCCTGACAGCGACTTCAC-3'
	Rev: 5'-GTGGCATGACTCTCCTCATC-3'

2.6.6. Transcript levels of cytokines in macrophages infected with mycobacteria

24 h post infection the cells were scraped from the plates and total RNA was isolated and qRT-PCR was carried out using mouse-specific primers (Table 2.11) obtained from Primer Bank (https://pga.mgh.harvard.edu/primerbank/) as mentioned in section 2.6.5. β-actin was used as internal control.

Table 2.11 List of primers for quantification of cytokines

Gene	Primer sequence	Gene	Primer sequence
IFN-γ	For: 5'-ACAGCAAGGCGAAAAAGGATG-3'	IL-6	For: 5'-CCAAGAGGTGAGTGCTTCCC-3'
	Rev: 5'-TGGTGGACCACTCGGATGA-3'		Rev: 5'-CTGTTGTTCAGACTCTCTCCCT-3'
TNF-α	For: 5'-CCCTCACACTCAGATCATCTTCT-3'	IL-10	For: 5'-GCTCTTACTGACTGGCATGAG-3'
	Rev: 5'-GCTACGACGTGGGCTACAG-3'		Rev: 5'-CGCAGCTCTAGGAGCATGTG-3'
IL-1β	For: 5'-GCAACTGTTCCTGAACTCAACT-3'	IL-12p40	For: 5'-TGGTTTGCCATCGTTTTGCTG-3'
	Rev: 5'-ATCTTTTGGGGTCCGTCAACT-3'		Rev: 5'-ACAGGTGAGGTTCACTGTTTCT-3'
IL-4	For: 5'-GGTCTCAACCCCCAGCTAGT-3'	IL-18	For: 5'-GACTCTTGCGTCAACTTCAAGG-3'
	Rev: 5'-GCCGATGATCTCTCTCAAGTGAT-3'		Rev: 5'-CAGGCTGTCTTTTGTCAACGA-3'

2.7. Studies on HupB as a iron transporter of ^{55}Fe

The interaction of HupB with mycobactin and carboxymycobactin and its role as an iron transporter was studied by three different approaches. First, uptake of ^{55}Fe by live organisms (mutant *vs* wild type and the complemented strains) was studied. Second, interaction of the ^{55}Fe-CMb with purified HupB and cell wall proteins of mutant *vs* wild type incorporated into liposomes were analysed. Thirdly, confirmation of HupB-siderophore interaction was done by direct interaction of the purified protein with HPLC-purified Fe-Mb and Fe-CMb by spectrofluorimetry and by circular dichroism (CD).

2.7.1. Growth of the mutant strain in ^{55}Fe-containing low and high iron medium and recovery of the label in carboxymycobactin and mycobactin

Reagents

a) 50 mM EDTA: Added 1.86 g of disodium EDTA.2H_2O to 80 mL of double-distilled water, adjusted pH to 4 with glacial acetic acid and volume made up to 100 mL

b) 0.1 M lithium acetate: Dissolved 0.65 g lithium acetate in 100 mL double-distilled water

c) Preparation of ^{55}Fe solutions for culture of mycobacteria

Stock: ^{55}Fe supplied (American Radiolabeled Chemicals, MO, USA) had a specific activity 10.18 mCi / mg in a final concentration 40.4 mCi / mL. The concentration of iron was 4 µg Fe / µL.

1 µL stock was diluted to 2000 µL to get a working solution containing 0.002 µg Fe / µL.

Low iron: 100 µL of working solution of ^{55}Fe was added to get 0.02 µg Fe / mL or 0.36 µM Fe

High iron: 100 µL ^{55}Fe (≡ 0.2 µg) + 14.75 µL cold Fe was added to get 12 µg Fe / mL or 214 µM Fe

d) HPLC purification of CMb and Mb

CMb and Mb was extracted and HPLC purified as per published protocols (Barclay *et al.*, 1985; Lane *et al.*, 1998). CMb and Mb were extracted from 100 mL cultures grown in low iron medium. The chloroform extracts of both Fe-Mb and Fe-CMb (section 2.3.6) were taken in a separating funnel, washed thrice with water to remove the excess ferric chloride and the excess water was removed. The sample was dried by rotary evaporation and the residue was dissolved in minimal quantity of chloroform and filtered though Nylon membrane filter to remove any insoluble material. Both Fe-Mb and Fe-CMb were separated by reverse phase HPLC on Water's C18 column (150 mm x 4.6 mm id) at a flow rate of 1 mL / min for 35 min and monitored continuously at 450 nm. The hydrophobic Fe-Mb was separated using a gradient (Table 2.12) of 0 to 100 % with buffer A (0.09% formic acid / 90% acetonitrile) and buffer B (0.1% formic acid in 60% acetonitrile) and 40% methanol. The Fe-CMb was separated using a gradient of 0 to

100% with buffer A (0.1% formic acid) and buffer B (0.09% formic acid in 90% acetonitrile).

Table 2.12. HPLC gradient for purification of Fe-Mb and Fe-CMb

Time (min)	Buffer A %	Buffer B %
2	100	0
32	0	100
33	0	100
35	100	0

Fractions with maximal absorbance at 450 nm were collected, concentrated by Speed vac system. The purity of the concentrated sample was determined by performing spectral scan ranging from 300 nm-600 nm by using acetonitrile as blank. The concentration of ferric complexes of siderophores was determined by using their extinction coefficients.

e) Preparation of desferri-CMb: One volume of 50 mM EDTA, pH 4.0 was added to the purified CMb (in acetonitrile) and incubated for 18 h at room temperature (Ryndak *et al.*, 2010a). The solution was extracted into chloroform, dried and the residue was re-suspended in 50% ethanol (prepared in iron-free water).

f) Preparation of ^{55}Fe-CMb: The desferri-CMb was mixed with 1 µM $^{55}FeCl_3$ and incubated for 10 min at room temperature. The ^{55}Fe-CMb was extracted into chloroform, washed twice with iron-free water to remove excess ^{55}Fe. The chloroform was evaporated and the residue was resuspended in 50% ethanol and aliquots were stored in -20°C.

g) Cocktail 'O' Scintillation fluid (Sisco Research Laboratories, India): This contained 6 g PPO and 0.2 g POPOP dissolved in 1 L toluene

Growth of mycobacteria in ^{55}Fe-containing medium: The mycobacterial strains *M.tb.*H37Rv, *M.tb.ΔhupB* and *M.tb.ΔhupB* / pMS101 were grown in high and low iron medium as mentioned in Section 2.3.5, except that ^{55}Fe was used in the culture medium and the cultures were harvested after 6 days of growth. Additionally, rabbit anti-HupB antibodies / pre-immune serum (final dilution of 1:500) was added to identical sets of cultures inoculated into low iron media.

The above experiment was done in two biological replicates, each of which was performed in duplicate. As it was planned to measure the

radioactivity in a) whole organisms, b) mycobactin recovered from the cell pellet and c) CMb from the culture filtrate, the required number of cultures for each of the two biological replicates were included.

The radioactivity associated with the cells was determined as follows. The cells were washed with 0.1 M lithium acetate (Sisco Research Laboratories, India) followed by two washes with 1 mL cold P & B media. The bacterial pellet was re-suspended in a total volume of 5 mL scintillation fluid and the radioactivity determined in a Liquid Scintillation Counter (TriCarb 2910 TR, Packard) set at the wide-open window setting.

Mycobactin from the cells was extracted with 100% ethanol o/n, the extract dried and re-suspended in 20 µL chloroform, added to scintillation fluid and the radioactivity counted. An identical preparation in 20 µL chloroform was used for analysis by Thin layer Chromatography performed on aluminium-backed silica gel plates (Merck Millipore, Darmstadt, Germany) using the solvent system consisting of petroleum ether: butanol: ethyl acetate (2:3:3). After the run, the plates were dried and exposed to Phosphor Screen for 2 days and the image was recorded with a Phosphor Imager (Molecular Imager PharosFX Plus System, Bio-Rad, CA, USA).

For the extraction of carboxymycobactin, one volume of 95% ethanol was added to the collected supernatant and CMb was extracted by adding one volume of chloroform. The extract was washed twice with water and dried. The extract was re-suspended in 20 µL chloroform and the same procedures were followed for determination of radioactivity and TLC as mentioned above.

2.7.2. Uptake of iron from ^{55}Fe-CMb by high and low-iron grown organisms

All the three mycobacterial strains were grown in high (214 µM Fe) and low (0.36 µM Fe) iron medium as described in Section 2.3.5. As uptake studies were performed with log phase organisms, the mycobacteria were harvested after 9 days of growth. The cultures were harvested, washed thrice with iron-free P & B media, prepared a cell suspension of 1 x 10^8 cells / mL of the respective high and low iron organisms in iron-free P & B medium. 1 mL was dispensed into 24-well plates (Corning, NY, USA), added 1 x 10^5 cpm of ^{55}Fe-CMb to each well and incubated at 37°C for 2 h with gentle rocking at 150 rpm. ^{55}Fe in whole cells and mycobactin was assayed as mentioned above in Section 2.7.1. In addition, uptake by low iron organisms was done upon pre-

incubation of the cell suspensions with rabbit anti-HupB antibodies / pre-immune sera (control) added at (1: 500 dilution).

2.7.3. Interaction of ^{55}Fe-CMb with liposome-entrapped rHupB or CHAPS-solubilised cell wall proteins

Reagents

a) 1 M CHAPS (3-[(3-Cholamidopropyl) dimethylammonio]-1-propanesulfonate): Dissolved 6.15 g CHAPS in 10 mL double-distilled water
b) 50 mM KH_2PO_4 / NaOH, pH 7.1: Dissolved 6.8 g KH_2PO_4 in 800 mL double-distilled water, adjusted pH to 7.1 with 10 N NaOH and volume made up to 1L
c) Solubilising buffer: 8 mM CHAPS in 50 mM KH_2PO_4, pH 7.1
d) Preparation of desferri-Mb: Iron was removed from the mycobactin by gently shaking the chloroform suspension with 1 mL of methanol and 1 mL of 6 M HCl. The resulting colourless chloroform solution was evaporated under a stream of N_2 gas to get desferri-Mb

Solubilisation of cell wall proteins with the non-denaturing detergent CHAPS: The cell wall was prepared from the mutant and wild type *M. tuberculosis* grown under in low iron P & B medium (Section 2.4.1). 200 µL of solubilising buffer was added to the cell wall pellet, solubilised by shaking at 4°C o/n and centrifuged at 18,000 rpm for 30 min at 4°C. The supernatant containing the CHAPS-solubilised envelope proteins was transferred into another tube. The CHAPS-solubilised envelope proteins were dialysed o/n against 400 volumes of 50 mM KH_2PO_4 pH 7.1 at 4°C to remove the detergent.

Preparation of liposomes

Phosphatidylcholine and cholesterol (Sigma), taken in molar ratio of 1:1 were solubilised in chloroform and dried as a thin film in an inert atmosphere using nitrogen gas. 300 µg total lipid was dried onto the walls of a test-tube. Identical sets using 50 nM desferri-Mb were also prepared.

Empty liposomes were prepared by adding 1 mL of the phosphate buffer to the lipid film and shaking vigorously for 30 s to get the milky suspension. Recombinant HupB or the CHAPS-solubilised mycobacterial cell wall proteins were incorporated as reported (Dover & Ratledge, 1996). 100 µg of the proteins in a total volume of 1 mL in 50 mM KH_2PO_4, pH 7.1 was added to prepare the

liposomes. Crude proteo-liposomes were formed by shaking the mixture vigorously for 30 s which appeared cloudy. This suspension was incubated with 50 nM ^{55}Fe-CMb (150,000 cpm) for 30 min at 37°C. The liposome-bound ^{55}Fe was retained by filtering the reaction mixture through 0.22 µ pore size GVWP filters (Millipore Corporation, MA, USA), washed with 2 mL of buffer to remove any unbound label. The filters were dried, transferred to a scintillation vial, added 5 mL scintillation fluid and measured the radioactivity as mentioned above.

2.7.4. Direct interaction of HupB with Mb and CMb: *in silico* analysis and validation by ligand-binding studies

2.7.4.1. *In silico* prediction of the tertiary structure of HupB using I-TASSER

Homology modeling of the mycobacterial HupB is not possible as there is no suitable template for the C-terminal region of HupB that is unique to mycobacteria. Also, the crystal structure of the full length HupB is not available and only the N-terminal region has been crystallised (Bhowmick *et al.*, 2014). Here, HupB protein (214 aa) of *M. tuberculosis* was modelled in I-TASSER (Iterative Threading ASSEmbly Refinement) server (Zhang, 2008). In this the structural templates are first identified by multiple threading approach that is based on prior statistical knowledge of the relationship between the structures in the PDB and the sequence of a protein which one wishes to model. The tertiary structure of the protein thus generated was confirmed using the Ramachandran map generated by PROCHECK tool (Laskowski *et al.*, 1993). In order to remove the steric clashes if any, the model was refined using ModRefiner (http://zhanglab.ccmb.med.umich.edu/ModRefiner/) and the level of disorder in the protein was checked with DISOPRED3 (Jones & Cozzetto, 2015). The modeled structure was visualized using Pymol Molecular Graphics viewer.

2.7.4.2. Docking of HupB with carboxymycobactin and mycobactin

CMb (accession number DB04043), Drugbank (http://www.drugbank.ca/) and Mb (CHEBI: 61174), ChEBI (https://www.ebi.ac.uk/chebi/) were obtained. SMILES file for CMb available in Drugbank was used to build a 3D structural (PDB) file in Avogadro (Hanwell *et al.*, 2012). For Mb, MOL file was converted

into SMILES in Open Babel (O'Boyle *et al.*, 2011) that was used to build a PDB file using Avogadro. Docking study was carried out using AutoDock/Vina (Weininger, 1988) after preparing the ligand and protein for software use in AutoDockTool (ADT) program. The protein PDB file was first modified in ADT by assigning polar hydrogen and merging non-polar hydrogen to the parent carbon atoms and removing water molecules. Both ligand and protein were saved as pdbqt files. AutoGrid was used for defining of docking area. The grid size was set to 58×42×40 xyz points with grid spacing of 1Å and grid center was designated at dimensions (x,y,z): 63.283, 63.42, 63.302. Since no specific binding site was known for HupB protein, the whole surface of the protein was chosen in the grid box (Blind Docking). Considering the ligands as rigid molecules, nine different conformations were generated by docking and the pose with lowest energy of binding was analysed using LigPlot+ (Laskowski & Swindells, 2011).

2.7.4.3. Direct interaction of rHupB with carboxymycobactin and mycobactin: spectrofluorimetry and circular dichroism to study protein-ligand interactions

Stock concentrations of Fe-CMb and Fe-Mb

a) Fe-CMb: The stock concentration was 253 µM. Titrations were done with 0.5 µM increasing concentration up to 15 µM and 3 µM for fluorescence spectroscopy and circular dichroism respectively
b) Fe-Mb: The stock concentration was 753 µM. Titrations were done with 2 µM increasing concentration up to 30 µM and 3 µM for fluorescence spectroscopy and circular dichroism respectively

Fluorescence spectroscopy: Soluble rHupB (purified as mentioned in Section 2.5.7.1) was dialysed o/n with 10 mM Tris-HCl, pH 7.4. The optimal concentration of the protein for the study was determined as follows. As HupB lacks tryptophan and tyrosine residues and contains four phenylalanine residues, the absorbance of the protein was measured at 205 nm. The extinction coefficient of HupB was calculated from the extinction coefficients (Table 2.13) of the amino acids and peptide bonds of HupB at 205 nm (Anthis & Clore, 2013). Using the formula [$\varepsilon_{205} = \Sigma (\varepsilon_i n_i) + \varepsilon_{bb} (r-1)$], the extinction coefficient for HupB at 205 nm was calculated to be 661,070 $M^{-1}cm^{-1}$ and the

concentration of HupB required for equilibrium binding studies was determined as 1.63 µM.

Table 2.13 Extinction coefficients of amino acids at 205 nm

Amino acid	Extinction coefficient ($M^{-1}cm^{-1}$)		Amino acid	Extinction coefficient ($M^{-1}cm^{-1}$)
W	20400.0000		C	690.0000
F	8600.0000		N	400.0000
Y	6080.0000		Q	400.0000
H	5200.0000		Cystine	2200.0000
M	1830.0000		Peptide BB	2780.0000
R	1350.0000			

Purified HupB, diluted in 10 mM Tris-HCl to get the required concentration of 1.63 µM was taken in a volume of 1 mL in the cuvette and subjected to spectrofluorimetry in JOBIN-YVON Fluoromax 3 (HORIBA, Kyoto, Japan) instrument using slit width of 5 at 20°C. The protein was excited with light at a wavelength of 263 nm and the emitted light was recorded from 295 nm to 350 nm.

The emission spectrum was recorded upon addition of increasing amounts of Fe-CMb and Fe-Mb. As ferri-siderophores are required to cross the mycobacterial cell envelope, interaction with the desferri-CMb was done as a control as it was not expected to bind HupB. The data generated was used to calculate the apparent binding constant by fitting the data points at 318 nm to a rectangular hyperbola by Non-linear Least Square Method. Best fit was obtained for minimal model of ligand binding to identical non-interacting binding sites.

Circular dichroism (CD): Far-UV CD experiment as a function of ligand concentration was performed to determine whether any structural changes are induced upon interaction of HupB with the siderophores. Pure protein and HupB pre-incubated for 10 min with varying concentrations of Fe-Mb and Fe-CMb (0-3 µM) and desferri-CMb (0-50 µM) in a total volume of 600 µL was subjected to CD spectroscopy. The spectra from 250-200 nm were recorded in the J-1500 Circular Dichroism Spectrometer (Jasco, Oklahoma, USA).

2.7.5. ChIP assay to establish that HupB regulated the genes *mmpL5, mmpS5, irtA* and *eccA3* associated with transport of iron

ChIP assay was done as described in Section 2.6.3.3. qRT-PCR was carried out using the primers for the promoter DNA of the genes *mmpL5, mmpS5, irtA* and *eccA3* (Table 2.14)

Table 2.14 List of primers for genes associated with iron transport

Upstream region of the gene	Primer sequence
mmpL5	For: 5'-TTTAGGCGGGTACGGCTCAG-3'
	Rev: 5'-CTCCTCGGAAAGTGGTTCTG-3'
mmpS5	For: 5'-CACGCTTGAGAGTTCCAATC-3'
	Rev: 5'-GACGCTCACAAGTTTCACTG-3'
irtA	For: 5'-GTTTGACCTTCGGTAAGGCA-3'
	Rev: 5'-CTGATACTCAGCCCGCGCAT-3'
eccA3	For: 5'-GGGCTACCAACGAAATGGAG-3'
	Rev: 5'-GCCGATCCGCCTGAACTTTG-3'

2.8. Lipid profile of *M.tb.ΔhupB* mutant

*M.tb.*H37Rv and *M.tb.ΔhupB* were grown in iron-regulated media as mentioned in section 2.3.5. The organisms were harvested at mid-logarithmic stage, washed twice with equal amounts of milliQ water, heat killed by incubating the cells at 80°C for an hour and freeze dried to get dry biomass.

2.8.1. Mycolic acids

All the solvents were procured from Sisco Research Laboratories, India. 1 mL of 20% tetrabutyl ammonium hydroxide was added to 100 mg of the dried cell pellet and heated for 20 h at 100°C in a heating block. This step, known as saponification hydrolyzes the mycolic acids present in the cell wall. The tubes were brought to room temperature before opening. 2 mL methylene chloride and 100 µL methyl iodide were added and the tubes were placed on a rotary mixer (Rotospin Rotary mixer, Tarsons) for 1 h at 25 rpm. The tubes were centrifuged at 5000 rpm for 1 min and the upper aqueous phase was discarded. The organic phase was washed with 1 mL 3 N hydrochloric acid followed by 1 mL distilled water, vortexed and centrifuged at 5000 rpm for 1 min. After discarding the upper aqueous phase, 2 g anhydrous sodium sulphate was added to the organic phase to remove any residual water, vortexed and centrifuged for 10 min at 5000 rpm. The organic phase was collected in a pre-

weighed tube, evaporated to dryness and the weight of the lipid residue was determined. The residue(s) from the different strains were dissolved in methylene chloride to obtain all the samples of equal concentration. 5 µL of each was subjected to TLC using the solvent system consisting of 40 mL of hexane: ethyl acetate (95:5 v/v). The TLC plate was placed in the chamber and the elution was carried out three times with complete drying after each elution. The TLC plates were dipped in a solution of 5% phosphomolybdic acid in ethanol and mycolic acids were detected by charring. Identification of mycolic acids was performed by comparison with previously published TLC analysis.

2.8.2. Non-polar lipids

2 mL of aqueous methanol (10 mL of 0.3% NaCl: 100 mL of methanol) and 1 mL of petroleum ether was added to 100 mg of dried biomass. This was mixed in a rotary mixer for 15 min and centrifuged for 5 min at 13,000 rpm. The upper layer, containing the non-polar lipids was transferred to a separate pre-weighed tube and 1 mL of petroleum ether was added to the lower layer and the same steps followed. The resulting upper layer was added to the first, dried completely and the weight of the lipid residue was determined. The non-polar lipids from each of the strains were dissolved in appropriate volume of chloroform: methanol (4:1; v/v) to get samples of equal concentration. If it appeared turbid and hazy due to the presence of proteins, it was filtered through PTFE filters. The samples were then stored at 4°C before further analysis

The non-polar lipids were subjected to TLC using the solvent systems (Camacho *et al.*, 2001; Slayden & Barry, 2001) listed in Table 2.15. All the lipids were detected by charring with 5% phosphomolybdic acid. Identification of mycolic acids was performed by comparison with previously published TLC analysis.

Table 2.15 Solvent system for separation of lipids by TLC

Solvent composition	Number of elutions	Lipids detected
Chloroform: methanol: water (90:10:1)	1	Sulpholipid-1, DAT
Petroleum ether: acetone (92:8)	3	PAT
Hexane: ether (9:1)	1	PDIM

2.8.3. Fatty acid methyl esters (FAME)

Fatty acid profiling was done commercially by GC-MS in Royal Life Sciences, Hyderabad.

2.8.4. ChIP assay to establish that HupB regulated the genes involved in the biosynthesis of mycolic acids, SL-1, PDIM, DAT and PAT

Following chromatin immunoprecipitation, qRT-PCR was carried out using sequence specific primers (Table 2.16) of the upstream regions of the genes involved in lipid biosynthesis.

Table 2.16 List of primers for genes associated with lipid biosynthesis

Upstream region of the gene	Primer sequence
fabD	For: 5'-GGACGGAAAGTGATCCAGAC-3'
	Rev: 5'-GCGCGGTGTAACAGATTATG-3'
kasA	For: 5'-CATCCAGAAGCTCGAGGAAG-3'
	Rev: 5'-ACTTGGACTCGGCCTCAAGC-3'
inhA	For: 5'-GGGCTACATCGACACCGATA-3'
	Rev: 5'-CCTCGGAAGCCAGGAAGCTG-3'
fadD32	For: 5'-GCGTACGTTGATGGCGGCCT-3'
	Rev: 5'-GACCCGACTGGGTCCTGCAC-3'
pks13	For: 5'-GCTCGACCACCAGCCCATCG-3'
	Rev: 5'-GATCTTGCCGCTGGAGGTTC-3'
papA1	For: 5'-ACCGCTGACAACTCTACTGG-3'
	Rev: 5'-GCTGTCGTCACAGTAAGAAC-3'
mmpL8	For: 5'-GTGACGGTAGATAGAGAAGC-3'
	Rev: 5'-TCCTCATCTGCTCCGCACGT-3'
papA3	For: 5'-TACGCGTCAGTCCCACAAAG-3'
	Rev: 5'-TCCTCGGCTCGATCTCAAAC-3'
pks4	For: 5'-GGCTGGCGGATTGGGTCGAC-3'
	Rev: 5'-CGTCCGGACGGGTCGGTGTG-3'
chp2	For: 5'-GGCTGCCAACTTTAATGTCG-3'
	Rev: 5'-CTGCCTCTGCATCGAGAATC-3'
mmpL10	For: 5'-CTGATTCATTCCCGGTGGTG-3'
	Rev: 5'-AGCCATCTCCGCCAGTGAAG-3'
fadD26	For: 5'-CCGGCACGTTTCAGAGCGGT-3'
	Rev: 5'-CGCCTTGTACTCCCATTCGG-3'
fadD28	For: 5'-GGCAAACCCCTGCTGAGCTG-3'
	Rev: 5'-GGGCATCACGTTACCGGCCA-3'
drrC	For: 5'-GGTCTCATGCCGTTAAAGCT-3'
	Rev: 5'-CTCACCTGTGAGGCTGTCTT-3'

2.9. Evaluation of clinical significance of HupB

2.9.1. Cell-mediated and humoral immune response to HupB

2.9.1.1. Study subjects

The study population comprising a total of 83 subjects within the age group of 16-70 years included two categories, namely pulmonary TB (PTB) and extrapulmonary TB (EPTB). Patients with HIV and other chronic infections like diabetes were excluded. Pulmonary TB included new cases (both sputum positive and negative) awaiting anti-tubercular therapy and subjects who are undergoing the therapy for less than a month. Defaulters included subjects who did not complete treatment and with symptoms of the disease. Extrapulmonary TB, often clinically diagnosed included subjects diagnosed with pleural effusion, lymphadenitis, ophthalmic Koch or miliary TB. Control subjects comprising of 30 healthy donors without any clinical symptoms of the disease were recruited randomly. 10 mL of blood was collected from the subjects in a BD Vacutainer coated with 158 USP units sodium heparin (Becton & Dickinson Ltd., NJ, USA) for isolation of peripheral blood mononuclear cells (PBMCs) and 4 mL in BD Vacutainer coated with silica (clot activator).

The study was approved by the Institutional Ethical Committee and Biosafety Committees with informed written consent obtained from all participants.

2.9.1.2. Isolation of peripheral blood mononuclear cells (PBMCs) from blood

The blood was diluted 1:1 with 0.9% NaCl and layered on 4 mL Histopaque (Sigma) taken in two 15 mL centrifuge tubes and centrifuged at 2000 rpm for 30 min. The buffy coat layer comprising of the PBMCs was washed with 6 mL RPMI 1640 (Sigma), re-suspended in 1 mL RPMI supplemented with 5% heat inactivated fetal bovine serum (Gibco) and 100 U/ml penicillin, 100 mg/ml streptomycin (Gibco). Any contaminating RBCs were removed by lysing them with 0.8% ammonium chloride followed by washing with 5 mL 1X PBS. The PBMCs were re-suspended in 1 mL RPMI 1640 and the number of viable cells was determined as follows.10 µL of the cell suspension was mixed with 30 µL RPMI and 10 µL of 0.5% Trypan blue. 10 µL of this was loaded onto a hemocytometer and the numbers of viable cells (cells that had not taken up the dye and were colourless) were counted.

Viable Cells / mL = Average number of viable cells per large square x (10^4 / mL) x (1 / dilution factor)

2.9.1.3. Preparation of full length HupB

The full length HupB was purified and concentrated as mentioned in section 2.5.6.1. The protein was passed through agarose beads bound with polymyxin B (Sigma) to remove endotoxin based on manufacturer instructions. The protein was filter-sterilised by passing through 0.2 µm filter (Millipore Corporation, MA, USA) before adding to lymphocyte cultures.

2.9.1.4. Lymphocyte proliferation assay

The cells were diluted to 1 x 10^6 cells / mL and 200 µL containing 2 x 10^5 cells was seeded in sterile 96-well flat-bottomed tissue culture plates (Corning, NY, USA). HupB (2.5 µg / mL), Purified protein derivative PPD (3 µg / mL; Span Diagnostics, India), Concanavalin A used as mitogen (1 µg / mL; Sigma) were added to the respective wells. Negative control included PBMCs minus any antigen / mitogen. Each set was done in triplicates and incubated at 37°C in a carbon dioxide incubator with 5% CO_2. After 72 hours, 150 µL of the culture supernatant from each well was removed and stored at -80°C for cytokine assays. 10 µL MTT (50 µg / mL) was added to the cells and incubated for 4 h at 37°C in an atmosphere of 5% CO_2. The plates were centrifuged at 2000 rpm for 10 min, discarded the supernatant and dissolved the purple formazan crystals in 100 µL DMSO (Qualigens, India). The absorbance was read at 570 nm with 630 nm as reference. The proliferation, expressed as stimulation index (SI) was calculated as the ratio of mean proliferative response in the presence and absence of antigen and a SI value ≥ 2 was considered as positive.

2.9.1.5. Assay of cytokines

The culture supernatants were assayed for IL-2, IL-4, IL-6, IL-8, IL-10, GM-CSF, IFN-γ and TNF-α using Bio-Plex Pro Human Cytokine Grp I Panel 8-Plex (Bio-Rad, CA, USA) as per manufacturer's instructions. Briefly, the 96-well plate layout was planned, the Bio-Plex 200 suspension array system was initialized and the assay reagents were equilibrated to room temperature. The system was calibrated after 30 min of initialization. The 'standards' vial was reconstituted with 500 µL of the appropriate diluents, vortexed and kept on ice for 30 min. The 8 point standard dilution series, the blanks and the 1X coupled beads in assay buffer were prepared. The filter plate was pre-wet with 100 µL

assay buffer and 50 µL 1X coupled beads was added. This was washed twice with 100 µL wash buffer. 50 µL of standards, blanks and samples were added, covered and incubated in the dark at RT with shaking at 300 rpm. After washing thrice with 100 µL wash buffer, 25 µL of detection antibody (prepared in detection antibody diluents) was added and incubated as mentioned above. 50 µL of streptavidin-PE was added after washing thrice and incubated for 10 min. This was washed thrice and the beads were re-suspended in 125 µL of assay buffer and incubated with shaking at 1100 rpm for 30 sec. Finally the plate was read using the Bio-Plex Manager software version 5.0 where the standard curves were calculated by a five-parameter regression formula. The mean concentration of each cytokine was expressed as pg / mL.

2.9.1.6. Indirect ELISA to detect anti-HupB antibodies in the sera of TB patients

Reagents

a) Bicarbonate buffer (pH 9.2): Dissolved 159 mg Na_2CO_3 and 293 mg $NaHCO_3$ in 90 mL double-distilled water, adjusted pH to 9.2 with 0.1 N HCl and made volume up to 100 mL. The solution was autoclaved and stored at 4°C
b) 0.1 M PBS (pH 7.2): Dissolved 8 g NaCl, 2.4 g KH_2PO_4, 14.4 g Na_2HPO_4 and 2 g KCl in 900 mL double-distilled water, adjusted pH to 7.2 with 0.1 N HCl, made volume up to 1 L and autoclaved
c) PBST: 0.1 M PBS containing 0.05% Tween 20
d) Blocking solution: 0.1 M PBS containing 5% FBS
e) Secondary antibody: Goat anti-human IgG-horse radish peroxidase conjugate (1:10,000; Sigma)
f) Substrate for horse radish peroxidase:
    - 0.05 M phosphate-citrate buffer (pH 5.0): Dissolved 5.11 g citric acid and 7.3 g Na_2HPO_4 in 900 mL double-distilled water, adjusted pH to 5.0 and made volume up to 1 L
    - 3, 3', 5, 5'-tetramethylbenzidine (TMB) substrate solution: Dissolved 1 mg TMB tablet in 10 mL of 0.05 M phosphate citrate buffer and added 3 µL of fresh 30% hydrogen peroxide prior to use

g) Stop solution: 1.25 M H_2SO_4.

When rHupB was used as antigen, the following procedure was used. A flat-bottomed polystyrene microtitre plates (Corning) was coated with 250 ng rHupB dissolved in 0.1 M bicarbonate buffer, pH 9.2 for 3 h at 37°C in a humid box, followed by o/n incubation at 4°C. The plates were washed three times with PBS-T and incubated with blocking solution for 2 h at 37°C. After washing, 100 µL of human serum (1:200 dilution) was added to the wells, incubated for 2 h at 37°C, washed three times with PBS-T and added 100 µL of secondary antibody (goat anti-human IgG peroxidase conjugate) and incubated for 2 h at 37°C. Colour was developed in the dark by adding 100 µL of freshly prepared TMB substrate solution, incubated in the dark for 10 min and the reaction was stopped by adding 100 µL of 1.25 M H_2SO_4. $OD_{450\ nm}$ was read in an ELISA reader (Model 680XR, BioRad, CA, USA).

The controls included antigen and antibody blanks, positive serum from a confirmed case of TB (with high titre of anti-HupB antibodies) and negative serum from a normal healthy control.

2.9.1.7. Statistical analysis

Data was analysed using GraphPad Prism software version 5.01 (GraphPad Software, Inc., San Diego, CA) and SigmaPlot software (Version 10.0; **Systat Software Inc.,** CA, USA). Results are represented as box plots where the upper quartile of the box represents the 75th percentile and the lower quartile of the box represents the 25th percentile. The line inside the box represents the median. Whiskers above and below the box indicate the 90th and 10th percentiles. Any data to the further extreme of the whiskers is termed as outlier. The non-parametric Mann–Whitney U test was used to compare the differences between the groups. The threshold for significance was set at $P < 0.05$ (two-tailed). Receiver-operating-characteristic curves (ROC) were calculated and expressed as areas under the curve (AUC), with an asymptotic 95% confidence interval (CI) using the MedCalc Statistical Software (Version 15.2.2; MedCalc Software, Ostend, Belgium).

2.9.2. ELISA with HupB fragments as antigens

2.9.2.1. Study subjects and serum collection

The study group consisted of 73 confirmed cases of TB. The patients were categorized into four groups, namely newly diagnosed cases of pulmonary TB (Group I), defaulters of anti-tubercular therapy (ATT) with varying periods of therapy (Group II), relapse cases with an earlier history of the disease (Group III) and extrapulmonary TB cases (Group IV) that included patients with pleural effusion and involvement of lymph nodes / meninges / spine / abdomen. Individuals with history of human immunodeficiency virus (HIV) infection and other chronic diseases like diabetes were excluded from the study. The control group (Group V) consisted of healthy endemic normals with no clinical evidence of disease. The study was approved by the Institutional Ethical Committee and Biosafety Committees with informed written consent obtained from all the subjects. Three millilitres of venous blood was collected from the study subjects, serum separated and stored at −80°C until use.

2.9.2.2. Serum iron profile

Assay of free iron, total iron binding capacity (TIBC), % saturation of serum transferrin and ferritin levels of all the serum samples was done commercially (Thyrocare, Mumbai, India).

2.9.2.3. Preparation of antigens: rHupB and recombinant HupB fragments

All the four antigens were purified as mentioned in Sections 2.5.6.1 and 2.5.6.2.

2.9.2.4. ELISA

Reagents

All the reagents used were similar as mentioned in section 2.9.1.6 except

a) Secondary antibody: Goat anti-human IgG alkaline phosphatase (1:5000; Bangalore Genei)
b) Substrate for Alkaline phosphatase (ALP)
    - Diethanolamine buffer (DEA): Dissolved 24.2 mL diethanolamine (Sigma) in 200 mL double-distilled water, adjusted pH to 9.8 with 0.1 N HCl, added 0.5 mM $MgCl_2$ and made up the volume to 250 mL
    - p-nitrophenyl phosphate (pNPP) substrate solution: Dissolved 1 pNPP tablet (5 mg) in 5 mL DEA buffer to get 1 mg / mL solution

ELISA was done essentially as described earlier for the first study. The four antigens were used at 500 ng concentration. Patients' serum was used at 1:100 dilution and the secondary antibody was goat anti-human IgG alkaline phosphatase conjugate (1:5000 dilution). 100 µL p-nitrophenyl phosphate was added as the substrate, incubated for 15 min and $OD_{405\ nm}$ was read in an ELISA reader.

2.9.2.5. Statistical analysis

Data were analysed using IBM SPSS Statistics Version 20 (IBM Corporation, New York, USA). One-way analysis of variance (ANOVA) and post-hoc Tukey's test was used to determine which pairs of means differed significantly. The bivariate correlation between serum iron profiles was determined using Pearson's correlation coefficient. In all analyses, $P < 0.05$ was considered statistically significant.

CHAPTER 3

RESULTS

3.1. Generation of the *hupB*-complemented strain *M.tb.ΔhupB* / pMS101

The complemented strain *M.tb.ΔhupB* / pMS101 was generated by transformation of *M.tb.ΔhupB* with pMS101 (Fig. 3.1). Recombinants were selected by growing them on Middlebrook 7H11 agar with kanamycin.

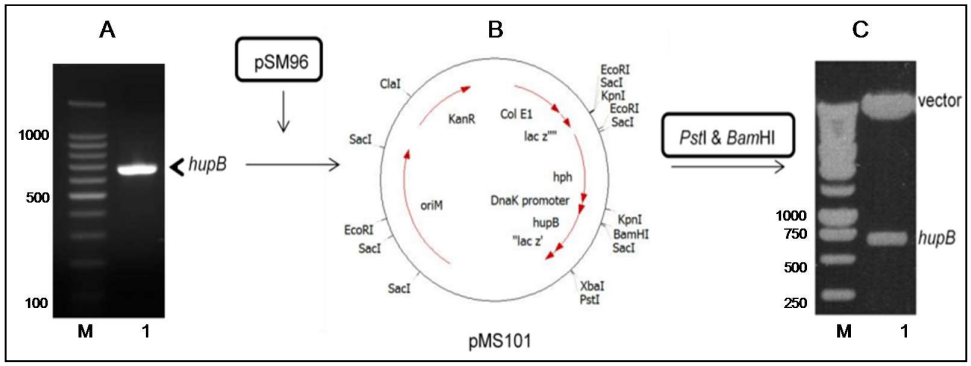

Fig. 3.1. Generation of pMS101. Panel A shows the 645 bp *hupB* amplicon cloned into pSM96 to generate pMS101 (Panel B). In Panel C, lane 1 shows the *hupB* fragment released upon double digestion of the recombinant plasmid with *Pst*I and *Bam*HI. M represents the ladder.

3.1.1. Constitutive expression of HupB in the complemented strain

As *hupB* in the complemented strain was under the control of the DnaK promoter, there was constitutive expression of HupB, with Fig. 3.2 showing that both high and low iron grown strains expressed HupB in equivalent concentrations. While the *hupB* KO strain showed no expression, iron-limited WT*M.tb.*H37Rv showed up-regulation of the protein.

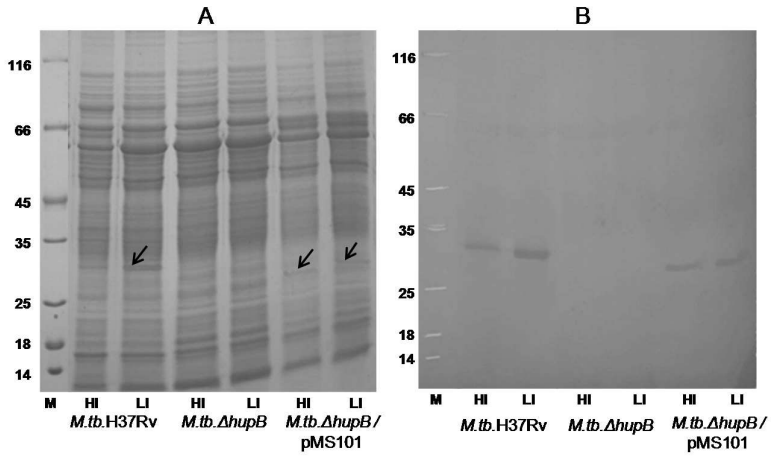

Fig. 3.2. Expression of HupB. Panels A and B show the SDS-PAGE and immunoblot analysis of whole cell sonicates (50 µg total protein) of high (144 µM Fe; HI) and low

iron (0.36 µM Fe; LI) *M.tb.*H37Rv, *M.tb.ΔhupB* and *M.tb.ΔhupB* / pMS101 respectively. SDS-PAGE was done on a 5-20% gradient gel, transferred onto nitrocellulose membrane and developed with rabbit anti-HupB antibodies diluted 1:2500. The arrows indicate HupB and M is the protein molecular weight marker.

3.2. Characterization of the *M.tb.ΔhupB* mutant strain

3.2.1. Growth of the mutant strain in media with different carbon sources

When *M.tb.*H37Rv, *M.tb.ΔhupB* and *M.tb.ΔhupB* / pMS101 were grown in Middlebrook 7H11 medium, *M.tb.ΔhupB* showed sparse growth (dysgonic) in all media, irrespective of the presence of glycerol or pyruvate or in the absence of both of them. The WT *M.tb.*H37Rv showed eugonic (dense growth) and rugose colonies in the presence of glycerol (Fig. 3.3). This phenotype was restored in the mutant upon *hupB* complementation.

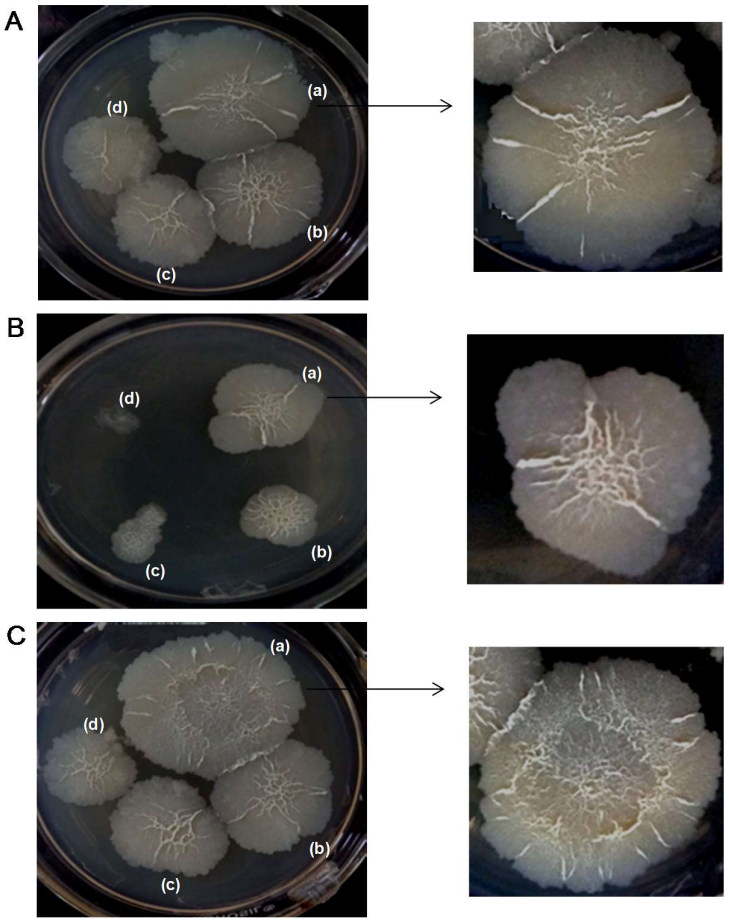

Fig. 3.3. Growth in Middlebrook 7H11 medium supplemented with OADC and glycerol. Panel A, B and C represents the growth of *M.tb.*H37Rv, *M.tb.ΔhupB* and *M.tb.ΔhupB* / pMS101 respectively when 10-fold serial dilutions (a, b, c and d represent

dilutions of 10^{-1}, 10^{-2}, 10^{-3} and 10^{-4} respectively) of McFarland#1 cell suspension were spotted on Middlebrook 7H11-OADC solid media supplemented with glycerol and incubated at 37°C for 4 weeks.

In OADC plates (Fig. 3.4) both WT and complemented strains were eugonic and these strains showed poor growth when pyruvate was used as a carbon source (Fig. 3.5).

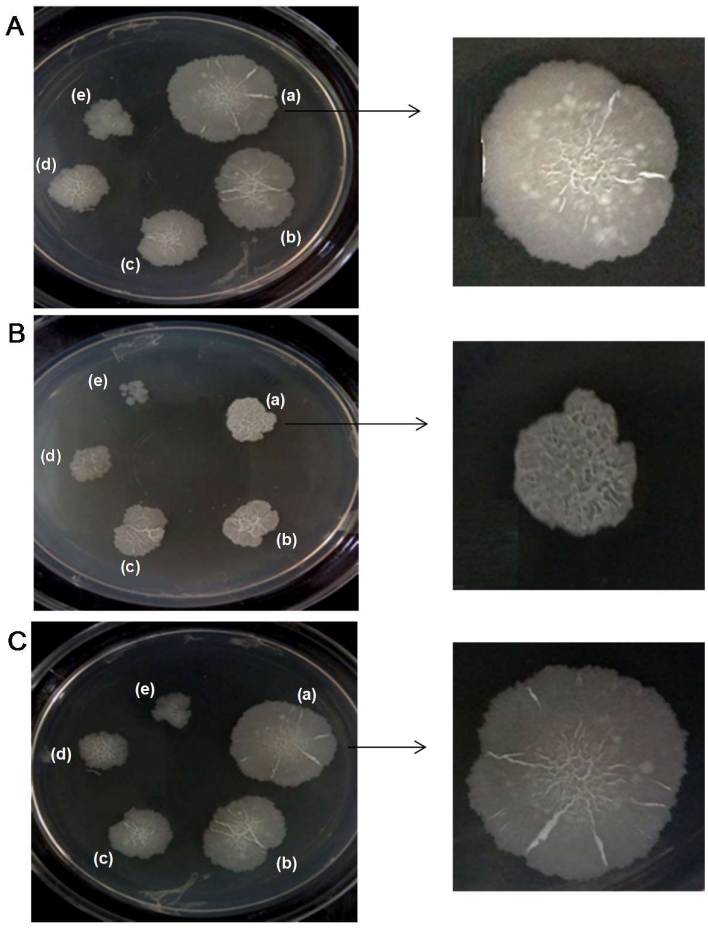

Fig. 3.4. Growth in Middlebrook 7H11 medium supplemented with OADC. Panel A, B and C represents the growth of *M.tb.*H37Rv, *M.tb.ΔhupB* and *M.tb.ΔhupB* / pMS101 respectively when 10-fold serial dilutions (a, b, c, d, e represent dilutions of 10^{-1}, 10^{-2}, 10^{-3}, 10^{-4} and 10^{-5} respectively) of McFarland#1 cell suspension were spotted on Middlebrook 7H11-OADC solid media and incubated at 37°C for 4 weeks.

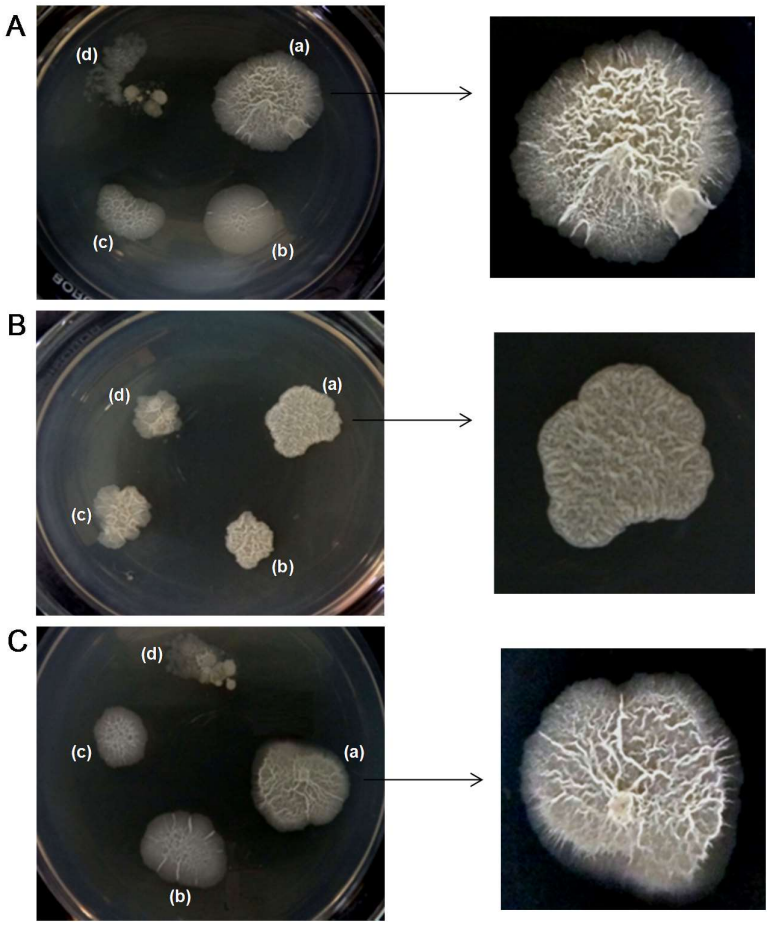

Fig. 3.5. Growth in Middlebrook 7H11 medium supplemented with OADC and pyruvate. Panel A, B and C represents the growth of *M.tb.*H37Rv, *M.tb.ΔhupB* and *M.tb.ΔhupB* / pMS101 respectively when 10-fold serial dilutions (a, b, c and d represent dilutions of 10^{-1}, 10^{-2}, 10^{-3} and 10^{-4} respectively) of McFarland#1 cell suspension were spotted on Middlebrook 7H11-OADC solid media supplemented with pyruvate and incubated at 37°C for 4 weeks.

3.2.2. Effect of iron levels on *M.tb.ΔhupB*

3.2.2.1. Growth in high and low iron media

When the growth of the three mycobacterial strains in liquid high and low iron Proskauer and Beck medium was monitored (Fig. 3.6, Panel A), the mutant strain exhibited an extended lag phase that was more pronounced in low iron medium. This was restored in the *hupB*-complemented strain that showed similar growth characteristics as the WT *M.tb*.H37Rv. When cultured in solid medium *M.tb.ΔhupB* showed less growth compared to WT that was restored in the complemented strain (Fig. 3.6, Panel B).

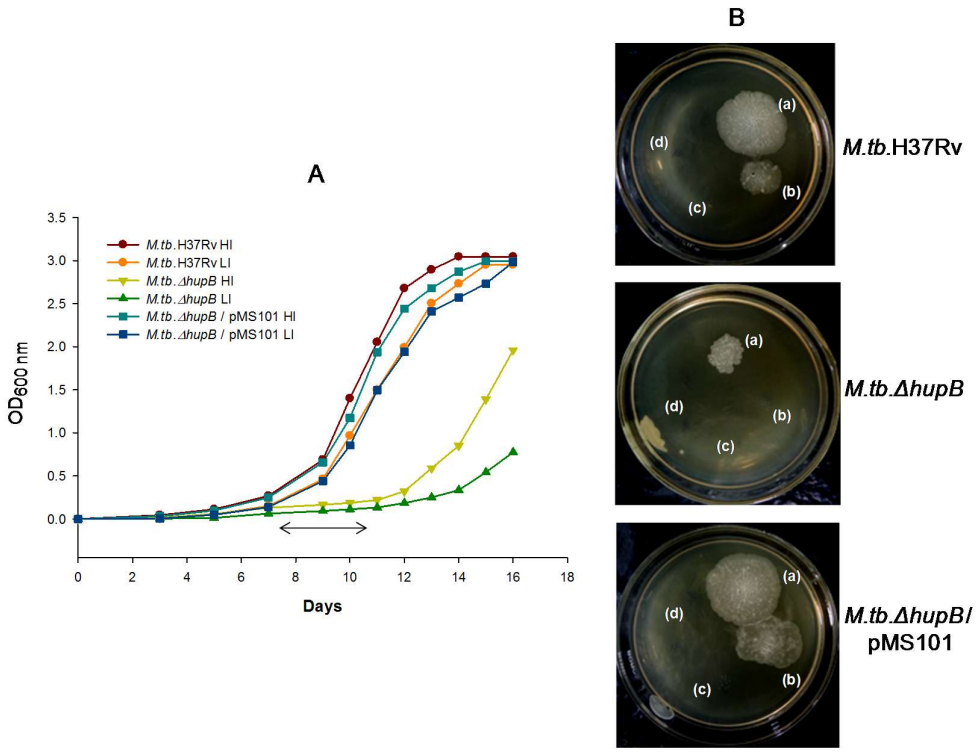

Fig. 3.6. Growth of *M.tb*.H37Rv, *M.tb.ΔhupB* and *M.tb.ΔhupB* / pMS101 strains in iron-regulated media. The three strains were grown under high iron (144 µM Fe; HI) and low iron (0.36 µM Fe; LI) conditions in Proskauer and Beck medium (Panel A). Growth was monitored by measuring the $OD_{600\ nm}$ over a period of 16 days. The experiment was repeated thrice and the figure represents data from one experiment. Lag phase is represented by (↔). In (Panel B) 10-fold serial dilutions (a, b, c and d represent dilutions of 10^{-1}, 10^{-2}, 10^{-3} and 10^{-4} respectively) of McFarland#1 cell suspension of all the three strains were spotted on Proskauer and Beck solid media with 0.36 µM Fe (LI) and incubated at 37°C for 4 weeks.

3.2.2.2. Low levels of carboxymycobactin and mycobactin in iron-limited *M.tb.ΔhupB* mutant strain

M.tb.ΔhupB in culture produced low levels of CMb and Mb

Iron-limited *M.tb.ΔhupB* cultured for 14 days (Fig. 3.7) showed a 3-5 fold lower expression of CMb (Panel A) and Mb (Panel B) when compared to *M.tb*.H37Rv. The siderophore levels were restored in the *hupB*-complemented strain with almost identical levels seen in iron-limited *M.tb.ΔhupB* / pMS101 and *M.tb.*H37Rv. Time course analysis over a period of 8 to 18 days showed low levels of Mb and CMb in the mutant that further confirmed the inability of the

mutant strain to produce optimal siderophores when deprived of iron (Fig. 3.7, Panels C & D). Reduction in mycobactin was more pronounced with almost a 9-fold difference on the eighth day when compared to WT *M.tb.*H37Rv.

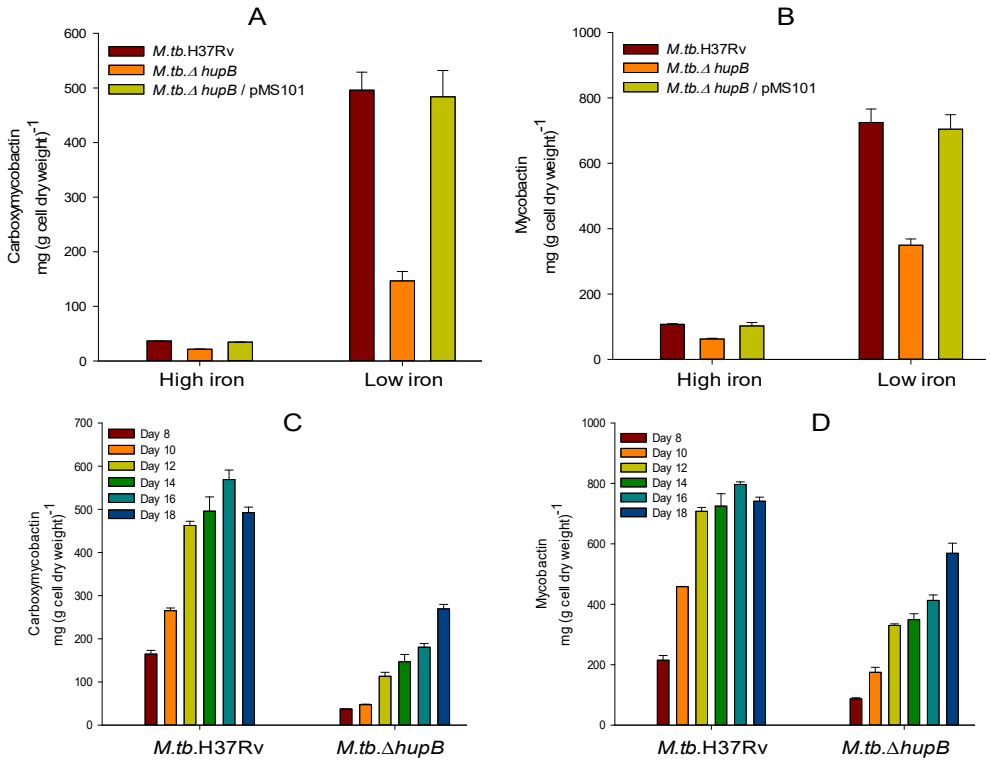

Fig. 3.7. Expression of low levels of mycobactin and carboxymycobactin by *M.tb.ΔhupB* mutant strain and their restoration to normal levels upon *hupB* complementation. The three strains were grown in high (144 µM Fe) and low (0.36 µM Fe) iron media. Panels (A) and (B) represent carboxymycobactin and mycobactin expressed by these organisms harvested after 14 days of growth. Panels (C) and (D) represent the time course of expression of the two siderophores by *M.tb*.H37Rv and the mutant strain grown in low iron media. The error bars represent standard deviation calculated from three identical experiments.

3.2.2.3. Reduction of transcript levels of *mbtA* and *mbtB* genes in *M.tb.ΔhupB*

Transcriptional profiling (microarray) carried out with high and low iron grown *M.tb.*H37Rv and *M.tb.ΔhupB* had shown a down-regulation of the *mbt* (siderophore biosynthesis) genes in *M.tb.ΔhupB* (Pandey *et al.*, 2014b). qRT-PCR of *mbtA* and *mbtB* normalized with 16S rRNA showed a positive 18- and 27-fold change respectively in the WT low *vs* high iron (Fig. 3.8). A down-

regulation of 8-fold and 6-fold for *mbtA* and *mbtB* was observed in low iron *M.tb.ΔhupB* when compared to low iron *M.tb.*H37Rv. The transcript levels were restored when the mutant was complemented with *hupB*.

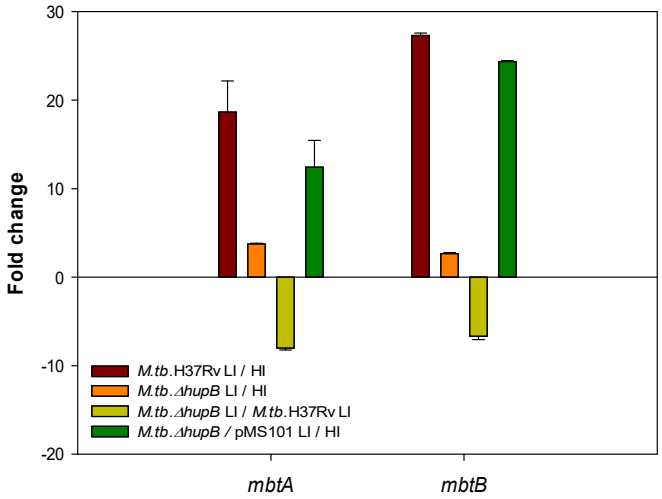

Fig. 3.8. qRT-PCR of *mbtA* and *mbtB*. The three strains were grown in high (144 µM Fe; HI) and low (0.36 µM Fe; HI) iron media. qRT-PCR was done with RNA isolated from the strains. The mRNA transcript levels in HI and LI organisms were normalised with 16S rRNA. The error bars represent standard deviation calculated from two identical experiments performed in duplicates.

3.2.2.4. ChIP assay: regulatory role of HupB on *mbtA* and *mbtB*

HupB box was identified in our earlier study in the promoter DNA of *mbtB* (Pandey *et al.*, 2014b). Here, ChIP assay was done to confirm the location of the HupB box at positions -40 and -72 of *mbtB* and *mbtA* respectively using the Percent Input Method for calculation. A positive enrichment was found in low iron *M.tb.*H37Rv with a 39-fold change and 5-fold change seen for *mbtB* and *mbtA* respectively when compared to high iron *M.tb.*H37Rv (Fig. 3.9, Panel A). *M.tb.ΔhupB* that did not express HupB did not show enrichment as the values were similar to the IgG controls.

Since it had been proved that HupB auto-regulates its own expression (Pandey *et al.*, 2014a), enrichment was also calculated for *hupB* (positive control) and few of the genes that did not have HupB box in their promoters and also not altered in the microarray (negative control), such as *mutT1, aroA, leuD* and *rpoB* (Fig. 3.9, Panel B). For *hupB,* there was a 100-fold more enrichment in the low iron *M.tb.*H37Rv compared to high iron while the mutant showed no

enrichment (Fig 3.9, Panel A). In the negative control genes there was no enrichment even in the WT *M.tb.*H37Rv low *vs* high iron.

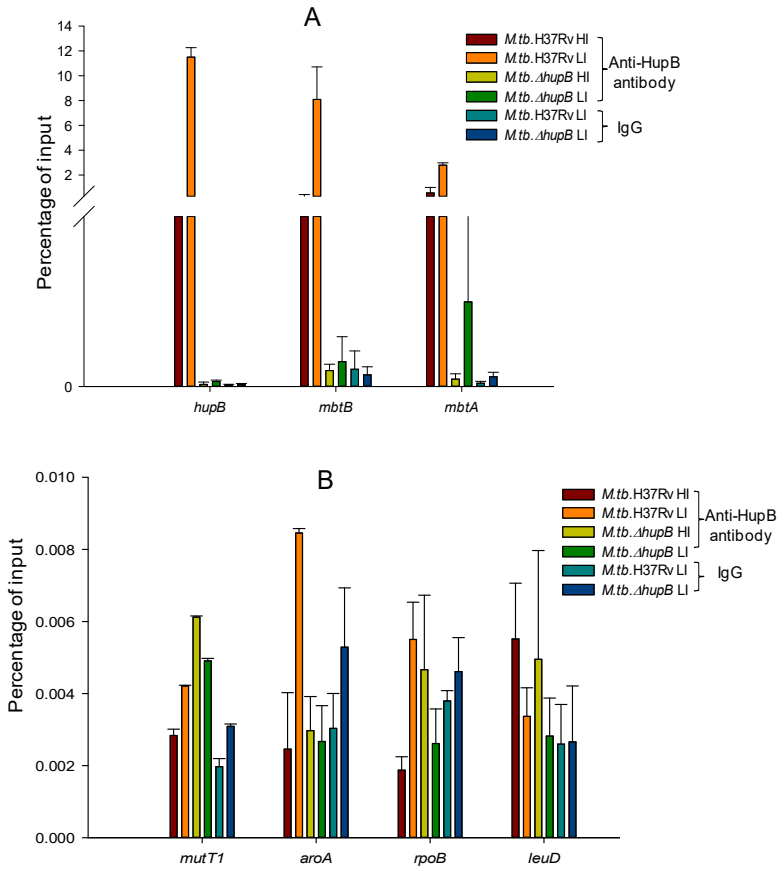

Fig. 3.9. ChIP assay and qRT-PCR of *hup B, mbtB* and *mbtA.* ChIP assay was carried out with DNA from WT and mutant strains using anti-HupB antibodies and IgG antibodies (control). qRT-PCR was done with primers for upstream regions of the selected genes. Panel A shows the genes whose upstream DNA contained a potential HupB box and Panel B, showing no change were genes that were not regulated by HupB. DNA enrichment was calculated using Percent Input Method. The error bars represent standard deviation calculated from two identical experiments performed in duplicates.

3.2.3. *In vivo* growth and survival of the mutant strain

3.2.3.1. Infectivity and growth within macrophages

The three mycobacterial strains grown in high and low iron media, when added to macrophages showed poor infectivity by the mutant unlike the WT (Fig. 3.10; Panel A). The number of cells recovered from the macrophages 4 h after infection was considered as those that gained entry into the macrophages (and time zero for studying the viability inside macrophages).

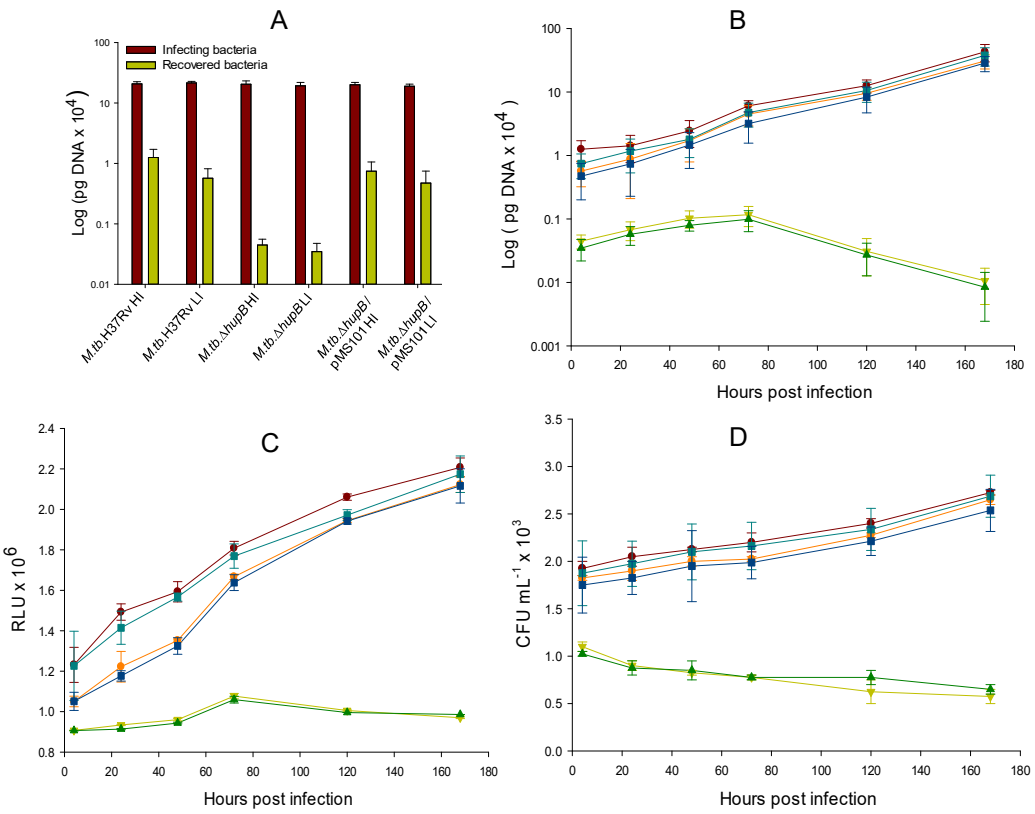

Fig. 3.10. Infectivity and survival of *M.tb*.H37Rv, *M.tb.ΔhupB* mutant and the *hupB*-complemented *M.tb.ΔhupB* / pMS101 strains inside macrophages. 1 x 10^6 cells of mouse peritoneal macrophages (RAW 264.7 cell line), seeded in a 6-well plate were infected with high iron (144 µM Fe) grown *M.tb*.H37Rv (—●—), *M.tb.ΔhupB* (—▼—) and *M.tb.ΔhupB* / pMS101 (—■—) strains and the respective low iron (0.36 µM Fe) grown *M.tb*.H37Rv (—●—) *M.tb.ΔhupB* (—▲—) and *M.tb.ΔhupB* / pMS101 (—■—) at MOI of 10:1. Infectivity of the strains determined by qRT-PCR is shown in panel A. The number of viable bacilli in each of the wells was assayed both by qRT-PCR analysis based on 16S rRNA (Panel B; RLU represents relative light units) and ATP assay (Panel C); this was assayed in triplicate. Two such identical experiments were done for each of the above strains. Panel (D) represents the colony forming units (CFU) by plating on Middlebrook 7H11 plates.

The role of HupB was reflected by the infectivity of the complement strain which was identical to the WT. In addition, the mutant strain could not survive inside the macrophages. This was evident in the number of bacteria recovered from days 0 to 7 as assayed by ATP assay, qRT-PCR and CFU analysis (Fig. 3.10, Panel B, C and D respectively). While both WT and mutant did not show increase in numbers till day 3, the WT strain showed gradual increase in

numbers after the third day with marginal difference seen between high and low iron organisms. The *M.tb.*Δ*hupB* mutant, irrespective of the iron status was unable to survive within the macrophages. The complemented strain behaved like the WT and was able to survive in the macrophages.

3.2.3.2. Increased ROS levels in macrophages infected with *M.tb.ΔhupB*

One of the mechanisms employed by the host cell to contain intracellular bacteria is the production of reactive oxygen species (ROS). The fluorescent dye 2',7'-dichlorodihydrofluorescein diacetate (H_2DCFDA) is a cell-permeant, the reduced form of which is used as an indicator for ROS produced by cells. Upon cleavage of the acetate groups by intracellular esterases and oxidation, the non-fluorescent H_2DCFDA is converted to the highly fluorescent 2',7'-dichlorofluorescein (DCF) that is used for measurement. All the three mycobacterial strains grown in high iron medium induced marginally higher levels of ROS in the macrophages when compared to the respective low iron organisms (Fig. 3.11).

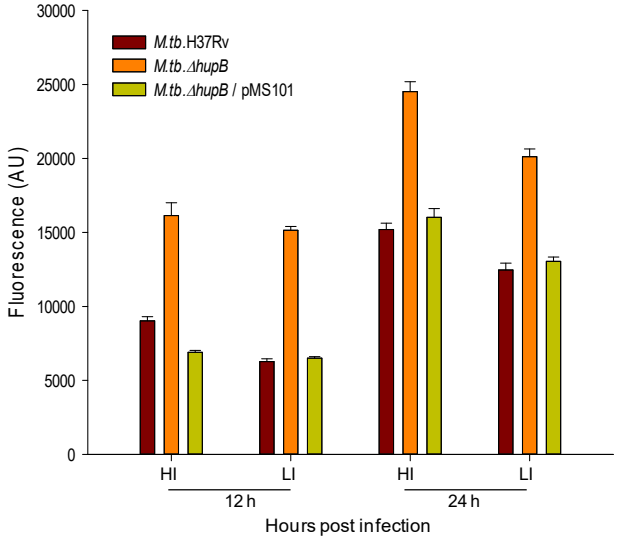

Fig. 3.11. ROS production by RAW 264.7 cells infected with the mycobacterial strains. RAW cells were infected with *M.tb.*H37Rv, *M.tb.ΔhupB* and *M.tb.ΔhupB* / pMS101 grown under high (144 µm Fe; HI) and low (0.36 µM Fe; LI) iron conditions at MOI of 10:1. 10 µM of H_2DCFDA dye was added and the fluorescence was measured 12 h and 24 h post infection in the TECAN Infinite M200 Microplate Reader by exciting at 488 nm and measuring the emitted light at 530 nm. The error bars represent standard deviation calculated from two identical experiments performed in duplicates.

The mutant-infected macrophages, however, irrespective of the iron condition produced approximately 2-fold more ROS compared to *M.tb.*H37Rv and *M.tb.ΔhupB* / pMS101. The findings were identical at 12 and 24 hours, with the overall levels being higher at 24 hours.

3.2.3.3. Up-regulation of ROS-inducing genes of macrophages infected with the mutant

Based on the increased ROS production in the macrophages infected with *M.tb.ΔhupB*, the transcript levels of genes associated with ROS production in the macrophages were evaluated. They included *NOX1* (encoding NADPH oxidases), *NOXA1* (encoding NOX-activating protein) and *NOS2* (encoding nitric oxide synthase). qRT-PCR showed an up-regulation in the transcript levels upon infection with high iron grown organisms compared to low iron (Table 3.1). The transcript levels of *NOX1*, *NOXA1* and *NOS2* were about 4-, 2- and 3-fold higher in macrophages infected with low iron *M.tb.ΔhupB vs* low iron *M.tb.*H37Rv (Fig. 3.12). A similar fold change was observed in the mutant *vs* *hupB*-complemented strain.

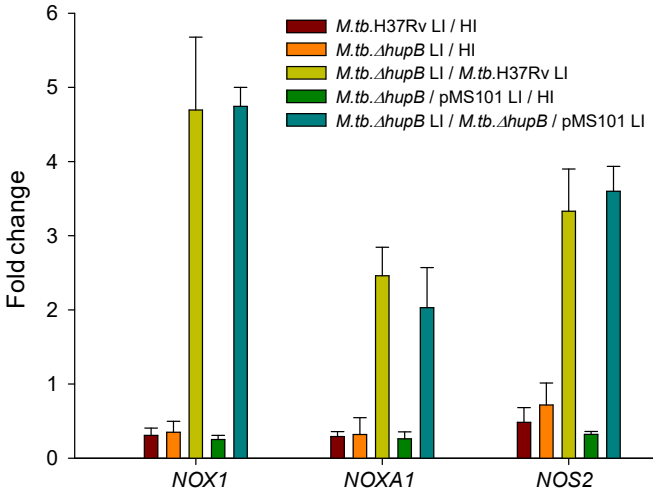

Fig. 3.12. Transcript levels of ROS-inducing genes of macrophages. RAW 264.7 cells were infected with high (144 µm Fe; HI) and low (0.36 µM Fe; LI) iron grown *M.tb.*H37Rv, *M.tb.ΔhupB* and *M.tb.ΔhupB* / pMS101 (MOI 10:1). Total RNA was extracted from the infected macrophages 24 h post infection and qRT-PCR was carried out for *NOX1, NOXA1* and *NOS2* using β-actin as internal control. The error bars represent standard deviation calculated from two identical experiments performed in duplicates.

Table 3.1 Iron-dependent up-regulation of the ROS-inducing genes

Gene	*M.tb.*H37Rv HI *vs* LI	*M.tb.ΔhupB* HI *vs* LI	*M.tb.ΔhupB* / pMS101 HI *vs* LI
NOX1	3.42 ± 1.09	3.14 ± 1.33	4.08 ± 0.91
NOXA1	3.50 ± 0.78	4.22 ± 3.02	4.07 ± 1.45
NOS2	2.26 ± 0.92	1.53 ± 0.63	3.14 ± 0.38

3.2.3.4. Transcript levels of oxidative stress enzymes of mycobacteria

ROS production is an innate immune strategy of the macrophages to control the growth of mycobacteria. To counter this, mycobacteria produces oxidative stress enzymes that quench the free radicals and peroxides either by oxidizing or reducing them. The expression levels of the genes *sodA, ahpC* and *katG* was examined after infection of macrophages. The expression of all the three genes was up-regulated in *M.tb.*H37Rv while it was down-regulated in *M.tb.ΔhupB*. The expression was restored in the complemented strain *M.tb.ΔhupB* / pMS101 (Fig. 3.13; Table 3.2).

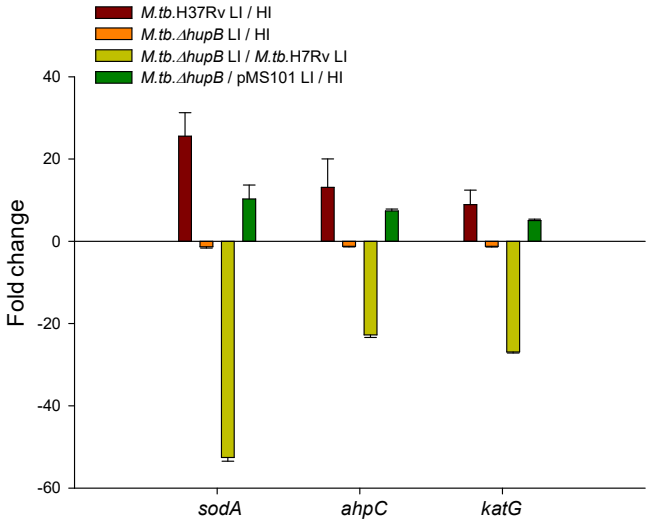

Fig. 3.13. Transcript levels of oxidative stress enzymes of mycobacteria. RAW 264.7 cells were infected with high (144 µm Fe; HI) and low (0.36 µM Fe; LI) iron grown *M.tb.*H37Rv, *M.tb.ΔhupB* and *M.tb.ΔhupB* / pMS101 (MOI 10:1). Total RNA was extracted from the infected macrophages 24 h post infection and qRT-PCR was carried out for *sodA, ahpC* and *katG* using 16S rRNA as internal control. The vertical bars represent the standard deviation of the mean from two independent experiments done in duplicates.

Table 3.2 Fold changes of *sodA, ahpC* and *katG*

Gene (Rv number)	Product	Fold change±SD			
		***M.tb.*H37Rv LI *vs* HI**	***M.tb.ΔhupB* LI *vs* HI**	***M.tb.ΔhupB* LI *vs* *M.tb.*H37Rv LI**	***M.tb.ΔhupB* / pMS101 LI *vs* HI**
sodA (Rv3846)	Superoxide dismutase	25.56 ± 5.69	-1.32 ± 0.32	-52.56 ± 0.89	10.29 ± 3.39
ahpC (Rv2428)	Alkyl hydroperoxide reductase C	13.11 ± 6.91	-1.22 ± 0.13	-22.74 ± 0.64	7.381 ± 0.45
katG (Rv1908c)	Catalase-peroxidase-peroxynitritase T	8.90 ± 3.52	-1.21 ± 0.19	-26.90 ± 0.27	5.042 ± 0.33

3.2.3.5. ChIP assay: influence of HupB on *sodA* and *ahpC*

HupB box was identified at position -47 (CGCGAAAATT) and -38 (AACCAAAATT) respectively of *sodA* and *ahpC* genes and was absent in the promoter DNA of *katG.* ChIP analysis showed approximately 3-fold (*sodA*) and 16-fold (*ahpC*) positive enrichment in *M.tb.*H37Rv low *vs* high iron while no enrichment was observed in the mutant that was identical to the IgG controls (Fig. 3.14).

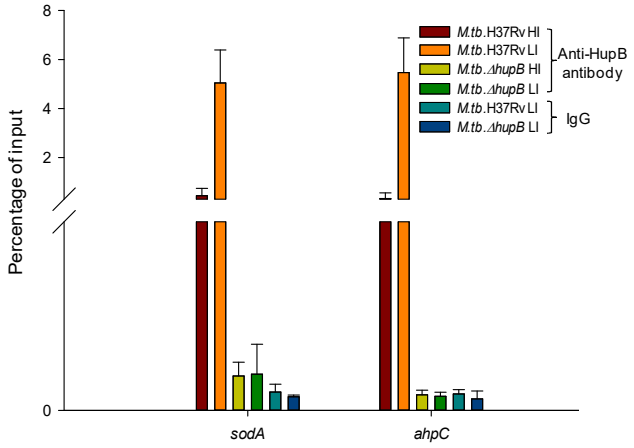

Fig. 3.14. ChIP followed by qRT-PCR analysis of oxidative stress enzymes of mycobacteria. ChIP was carried out using anti-HupB antibodies as detailed in Material and Methods. IgG antibodies were used as control. qRT-PCR was performed using primers designed for the upstream regions of *sodA* and *ahpC*. DNA enrichment was calculated using Percent Input Method. The error bars represent standard deviation calculated from two identical experiments performed in duplicates.

3.2.3.6. *M.tb.ΔhupB* elicits a pro-inflammatory immune response

The expression of pro-inflammatory and anti-inflammatory cytokines from macrophages infected with the three mycobacterial strains grown in iron-regulated media was compared. IFN-γ, TNF-α, IL-1β, IL-4, IL-6, IL-10, IL-12 and IL-18 transcript levels were analysed 24 h post infection (Fig. 3.15). The influence of iron was prominent in cytokine production as the levels of IFN-γ, TNF-α, IL-1β and IL-18 were low for *M.tb.*H37Rv low *vs* high iron while the transcript levels of IL-6, IL-12, IL-4 and IL-10 increased when iron-limited organisms were used for infection. In the mutant low *vs* high iron, only IL-6 showed up-regulation. Low iron grown *M.tb.ΔhupB* elicited significantly higher levels of IFN-γ, TNF-α, IL-1β, IL-12 and IL-18 compared to low iron *M.tb.*H37Rv while the reverse was observed for IL-4, IL-6 and IL-10. The complemented strain behaved similar to the WT.

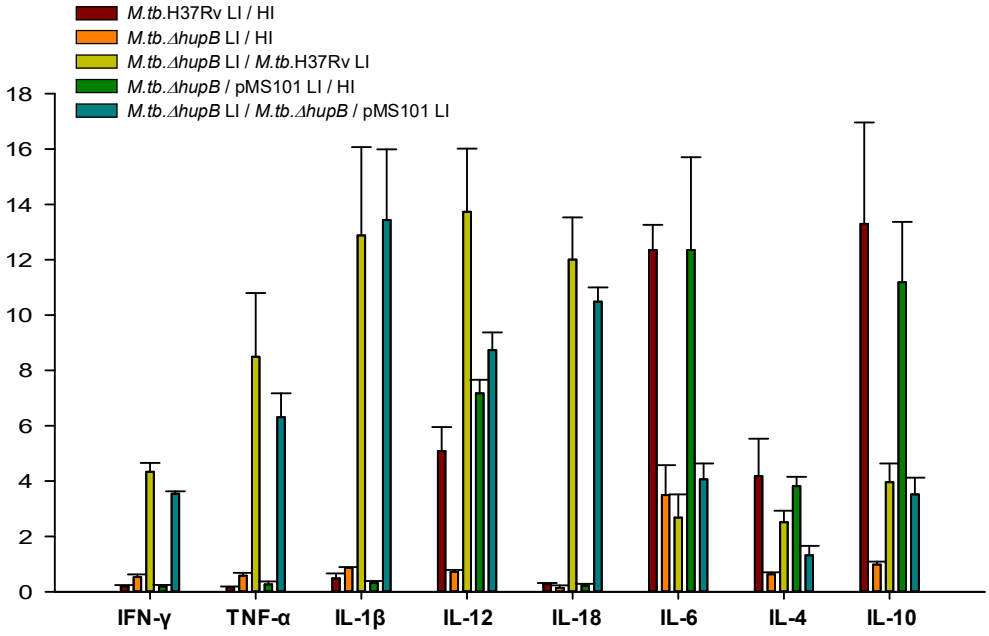

Fig. 3.15. Transcript levels of cytokines induced in macrophages upon infection. RAW 264.7 cells were infected with high (144 μM Fe; HI) and low (0.36 μM Fe; LI) iron grown *M.tb.*H37Rv, *M.tb.ΔhupB* and *M.tb.ΔhupB* / pMS101 (MOI 10:1). Total RNA was extracted from the infected macrophages 24 h post infection and qRT-PCR was carried out for IFN-γ, TNF-α, IL-1β, IL-4, IL-6, IL-10, IL-12 and IL-18 using β-actin as internal control. The error bars represent standard deviation calculated from two identical experiments performed in duplicates.

3.3. Role of HupB as an iron transporter in *M. tuberculosis*

3.3.1. Mutant strain *M.tb.ΔhupB* is defective in uptake of iron

3.3.1.1. Uptake of inorganic ^{55}Fe by WT *M.tb*.H37Rv and *M.tb.ΔhupB* and recovery of the label in mycobactin and carboxymycobactin

When the three strains *M.tb*.H37Rv, *M.tb.ΔhupB* and the *hupB*-complemented *M.tb.ΔhupB* / pMS101 were grown in the presence of inorganic ^{55}Fe supplied at established high (214 μM Fe) and low (0.36 μM Fe) iron concentrations respectively for 6 days, the recovery of the label was measured in iron-replete and iron-limited organisms and was traced in Mb and CMb. In iron replete WT *M.tb*.H37Rv (that does not express HupB) and *hupB* KO mutant, there was poor uptake that explained the low recovery of the label in Mb and CMb (Table 3.3). The complemented strain, constitutively expressing HupB showed increased incorporation in both Mb and CMb as the organisms were able to take up higher levels of iron.

Table 3.3 Recovery of ^{55}Fe in whole cells, Mb and CMb

Strain		Radioactivity in whole cell Mean±SD	% (in whole cells)	Radioactivity in Mb Mean±SD	% (in Mb)	Radioactivity in CMb Mean±SD	% (in CMb)
M.tb.H37Rv	HI	27993.5 ± 690.40	13.20	11560.25 ± 1330.62	5.45	12307.5 ± 1195.03	5.81
	LI	125276.8 ± 3899.53	53.08	74514.25 ± 1264.81	31.57	41485.25 ± 929.32	17.58
	Anti-HupB antibodies	28347.5 ± 1366.16	12.01	13483.75 ± 918.18	5.71	19544 ± 896.85	8.28
	Pre-immune serum	122801.3 ± 883.22	52.03	74560.75 ± 1004.75	31.59	39356 ± 1273.46	16.68
M.tb.ΔhupB	HI	28602.25 ± 906.69	13.49	11103 ± 175.21	5.24	10784 ± 886.78	5.08
	LI	28502 ± 1221.12	12.08	11325.5 ± 874.73	4.79	12014.25 ± 468.31	5.09
	Anti-HupB antibodies	29391.25 ± 711.01	12.45	11463.75 ± 1061.72	4.86	13002.5 ± 1001.94	5.51
	Pre-immune serum	27726 ± 741.28	11.75	11110.5 ± 869.52	4.71	12281.25 ± 822.44	5.20

M.tb.ΔhupB / pMS101	HI	92888 ± 1856.46	43.82	49095 ± 1236.14	23.16	39008.5 ± 1399.51	18.40
	LI	94188.5 ± 541.61	39.91	51855 ± 880.29	21.97	38420.75 ± 735.37	16.28
	Anti-HupB antibodies	27484.5 ± 755.72	11.65	11842.75 ± 1450.04	5.02	20577 ± 640.01	8.72
	Pre-immune serum	94401.5 ± 1286.96	40.00	51417 ± 831.85	21.79	38994.5 ± 762.69	16.52

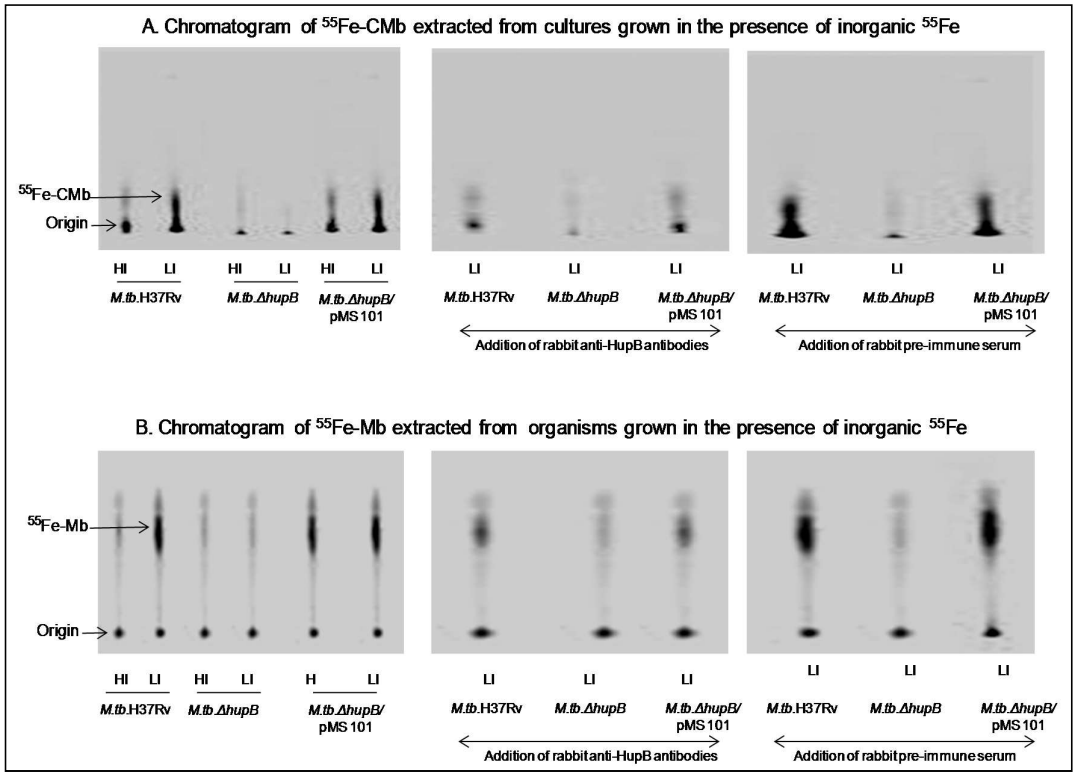

Fig. 3.16. Recovery of ^{55}Fe in Mb and CMb by thin-layer chromatography (TLC). ^{55}Fe-CMb (Panel A) and ^{55}Fe-Mb (Panel B) were subjected to TLC as detailed in Section 2.7.1 and radioactivity was recorded with a Phosphor Imager (BioRad).

When the organisms were grown in low iron medium, the WT *M.tb*.H37Rv effectively acquired iron (53.08%, Table 3.3) with a marked incorporation of the radiolabel into both Mb (31.57%) and CMb (17.58%). The specificity of this uptake can be attributed to HupB as anti-HupB antibodies, unlike the pre-immune serum drastically reduced the label in whole cells and the two siderophores. The role of HupB in uptake of iron was additionally established by the finding that iron-limited *M.tb.ΔhupB* was unable to take up the metal ion and addition of anti-HupB antibodies had no effect as this strain

does not express HupB. ^{55}Fe in the two siderophores, presented in Table 3.3 was also identified by TLC (Fig. 3.16, Panels A and B).

3.3.1.2. *M.tb.ΔhupB* fails to take up ^{55}Fe from ^{55}Fe-CMb

Our earlier studies (Pandey *et al.*, 2014b) established that the *hupB* KO strain *M.tb.ΔhupB* was defective in siderophore biosynthesis. As the low iron uptake in the mutant strain (shown above) could have resulted due to low carboxymycobactin / mycobactin expression, uptake of iron from ^{55}Fe-CMb was done to establish the possible role of HupB as an iron transporter. Fig. 3.17 shows that the mutant strain was unable to take up the metal ion from ^{55}Fe-CMb and there was negligible radioactivity in Mb extracted from these cells. This is in sharp contrast to the iron-limited WT *M.tb.*H37Rv that effectively acquired iron from ^{55}Fe-CMb, with a significant amount recovered in mycobactin. Anti-HupB antibodies inhibited this uptake, an anticipated finding. Similarly, the complemented strain acquired iron from ^{55}Fe-CMb, irrespective of their iron status, with the process inhibited by anti-HupB antibodies.

It was observed that ~80% of the radiolabel was recovered in Mb in the WT *M.tb.*H37Rv upon incubation with ^{55}Fe-CMb for 2 h. Uptake and recovery of iron, when studied every 15 min (Fig. 3.18) showed that there was a steady increase of the radiolabel in Mb that paralleled the uptake by whole organisms for 60 min, after which the amount of the iron incorporated into Mb was relatively less compared to the uptake by whole cells.

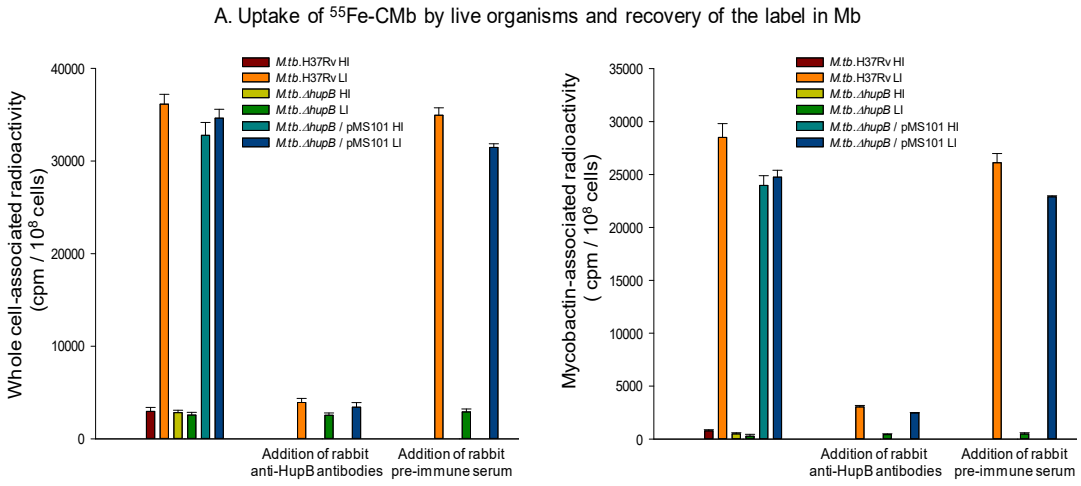

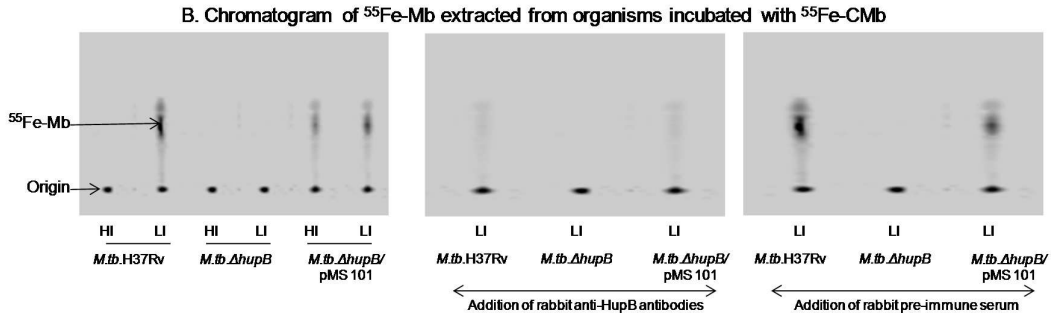

Fig. 3.17. Uptake of ^{55}Fe-CMb and recovery of the label in Mb. The three mycobacterial strains were grown in high (HI) and low (LI) iron media for 9 days. 1 x 10^8 cells / mL were incubated with 1 x 10^5 cpm of ^{55}Fe-CMb at 37°C for 2 h. The radioactivity recovered was measured in whole cells and in Mb in the absence and presence of anti-HupB antibodies. Panel A shows the cpm as measured in a liquid scintillation counter. The error bars represent standard deviation calculated from two identical experiments performed in duplicates. Panel B represents the label in Mb separated by TLC.

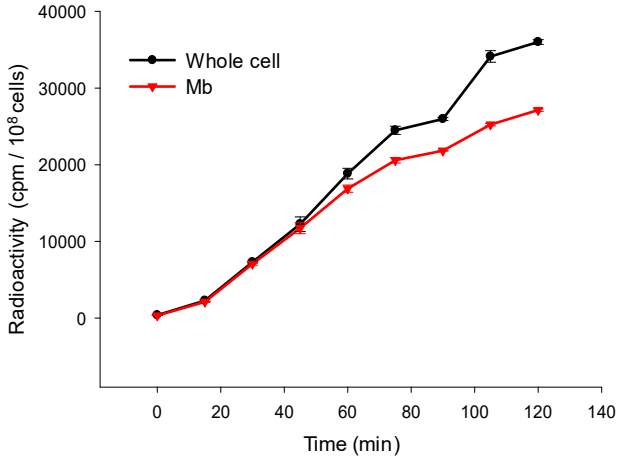

Fig. 3.18. ^{55}Fe from ^{55}Fe-CMb is recovered in Mb in *M.tb.*H37Rv - a time course study. 1 x 10^5 cpm of ^{55}Fe-CMb was added to 1 x 10^8 low iron *M.tb.*H37Rv cells and incubated at 37°C. The radioactivity was measured for 2 h at 15 min intervals in whole cells and Mb. The error bars represent standard deviation calculated from two identical experiments performed in duplicates.

3.3.1.3. ^{55}Fe-CMb uptake by liposomes: role of HupB in iron uptake

To study further the interaction of HupB with Fe-CMb, purified rHupB was incorporated into liposomes (with and without Mb) followed by incubation with ^{55}Fe-CMb. Liposomes prepared with Mb and rHupB showed maximal radioactivity (Fig. 3.19) with the interaction of ^{55}Fe-CMb being considerably less

in liposomes containing only rHupB. The direct transfer of iron from ^{55}Fe-CMb to Mb was ruled out as negligible label was recovered in liposomes containing only Mb.

In addition, the proteo-liposomes prepared from CHAPS-solubilised cell wall preparations of iron-limited WT *M.tb.*H37Rv, unlike that of the *hupB* KO mutant strain showed strong reactivity with ^{55}Fe-CMb (Fig. 3.19).

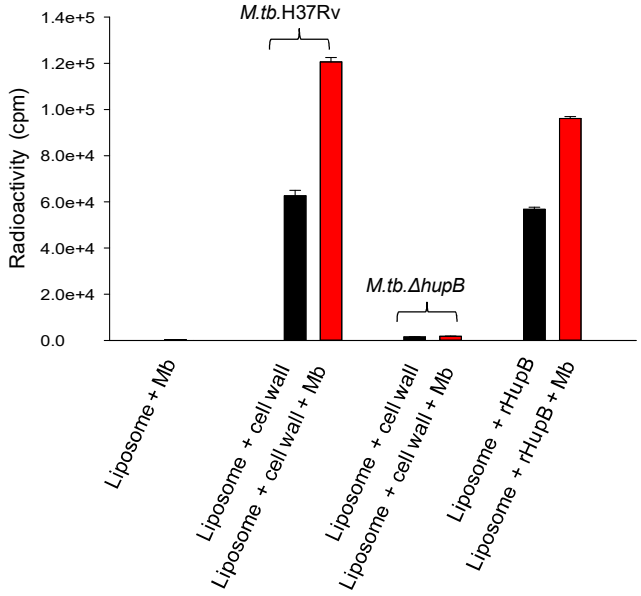

Fig. 3.19. Interaction of ^{55}Fe-CMb with HupB-containing liposomes. The following liposomes were prepared (detailed in Section 2.7.3): a) with desferri-Mb (50 nM), b) 100 µg CHAPS-solubilised cell wall proteins from *M.tb.*H37Rv and *M.tb.ΔhupB* without desferri-Mb, c) same as (b) but with added desferri-Mb, d) purified HupB and e) purified rHupB and desferri-Mb. The proteo-liposomes were incubated with 50 nM (≡1.5 x 10^5 cpm) ^{55}Fe-CMb for 30 min and after suitable washes; radioactivity associated with the liposome was measured. The error bars represent standard deviation calculated from two identical experiments performed in duplicates.

3.3.2. Direct interaction of HupB with mycobactin and carboxymycobactin: *in silico* analysis and ligand-binding studies

3.3.2.1. *In silico* prediction of tertiary structure of HupB

As the crystal structure of the full length (214 aa) HupB is not available, the protein was modeled using I-TASSER (Fig. 3.20, Panel A). The model was validated using PROCHECK server and from the Ramachandran plot generated (Fig. 3.20, Panel B), it is evident that 62.6% of the model was falling in the most

favoured regions, 30.5% in additional allowed regions, 4.8% in generally allowed regions while only 2.1% residues were in the disallowed regions. The model when subjected to refinement using ModRefiner showed no significant improvement. DISOPRED3 showed disorder confidence levels against the sequence positions as a solid blue line (Fig. 3.20, Panel C). The dashed horizontal line (in grey) marks the threshold above which amino acids are regarded as disordered. It was evident that the C-terminus of the protein is disordered from amino acid 100 onwards as the confidence level was found to be very high from the threshold level.

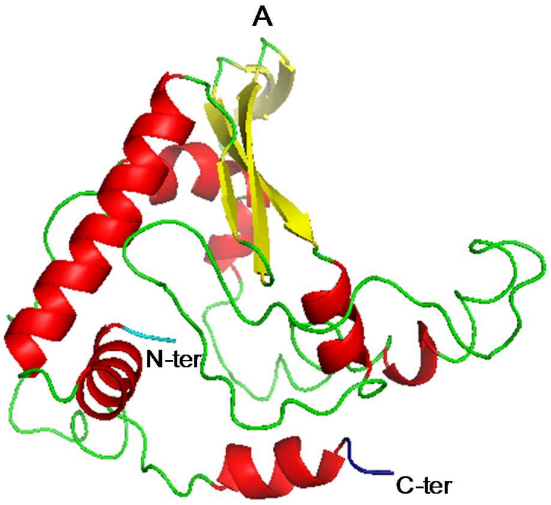

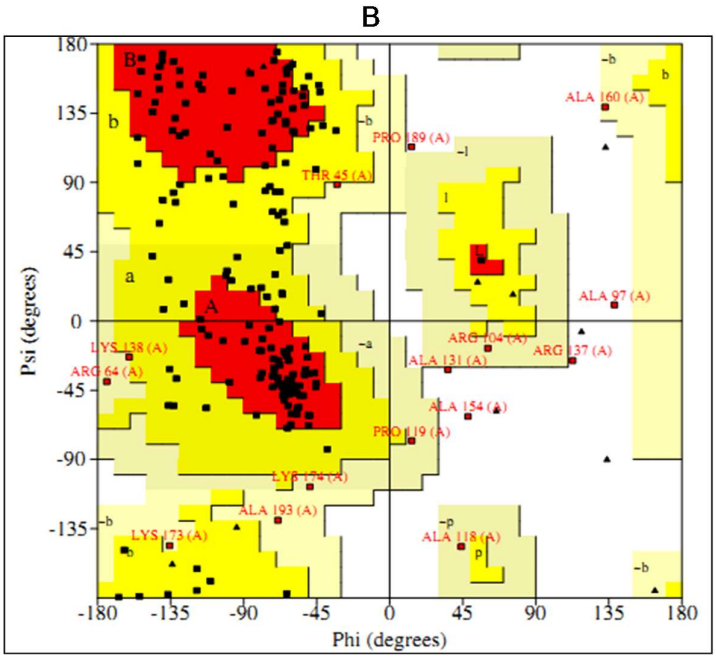

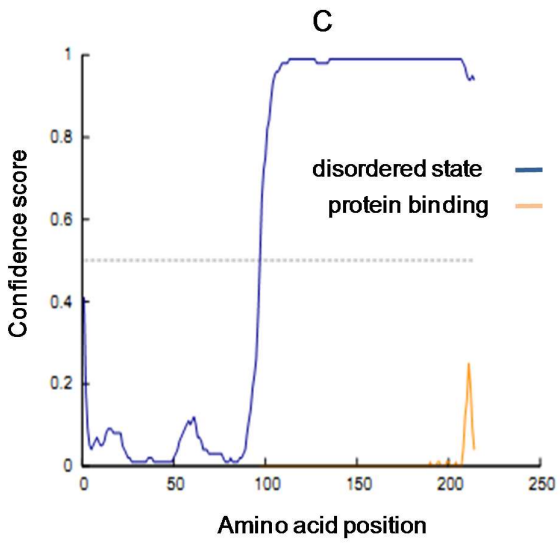

Fig. 3.20. *In silico* modeling of HupB of *M. tuberculosis*. Panel A shows the tertiary structure of full length (214 aa) protein generated using I-TASSER. The α-helices are shown in red, β-sheets in yellow while the loop regions are represented in green. Panel B and C show the Ramachandran plot and the DISOPRED3 analysis data.

3.3.2.2. Docking of Fe-CMb and Fe-Mb to HupB

The modelled HupB was used to study the interaction of the two ferri-siderophores by docking with AutoDock/Vina (Fig. 3.21, Panel A). The mode of binding (Panel B) to Fe-CMb included a combination of H-bonding (Val89, Ser109, Thr141, Thr208 and Lys 205) and hydrophobic interactions (Gly46, Phe47, Phe85, Val88, Leu95, Ala108, Pro100 and Ala140) with Fe-Mb showing predominantly hydrophobic interactions involving Met1, Ile44, Phe47, Phe50, Phe85, Val88, Val89, Leu95, pro100, Ala108, ser109, Thr208, Arg211.

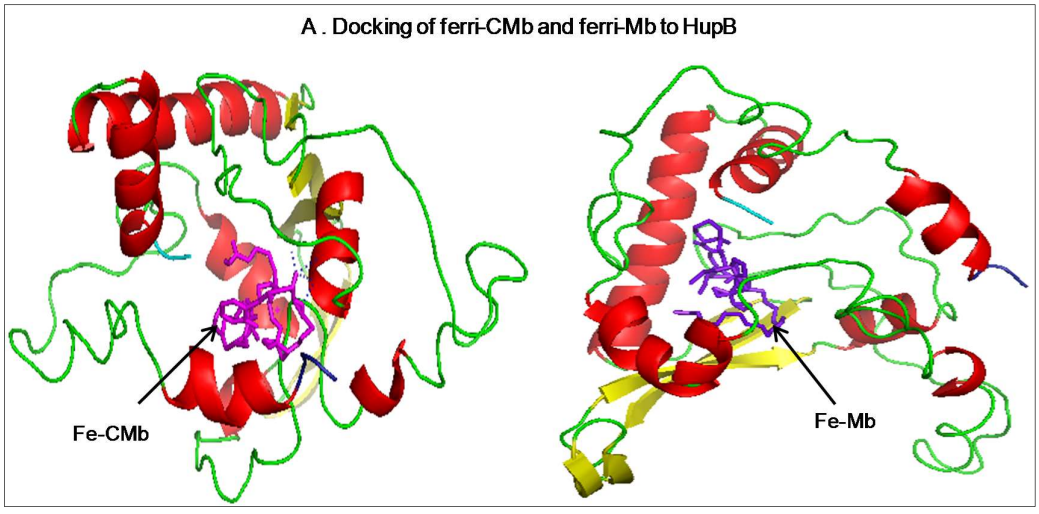

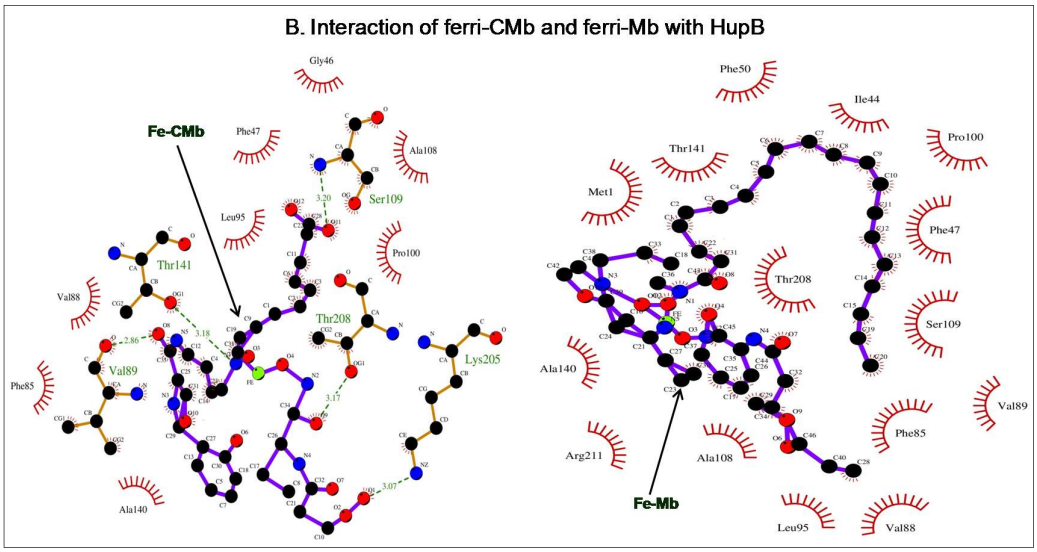

Fig. 3.21. Docking of Fe-CMb and Fe-Mb to HupB. Panel A shows the docking of the three-dimensional structures of Fe-CMb (Fe^{3+}-CMb) and Fe-Mb (Fe^{3+}-Mb) to HupB using Autodock/Vina. Panel B shows the interacting amino acids with HupB where the red arcs with amino acid codes are the residues of the protein interacting with the ligands (the backbone is represented by dots and lines). This analysis was done using LigPlot+.

3.3.2.3. Ligand-binding studies: experimental validation of interaction of ferri-siderophores with HupB

Preparation of rHupB

In our earlier studies, HupB was predominantly obtained as an insoluble protein (Sivakolundu *et al.*, 2013). Here, it was re-cloned into pET22b (+) vector (Fig. 3.22, Panel A) and obtained as a soluble protein (Fig. 3.22, Panel B). The affinity chromatography-purified HupB is shown as a single band by Coomassie blue staining and immunoblot analysis with commercial anti-His and rabbit anti-HupB antibodies respectively.

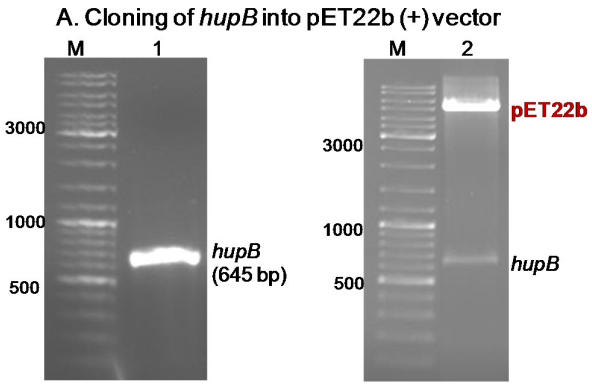

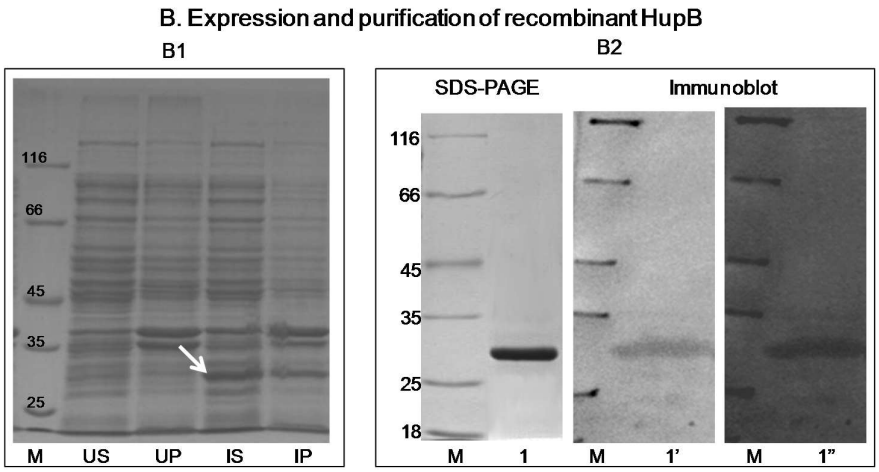

Fig. 3.22. Cloning, expression and purification of rHupB. The full length *hupB* of *M. tuberculosis* was cloned into pET22b (+) vector (Panel A) where lane 1 represents the *hupB* amplicon, lane 2 represents clone confirmation by double digestion with *Bam*HI and *Hin*dIII and M represents the ladder. Panel B shows the expression profile of HupB (B1) and the profile of the purified protein obtained in soluble form (B2). US and UP represent un-induced supernatant and pellet while IS and IP represent IPTG-induced supernatant and pellet. The arrow (white) indicates rHupB in the supernatant. The purified protein was verified by SDS-PAGE (lane 1) and by immunoblotting with rabbit anti-HupB antibody (lane 1') and commercial anti-His antibody (lane 1''). M represents protein molecular weight marker.

3.3.2.4. CD spectral data of HupB-siderophore interaction

Figure 3.23 shows the changes in the spectral data of purified HupB upon interaction with the two ferri-siderophores added at increasing concentrations. At 3 μM of Fe-CMb, HupB showed a positive increase in ellipticity that indicated loss in secondary structure of the protein upon binding with Fe-CMb (Fig. 3.23, Panel A). Notable was the marked change in optical ellipticity upon addition of Fe-Mb at the same concentration, indicating an increase in the ordered secondary structure of the protein (Fig. 3.23, Panel B). It was observed that only the ferric-forms of the two siderophore interacted with the protein, with the desferri-CMb showing poor interaction even at concentrations as high as 50 μM (Fig. 3.23, Panel C).

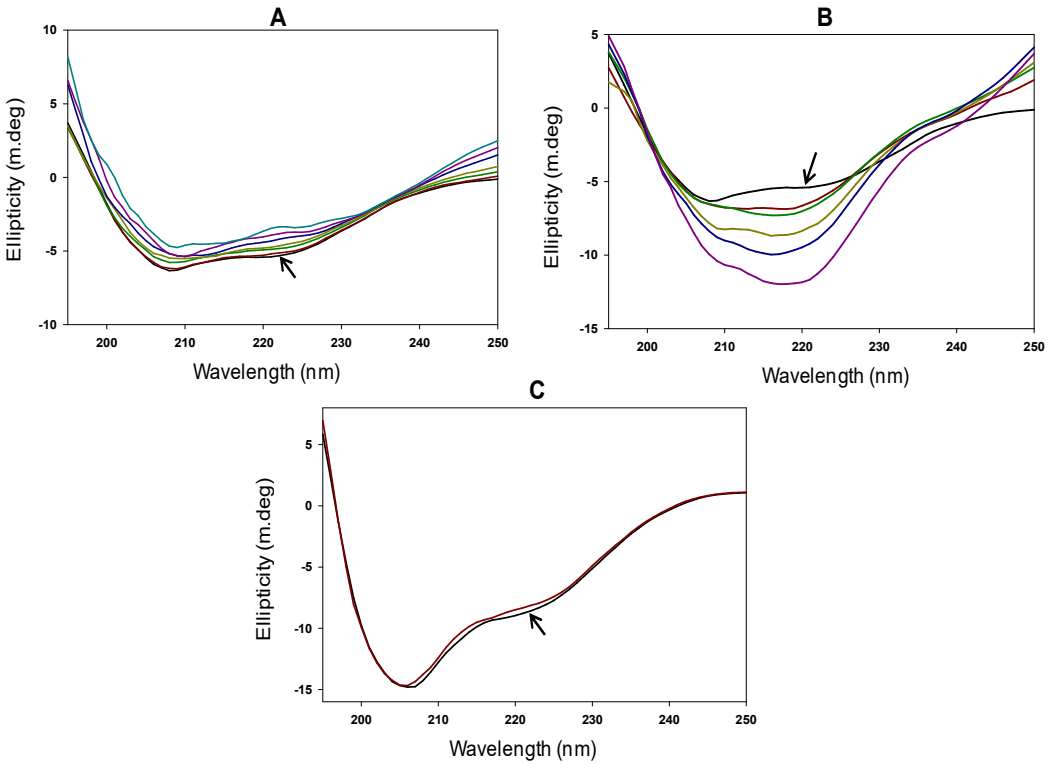

Fig. 3.23. Circular dichroism studies: spectral data of HupB interaction with Fe-CMb and Fe-Mb. Far-UV CD spectra of HupB taken from 250-200 nm is indicated by an arrow. Panels A and B show the CD spectra of HupB in the presence of increasing concentrations of Fe-CMb and Fe-Mb respectively. Panel C shows the spectral data upon addition of desferri-CMb (50 μM).

3.3.2.5. Spectrofluorimetry: equilibrium titrations and determination of Kd values of HupB: Fe-CMb and HupB: Fe-Mb interactions

When Fe-CMb was added to HupB and subjected to spectrofluorimetry, the intensity of the emitted light increased (Fig. 3.24, Panel A) and was accompanied by a shift from 320 nm to 314 nm (blue shift), indicative of ligand-receptor interaction. While an increase in the fluorescence was seen in the presence of Fe-Mb (Panel B), it was not as appreciable as seen with Fe-CMb and no spectral shift was seen. When desferri-CMb was used as the ligand molecule, no appreciable changes were seen at low concentrations of the added ligand and a decrease in fluorescence was noted at high concentrations of the desferri-siderophore.

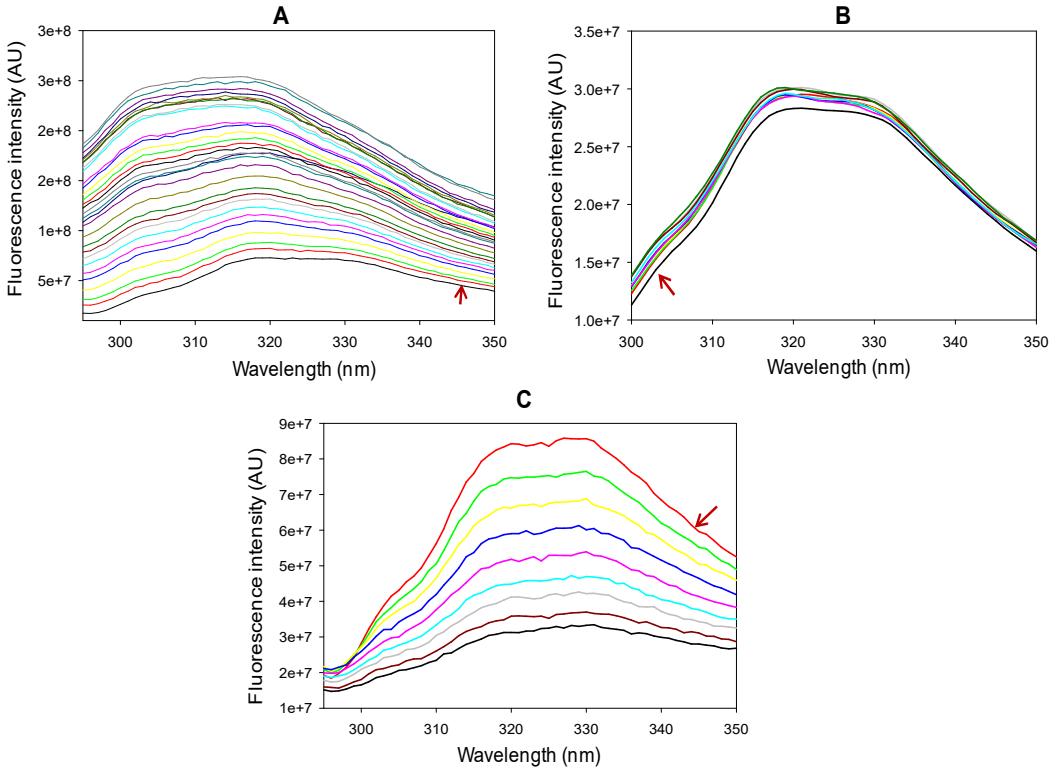

Fig. 3.24. Spectrofluorimetric analysis of the interaction of HupB with Fe-CMb and Fe-Mb. HupB was taken at a concentration of 1.63 μM and the emission spectrum was recorded from 300-350 nm; the red arrow shows the spectrum of the purified protein. Panels A and B show the spectral changes upon addition of Fe-CMb and Fe-Mb respectively. The former was added as 0.5 μM aliquots to a maximum concentration of 15 μM and Fe-Mb was added as 2 μM aliquots to a maximum of 30 μM. Panel C shows the spectral changes in HupB upon addition of high concentrations of desferri-CMb (50 μM aliquots to a maximal concentration of 350 μM).

Using the data points at 318 nm, the binding constants were determined using two methods. When the binding isotherms were plotted and fitted to a One-binding site model using non-linear least square method and by Scatchard plot analysis (Fig. 3.25, Panel B), it was apparent that both Fe-CMb and Fe-Mb showed moderate binding affinity to HupB with K_d values of 22.42 μM and 38.76 μM respectively. The desferri-CMb exhibited a very weak binding (K_d = 769 μM).

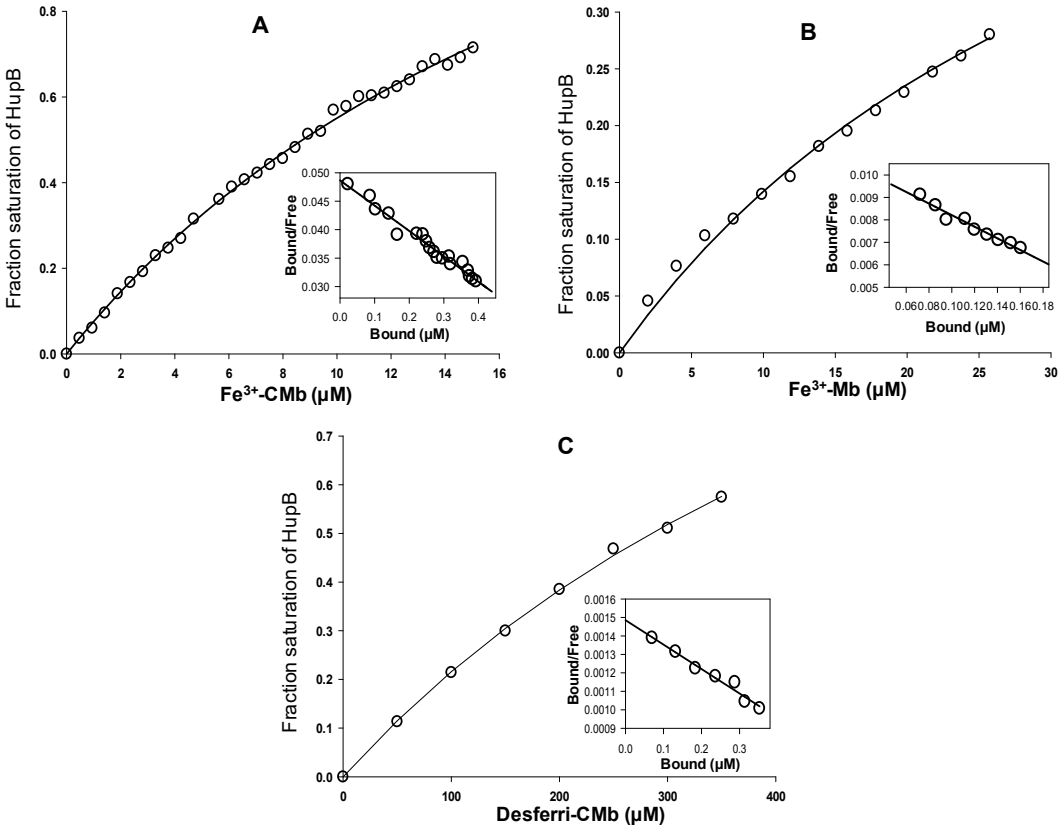

Fig. 3.25. Determination of the binding constants of HupB interactions with the ferri-siderophores. The binding constants were calculated using both One-binding site model and Scatchard plot (inset) using the data points at 318 nm.

3.3.3. Validation of microarray analysis by ChIP assay: influence of HupB on the transcript levels of *mmpL5, mmpS5, irtA* and *eccA3*

Microarray analysis of the *hupB* KO mutant showed that several genes (listed in Table 3.4) associated with siderophore export and uptake were down-regulated (Pandey *et al.*, 2014b). Here, ChIP assay followed by qRT-PCR analysis for the genes *mmpL5, mmpS5, irtA* and *eccA3* (latter is part of ESX machinery shown in Table 3.4) showed a positive enrichment for low iron *vs* high iron *M.tb.*H37Rv; the IgG controls showed no enrichment. None of these genes showed enrichment in the *hupB* KO mutant strain, with values being identical to the IgG controls (Fig. 3.26). The sequence and location of the HupB box with reference to the start site and the fold difference in enrichment in *M.tb.*H37Rv low *vs* high iron is given in Table 3.5.

Table 3.4 Microarray analysis of the differential expression of genes in *M.tb.ΔhupB*

Gene / Rv number	Fold change (expression of mRNA)		Gene product
	WT LI / HI*	Mutant LI / WT LI*	
Genes involved in export of siderophores			
mmpL5 / Rv0676c	2.7267	-3.1554	Probable conserved transmembrane transport protein MmpL5
mmpS5 / Rv0677c	1.7504	-3.2452	Possible conserved membrane protein MmpS5
mmpL4 / Rv0450c	0.6817	-1.4021	Probable conserved transmembrane transport protein MmpL4
mmpS4 / Rv0451c	1.4026	-1.5491	Possible conserved membrane protein MmpS4
Genes involved in uptake of siderophores			
irtA / Rv1348	3.8448	-2.3819	Iron-regulated transporter IrtA
irtB / Rv1349	3.7224	-2.2015	Iron-regulated transporter IrtB
ESX-3 secretion system involved in siderophore-mediated iron uptake			
$eccA_3$ / Rv0282	1.7543	-1.3680	ESX conserved component EccA3. ESX-3 type VII secretion system protein
$eccB_3$ / Rv0283	1.5827	-1.9801	ESX conserved component EccB3. Possible membrane protein
$eccC_3$ / Rv0284	1.8809	-1.6310	ESX conserved component EccC3. Possible membrane protein
$espG_3$ / Rv0289	1.7913	-2.7083	ESX-3 secretion-associated protein EspG3
$eccD_3$ / Rv0290	1.9662	-2.9816	ESX conserved component EccD3. Probable transmembrane protein
$eccE_3$ / Rv0292	1.7946	-2.3291	ESX conserved component EccE3. Probable transmembrane protein

*LI and HI represent organisms grown in low and high iron media respectively

Table 3.5 Interaction of HupB with the promoter region of *mmpL5, mmpS5, irtA* and *eccA3*: location of HupB box and interactions in ChIP assay

Upstream region of the gene	Putative HupB-binding motif	Location of HupB box	Mismatch	Fold difference *M.tb.*H37Rv LI *vs* HI
	Consensus sequence: 5'-CACTAAAATT-3'			
mmpL5	TACTGAAATC	-19	3	8
mmpS5	CTCTGAAATC	-71	3	7
irtA	CCCTTAGATT	-199	3	3
eccA3	CTCAAAGCTT	-109	4	15

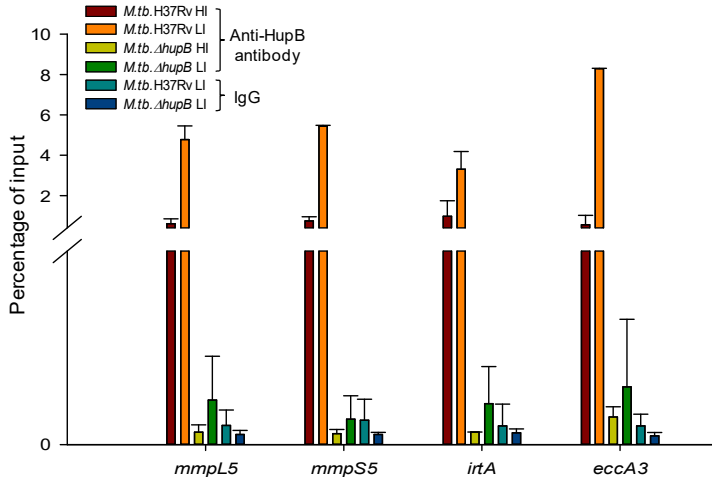

Fig. 3.26. ChIP followed by qRT-PCR analysis of *mmpL5, mmpS5, irtA* and *eccA3*. ChIP was carried out using anti-HupB antibodies for pull down of HupB-regulated genes; IgG antibodies were used as control. qRT-PCR was performed using primers designed for the upstream regions of *mmpL5, mmpS5, irtA* and *eccA3*. DNA enrichment was calculated using Percent Input Method. The error bars represent standard deviation calculated from two identical experiments performed in duplicates.

3.4. Altered lipid profile in *hupB* KO mutant strain of *M. tuberculosis*

Altered colony morphology and low transcripts of gene products associated with different lipid biosynthetic pathways in the *hupB* KO mutant (Pandey *et al.*, 2014) led us to analyze the role of HupB in the expression of some of these genes. Two approaches were made, namely to quantitate the various lipid levels and secondly to perform ChIP assay to study if HupB played any regulatory role on the expression of the genes reflected in the microarray analysis. The different lipids including fatty acids, mycolic acids, phthiocerol

dimycocerosate (PDIM), sulpholipid-1 (SL-1), diacyl trehalose (DAT), penta-acyl trehalose (PAT) were quantitated after extraction from the respective strains using established protocols as mentioned in Materials and Methods (Section 2.8). The role of HupB in the transcriptional regulation of the genes involved in the biosynthesis of these lipids was ascertained by first identifying HupB box in the upstream region of the genes followed by chromatin immunoprecipitation and qRT-PCR.

3.4.1. Extraction and analysis of lipids from the mutant and WT mycobacterial strains

3.4.1.1. Fatty acids

The levels of fatty acids in *M.tb.ΔhupB* showed a decrease in tetradecanoic (14:0; 1.7-fold), palmitic (16:0; 2-fold) and tuberculostearic (18:0-10Me; 2.5-fold) acids and increase in stearic (18:0; 1.6-fold) acid; the long chain fatty acid arachidic acid (20:0) was present only in the mutant. The mutant had a greater proportion of long chain unsaturated fatty acids such as oleic acid (18:1 ω9c; 1.2-fold), cis-vaccenic acid (18:1 ω7c; 2.4-fold) and linoleic acid (18:2 ω6,9c; 2.3-fold) and interestingly showed the expression of three unique fatty acids, 15:0 (pentadecylic acid), 17:0 (margaric acid; 4.4-fold) and 17:1 ω8c (margaroleic acid) (Fig. 3.27).

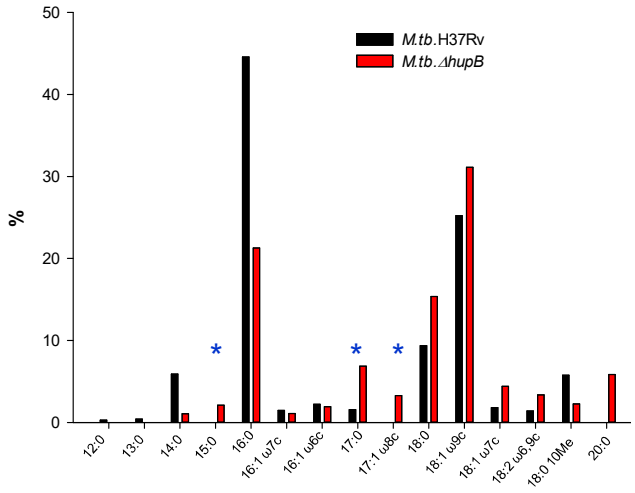

Fig. 3.27. Fatty acid profiling of *M.tb.*H37Rv and *M.tb.ΔhupB* using GC-MS. Fatty acids were extracted from log-phase cultures of *M.tb*.H37Rv and *M.tb.ΔhupB* grown in low iron medium (0.36 μM Fe) as described in Materials & Methods. Fatty acid profiling was performed commercially (Royal Life Sciences, Hyderabad) by GC-MS. The unique fatty acids are indicated by an asterisk (*).

3.4.1.2 Mycolic acids

Fig. 3.28 shows the mycolic acid profile of the WT and the *hupB* KO mutant strains, as analyzed by TLC. While all the three forms of mycolic acid namely α-, methoxy- and keto-mycolates were expressed by both strains, their levels were relatively lower in the mutant strain.

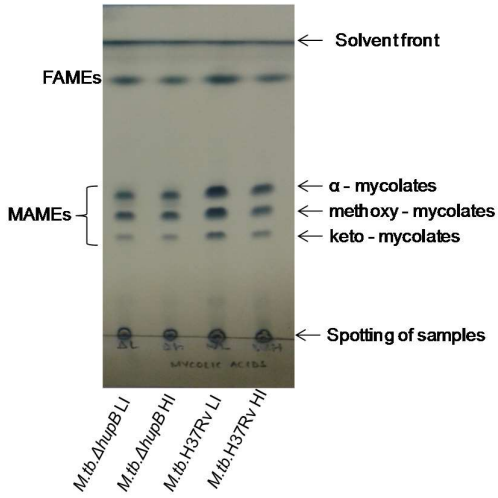

Fig. 3.28. TLC of mycolic acids extracted from the mycobacterial strains. The mycolic acids were extracted from log-phase cultures of *M.tb.*H37Rv and *M.tb.ΔhupB* grown under high (144 µm Fe; HI) and low (0.36 µM Fe; LI) iron conditions. Equal concentrations of the above extract were loaded on the TLC plate and separated using hexane: ethyl acetate (95: 5) as the solvent system. Fatty acid methyl esters (FAME) are also separated along with the mycolic acids.

3.4.1.3. Non-polar lipids: SL-1, PDIM, DAT and PAT

The non-polar lipids include the SL-1, PDIM, DAT and PAT that were extracted using specific solvents as reported in established protocols (Camacho *et al.*, 2001; Slayden & Barry, 2001). TLC (Fig. 3.29) of the different lipids showed that SL-1 and DAT (Panel A), PAT (Panel B) and PDIM (Panel C) were relatively less in *M.tb.ΔhupB* compared to the WT *M.tb.*H37Rv. It was also observed that these lipids were expressed in relatively higher levels in iron-limited WT *M.tb.*H37Rv when compared to the respective iron-replete organisms. The “cord factor” trehalose dimycolate (TDM) was also separated along with SL-1 and DAT as the solvent system chloroform: methanol: water (90:10:1) has been shown to separate TDM (Habermehl, 2012). PAT and an unknown lipid were identified with the solvent system petroleum ether: acetone (92:8) while the solvent system hexane: ether (9:1) separated only PDIM.

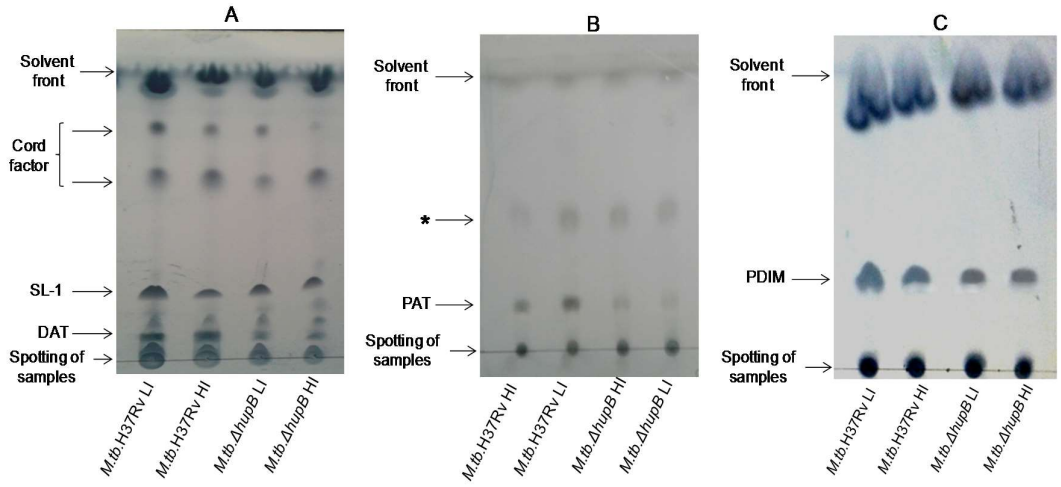

Fig. 3.29. TLC of non-polar lipids extracted from *M.tb.*H37Rv and *M.tb.ΔhupB*. The non-polar lipids were extracted using methanol and petroleum ether from log-phase cultures of *M.tb.*H37Rv and *M.tb.ΔhupB* grown under high (144 µm Fe; HI) and low (0.36 µM Fe; LI) iron conditions. The lipid extract were collected in pre-weighed tubes and the weight of the lipid residues were determined. The residues were dissolved in methylene chloride to obtain samples of equal concentration. They were then subjected to TLC plate using the respective solvent systems as mentioned in Materials and Methods. Unknown lipid is indicated with *.

3.4.2. Identification and functionality of HupB box upstream of genes associated with lipid biosynthesis

Microarray analysis of the *hupB* KO mutant showed that several genes (listed in Table 3.6) associated with the biosynthesis of mycolic acids and surface exposed lipids were down-regulated (Pandey *et al.*, 2014b). Bioinformatic analysis identified the 10 bp HupB box upstream of several genes whose translated products are associated with lipid biosynthetic pathways as shown in Table 3.7.

When the functionality of the HupB box was analyzed by ChIP assay and qRT-PCR, there was positive enrichment for several of the genes listed in Table 3.8 for low iron *vs* high iron *M.tb.*H37Rv when anti-HupB antibodies were used in the assay as compared with the normal IgG controls. In the *hupB* KO mutant that does not express HupB, there was no such enrichment and the findings were identical to the IgG controls (Fig. 3.30), implicating HupB as a transcriptional regulator protein (Table 3.7).

Table 3.6. Microarray analysis of *M.tb.ΔhupB*: altered mRNA transcripts of genes involved in lipid biosynthesis

Gene / Rv number	Fold change (expression of mRNA)		Gene product
	WT LI / HI*	Mutant LI / WT LI*	
Mycolic acid			
fas / Rv2524c	0.7840	-1.6226	Probable fatty acid synthase Fas
fabD / Rv2243	0.0473	-1.5877	Malonyl-CoA:ACP transacylase
acpM / Rv2244	-0.1468	-1.1639	Meromycolate extension acyl carrier protein AcpM
kasA / Rv2245	0.2245	-1.1389	β-Ketoacyl-ACP synthase
kasB / Rv2246	-0.0020	-1.3654	β-Ketoacyl-ACP synthase
accD6 / Rv2247	0.0362	-1.4215	Acetyl/propionyl-CoA carboxylase (beta subunit) AccD6
inhA / Rv1484	0.1035	-1.1285	NADH-dependent enoyl-ACP reductase
pks13 / Rv3800c	-0.1810	-1.0941	Polyketide synthase-13
fabD32 / Rv3801c	-0.2145	-1.0016	Fatty-acid-AMP ligase FadD32
SL-1			
pks2 / Rv3825c	0.2837	-1.6915	Polyketide synthase Pks2
papA1 / Rv3824c	0.0802	-1.6008	Polyketide synthase associated protein PapA1
mmpL8 / Rv3823c	0.1924	-1.3525	Transmembrane transport protein
PDIM			
fadD26 / Rv2930	0.6015	-0.3592	Fatty-acid-AMP ligase FadD26
fadD28 / Rv2941	-0.2980	-1.1337	Fatty-acid-AMP ligase FadD28
drrC / Rv2938	0.0080	-0.6557	Integral membrane protein ABC transporter DrrC
DAT and PAT			
papA3 / Rv1182	-0.3505	-4.6442	Polyketide synthase associated protein PapA3

pks4 / Rv1181	-0.2466	-2.8671	Polyketide synthase-4
chp2 / Rv1184c	-0.2872	-1.2988	Acyltransferase
mmpL10 / Rv1183	0.2518	-2.7384	Transmembrane transport protein

*LI and HI represent organisms grown in low and high iron media respectively

Table 3.7 Location of HupB box in the promoter regions of genes associated with lipid biosynthesis and validation of the functionality of the HupB box by ChIP / qRT-PCR

Gene (Rv number)	HupB box			Fold difference WT LI / HI	Fold difference WT LI / mutant LI
	Sequence	**Location**	**Mismatch**		
	Consensus sequence: 5'-CACTAAAATT-3'				
Mycolic acid					
fabD (Rv2243)	TACAAAAACC	-73	4	30	670
kasA (Rv2245)	CGCGAAGATT	-69	3	27	543
inhA (Rv1484)	CGCTGCAATT	-158	3	9	227
pks13 (Rv3800c)	CATCAAGATT	-179	3	10	873
fadD32 (Rv3801c)	CCTTAACATT	-76	3	36	822
SL-1					
papA1 (Rv3824c)	CACTAGAGCT	-201	3	5.5	241
mmpL8 (Rv3823c)	CACGTAAATT	-76	2	14	242
PDIM					
fadD26 (Rv2930)	CAATAAACTT	-121	2	30	450
fadD28 (Rv2941)	CGGTAACGTG	-199	5	20	306
drrC (Rv2938)	CGTTAAAGTT	-32	3	19	202

DAT and PAT					
papA3 (Rv1182)	CACAAAGATC	-131	3	6	580
pks4 (Rv1181)	CAGTCGAGTT	-106	4	12	421
chp2 (Rv1184c)	GACTAAGATA	-34	3	11	549
mmpL10 (Rv1183)	CGCTGAAGTC	-105	4	14	435

The location of the HupB box sequence is with reference to the start site; Mismatch from the 10 bp HupB-binding motif in the *mbtB* promoter DNA

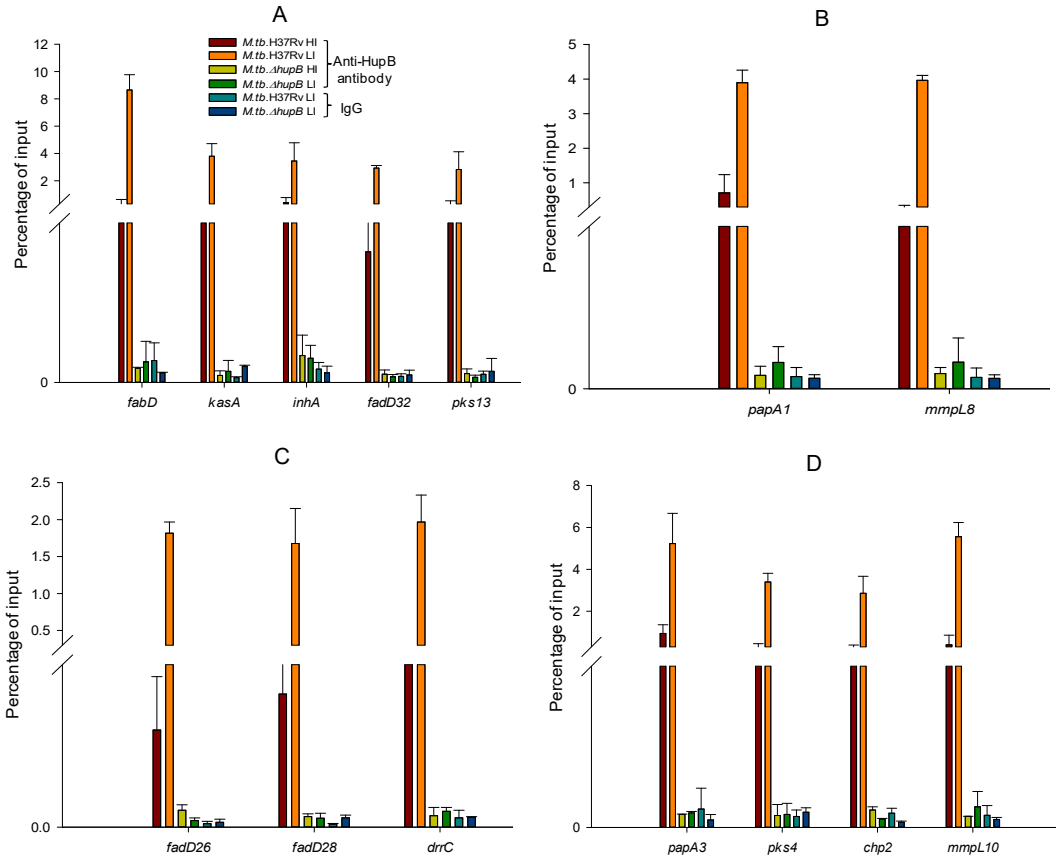

Fig. 3.30. ChIP followed by qRT-PCR analysis of genes involved in the biosynthesis of mycolic acids, SL-1, PDIM, DAT and PAT. ChIP was carried out using anti-HupB antibodies for pull down of HupB-regulated genes from the genomic DNA of WT *M.tb.*H37Rv and the mutant *M.tb.ΔhupB*; IgG antibodies were used as control. qRT-PCR was performed using primers designed for the upstream regions of mycolic acid synthesis genes *fabD, kasA, inhA, fadD32* and *pks13* (Panel A), SL-1 biosynthesis genes *papA1* and *mmpL8* (Panel B), PDIM biosynthesis genes *fadD26,*

fadD28 and *drrC* (Panel C), DAT and PAT biosynthesis genes *papA3, pks4, chp2 and mmpL10* (Panel D). DNA enrichment was calculated using Percent Input Method. The error bars represent standard deviation calculated from two identical experiments performed in duplicates.

3.5. Clinical significance of HupB

3.5.1. Cell-mediated and humoral immune response of TB patients to HupB

3.5.1.1. Demographic data

Table 3.8 shows the demographic data of the 83 TB patients and 30 healthy controls. Alcohol and tobacco abuse were commonly seen in male subjects. The PTB cases included 36 newly diagnosed cases and 24 cases of defaulters of previously initiated anti-tubercular therapy (ATT) who presented with symptoms of the disease. The former included 39% cases who had not started ATT while the others were in their initial stages of medication (not more than one month). The EPTB cases comprised of 20 pleural effusion cases, 2 lymphadenitis cases and 1 ophthalmic Koch.

Table 3.8 Demographic data of the study groups

S. No.	Group	Sample size (n)	Age (years)	Sex		AFB positivity	
				Male	Female	(+)	(-)
1.	Pulmonary TB (PTB)*	60	38.2 ± 13.71	51	9	49	11
2.	Extrapulmonary TB (EPTB)	23	28.48 ± 12.94	15	8	2	21
3.	Healthy controls	30	26.43 ± 3.53	25	5	ND	

*Three cases of miliary TB were included in this group (as per WHO guidelines)

ND= Not determined

3.5.1.2. Immunoproliferative response of PBMCs of TB patients to HupB

There was a statistically significant higher proliferative response of the PBMCs of TB patients *vs* healthy controls to HupB (Fig. 3.31, Panel A) compared to PPD, particularly in EPTB cases (P = 0.0001). Table 3.9 summarizes the mean stimulation index (SI) and ROC curves of the HupB-mediated immune-

proliferation of the PBMCs of TB patients and healthy controls. HupB elicited maximal proliferation in EPTB patients (mean SI of 3.653±0.55), higher than that seen in the PTB group (mean SI of 3.194±1.08), with a three-fold lower SI in the healthy controls that complement our previous reports of HupB as a marker in EPTB (Sivakolundu *et al.*, 2013; Sritharan *et al.*, 2015). With the conventionally used PPD, a lower SI was seen that was almost identical in both the TB groups. Based on the sensitivity and specificity, the performance of HupB was superior to PPD (Table 3.10). The mitogen ConA elicited the anticipated higher proliferation of the PBMCs of both patients and healthy controls (Fig. 3.31, Panel B).

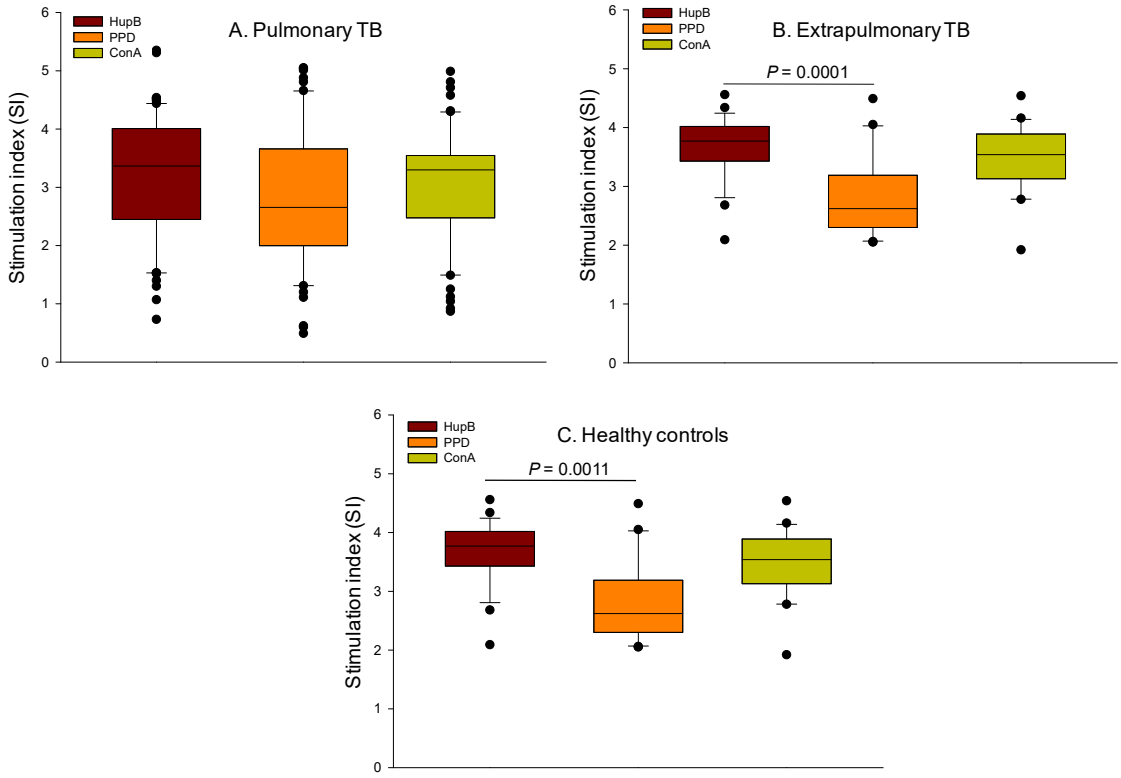

Figure 3.31. Proliferation of PBMCs of TB patients and healthy controls to HupB, PPD and ConA. The reaction set-up is as described in Section 2.9.1.4. The experiments were done in triplicates. The figure shows Tukey box plots drawn to represent the stimulation index (SI) of pulmonary TB (Panel A), extrapulmonary TB (Panel B) and healthy controls (Panel C) to the antigens HupB, PPD and the mitogen ConA. The box boundaries display the median and inter-quartile ranges; whiskers display the maximum and minimum values excluding the outliers (shown as points). The threshold for significance was set at P<0.05.

Table 3.9 T cell proliferation of PBMCs of PTB and EPTB patients to HupB

Antigen	Stimulation index mean±SD			Area under the ROC curve					
	PTB	EPTB	HC	AUC	SE	95% CI		% Sensitivity	% Specificity
HupB	3.194 ± 1.08	3.653 ± 0.55	1.378 ± 0.26	0.892	0.0358	0.766	0.97	81.71	96.77
PPD	2.830 ± 1.20	2.792 ± 0.67	1.643 ± 0.38	0.781	0.0468	0.693	0.853	70.89	85.29

PTB: pulmonary TB; EPTB: extrapulmonary TB; HC: healthy controls; AUC: area under the curve; SE: standard error; CI: confidence interval. The significance threshold was set at P<0.0001. The mean SI obtained with the mitogen ConA was 3.068±1.00, 3.465±0.57 and 3.248±0.49 respectively when added to PBMCs from PTB, EPTB and HC subjects.

3.5.1.3. Cytokine profile

The HupB-treated PBMCs of TB patients showed statistically significant differences in the levels of several cytokines when compared to healthy controls (Fig. 3.32). Their IFN-γ (Panel A) levels were low, with the median [interquartile range (IQR)] being 122.5 [110.5–135] pg / mL in PTB cases and 151.0 [113.0-184] pg / mL for EPTB cases; the median value in healthy controls was 228.5 [190.3-276.3] pg / mL. The TNF-α (Panel B) levels in the EPTB group was notably high with a median value of 1239 [593.5 - 2015] pg / mL when compared to 749.5 [590.3 - 896.5] pg / mL obtained with the healthy control group; the PTB group showed the least median value of 458.0 [278 - 811] pg / mL. Both IL-6 (Panel C) and IL-8 (Panel D) were high in the two patient groups, with the former reaching median [IQR] = 20642 [19733 - 21463] pg / mL in PTB group and median value of 21251 [20354 - 22123] pg / mL in the EPTB group as against the median value of 17456 [16807-17872] pg / mL in the healthy controls. Similarly, IL-8 showed median values of 9276 [8912 - 9610] pg / mL in PTB group and 9319 [9119 - 9501] pg / mL in the EPTB cases as compared to 8658 [8260 - 8796] pg / mL in the healthy controls.

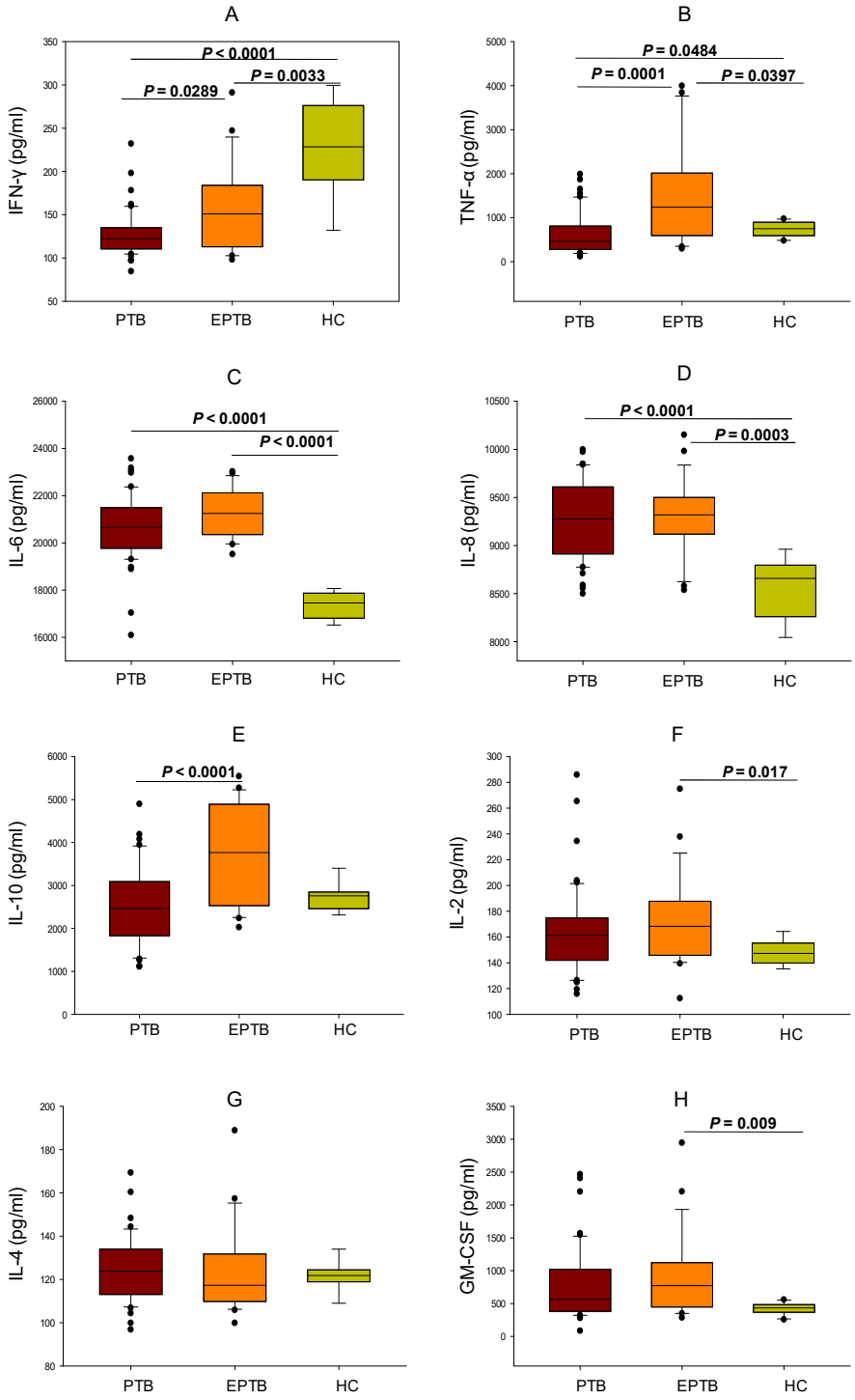

Figure 3.32. Cytokine profile upon stimulation of PBMCs of TB patients with HupB. The culture supernatants of the PBMCs stimulated with HupB were assayed as detailed in Materials and Methods. The Tukey box plots representing the levels of IFN-γ (Panel A), TNF-α (Panel B), IL-6 (Panel C), IL-8 (Panel D), IL-10 (Panel E), IL-2 (Panel F), IL-4 (Panel G) and GM-CSF (Panel H) expressed by PTB (n=50), EPTB (n=23) and HC (n=9) are shown where the box boundaries display the median and

inter-quartile ranges; whiskers display the maximum and minimum values excluding the outliers (shown as points). The threshold of significance was set at P<0.05.

Interestingly, EPTB group showed the maximal amounts of IL-10 (Panel E) upon stimulation with HupB, with a median value of 3768 [2530 - 4893] pg / mL). The value was comparatively lower in PTB cases (median value of 2295 [1641-3044] pg / mL) with the healthy controls showing a median value of 2760 [2460 - 2848] pg / mL). IL-2 (Panel F) and IL-4 (Panel G) levels were identical in the patient and the control groups. GM-CSF (Panel H) levels were elevated in both the patient groups, with the EPTB cases, median 771.3 [446.8 - 1121] pg / mL producing relatively higher levels than the PTB subjects (median = 564.8 [379.8 - 1021] pg / mL as compared to 433.1 [366.2 - 484.4] pg / mL expressed by the healthy controls.

3.5.1.4. Pro-inflammatory and anti-inflammatory cytokine ratios

The balance between pro-inflammatory and anti-inflammatory cytokines is crucial for the clinical outcome of any disease. The relative expression of the biomarker signatures IFN-γ, IL-10 and TNF-α (Fig 3.33) were found to be statistically significant in EPTB *vs* healthy controls. These results strongly suggest a shift towards anti-inflammatory host immune response during active disease and that cytokine ratios could be utilized to differentiate between PTB and EPTB using HupB as an antigen.

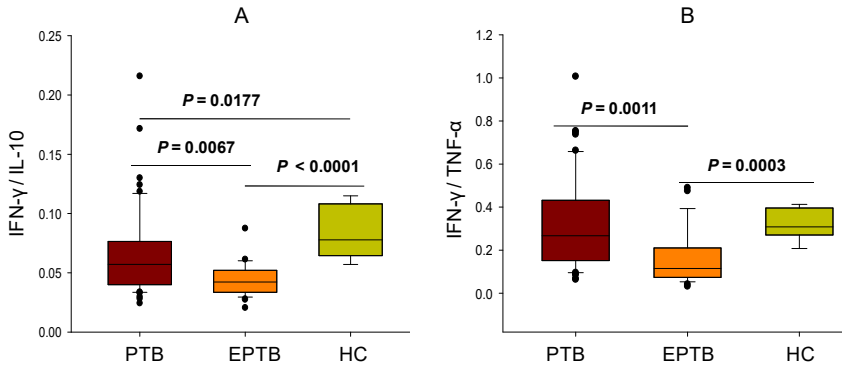

Figure 3.33. Relative expression of IFN-γ, IL-10 and TNF-α by PBMCs stimulated with HupB. The ratio of IFN-γ / IL-10 (Panel A) and IFN-γ / TNF-α (Panel B) are represented as Tukey box plots for PTB, EPTB and healthy controls (HC). The box boundaries display the median and inter-quartile ranges and the whiskers display the maximum and minimum values excluding the outliers that are shown as points. The threshold for significance was set at P<0.05.

3.5.1.5. High titres of circulating anti-HupB antibodies in TB patients

The circulating levels of anti-HupB antibodies in both PTB and EPTB patients were high when compared to the healthy controls, as was observed in our earlier studies (Sivakolundu *et al.*, 2013) (Fig. 3.34); the levels were statistically significant ($P < 0.0001$) when compared to the healthy controls. The mean titre of anti-HupB antibodies in PTB (0.655±0.254) and EPTB (0.614±0.241) patients were almost identical, with a fold increase of 5 and 4.7 respectively when compared to healthy controls (0.131±0.016).

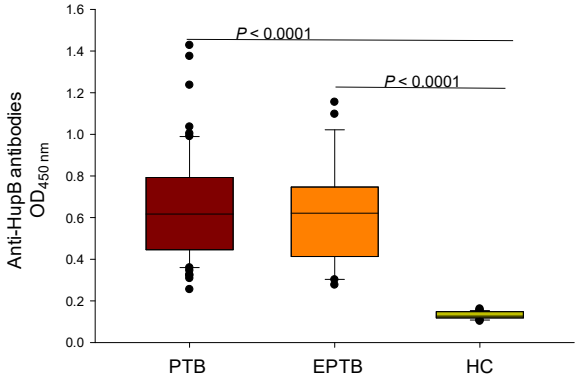

Fig. 3.34. Titre of anti-HupB antibodies in the serum of TB patients and healthy controls. Serum samples were tested for anti-HupB antibodies in triplicate in PTB, EPTB and healthy controls (HC). The figure shows Tukey box plots drawn to represent the titre of anti-HupB antibodies. The box boundaries display the median and inter-quartile ranges and the whiskers display the maximum and minimum values excluding the outliers that are shown as points. The threshold for significance was set at P<0.05.

3.5.2. Diagnostic potential of HupB

3.5.2.1. Heterogeneity of mycobacterial HupB

HupB expressed by different mycobacterial species differs in length and sequence. Compared to the 214 aa long protein present in *M. tuberculosis*, it is smaller in BCG (205 aa), *M. leprae* (200 aa), *M. avium* (169 aa) and *M. abscessus* (145 aa) and bigger in *M. ulcerans* (229 aa), *M. marinum* (220 aa) and *M. vaccae* (223 aa). These variations are seen predominantly in the C-terminal end containing a large number of alanine residues and the positively charged lysine (K) and arginine (R) that render the protein a high pI value of 12.5. To identify the sequence variation of HupB among mycobacteria, HupB sequences of various mycobacterial species were collected from NCBI (National Center for Biotechnology Information, Bethesda MD, USA) repository.

The sequences were subjected to multiple sequence alignment (T-Coffee, Ver.10.00.r1580) (Notredame *et al.*, 2000) with three randomly chosen fragments of the 214 aa HupB from *M. tuberculosis*, namely HupB-F1 (aa 1-71), HupB-F2 (aa 63-161) and HupB-F3 (aa 164-214) to determine the most conserved and most variable regions of HupB across mycobacterial species.

HupB-F1 showed almost 100% similarity among mycobacteria (Fig. 3.35, Panel A), with moderate level of variation seen with the HupB-F3 region (Fig. 3.35, Panel B).

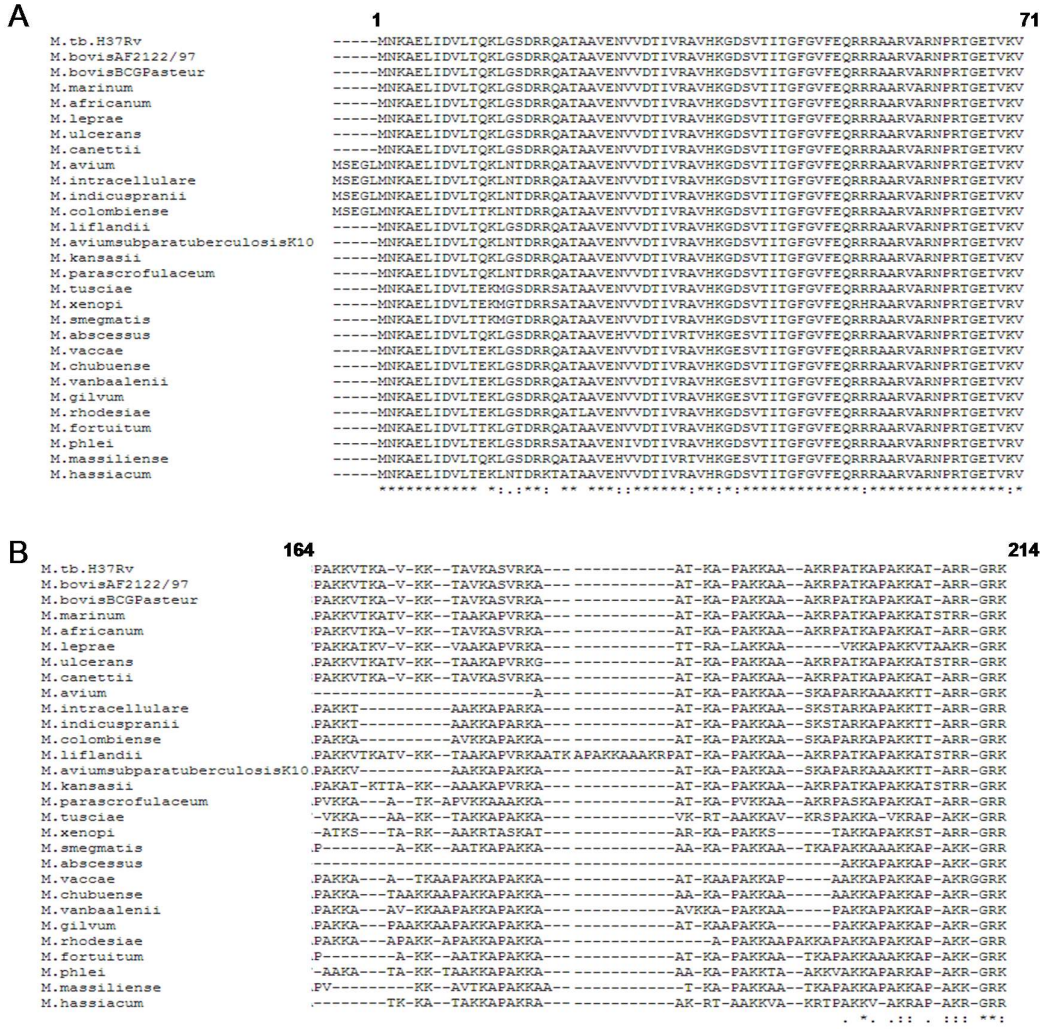

Fig. 3.35. Multiple sequence alignment of HupB-F1 and HupB-F3 from different mycobacterial species. The amino acid sequence of HupB-F1 (Panel A) and HupB-F3 (Panel B) fragment spanning aa 1-71 and 164-214 respectively from different mycobacteria (See Fig. 3.38 for Accession Nos.) were subjected to multiple sequence alignment using T-Coffee where the symbols (*), (:) and (.) represents identical sequences, conserved substitutions and semi-conserved substitutions respectively.

Notable was the high degree of variation in the HupB-F2 fragment (Fig. 3.36, Panel A) carrying deletions of varying stretches of amino acids. Of significance is the 9 aa deletion observed in the vaccine strain *M. bovis* BCG, also seen in the field strain *M. bovis* AN5, both possessing a total of only 205 aa. These two members of the *M. tuberculosis* complex lack this stretch of amino acids (aa 137 to 144 relative to that in *M. tuberculosis*) present in other members (Fig. 3.36, Panel B). Analysis revealed large deletions in *M. leprae* (aa 118-127), *M. avium* and *M. abscessus* (aa 107-140) (indicated by arrows in Fig. 3.36, Panel A); in *M. avium*, in addition to the deletion of aa 124-129, a large stretch of residues between 153-186 are missing, accounting for the small size of the protein with a total of only 169 aa.

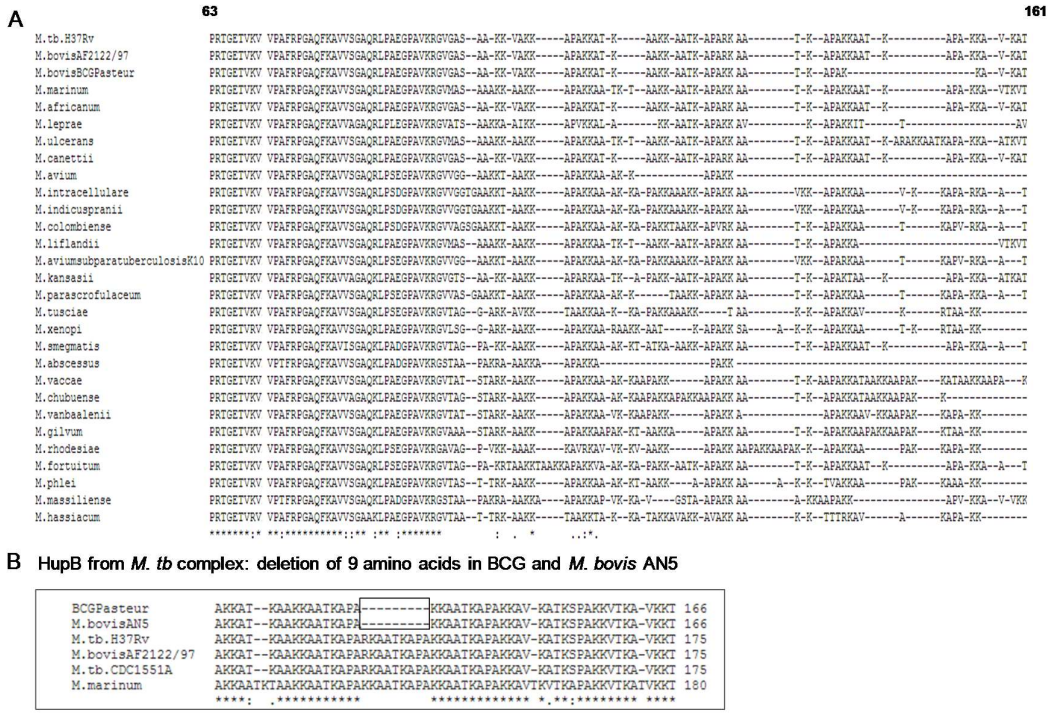

Fig. 3.36. Multiple sequence alignment of HupB-F2 from different mycobacterial species. The amino acid sequence of HupB-F2 fragment spanning aa 63 - 161 from different mycobacteria (Panel A) and HupB from *M.tb.* complex showing a 9 aa deletion in BCG Pasteur and *M. bovis* AN5 (Panel B) were subjected to multiple sequence alignment using T-Coffee where the symbols (*), (:) and (.) represents identical sequences, conserved substitutions and semi-conserved substitutions respectively.

3.5.2.2. HupB-based phylogenetic analysis reveals clustering of pathogenic mycobacteria

As the N-terminal 90 aa of mycobacterial HupB shows similarity with the HU protein of *E. coli*, we studied the phylogeny of HupB among bacteria. It is evident from Fig. 3.37 that HupB of *M. tuberculosis* H37Rv formed a separate cluster with genetic relatedness to its homologues in *Nocardia* and *Rhodococcus*. Phylogenetic analysis was done using MEGA tool (Ver. 5)(Tamura *et al.*, 2011). ClustalW software (inbuilt into MEGA5) utilizing the BLOSUM score matrix was used for pair-wise and multiple sequence alignment. The phylogenetic tree was constructed utilizing the neighbour-joining method. The robustness of the tree was determined using bootstrapping with 5000 replicates.

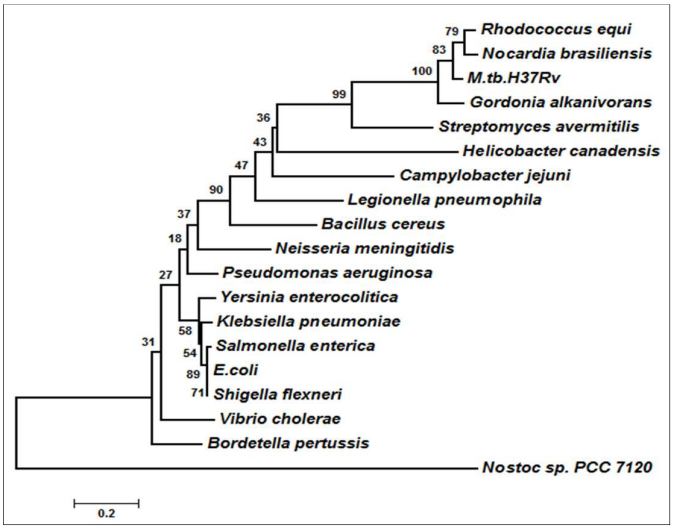

Fig. 3.37. Evolutionary relatedness of HupB from *M. tuberculosis* with homologs in other bacteria. The phylogenetic tree of HupB from different bacteria was constructed using the MEGA software tool (See Materials & Methods details). The robustness of the tree was determined using bootstrapping with 5000 replicates. *M. tuberculosis* H37Rv (NP_217502.1), *E. coli* (P0ACF4.1), *Pseudomonas aeruginosa* (NP_250495.1), *Shigella flexneri* (P0ACF7.1), *Campylobacter jejuni* (AAA60954.1), *Klebsiella pneumonia* (CCI78545.1), *Bordetella pertussis* (CAB53382.1), *Salmonella enterica* (NP_455048.1), *Yersinia enterocolitica* (CAL13166.1), *Vibrio cholera* (YP_001217452.1), *Neisseria meningitides* (YP_003083230.1), *Legionella pneumophila* (AAU27935.1), *Helicobacter canadensis* (EES89509.1), *Rhodococcus equi* (YP_004007817.1), *Streptomyces avermitilis* (BAC70395.1), *Nocardia brasiliensis*

(YP_006811262.1), *Bacillus cereus* (WP_001972967.1), *Gordonia alkanivorans* (WP_006359371.1), *Nostoc sp.* PCC 7120 (AAB64438.1).

Evolutionary relationship of HupB among mycobacteria revealed nine clusters, with several showing low bootstrap values at the nodes (Fig. 3.38). *Mycobacterium tuberculosis* H37Rv, *M. bovis* AF2122/97, *M. bovis* BCG Pasteur, *M. africanum* and *M. canettii*, belonging to *M. tuberculosis* complex formed a single cluster (I) with 100% bootstrap value. *Mycobacterium marinum*, though belonging to *M. tuberculosis* complex formed a separate cluster with *M. ulcerans* (IIb; with 99% bootstrap value); *M. liflandii* formed the sister cluster IIa. It is interesting to note that *M. leprae* and *M. kansasii* clustered together (III). While *M. xenopi* and *M. phlei* are the lone members in clusters IV and V, the other clusters contained several members grouped into sub-clusters. The non-pathogens, for example, *M. smegmatis*, *M. gilvum*, *M. vanbaleneii* and *M. vaccae* are well separated from the pathogens.

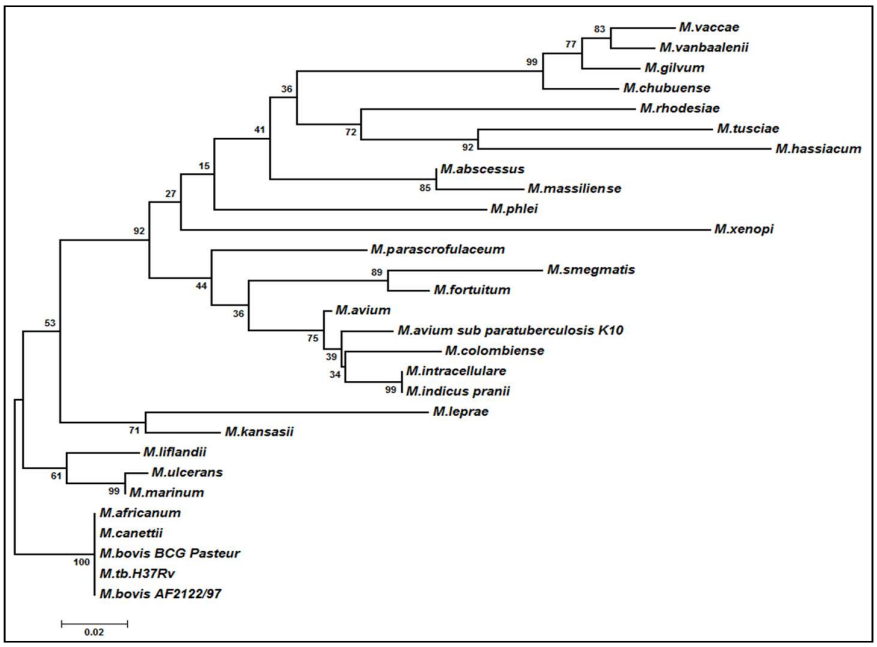

Fig. 3.38. Phylogenetic tree depicting the genetic relatedness of HupB among various mycobacterial species. The MEGA software tool was used to construct the phylogenetic tree based on the amino acid sequence of HupB (Rv2986c) from *M. tuberculosis* and other mycobacteria. The accession numbers of the sequences used include *M. tuberculosis* H37Rv (NP_217502.1), *M. bovis* AF2122/97 (NP_856655.1), *M. bovis* BCG Pasteur (YP_979091.1), *M. africanum* (CCC28061.1), *M. marinum* (YP_001850032.1), *M. leprae* (NP_302157.1), *M. ulcerans* (YP_905888.1), *M. canettii*

(YP_004746427.1), *M. avium* (WP_019305641.1), *M. intracellulare* (YP_005339200.1), *M. colombiense* (WP_007775502.1), *M. liflandii* (YP_007368301.1), *M. avium* sub *paratuberculosis* K10 (NP_961958.1), *M. kansasii* (WP_023372192.1), *M. parascrofulaceum* (WP_007171327.1), *M. tusciae* (WP_006242212.1), *M. xenopi* (WP_003922105.1), *M. smegmatis* (AFP38797.1), *M. abscessus* (WP_016892885.1), *M. vaccae* (WP_003928676.1), *M. chubuense* (YP_006452321.1), *M. vanbaalenii* (YP_952958.1), *M. gilvum* (YP_001135482.1), *M. rhodesiae* (WP_005141740.1), *M. fortuitum* (WP_003881138.1), *M. phlei* (WP_003889233.1), *M. massiliense* (YP_006521553.1), *M. hassiacum* (WP_005626473.1), *M. indicus pranii* (YP_006730812.1). The robustness of the tree was determined using bootstrapping with 5000 replicates.

3.5.2.3. Cloning, expression and purification of HupB-F1, HupB-F2 and HupB-F3 fragments

The three *hupB* fragments were amplified (Fig. 3.39, Panel A) and successfully cloned into pET22b (+) vector which was confirmed by sequencing. Plasmids from positive clones were used to re-transform *E. coli* BL21 (DE3). The antigen fragments HupB-F1, HupB-F2 and HupB-F3 were expressed as recombinant proteins.

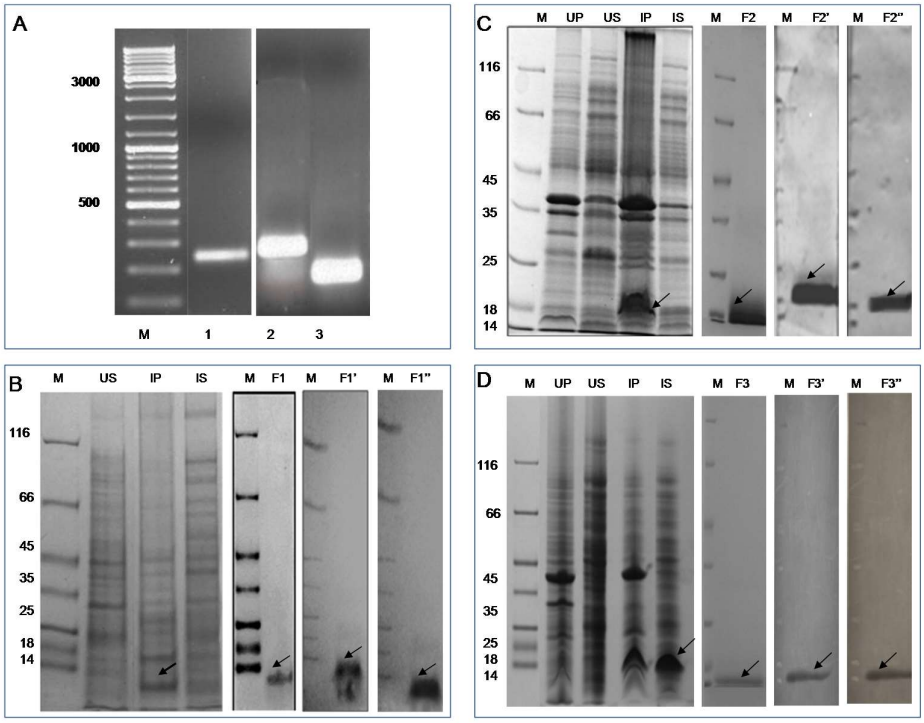

Fig. 3.39. Cloning, expression and purification of HupB-F1, HupB-F2 and HupB-F3. Panel A shows the amplified products of the three *hupB* fragments, *hupB-F1* (lane

1), *hupB-F2* (lane 2) and *hupB-F3* (lane 3) that were cloned into pET22b (+) vector. Panels (B), (C) & (D) represent the expression and purification of rHupB-F1, rHupB-F2 and rHupB-F3 respectively. Each of the lanes were loaded with 30 µg total protein and subjected to Tris-Tricine gel electrophoresis on a 10% gel. UP and US represent uninduced pellet and supernatant and IP and IS represent induced pellet and supernatant respectively; M is the molecular weight marker. F1, F2 & F3 in the three panels represent the respective purified protein and lanes F1', F2' and F3' are the corresponding immunoblots developed with rabbit anti-HupB antibody while lanes F1'', F2'' and F3'' are the corresponding immunoblots developed with anti-His antibody. The gel was scanned and molecular masses determined by UVP Vision Works LS Image Acquisition and Analysis software.

The purified proteins (Fig. 3.39, Panels B, C & D) showed altered mobility when subjected to electrophoresis with values of 12.5, 18.2 and 11.07 kDa respectively, as against their calculated molecular masses of 7.8, 10.9 and 5.6 kDa. All the three fragments were immunoblotted with anti-His antibodies and rabbit anti-HupB antibody raised against the full length HupB protein.

3.5.2.4. Demographic data

The five study groups included 72 TB patients categorized as pulmonary TB new cases, pulmonary TB defaulters, pulmonary TB relapse cases and extrapulmonary TB and healthy controls. Table 3.10 shows the various subject groups along with the demographic data of patients and controls.

Table 3.10 Demographic data of the study groups

Study group			Sample size (n)	Age (years) Mean ± SD	Male	Female
I	Pulmonary TB (PTB)	New cases	29	46.4 ± 18.5	23	6
II		Defaulters	15	46.2 ± 15.6	8	7
III		Completely treated relapse cases	13	50.6 ± 11.3	9	4
IV		Extrapulmonary TB (EPTB)	15	33.4 ± 18.1	5	10
V		Healthy controls	10	25.3 ± 10.4	5	5

3.5.2.5. High titre of antibodies against HupB-F2 in the serum of TB patients with recurrence of the disease and in extrapulmonary TB

Serum from all four groups of TB patients showed high levels of antibodies against the full-length HupB, as observed in our earlier study (Sivakolundu *et al.*, 2013), the levels being more in case of extrapulmonary TB (Group IV). Another interesting observation was that anti-HupB antibodies were maximal in patients in whom the disease recurred after the completion of therapy (Group III) when compared to normal healthy controls (Table 3.11). Among the HupB fragments, while all of them performed well as antigens, HupB-F2 was found to be highly promising. This antigen, found to be reactive in all groups of TB patients, is of considerable diagnostic potential in relapse cases (Group III) and in extrapulmonary TB (Group IV). In the latter, the high titre (approximately 5–6-fold) when compared to healthy controls (Table 3.11, Fig. 3.40) was statistically significant ($P < 0.05$) and was found to be better than the full-length HupB. In relapse cases (Group III), HupB-F2 and full-length HupB and in EPTB (Group IV), HupB-F2 showed good potential as antigens.

Table 3.11 Performance of HupB-F2 in the ELISA-based detection of anti-HupB antibodies in the serum of TB patients and healthy controls

Study group		HupB FL	HupB F1	HupB F2	HupB F3
I	New cases	0.596 ± 0.407*	0.494 ± 0.180*	0.708 ± 0.204*	0.430 ± 0.211*
II	Defaulters	0.468 ± 0.167**	0.506 ± 0.198*	0.595 ± 0.287*	0.381 ± 0.243
III	Relapse	0.877 ± 0.572***	0.545 ± 0.199*	0.760 ± 0.215*	0.344 ± 0.130
IV	EPTB	0.519 ± 0.281	0.434 ± 0.137*	0.695 ± 0.233*	0.520 ± 0.257*
V	Healthy controls	0.157 ± 0.081	0.189 ± 0.125	0.12 ± 0.023	0.184 ± 0.043

*Mean difference is significant at the 0.05 level vs healthy controls

**Mean difference is significant at the 0.05 level vs relapse TB cases

***Mean difference is significant at the 0.05 level vs healthy controls and defaulters

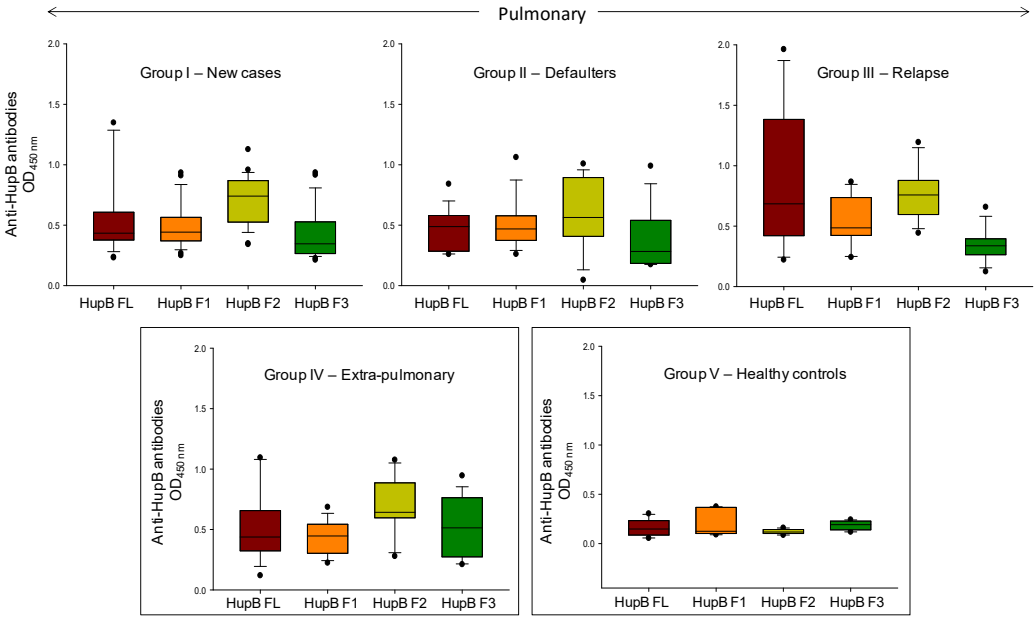

Fig.3.40. ELISA: immunoreactivity of HupB and its fragments with serum from TB patients and normal healthy controls. The figure shows Tukey box plots drawn to represent the titre of antibodies against the full length HupB (HupB-FL), HupB-F1, HupB-F2 and HupB-F3 respectively. The five study groups included new active pulmonary TB cases (Group I), pulmonary TB defaulters (Group II), relapse cases (Group III), extrapulmonary TB (Group IV) and normal healthy controls (Group V). The box boundaries display the median and inter-quartile ranges, whiskers display the maximum and minimum values excluding the outliers, shown as points.

3.5.2.6. Antibodies against HupB-F2 showed maximal correlation with serum iron status: Pearson's correlation analysis

Negative correlation of titre of the circulating anti-HupB antibodies with serum iron status of TB patients was reported earlier with full length HupB (Sivakolundu *et al.*, 2013). Here, the maximal correlation was seen with HupB-F2 as shown by Pearson's correlation analysis (−0.415; Table 3.12). TB patients in this study group also showed low values of serum iron, total iron-binding capacity (TIBC) and % saturation of serum transferrin when compared to healthy controls (Table 3.13; Fig. 3.41). Serum iron showed 2.5–3-fold decrease ($P < 0.05$) and there was 50% reduction in iron saturation of serum transferrin in patients (Groups I–IV) when compared to normals (Group V). The serum ferritin level was found to be 3-fold higher in TB patients than normal controls.

Table 3.12 Negative correlation of anti-HupB antibodies with serum iron and comparison of HupB-F2 vs full length HupB (Pearson's correlation analysis)

	Iron	TIBC	Transferrin	Ferritin	HupB-FL	HupB-F1	HupB-F2	HupB-F3
Iron	1	0.342**	0.914**	0.080	-0.153	-0.334**	-0.415**	-0.273*
TIBC	-	1	0.011	-0.512**	-0.085	-0.213	-0.191	-0.047
Transferrin	-	-	1	0.310**	-0.120	-0.282*	-0.358**	-0.214
Ferritin	-			1	-0.013	-0.115	-0.115	-0.114
HupB-FL					1	0.386**	0.389**	0.014
HupB-F1						1	0.544**	0.125
HupB-F2							1	0.226*
HupB-F3			-					1

** Correlation is significant at the 0.01 level (2-tailed)

* Correlation is significant at the 0.05 level (2-tailed)

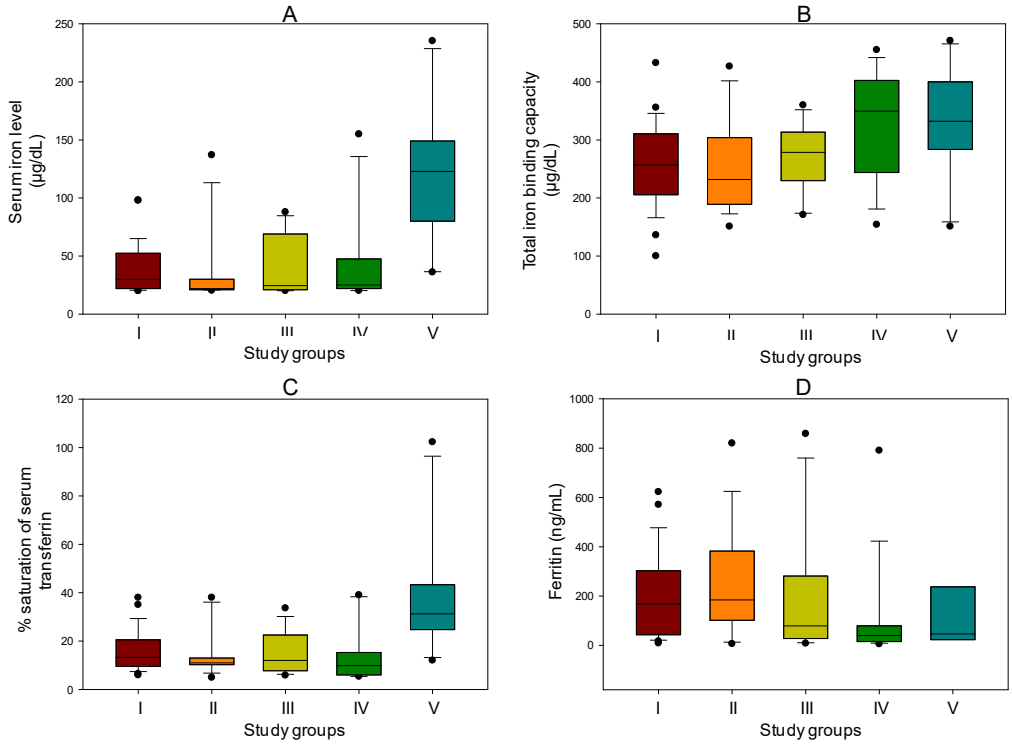

Fig. 3.41. Serum iron profile of TB patients and endemic normals. Panels A – D represent the serum iron, total iron-binding capacity (TIBC), percent saturation of serum transferrin and ferritin levels in Groups I – V representing new active cases of

pulmonary TB, pulmonary TB defaulters, relapse cases, extrapulmonary TB and endemic normal controls. The box boundaries display the median and inter-quartile ranges and the whiskers display the maximum and minimum values excluding the outliers, indicated as points.

Table 3.13 Serum iron profile in the various study groups

Study group		Serum iron (µg / dL)	TIBC (µg / dL)	% saturation of serum transferrin	Ferritin (ng / mL)
I	New cases	37.89 ± 21.84*	254.20 ± 73.21**	15.51 ± 8.42*	290.47 ± 351.81
II	Defaulters	37.13 ± 33.80*	257.28 ± 81.15	14 ± 9.34*	305.64 ± 318.92
III	Relapse	41.82 ± 25.77*	271.71 ± 58.08	15.33 ± 8.61*	349.14 ± 475.96
IV	EPTB	46.08 ± 42.46*	326.84 ± 87.6	14.26 ± 11.5*	97.35 ± 197.04
V	Healthy controls	119.65 ± 58.58	332.46 ± 91.87	37.68 ± 24.75*	308.61 ± 609.22

*Mean difference is significant at the 0.05 level *vs* healthy controls

**Mean difference is significant at the 0.05 level *vs* extrapulmonary TB cases

CHAPTER 4

DISCUSSION

HupB in *M. tuberculosis* is a 214 amino acid protein, rich in basic amino acids lysine and arginine in the C-terminal region. The protein, expressed by all mycobacteria shows considerable structural heterogeneity in the mycobacterial-specific C-terminal region. It is variously called in different mycobacterial species and assigned different functions (detailed in Chapter 1). The suggested roles of the protein in adhesion, recombination, protection of DNA from oxidative stress and as a transcriptional regulator necessitates its varied localization, which is supported by its presence as a nucleoid associated protein (Prabhakar *et al.*, 1998) and as a cell wall-associated surface protein (Pethe *et al.*, 2002; Yeruva, 2012). The first report of HupB as an iron-regulated protein was from our lab (Yeruva *et al.*, 2006) with subsequent characterization of the protein as a transcriptional regulator of mycobactin biosynthesis (Pandey *et al.*, 2014b). In this study, we provide experimental evidence to demonstrate its additional role in iron metabolism as an iron transporter by functioning as a receptor for Fe-CMb. From the microarray analysis of the *hupB* KO mutant strain *M.tb.ΔhupB*, the multi-functional role of the protein in *M. tuberculosis* was evident. In this study, its regulatory role in the biosynthetic pathways of mycobacterial lipids was addressed. The clinical significance of the protein and its diagnostic potential is highlighted by demonstrating the influence of the protein in triggering the expression of anti-inflammatory cytokines, with the resulting Th2 response accounting for the significantly high levels of circulating anti-HupB antibodies in extrapulmonary TB patients. This implicates its role as an adherence factor in promoting the establishment of the pathogen in extrapulmonary sites that however, needs further studies to conclude its role in dissemination.

In solid media, the growth of *M.tb.ΔhupB* was notably reduced that was however restored in the *hupB*-complemented strain, implying the requirement of HupB for normal growth of the pathogen. In liquid medium maintained under high and low iron conditions, the mutant exhibited an extended lag phase but showed optimal growth, though relatively less than that of the WT and *hupB*-complemented strains. It is likely that the mutant, through repeated passages in these axenic media had adapted to the *in vitro* growth conditions. The mutant strain however showed poor infectivity and survival inside the macrophages.

Three different methods of determination of viable bacilli, namely ATP assay, real time PCR using 16S rRNA as target sequence and CFU counts pointed to the low viability and poor growth of the mutant strain inside the macrophages. This inability to grow inside the macrophages can be attributed to several factors, namely the inability to acquire iron, failure to counter the oxidative stress and due to altered lipid metabolism, each of which is discussed below.

HupB and siderophore-mediated iron acquisition

All mycobacteria, including *M. tuberculosis* require iron for their growth. As detailed in Chapter 1 (Review of Literature), iron is scarce and mycobacteria express siderophores to acquire insoluble or protein-bound iron. Mycobacterial siderophores namely the mycobactins, carboxymycobactins and exochelins are well characterized chemically but the mechanism of iron uptake by these molecules is not completely understood. The first iron-regulated envelope protein to be characterized as a siderophore receptor was IREP-29 in *M. smegmatis* that was demonstrated to be a receptor for ferri-exochelin (Hall *et al.*, 1987). In the study, using specific antibodies against IREP-29 that blocked the protein in live organisms, uptake of iron from ferri-exochelin MS was inhibited. The specificity of the receptor for ferri-exochelin MS was confirmed by direct interaction of the two molecules using affinity chromatography (Dover & Ratledge, 1996). In this study, HupB is established as a receptor for Fe-CMb. Experimental evidence is provided to demonstrate that the protein, upon binding the extracellular siderophore mediates the transfer of the iron to mycobactin localized in the cell envelope.

The biosynthetic machinery for exochelin, the extracellular siderophore produced by non-pathogens is absent in the genome of *M. tuberculosis*, making the mycobactin-carboxmycobactin machinery the sole iron uptake machinery. With the deciphering of the mycobactin biosynthetic machinery (Quadri *et al.*, 1998) and demonstrating the essentiality of this machinery (De Voss *et al.*, 2000), the ability to synthesise mycobactin is now established as a contributing virulence determinant. De Voss *et al*., generated the *mbtB* KO mutant of *M. tuberculosis*, lacking the first gene *mbtB* in the *mbt* operon and demonstrated through disruption of the mycobactin biosynthesis that it was essential for the

entry and survival of the pathogen inside macrophages. The requirement for the optimal functioning of the *mbt* biosynthetic machinery was also reported from our lab (Pandey *et al.*, 2014b). In the efforts to characterize the role of HupB, it was observed that the *hupB* KO mutant, unable to produce optimal levels of mycobactin and carboxymycobactin failed to multiply inside macrophages, unambiguously pointing to the essentiality of the siderophore machinery in this pathogen (Pandey *et al.*, 2014b).

In this study, when iron uptake, supplied as ^{55}Fe was studied, >50% of the label was recovered in the WT organisms, with a significant amount in the two siderophores. The low label recover in *M.tb.ΔhupB* can be reasoned due to the low production of Mb and CMb due to the absence of HupB needed to transcribe the *mbt* genes by functioning as a positive transcriptional regulator of the *mbt* operon. Interestingly, though, the mutant strain was unable to assimilate iron when given as ^{55}Fe-CMb. This clearly pointed to the need for the presence of HupB in taking up the iron associated with the extracellular siderophore CMb. This strengthened our hypothesis that HupB played an additional role of an iron transporter that was based on the following observations. First, HupB can bind iron, as reported by our lab and by others (Takatsuka *et al.*, 2011); the latter further demonstrated that it possessed ferroxidase activity, by virtue of which it can convert ferrous iron to the ferric form. Second, it is present on the cell surface (Pethe *et al.*, 2002; Yeruva, 2012) and thirdly, our earlier studies (Yeruva, 2012) showed that it can interact with both the ferri-siderophores. Thus, the inability of the *M.tb.ΔhupB* strain to take up the iron from the ^{55}Fe-CMb indicated HupB as a possible receptor for Fe-CMb. When the HupB in the WT strain was blocked by pre-incubating the organisms with rabbit anti-HupB antibodies, uptake of iron from ^{55}Fe-CMb was inhibited; the specificity of this inhibition can be inferred from the fact that this inhibition was not seen with the pre-immune serum obtained from the same animal used for immunization.

Chromatographic separation of Mb established without any doubt, the transfer of iron from ^{55}Fe-CMb to Mb fraction upon uptake of the former by the live WT organisms. This process does not occur upon blocking of HupB with anti-HupB antibodies and in the mutant strain, implicating the need for HupB to

mediate this process of iron transfer. In the WT strain, the levels of the label was almost identical in the whole cells and in Mb fraction, a feature that was further confirmed in the time course assay in which the periodic monitoring of the label over a period of one hour showed that the label in Mb paralleled that taken up by whole cells. The Mb-associated iron plateaued after one hour, suggesting that the iron was probably being internalized for metabolic purposes as the total radioactivity in whole cells continued to rise when studied over a period of two hours. It may be re-called that an *in vitro* assay had shown that purified CMb can remove iron from host high-affinity iron-binding molecules and transfer it to Mb (Gobin & Horwitz, 1996b). The role of HupB as an iron transporter was further substantiated by incorporating the protein into liposomes. The liposome-mediated uptake of ^{55}Fe-CMb showed that HupB facilitated the transfer of iron from the externally added ^{55}Fe-CMb to Mb on the inside. These artificial membranes prepared with HupB acquired higher levels of iron in the presence of desferri-Mb. The presence of the label in HupB-liposomes possibly occurs due to the iron-binding property of the protein, but the higher label in the presence of Mb implies the chelation of iron by Mb owing to its high affinity for iron. The negligible radioactivity in the control liposomes containing only desferri-Mb (minus HupB) clearly ruled out the direct transfer of the metal ion from ^{55}Fe-CMb to Mb. Further evidence for the role of HupB came from liposomes prepared from HupB-positive cell wall proteins from the iron-limited WT strain that was able to take up high levels of ^{55}Fe-CMb when compared to traces of the label in the HupB-deficient cell wall proteins from the mutant strain.

All the above evidence pointed to HupB functioning as a receptor for Fe-CMb, with subsequent transfer of the metal ion to Mb, the exact mechanism of which remains to be unraveled. It is therefore necessary to demonstrate that the protein can interact with both the siderophores. This was done using both *in silico* and experimental tools. As the C-terminal region was unique to mycobacteria, there was no suitable template for homology modeling. Hence, the I-TASSER program was chosen for determining the tertiary structure of the full length protein. Since only 62% of the amino acids were within the allowed regions in the Ramachandran plot generated from the model, the level of

disorder was assessed that showed it to be restricted to the C-terminal region. Docking studies identified the interacting amino acids in HupB that revealed the hydrophobic bonds in Fe-Mb interactions and both hydrogen and hydrophobic bonds in the binding with Fe-CMb. Experimental validation of HupB-siderophore interactions were studied by spectrofluorimetry and CD analysis. The binding of Fe-CMb with HupB is indicative of receptor-ligand interaction as it was associated with increase in the intensity of the emitted light and shift of the absorption maximum from 320 nm to 314 nm called as 'blue shift'. Such spectral changes often indicate conformational changes in the protein upon interaction with the specific ligand. Here, it must be pointed out the interaction was specific with the Fe-CMb, with poor interaction with the desferri form of the siderophore. HupB also bound Fe-Mb, as seen from both spectrofluorimetric and CD spectral changes. In the former, while no spectral shift was seen, indicating its interaction with the protein is different from that of Fe-CMb interaction, there was increase in the intensity of the emitted light. The K_d values, showing the binding affinities of the two ferri-siderophores with HupB were calculated from the spectrofluorimetric data. The K_d values of 22.42 μM and 38.76 μM for Fe-CMb and Fe-Mb reflect almost similar values and indicate that the protein possesses moderate affinity for both the siderophores. Such interactions are probably necessary to facilitate quick binding and release of the iron during the transport process, which would otherwise be slowed down if there was a strong affinity receptor-ligand interaction. CD spectral data, generated upon addition of the two ferri-siderophores to HupB revealed changes in the secondary structure of the protein. A downward deflection in the value of ellipticity indicated an increase in ordered secondary structure, or as interpreted usually, an increase in the α-helical content of the protein (Akyol *et al.*, 2004). CD showed that the largely α-helical structure of HupB becomes further ordered upon addition of Fe-Mb but with the addition of increasing concentrations of Fe-CMb there was a gradual loss in its ordered secondary that was evident in the positive increase in ellipticity. Binding of HupB was specific only for the ferric forms of the siderophores as the desferri-CMb was unable to induce any structural changes in the protein even at high concentrations.

In the transport of iron in *M. tuberculosis*, reviewed recently (Fig. 4.1) (Sritharan, 2016) in which HupB was hypothesized to be an iron transporter, our studies here firmly establish it as a cell surface receptor. We propose that the internalization process is different from that of known transport systems in Gram negative bacteria in that HupB interacts with Fe-CMb and mediates the transfer of iron, by virtue of its Fe^{3+}-binding property to the desferri-Mb localized near the cytoplasmic membrane. This explains the presence of the two siderophores warranted by the lipid-rich nature of the cell envelope. When the iron is transferred to the Mb, the IrtAB localized in the cytoplasmic membrane facilitates the internalization of the iron from the Fe-Mb after reducing the iron from Fe^{3+} to Fe^{2+} by its reductase activity exhibited by IrtA subunit of the protein.

The recently hypothesised transporter role of HupB (Sritharan, 2016) is established in this study by demonstrating it as a receptor for Fe-CMb and mediating the transfer of iron to the desferri-Mb in the cell envelope

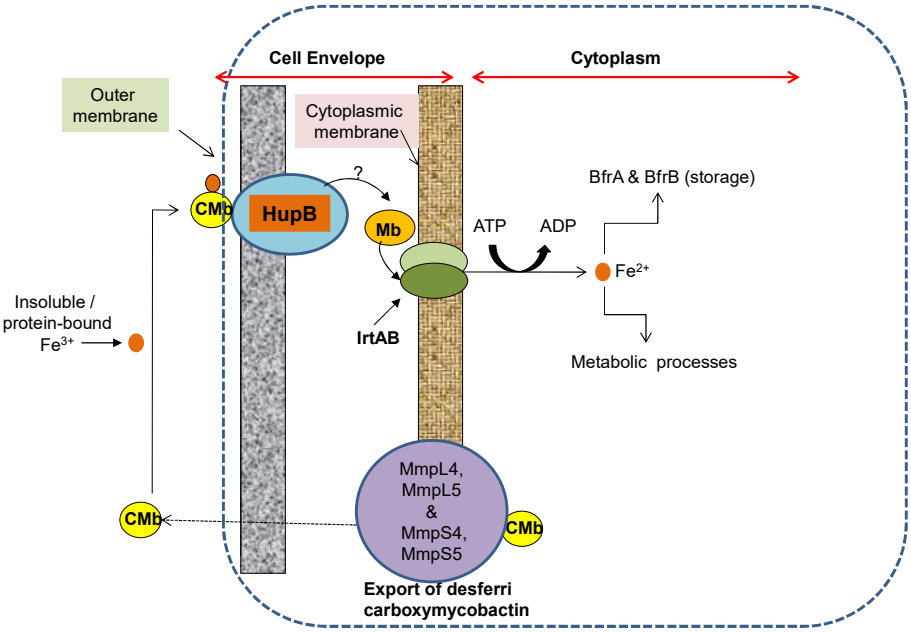

Fig. 4.1. Proposed model for HupB-mediated iron acquisition in *M. tuberculosis*. Adapted from Sritharan, 2016. The siderophores carboxymycobactin (CMb) and mycobactin (Mb) are exported across the cytoplasmic membrane by the MmpS4/5 and MmpL4/5 transporter proteins. The extracellular desferri-CMb chelates Fe^{3+} present as insoluble or protein-bound iron. The ferri-CMb interacts with HupB present on the cell envelope that mediates the transport of Fe^{3+} from Fe-CMb to Mb present within the cell

envelope. Fe^{3+} from the Mb is reduced to Fe^{2+} and transferred to the cytoplasmic space in an ATP-dependant manner by the IrtAB transporters present on the inner membrane. Once inside, the metal ion is utilised for the various metabolic processes and the excess iron is stored in BfrA and BfrB.

HupB is a DNA-binding protein and functions as a transcriptional regulator. The lysine and arginine-rich C-terminal end must bind the negatively charged DNA. Studies from our lab first demonstrated HupB as a positive transcriptional regulator of mycobactin biosynthesis (Pandey *et al.*, 2014b) by binding to the *mbtB* promoter DNA. This was ascertained by mobility shift and DNA footprinting assays that identified the 10 bp HupB box (5'-CACTAAAATT-3'). The location of this box is upstream of the 'iron / IdeR box' to which the negative regulator IdeR binds as IdeR-Fe^{2+} complex under iron-replete conditions. HupB functions as a positive regulator of mycobactin biosynthesis when the intracellular iron levels drop that do not favour the formation of the IdeR-Fe^{2+} complex (Pandey *et al.*, 2014a). The HupB box was also identified in several other iron-regulated genes. It was present upstream of the *hupB* gene itself and regulation by HupB on its own expression was demonstrated earlier (Pandey *et al.*, 2014a). In this study, we extended our studies to establish further the regulatory role of HupB in iron transport based on the low mRNA transcripts of several genes associated with export or uptake in the HupB minus mutant strain. The *irtA*, *mmpL5* and *mmpS5* that had putative HupB box in their promoter DNA were analysed by chromatin immunoprecipitation using specific anti-HupB antibodies. ChIP assay identifies protein-DNA interactions by using the protein-specific antibodies to precipitate the specific DNA sequences, the enrichment of which gives as assessment of the interaction of the protein with the promoter DNA of the specific sequences. The fold enrichment is then assessed by real time PCR that gave 3-fold gene enrichment for *irtA* while it was 8- and 7-fold for *mmpL5* and *mmpS5* respectively. A reduction in the levels of MmpS4, MmpS5, MmpL4 and MmpL5 in *M. tuberculosis* will result in the accumulation of the desferri-CMb (Wells *et al.*, 2013) as double KO mutants of lacking these genes were unable to export the desferri-CMb to the outside, without any impairment in the uptake of Fe-CMb. As HupB regulates the expression of both IrtA and IrtB, any reduction of IrtAB will affect internalization

of the iron from Fe-Mb into the cytosol. The expression of *eccA3* of the *esx-3* operon was reduced in the absence of HupB, ChIP data showed a 15-fold enrichment. This machinery, shown to play a role in mycobactin-mediated iron acquisition is essential for growth *in vitro* (Serafini *et al.*, 2009; Siegrist *et al.*, 2009). While the inability of the *hupB* negative mutant strain to grow inside macrophages is a resultant effect of one or more of its roles in iron acquisition, the overall observation is that the mutant strain produces negligible Mb and CMb and cannot take up iron from the externally supplied Fe-CMb. It can thus be concluded that HupB in *M. tuberculosis* functions as an iron sensor and controls its own level and that of the other components of iron transport besides playing the important role in the uptake of iron by interacting with both the siderophores. The study has helped to gain a better understanding of the mechanistic details of the siderophore machinery in *M. tuberculosis*.

Regulatory role of HupB in lipid biosynthesis in M. tuberculosis

Mycobacterial cell wall lipids are unique and include the mycolic acids and several types of surface-exposed lipids and glycolipids that are associated non-covalently with the mycolic acids. These form the protective layer that serves as an effective barrier and protect the pathogen from the harsh environment of the macrophages. Thus, the cell wall lipids of *M. tuberculosis* contribute to the virulence of the pathogen. Hence, a disruption of any of the biosynthetic pathways or reduced expression of these lipids will have a profound effect on the organization of the cell envelope and susceptibility of the pathogen to several external factors. Here, our findings reflect the important role of HupB in lipid biosynthesis. The HupB-deficient mutant strain, when grown in different solid media showed marked reduction in the growth and changes in cell morphology. Our hypothesis on the possible role of HupB in lipid biosynthesis was framed based on the down-regulation of genes associated with lipid metabolic pathways in the microarray data of the mutant strain of *M. tuberculosis* (Pandey *et al.*, 2014b). In this study, the role of HupB in lipid metabolism was investigated by comparing the levels of various lipids including fatty acids, mycolic acids, phthiocerol dimycocerosate (PDIM), sulpholipid-1 (SL-1), diacyl trehalose (DAT), penta-acyl trehalose (PAT) in the mutant with that expressed by the WT organisms. The regulatory role of HupB in lipid

biosynthetic pathways was established by first identifying the HupB box in the promoter DNA of genes with altered transcripts in the microarray analysis and by experimentally demonstrating the role of HupB by ChIP assay. While this study did not include analysis of organisms recovered from infected macrophages, it is highly likely that the changes in lipid content and profile could be one of the contributing factors to the increased susceptibility of these organisms to conditions like oxidative stress accounting for their inability to survive inside macrophages.

Extractions of the different lipids were done using established protocols. The mutant strain showed an overall decrease in several of the saturated long chain fatty acids, with an increase in unsaturated fatty acids. In addition, the mutant strain produced three unique fatty acids namely, pentadecylic, margaric and margaroleic acids; additional studies are needed to understand their role and relevance to the pathogen. Mycolic acids and surface exposed lipids was ~50% less compared to the WT H37Rv which was apparent from the total weight of the extracted lipids. Biochemical analysis by thin-layer chromatography revealed that though there was an overall reduction in the mycolic acids, the relative amounts of all the three forms namely α-, methoxy- and keto-mycolates were identical. Similarly, there were relatively lower levels of the non-polar lipids SL-1, PDIM, DAT and PAT in the mutant strain, with maximal expression of these lipids by WT organisms grown in iron-limiting media. The regulatory role of HupB in the biosynthetic pathways of the different lipids is based on the data from the ChIP analysis and is discussed in detail below.

The biosynthetic pathways of most of the above lipids are well delineated. Mycolic acids are synthesized by the participation of both the fatty acid synthase (FAS) systems FAS-I and FAS-II, a feature unique to mycobacteria because most bacteria do not elaborate the FAS-I system that is normally found only in eukaryotes. These unusually long fatty acids are synthesised by repetition of several cycles of addition of the acyl moieties involving several different types of reactions including condensation, ketoreduction, dehydration, enoyl reduction etc, catalysed by different enzymes (Fig. 4.2). In the FAS-I system, the acyl moieties are activated via a thioester

linkage to CoA and in the FAS-II system, an acyl carrier protein (ACP) encoded by *acpM* is involved (Fig. 4.2). The FAS-I system synthesises short-chain fatty acids. The *M. tuberculosis* FAS-II system is dependent on the acyl CoA moieties generated by the FAS-I system as it cannot synthesise *de novo* (Kremer & Besra, 2005). The FabD catalyses the transacylation of malonyl CoA with holo-ACP to generate malonyl-ACP that functions as the elongation substrate needed by the FAS-II system for synthesizing mycolic acid. The enzyme β-ketoacyl ACP synthase (FabH) forms a pivotal link between the last cycle of FASI and the first cycle of the FASII system. It mediates the condensation of acyl-CoA products of FASI with malonyl-ACP forming medium length ketoacyl-ACP, the initial substrates of FASII. After reduction by the β-keto-acyl-ACP reductase MabA, dehydration by the β-hydroxyl dehydratases HadAB and HadBC and reduction by the enoyl-CoA reductase InhA, either the β-ketoacyl-ACP synthase KasA or KasB catalyzes the condensation of the resulting product with malonyl-ACP units, thereby initiating the next round of elongation.

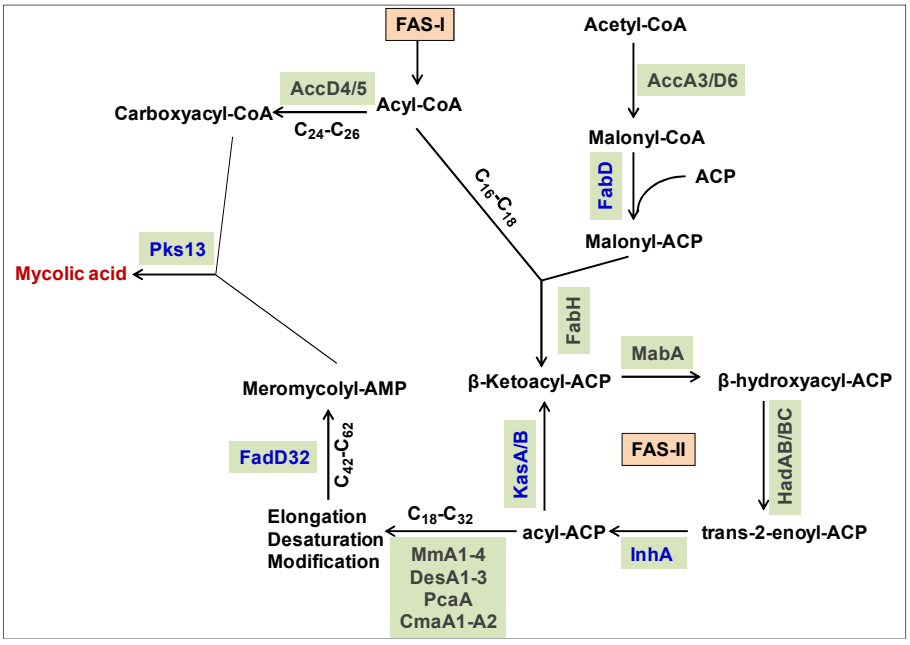

Fig. 4.2. FAS-II mycolic acid biosynthetic pathway in *M. tuberculosis*. The figure adapted from Jankute *et al.,* 2015 shows the acyl-CoA moieties synthesized by the FAS-I system serving as the substrate for the subsequent additions of fatty acyl chains to form the long chain mycolic acid. The enzymes in this biosynthetic pathway,

influenced by HupB are highlighted in blue. Abbreviations: ACP, acyl carrier protein; AMP, adenosine monophosphate; CoA, coenzyme A.

This cycling continues until the acyl chain reaches $C_{42–62}$, forming the saturated long-chain meromycolate after which various modifications are made to the chain providing functional groups to the meromycolate scaffold. The meromycolate is activated for the Claisen-type condensation by the generation of a meromycolyl-AMP by FadD32 (fatty acyl-AMP ligase). This meromycolyl-AMP substrate is linked to the α-alkyl short chain ($C_{22–24}$) in a reaction catalyzed by Pks13 (polyketide synthase) to produce α-alkyl-β-keto-mycolic acid.

As mentioned above, Acyl carrier protein (ACP) mediates the transfer of acyl intermediates between the enzymes. It must be mentioned that *acpM* transcripts (encoding ACP) are low in the mutant strain. The enzyme malonyl-CoA: ACP transacylase (FabD) is essential for mycolic acid biosynthesis. In this study, the ChIP assay showed a 30 fold enrichment of this gene, indicating the binding of HupB to the HupB box located -73 bp upstream of the start point in the promoter DNA of *fabD*. Similarly, *kasA* (encoding β-Ketoacyl-ACP synthase) and *fadD32* (encoding fatty-acid-AMP ligase) with HupB boxes in their promoter DNA showed 27 and 36-fold gene enrichment in the ChIP assay. Two other genes, identified in the ChIP assay include *inhA* (encoding enoyl-ACP reductase) and *pks13* (encoding polyketide synthase) with 9 and 10-fold enrichment. Though there was less than 2-fold reduction in the mRNA transcripts of these genes in the mutant strain (Pandey *et al.*, 2014b), the presence of the HupB box and the notable fold changes in the ChIP assay led us to propose that HupB binds to the HupB box upstream of these genes and promote their transcription. This however needs to be experimentally proved by electrophoretic mobility shift assays (EMSA) and DNA footprinting analysis. It may be mentioned that *kasB*, co-transcribed with *kasA* is also down-regulated in the mutant. Modification in the mycolic acid chain such as desaturation, addition of cis- or trans-cyclopropane rings, addition of keto or methoxy groups occurs while the meromycolate chain is still attached to the ACP and requires enzymes like desaturases (DesA1, DesA2 and DesA3), cyclopropane mycolic acid synthases (CmaA1, CmaA2 and PcaA) and methyltransferases (MmaA1-4) which were not altered by HupB. This explains the detection of all the three

forms of mycolic acids in the mutant though the overall expression in considerably lower than the WT strain.

Sulpholipid-1 (SL-1) is one remarkable lipid which is thought to mediate specific host-pathogen interactions during infection. Though the pathway has been well studied, the final step resulting in the production of mature SL-1 and the role of MmpL8 in this is yet to be determined (Converse *et al.*, 2003; Kumar *et al.*, 2007). The proteins involved in the assembly of SL-1 (Fig. 4.3) are sulfotransferase (Stf0), the polyketide synthase Pks2 that synthesizes the phthioceranoyl and hydroxyphthioceranoyl lipids that occupy the 6-, 6'-, and 3'-positions of SL-1, the polyketide synthase associated proteins PapA1 and PapA2 that carry out acylations of the sulfated product to form SL-1 intermediates (SL_{659} and SL_{1278} and the transporter protein MmpL8 that transports the final product SL-1 to the cell exterior. A reduction in the transcript levels of *pks2, papA1* and *mmpL8* in the KO mutant led to the search for HupB boxes in the promoter DNA of these genes. ChIP assay corroborated the regulatory role of HupB as 5.5-fold and 14-fold enrichment was observed in the *papA1* and *mmpL8* genes.

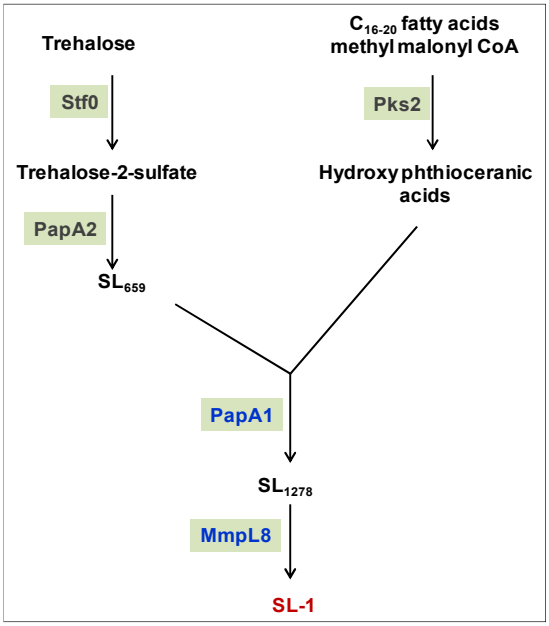

Fig. 4.3. SL-1 biosynthetic pathway in *M. tuberculosis*. Adapted from Kumar *et al.,* 2007. Trehalose is first sulfated by Stf0 to form trehalose-2-sulfate (T2S). PapA2, specific for T2S, then acylates the 2'-position of T2S to form SL_{659}. A (hydroxy) phthioceranic acid is then synthesized by Pks2 and transferred directly by PapA1 onto

SL_{659} to generate SL_{1278}. The diacylated SL_{1278} may be flipped by across the plane of the cell membrane, allowing it to be further modified into mature SL-1 before delivery to the cell wall. The enzymes in this biosynthetic pathway, influenced by HupB are highlighted in blue.

MmpL8 is an essential protein for SL-1 biosynthesis as KO strains of M. tuberculosis show poor growth and survival in mouse models (Converse *et al.*, 2003) probably due to the accumulation of the SL-1 intermediate SL_{1278} or due to the transport of molecules along with SL-1 that mediate various host-pathogen interactions. Lack of MmpL8 also results in a less effective suppression of protective immune response (Domenech *et al.*, 2004), which could probably lead to growth attenuation.

2,3-diacyltrehaloses (DAT) and penta-acyltrehaloses (PAT) not only play a structural role in the cell envelope but also contribute to the ability of *M. tuberculosis* to multiply and persist in the infected host, promoting the intracellular survival of the bacterium and modulating host immune responses. The pathway for the synthesis of DAT and PAT is illustrated in Fig. 4.4. The formation of DAT occurs on the cytosolic face of the plasma membrane through the action of PapA3 (polyketide synthase associated protein) and Pks3/4 (polyketide synthases); that of PAT occurs on the periplasmic face via trans-esterification reactions between DAT substrates catalyzed by the acyltransferase Chp2. The integral membrane transporter MmpL10 is essential for DAT to reach the cell surface, and its presence in the membrane is required for Chp2 to be active (Belardinelli *et al.*, 2014). The DAT and PAT biosynthesis is greatly influenced by HupB as the reductions in the transcript levels of the associated genes were more than 2-fold with *papA3* showing a notable 4.5-fold reduction in the mRNA transcripts. ChIP assay confirmed the functionality of the HupB boxes in the promoter DNA of these genes, as seen by the 6-, 12-, 11- and 14-fold enrichment for *papA3, pks4, chp2* and *mmpL10*.

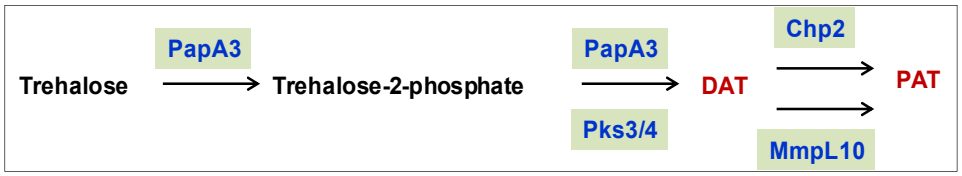

Fig. 4.4. DAT and PAT biosynthetic pathway in *M. tuberculosis.* Adapted from (Touchette *et al.*, 2015). The acyltransferase PapA3 initiates DAT and PAT biosynthesis on the cytosolic face of the plasma membrane by transferring a palmitoyl group to the 2-position of one of the glucosyl residues of trehalose to form trehalose 2-palmitate. PapA3 next transfers a mycolipenoyl group, synthesized by the polyketide synthase Pks3/4, to the 3-position of trehalose 2-palmitate to yield DAT. DAT is then flipped across the plasma membrane either by an as yet unknown flippase or by MmpL10 and further elaborated with mycosanoyl, mycolipenoyl, and/or mycolipanolyl chains by Chp2 on the periplasmic face of the plasma membrane to form the penta-acylated PAT. DAT serves both as the donor and acceptor substrate in these Chp2-mediated transesterification reactions. DAT and PAT are taken up by MmpL10 and / or by other unknown enzymes located on the periplasm or outer membrane and exported to the cell surface. The enzymes in this biosynthetic pathway, influenced by HupB are highlighted in blue.

PDIM, found in the outermost layers of the cell envelope are the major waxes of the tubercle bacillus (Ortalo-Magne *et al.*, 1996). The pathway for the synthesis of DAT and PAT is illustrated in Fig. 4.5. The genes *mas* (mycocerosic acid synthase) and *ppsA-E* (ppolyketide synthases) responsible for the synthesis of mycocerosic acids and phthiocerol / phenolphthiocerol respectively were not altered in the *hupB* KO mutant indicating that the initial steps were not influenced by HupB. The enzyme Mas is an iterative polyketide synthase that acts like FASI but produces $C_{29\text{-}32}$ mycocerosic acids after several rounds of extension on a C_{18} fatty acid precursor, using methylmalonyl-CoA instead of malonyl-CoA, which is the source of the methyl branches of mycocerosic acids. PpsA-E are type I modular polyketide synthases that elongate a $C_{20\text{-}22}$ fatty acid chain by reduction and decarboxylation to produce phthiocerols. The two acyl-CoA synthases FadD26 and FadD28 catalyze acyl-transfer reactions releasing phthiocerol and mycocerosic acids from their respective synthases (PpsA-E and Mas) (Camacho *et al.*, 2001; Cox *et al.*, 1999). The transcript level of the gene *fadD28* was reduced in the KO mutant

and the ChIP data showed a 30-fold and 20-fold enrichment for *fadD26* and *fadD28,* thus substantiating the effect of HupB at an intermediary step of PDIM biosynthesis. Export of PDIM is mediated by MmpL7, a membrane transport protein and DrrC, an ABC transporter is required to transfer the PDIM to the cell surface (Camacho *et al.*, 2001). HupB box was surprisingly found in the promoter DNA of *fadD26* and *drrC* genes though the microarray data showed no alteration in the transcript levels. A 19-fold enrichment was observed in *drrC*, thus showing that HupB has an effect on the transport of PDIM.

From the above, it is certain that HupB has a role to play in several of the lipid biosynthetic pathways. While no disruption of the various pathways were observed, evident from the chromatograms of the different lipids, it is likely that the potentiating role of HupB in lipid biosynthesis, not exerted in the mutant strain accounts for the reduced lipid levels in the mutant strain, an observation also seen with mycobactin biosynthesis. The significance of these findings needs to be validated in an *in vivo* environment to understand the impact of these changes on the survival of the organism.

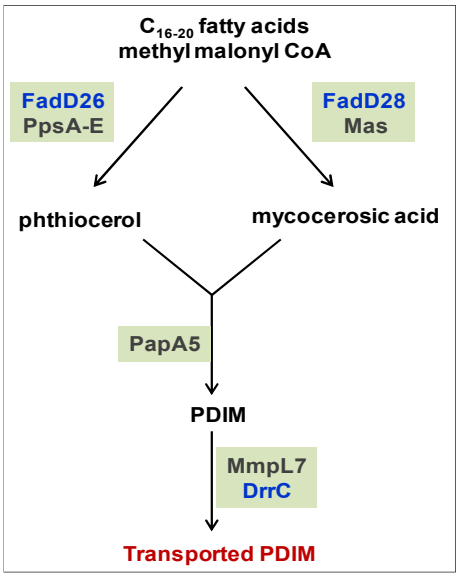

Fig. 4.5. PDIM biosynthetic pathway of *M. tuberculosis*. Adapted from (Jain *et al.*, 2007). Pps, phthiocerol synthase; Mas, mycocerosic acid synthase. PDIM consists of two mycocerosic acids esterified to phthiocerol. Mas synthesizes the methyl branched mycocerosic acids through successive additions of MMCoA whereas PpsA-E synthesize phthiocerol. FadD26 and FadD28 are responsible for activating straight chain fatty acids for transfer to Pps and Mas, respectively. PapA5 is an acyltransferase

responsible for the transfer of mycocerosic acids to phthiocerol to form PDIM. MmpL7 and DrrC are required for transport of PDIM to the cell wall. The enzymes in this biosynthetic pathway, influenced by HupB are highlighted in blue.

Survival of the hupKO mutant inside macrophages

The host immune system comprising of macrophages, neutrophils and other phagocytic cells mount a complex antimicrobial response to kill or limit the proliferation of *M. tuberculosis.* The major antimicrobial molecules are reactive oxygen intermediates (ROI) and reactive nitrogen intermediates (RNI) (Nathan & Ehrt, 2004). Although the generation of ROI and RNI is less in eukaryotic cells, the evolution of specialized systems for the expression of both the reactive species, nitric oxide synthase 2 / inducible nitric oxide synthase (NOS2 / iNOS) and NADPH phagocyte oxidase (Phox) gives the macrophages an added advantage in containment of infection (Zahrt & Deretic, 2002). NADPH oxidase generates ROI through the reduction of molecular oxygen to form superoxide and its dismutation and decomposition products, hydrogen peroxide and hydroxyl radical (Saran *et al.*, 1999). Iron serves as the catalyst in the Fenton reaction generating ROI (Fenton, 1894). The nitric oxide synthase uses L-arginine to generate nitric oxide which is further oxidized to nitrite, nitrogen dioxide and nitrate. The reaction of nitric oxide with cysteine sulfhydryls results in the generation of nitrosothiols and sulfenic acids (Nathan & Shiloh, 2000). Another category of reactive intermediates occurs by the interaction of the products of NADPH oxidase and NOS2 such as the generation of peroxynitrite by the reaction of superoxide with nitric oxide (Pacelli *et al.*, 1995). The production of ROI is also likely to be regulated by the expression of specific cytokines. Cytokines such as IFN-γ, TNF-α and IL-1β are known to activate NOX (Zahrt & Deretic, 2002) NOS2 transcription (Stuehr & Marletta, 1985) whereas the synergistic action of TNF-α and IFN-γ has been reported to be critical for NOS2 induction and the subsequent RNI-mediated antimycobacterial activity (Mohan *et al.*, 2001).

When the mutant strain *M.tb.ΔhupB* was added to macrophages, there was poor infectivity when compared to the WT strain and the organisms that had gained entry failed to survive and multiply inside the macrophages. While

the defective iron uptake and alteration in the lipid levels contribute to its inability to grow inside the macrophages, our findings also show that the mutant strain is unable to cope up with the oxidative stress mounted by the macrophages. The ROI and RNI are toxic to the pathogen as they can damage macromolecules including DNA, lipids and proteins (Zahrt & Deretic, 2002). The WT organisms resist the phagocyte oxidative burst by the elaboration of oxidative stress enzymes, superoxide dismutases (iron-dependent SodA and copper/zinc-dependent SodC) which convert superoxides to hydrogen peroxides which are then acted upon by the catalase-peroxidase (KatG) to form water and molecular oxygen. Another enzyme, alkyl hydroperoxide reductase (AhpC) acts on the organic peroxides and reduces them to their non-toxic alcohol forms (Dussurget & Smith, 1998). As iron plays an important role in the generation of reactive intermediates, both iron replete and iron-limited organisms of *M.tb.*H37Rv, *M.tb.ΔhupB* and *M.tb.ΔhupB* / pMS101 were used for infection studies. It was observed that iron replete organisms produced comparatively more ROI and RNI than the iron-limited organisms as reflected by the >2-fold increase in the transcript levels of *NOX1* (NADPH oxidase), *NOXA1* (NADPH oxidase activator 1) and *NOS2* (nitric oxide synthase). The WT strain effectively countered this oxidative stress by expressing higher levels of SodA, AhpC and KatG, as reflected by the 25-, 13- and 9-fold increase of their transcript levels. Moreover, it was seen that the expression of pro-inflammatory cytokines such as IFN-γ, TNF-α, IL-1β which are known to induce production of ROI and RNI were reduced under iron limitation, thus the effect of oxidative stress on the bacteria is less when compared to high iron conditions. A direct effect of HupB in dealing with oxidative stress is a possibility. HupB can bind iron (Takatsuka *et al.*, 2011) and prevent it from catalyzing the formation of the free radicals *via* the Fenton reaction.

The mutant strain showed low levels of *sodA, katG* and *ahpC*, making it vulnerable to the increased ROS and RNI that are produced due to increased activity of the NOX1, NOXA1 and NOS2 and indirectly through the increased expression of IFN-γ, TNF-α and IL-1β which were 4-, 8- and 12-fold higher. Among the three genes, HupB is likely to influence *sodA* and *ahpC*, as these genes show the HupB box in their promoter DNA that was recognized by HupB,

as demonstrated by ChIP assay, which showed a 3- and 16-fold enrichment. It appears that HupB has no regulatory role on *katG*, which is controlled by the iron regulator FurA. In addition, the susceptibility of the mutant strain to the prevailing conditions within the macrophages could also be contributed by the changes in the lipid composition in the cell wall. LAM, PGL-1 and cyclopropanated mycolic acids are known to provide protection by scavenging the oxygen radicals (Flynn & Chan, 2001) while LAM along with TDM has been reported to prevent phagosomal maturation *in vitro* (Sakamoto, 2012).

Thus, the reduced survival of the mutant inside the macrophages could be contributed by one or more of the above factors.

Clinical significance of HupB: potential as a diagnostic marker in pulmonary and extrapulmonary TB patients

Earlier studies in the lab established the clinical significance of HupB by demonstrating the expression of the protein in TB patients who showed high titres of circulating anti-HupB antibodies (Sivakolundu *et al.*, 2013; Yeruva *et al.*, 2006). There was a strong negative correlation of their levels with the serum iron status, with TB patients presenting low serum iron when compared to the endemic normal controls. The serum ferritin values were elevated with some patients showing unusually high values, indicating the shift of free iron to the storage form. While the iron-limiting conditions prevailing in TB patients is due to the withholding of iron by the mammalian host as a component of innate immunity (Kochan, 1977), it is equally possible that the lower socio-economic strata of individuals with malnutrition and anemia are susceptible to infection. With the serum titre of anti-HupB antibodies being high in TB patients, when compared to the endemic normal and patient contacts, it was notable that maximal levels were observed in the serum of EPTB cases (Sivakolundu *et al.*, 2013). This is of diagnostic interest, as a reliable and specific laboratory diagnostic test is not available for such patients when compared to PTB cases. The diagnosis of EPTB is often based on clinical symptoms, as the biological samples obtained from other locations other than sputum often are paucibacillary, thus making culture confirmation or AFB testing impractical.

HupB is expressed not only by *M. tuberculosis* but also by other mycobacteria. As our earlier studies were done with the full length HupB protein, an antigenic determinant of HupB was identified in this study for increasing the specificity of diagnosis (Sritharan *et al.*, 2015). *In silico* analysis of the protein from different mycobacteria revealed considerable heterogeneity in the size and sequence of the protein among mycobacteria, with the protein restricted to 145 aa in *M. abscessus* to a larger protein of 229 aa in *M. ulcerans*. Phylogenetic analysis reflecting the evolutionary changes grouped the pathogens from the non-pathogens based on the variations in HupB (Sritharan, 2016), making the latter a potential phylogenetic marker along with others such as *recA*, *rpoB* and 16S rRNA (Blackwood *et al.*, 2000; Kim *et al.*, 1999; Tortoli, 2003). In addition, the members of the *M. tuberculosis* complex formed a separate clade showing the usefulness of the protein in grouping genetically identical members. Of relevance is the observation that HupB can be used to differentiate *M. tuberculosis* from some field strains of *M. bovis* and the vaccine strain *M. bovis* BCG that express a 205 aa protein, with the 9 missing amino acids in the C-terminal end of the protein resulting due to a 27 bp deletion in the *hupB* gene. A PCR-based test (Prabhakar *et al.*, 2004), using suitable combination of primers for identifying the region of deletion was reported that could differentiate *M. tuberculosis* from BCG and *M. bovis* strains. As highlighted in Results, maximal sequence variation was observed in the C-terminal region. Experimentally, when three antigenic fragments of HupB, cloned and expressed as recombinant antigens were evaluated for their diagnostic potential, the antigenic fragment HupB-F2 of *M. tuberculosis*, bearing amino acids 63-161 performed well as an antigen when compared to HupB-F1 (aa 1-71) and HupB-F3 (aa 164- 214) and the full length protein (Sritharan *et al.*, 2015). This was not surprising as sequence alignment clearly showed high antigenic diversity within this region. The N-terminal fragment HupB-F1 is highly conserved in mycobacteria and is homologous to the HU protein of *E. coli*, thus lowering its potential as a marker. As HupB-F3 also did not show promising results in the screening, HupB-F2 fragment was considered a strong candidate as a marker. Another notable feature of HupB-F2 is that it contains the 9 amino acids reportedly missing in the vaccine strain *M. bovis* BCG that would make

HupB-F2 a good candidate to identify TB-infected individuals and differentiate from BCG vaccinated individuals.

Using HupB-F2 as antigen, TB patients diagnosed clinically and by conventional laboratory investigations as positive showed significantly high titres of antibodies against this fragment when compared with the control group. As was reported earlier (Sivakolundu *et al.*, 2013), the antibody levels showed negative correlation with the serum iron status. The significantly high levels in patients with relapse of the disease ($P<0.05$ compared to healthy controls) strongly suggest the longer exposure of the bacilli (possibly in dormant state) to iron-limiting conditions within the human host. It is evident that HupB evokes a strong humoral response, indicative of a Th2 response. In addition, the markedly high levels in EPTB cases strongly suggests the role of this protein as an adhesion molecule as seen with other mycobacteria, namely *M. leprae* in which the HupB homologue called laminin-binding protein (LBP) is necessary to bind Schwann cells (Shimoji *et al.*, 1999). In addition, studies with another iron-regulated protein HBHA (heparin-binding hemagglutinin adhesin) in *M. tuberculosis*, which shares several features with HupB has been established as an adhesion molecule promoting adherence of the pathogen to epithelial cells (Pethe *et al.*, 2001; Pethe *et al.*, 2002). Based on the similarity between HBHA and HupB, by virtue of their surface localization, lysine and arginine-rich C-terminus, methylation pattern and regulation by iron levels, HupB is a strong candidate as an adherence factor. Further detailed studies are needed to establish the role of HupB in EPTB. This will help to apply HupB as a definitive marker for EPTB that suffer from the disadvantage of proper laboratory diagnosis by conventional tests like smear examination of sputum, culture and chest X-ray as done for pulmonary TB. In fact, PCR amplification of *hupB* and *IS*6110 (Soto *et al.*, 2012) identified *M. tuberculosis* in a case of Takayasu's arteritis due to infection of the arteries by this pathogen.

Considering the low-iron environment prevailing in the human host and the expression of HupB *in vivo* (Sivakolundu *et al.*, 2013), this study strengthens the potential of HupB as a biomarker, specifically for EPTB patients. The high level of antibodies in the serum of TB patients led us to study the cytokine profile of the peripheral blood mononuclear cells to HupB. The

immune system of the human host first senses the presence of the pathogen via the macrophages and dendritic cells, followed by interplay between the macrophages and T cells that aim to target the killing of the pathogen by the production of cytokines. Among the cytokines, IFN-γ and TNF-α are the major players and are produced by T cells and NK cells. The effectiveness of these pro-inflammatory cytokines is determined by their relative amounts of expression and the levels of the anti-inflammatory cytokines, predominantly IL-10. It is reported that the relative amounts of cytokines like IFN-γ, TNF-α, IL10 and IL-6 determine not only the severity of the disease but also its localization in extrapulmonary loci (Hasan *et al.*, 2009; Jamil *et al.*, 2007; Sahiratmadja *et al.*, 2007). As it is well known that *M. tuberculosis* can disseminate to other sites and reside as dormant bacilli or be activated to produce disease manifestations in these compartments (Sharma & Mohan, 2004), mycobacterial antigens must play defined roles in influencing the host immune response. Here, HupB shifts the immune response to Th2 type.

In this study, both PTB and EPTB patients elicited a heightened immune response, both pro- and anti-inflammatory to HupB as antigen. In fact, HupB proved to be a better antigen in stimulating the T cell response in TB patients (both pulmonary and extrapulmonary) compared to PPD. Low levels of IFN-γ, a pro-inflammatory cytokine were produced by both groups of TB patients compared to the significantly higher levels in healthy controls. IFN-γ is the principal mediator of macrophage activation and protection of the human host against development of the disease by *M. tuberculosis* (Van Crevel *et al.*, 2002). Considering the role of HupB in iron acquisition, it must be pointed out that IFN-γ plays an additional role of decreasing the availability of iron, essential for the growth of the pathogen. In a healthy individual, this cytokine activates human monocytes, resulting in down-regulation of the surface-expressed transferrin receptor (TfR) that is necessary for internalizing the iron into the phagocytic cell, thereby limiting iron to the intracellular pathogen (Boelaert *et al.*, 2007). Further studies are needed to study the interrelationship between iron levels, HupB and IFN-γ production. It is also reported that in endemic populations exposed to tuberculous and environmental mycobacteria, the *M.*

tuberculosis-induced IFN-γ production as well as IFN-γR signaling were significantly down-regulated during active TB (Sahiratmadja *et al.*, 2007).

In EPTB patients, there is maximal expression of IL-10 by PBMCs stimulated with HupB, which coupled with low IFN-γ points to HupB as a possible factor for establishment of the pathogen in extrapulmonary loci in these patients. IL-10 is a potent suppressor of IFN-γ synthesis by helper T cells and by NK cells that causes inhibition of antigen presentation to Th1 cells (Torres *et al.*, 1998) and plays an anti-inflammatory role through the inhibition of IL-12 expression (Giacomini *et al.*, 2001; Sahiratmadja *et al.*, 2007). It may be noted that the IL-10 levels were not elevated in the PTB patients, who however responded to HupB with low IFN-γ levels. These observations led us to propose HupB as a marker for EPTB diagnosis. This finding needs to be strengthened by screening a larger number of EPTB cases with HupB. Further, it will be interesting to see if IL-10 can be used as a pre-treatment marker, as reported in a study (Priya *et al.*, 2009) in which high levels of IL-10 were expressed in response to recombinant Ag 85A, a 32 kDa protein, by the PBMCs of TB patients before chemotherapy, with the levels showing time-dependent decrease upon chemotherapy.

In contrast to the IFN-γ and IL-2 production, TNF-α production was significantly increased in EPTB patients showing that protective immune response is not impaired during active TB. TNF-α, another pro-inflammatory cytokine acting synergistically with IFN-γ causes the release of reactive nitrogen intermediates that target the pathogen (Hernandez-Pando & Rook, 1994). This cytokine is also known to trigger granuloma formation and limit the progression of the disease. But, at high levels, it can cause severe host tissue damage (Van Crevel *et al.*, 2002). The ratio of IFN-γ / TNF-α also showed a significant decrease in EPTB compared to PTB. The IFN-γ / IL-10 and IFN-γ / TNF-α ratio were found to be suggestive of an anti-inflammatory immune response to HupB and could be utilized to differentiate between PTB and EPTB; thus they are useful biomarker signatures.

The pattern of expression of IL-4 and IL-6 to HupB stimulation indicated promotion towards disease development. IL-4 was unaltered in the patient

group, a feature also reported in other studies (Zhang *et al.*, 1995a). Suppression of IFN-γ, along with the maintenance of the steady-state of IL-4 production was considered to contribute to the persistence of the pathogen and thus the progression of tuberculosis in susceptible individuals (Bhattacharyya *et al.*, 1999). Another possibility for lower protection in all the TB patients could be the induction and activity of IL-6, a pleiotropic cytokine and a B cell growth and differentiation factor, that was significantly high in all the TB cases compared to the healthy individuals. IL-6 secreted by *M. tuberculosis* - infected macrophages inhibits the responses of uninfected macrophages to IFN-γ suggesting that this inhibitory property of IL-6 could be exploited to evade eradication by a cellular immune response (Nagabhushanam *et al.*, 2003). Both the patient groups secreted high levels of IL-8, an early response of macrophages after phagocytosis of the pathogen. Its production serves to attract both acute and chronic inflammatory cells of active infection and thus participates in the process of containment of the pathogen (Matsushima & Oppenheim, 1989).

Th2 immune response due to increased secretion of IL-4, IL-10 and IL-5 results in increased antibody production due to their role in potentiating B-cell differentiation and activation (Howard & Zwilling, 1999a). When PPD was used as a stimulant, high levels of IL-4 and IgG antibodies were detected in TB patients, thus inducing a Th2 response whereas in the healthy controls, the levels of IL-2 and IFN-γ were high indicating a Th1 pattern (Sánchez *et al.*, 1994). Similarly, two other antigens of 38 kDa and 19 kDa induced high levels of IL-4 and reduced IFN-γ with a prominent humoral immune response, thus following a Th2 pattern (Surcel *et al.*, 1994). Humoral response to mycobacterial antigens such as antigen 85A, 85B, ESAT-6, 30 kDa protein has also been reported earlier (Macedo *et al.*, 2010; Torres *et al.*, 1998). Here, the cytokines produced by the PBMCs of TB patients to HupB and the high circulating anti-HupB antibodies (Sivakolundu *et al.*, 2013; Sritharan *et al.*, 2014) is due to the Th2 pattern, thus triggering a strong humoral response.

Our earlier reports and the observations in this study reflect the diagnostic potential of HupB. We have also identified an antigenic determinant HupB-F2 for increasing the specificity of the diagnosis. Of significant clinical relevance will be the use of HupB as a marker for EPTB, a form of the disease

that is often diagnosed only clinically, with detection of granuloma in biopsy samples sometimes adding to the confirmation of the disease.

Conclusions and Future Perspectives

HupB is an essential protein required for the growth and survival of *M. tuberculosis* inside macrophages. Our earlier reports and the findings in this study unequivocally strengthen the important role played by HupB in iron homeostasis, both as an iron transporter and as a transcriptional regulator of not only mycobactin but also several iron transport proteins. By virtue of its DNA-binding property, specifically to the HupB box, it is observed to influence the expression of several genes and here, its role in lipid biosynthesis was studied. HupB, as analysed by the ChIP assay bound the HupB box in the promoter DNA of genes, the products of which are components of the biosynthetic pathways of cell wall lipids. Also, there was a reduction in the lipid levels in the *hupB* KO strain. While these observations pointed to the influence of HupB in these pathways, further work is needed to study the exact mechanism of action and identify other interacting proteins / factors.

HupB as an adherence factor is reflected not only by the function of the homologous protein in other mycobacteria like *M. leprae*, but also by the antibodies against the protein in EPTB patients. This role of the protein in *M. tuberculosis* must be explored further as it can help to develop it as a marker in this form of the disease that is often difficult to diagnose due to the paucibacillary nature of the biological samples used for analysis. The HupB-F2 region of the protein offers a lot of scope for developing a diagnostic test, either for antigen / antibody detection or by molecular methods such as PCR / Real time PCR.

In conclusion, HupB is a protein of clinical relevance that can be explored as a diagnostic marker. Possible potential as a vaccine candidate can also be explored that however may be limited by some structural similarities in its C-terminal region with that of the histone proteins in the mammalian host.

CHAPTER 5

SUMMARY

HupB, a 28 kDa IREP of *M. tuberculosis,* is expressed under iron-limitation and plays an important role in the biosynthesis of siderophores and its own expression. To functionally characterize HupB, a *hupB* deletion mutant *M.tb.ΔhupB* and a *hupB*-complemented strain *M.tb.ΔhupB* / pMS101 was generated. The focus of this study was to identify additional roles of HupB in *M. tuberculosis* such as in iron transport, survival in host cells, lipid biosynthesis and study the significance of its expression *in vivo*. The following are the salient observations from the study

1. **HupB influences growth and phenotype:** *M.tb.*H37Rv, *M.tb.ΔhupB* and *M.tb.ΔhupB* / pMS101 were grown on OADC containing Middlebrook 7H11 solid media. When glycerol was used as a carbon source *M.tb.*H37Rv showed eugonic (abundant) growth and rugose morphology. *M.tb.ΔhupB* showed a rugose, dysgonic (sparse) growth while the phenotype was regained in the complemented strain. In the presence of pyruvate as the sole carbon source, decrease in growth was observed in *M.tb.*H37Rv but the rugosity was maintained. The mutant *M.tb.ΔhupB* showed dysgonic growth and a less rugose morphology while the phenotype was restored in the complemented strain. When grown in Proskauer and Beck minimal media under iron-regulated conditions, the mutant strain exhibited a prolonged lag phase that was more pronounced under low iron conditions. This was restored in the *hupB*-complemented strain that showed similar growth characteristics as the wild type *M.tb*.H37Rv.

2. **HupB regulates siderophore biosynthesis**
   Iron-limited *M.tb.ΔhupB* showed significantly lower expression of Mb and CMb when compared to *M.tb*.H37Rv, as revealed by time course assay. The levels were restored upon complementing the mutant with *hupB*. In agreement with the low mRNA transcripts of the *mbt* genes in microarray analysis, qRT-PCR showed low levels of *mbtB* and *mbtA*. ChIP assay showed a positive enrichment when the upstream region of *mbtB* was amplified by qRT-PCR showing that HupB bound to the HupB-box in the promoter region, implicating its role in regulating their expression.

3. **HupB is essential for *M. tuberculosis* to survive inside macrophages**

When all the three strains were used to infect macrophages, the recovery of the organisms 4 h after infection showed that the mutant's entry into the macrophage was restricted compared to the wild type strain. Further, those mutant organisms that gained entry failed to survive inside the macrophages. This was evident in the significantly reduced number of bacteria recovered from days 0 to 7 as assayed by qRT-PCR, ATP assay and CFU analysis. It is likely that the inability to acquire iron due to low production of the siderophores contributed to the inability of the mutant to survive inside macrophages.

The macrophages produce reactive oxygen and nitrogen intermediates to eliminate the pathogen. The inability of the KO mutant to survive within macrophages could be attributed to their inability to counter the host response which was evident from the high levels of ROS in the macrophages 12 h and 24 h post infection. On the other hand, the ROS levels were 2-fold lower when *M.tb.*H37Rv and the complemented strain were used to infect the macrophages. The transcript levels of *sodA, ahpC* and *katG* encoding the oxidative stress in the pathogen that detoxify the ROS showed significantly low levels in the mutant compared to the wild type and *hupB*-complemented strain. Positive enrichment in ChIP assay also demonstrated that the oxidative stress genes *sodA* and *ahpC* are regulated by HupB. The high levels of ROS in the mutant correlated with the rise in *NOX1, NOXA1* and *NOS2* transcripts. Higher expression of pro-inflammatory cytokines such as IFN-γ and TNF-α known to induce the production of ROS was also observed in the mutant compared to the WT *M.tb.*H37Rv

4. **HupB functions as an iron transporter and mediates transfer of iron from the extracellular Fe-CMb to the desferri Mb in the cell envelope**

When ^{55}Fe-CMb was used as the source of iron, maximum radiolabel was recovered in the whole cells of the iron-limited WT *M.tb.*H37Rv while the mutant was found to be defective in iron uptake. Blocking of WT organisms with anti-HupB antibodies drastically reduced incorporation of ^{55}Fe in the iron-limited WT implicating the role of HupB as the pre-immune sera showed

no effect. Time course uptake of ^{55}Fe-CMb done with low iron grown *M.tb.*H37Rv showed that more than 90% of the radioactivity was recovered from Mb at 15, 30 45 and 60 min showing that iron was transferred from CMb to Mb.

The interaction of HupB with ferri-CMb was studied by incorporating the purified protein in liposomes. The radiolabel associated with the HupB-entrapped liposome, higher than empty liposomes showed an increase when mycobactin was included along with HupB during liposome preparation. The experiments, when repeated with CHAPS-solubilised cell wall proteins of the mutant (HupB-negative) and wild type organisms confirmed the role of HupB in iron uptake.

In silico modeling of HupB was done using I-TASSER and the siderophores were docked with it. Ferri-CMb interaction involved both H-bonding and hydrophobic interactions while ferri-Mb had only hydrophobic interactions with HupB. Far-UV CD spectra of HupB alone and with increasing concentrations of siderophores showed no structural changes with desferri-CMb, marginal change with ferri-CMb while a significant change in optical ellipticity was observed with ferri-Mb. Binding constants calculated using fluorescence titration experiments showed that both ferri-Mb (K_d = 38.76 µM) and ferri-CMb (K_d = 22.42 µM) have moderate binding affinities for HupB while desferri-CMb (K_d = 769 µM) exhibited weak binding.

5. **HupB influences the fatty acid profile and plays a role in the biosynthesis of several lipids including mycolic acids, sulfolipid-1, phthiocerol dimycocerosate, diacyl trehalose and penta-acyl trehalose**

Fatty acid profiling revealed an increase in the percentage of unsaturated fatty acids in the mutant compared to the WT. Arachidic acid (20:0) and certain unique fatty acids, pentadecylic (15:0) and margaroleic acid (17:1 ω8c) were present only in *M.tb.ΔhupB*. Biochemical analysis of the extracted mycolic acids and surface exposed lipids showed reduced levels in the mutant. The regulatory role of HupB was confirmed by ChIP assay as positive enrichment was observed for few of the genes involved in the biosynthesis of these lipids; like *fabD, kasA, inhA, fadD32* and *pks13*

(mycolic acids); *papA1* and *mmpL8* (SL-1); *papA3, pks4, chp2* and *mmpL10* (DAT, PAT); *fadD26, fadD28* and *drrC* (PDIM).

6. HupB elicits a Th2 response in tuberculosis patients

The study done on pulmonary and extrapulmonary TB patients showed a statistically significant higher proliferative response of the PBMCs to HupB when compared to healthy controls (in EPTB cases P = 0.0001). Based on the sensitivity and specificity, the performance of HupB was superior to PPD. The low IFN-γ / IL-10 and IFN-γ / TNF-α ratio along with the heightened humoral response in TB patients, more so in EPTB cases, suggested a shift towards Th2 immune response to HupB.

7. High levels of anti-HupB antibodies in EPTB patients reflects the diagnostic potential of HupB

HupB elicited a strong humoral immune response as high titres of anti-HupB antibodies were detected in the serum of TB patients. Among the HupB fragments, maximal titres were seen with HupB-F2. This antigen, found to be reactive in all groups of TB patients, is of considerable diagnostic potential in relapse cases and in EPTB. In the latter, the high titre (approximately 5 to 6-fold) when compared to healthy controls was statistically significant ($P < 0.05$) and was found to be better than the full-length HupB. In relapse cases, both HupB-F2 and full-length HupB showed good potential as antigens. A negative correlation with serum iron levels (-0.415; Pearson correlation analysis) was observed with HupB-F2. The HupB-F2 region, showing marked sequence variation among the protein expressed in different mycobacterial species is a potential candidate for identification of *M. tuberculosis* as this region carries the 9 amino acids that is deleted in the vaccine strain M. bovis BCG making it possible to differentiate TB infected patients from BCG vaccinated individuals.

Thus, our studies have given a better understanding of iron acquisition in this pathogen, highlighting the multiple roles of HupB, which can be called a ‘moonlighting protein’ and offering an useful diagnostic marker for the screening of TB patients, specifically EPTB cases.

CHAPTER 6

BIBLIOGRAPHY

Abdallah, A. M., van Pittius, N. C. G., Champion, P. A. D., Cox, J., Luirink, J., Vandenbroucke-Grauls, C. M., Appelmelk, B. J. & Bitter, W. (2007). Type VII secretion—mycobacteria show the way. *Nature reviews microbiology* **5**, 883-891.

Adilakshmi, T., Ayling, P. D. & Ratledge, C. (2000). Mutational analysis of a role for salicylic acid in iron metabolism of Mycobacterium smegmatis. *Journal of bacteriology* **182**, 264-271.

Akyol, Z., Bartos, J. A., Merrill, M. A., Faga, L. A., Jaren, O. R., Shea, M. A. & Hell, J. W. (2004). Apo-calmodulin binds with its C-terminal domain to the N-methyl-D-aspartate receptor NR1 C0 region. *Journal of Biological Chemistry* **279**, 2166-2175.

Algood, H. M. S., Lin, P. L., Yankura, D., Jones, A., Chan, J. & Flynn, J. L. (2004). TNF influences chemokine expression of macrophages in vitro and that of CD11b+ cells in vivo during Mycobacterium tuberculosis infection. *The Journal of Immunology* **172**, 6846-6857.

Aliprantis, A. O., Yang, R. B., Weiss, D. S., Godowski, P. & Zychlinsky, A. (2000). The apoptotic signaling pathway activated by Toll-like receptor-2. *The EMBO journal* **19**, 3325-3336.

Andrei, C., Dazzi, C., Lotti, L., Torrisi, M. R., Chimini, G. & Rubartelli, A. (1999). The secretory route of the leaderless protein interleukin 1β involves exocytosis of endolysosome-related vesicles. *Molecular biology of the cell* **10**, 1463-1475.

Anthis, N. J. & Clore, G. M. (2013). Sequence-specific determination of protein and peptide concentrations by absorbance at 205 nm. *Protein Science* **22**, 851-858.

Appelberg, R., Orme, I., De Sousa, M. P. & Silva, M. (1992). In vitro effects of interleukin-4 on interferon-gamma-induced macrophage activation. *Immunology* **76**, 553.

Åslund, F., Zheng, M., Beckwith, J. & Storz, G. (1999). Regulation of the OxyR transcription factor by hydrogen peroxide and the cellular thiol—disulfide status. *Proceedings of the National Academy of Sciences* **96**, 6161-6165.

Barclay, R., Ewing, D. & Ratledge, C. (1985). Isolation, identification, and structural analysis of the mycobactins of Mycobacterium avium, Mycobacterium intracellulare, Mycobacterium scrofulaceum, and Mycobacterium paratuberculosis. *Journal of bacteriology* **164**, 896-903.

Bartos, P., Falkinham, J. & Pavlik, I. (2004). Mycobacterial catalases, peroxidases, and superoxide dismutases and their effects on virulence and isoniazid-susceptibility in mycobacteria-a review. *Veterinarni Medicina-UZPI (Czech Republic)*.

Belardinelli, J. M., Larrouy-Maumus, G., Jones, V., de Carvalho, L. P. S., McNeil, M. R. & Jackson, M. (2014). Biosynthesis and translocation of unsulfated acyltrehaloses in Mycobacterium tuberculosis. *Journal of Biological Chemistry* **289**, 27952-27965.

Belisle, J. T., Vissa, V. D., Sievert, T., Takayama, K., Brennan, P. J. & Besra, G. S. (1997). Role of the major antigen of Mycobacterium tuberculosis in cell wall biogenesis. *Science* **276**, 1420-1422.

Bertrand, T., Eady, N. A., Jones, J. N., Nagy, J. M., Jamart-Grégoire, B., Raven, E. L. & Brown, K. A. (2004). Crystal structure of Mycobacterium tuberculosis catalase-peroxidase. *Journal of Biological Chemistry* **279**, 38991-38999.

Bhattacharyya, S., Singla, R., Dey, A. & Prasad, H. (1999). Dichotomy of cytokine profiles in patients and high-risk healthy subjects exposed to tuberculosis. *Infection and immunity* **67**, 5597-5603.

Bhowmick, T., Ghosh, S., Dixit, K., Ganesan, V., Ramagopal, U. A., Dey, D., Sarma, S. P., Ramakumar, S. & Nagaraja, V. (2014). Targeting Mycobacterium tuberculosis nucleoid-associated protein HU with structure-based inhibitors. *Nature communications* **5**.

Birnboim, H. C. & Doly, J. (1979). A rapid alkaline extraction procedure for screening recombinant plasmid DNA. *Nucleic Acids Res* **7**, 1513-1523.

Blackwood, K. S., He, C., Gunton, J., Turenne, C. Y., Wolfe, J. & Kabani, A. M. (2000). Evaluation of recA sequences for identification of Mycobacterium species. *Journal of clinical microbiology* **38**, 2846-2852.

Bloch, H. (1950). Studies on the virulence of Tubercle bacilli isolation and biological properties of a constituent of virulent organisms. *The Journal of experimental medicine* **91**, 197-218.

Boehme, C. C., Nabeta, P., Hillemann, D. & other authors (2010). Rapid molecular detection of tuberculosis and rifampin resistance. *New England Journal of Medicine* **363**, 1005-1015.

Boelaert, J. R., Vandecasteele, S. J., Appelberg, R. & Gordeuk, V. R. (2007). The effect of the host's iron status on tuberculosis. *The Journal of infectious diseases* **195**, 1745-1753.

Bordier, C. (1981). Phase separation of integral membrane proteins in Triton X-114 solution. *The Journal of biological chemistry* **256**, 1604-1607.

Boshoff, H. I. & Barry, C. E. (2005). Tuberculosis—metabolism and respiration in the absence of growth. *Nature Reviews Microbiology* **3**, 70-80.

Braibant, M., Gilot, P. & Content, J. (2000). The ATP binding cassette (ABC) transport systems of Mycobacterium tuberculosis. *FEMS microbiology reviews* **24**, 449-467.

Brennan, P. J. & Nikaido, H. (1995). The envelope of mycobacteria. *Annual review of biochemistry* **64**, 29-63.

Broaddus, V. C., Hébert, C. A., Vitangcol, R. V., Hoeffel, J. M., Bernstein, M. S. & Boylan, A. M. (1992). Interleukin-8 is a major neutrophil chemotactic factor in pleural liquid of patients with empyema. *American Review of Respiratory Disease* **146**, 825-825.

Brooks, B. W., Young, N., Watson, D., Robertson, R., Sugden, E., Nielsen, K. & Becker, S. (1991). Mycobacterium paratuberculosis antigen D: characterization and evidence that it is a bacterioferritin. *Journal of clinical microbiology* **29**, 1652-1658.

Bullen, J., Griffiths, E. & Edmiston, C. E. (1999). Iron and infection: molecular, physiological and clinical aspects. *Shock* **12**, 410.

Byrd, T. (1997). Tumor necrosis factor alpha (TNFalpha) promotes growth of virulent Mycobacterium tuberculosis in human monocytes iron-mediated growth suppression is correlated with decreased release of TNFalpha from iron-treated infected monocytes. *Journal of Clinical Investigation* **99**, 2518.

Calder, K. M. & Horwitz, M. A. (1998). Identification of iron-regulated proteins of Mycobacterium tuberculosis and cloning of tandem genes encoding a low iron-induced protein and a metal transporting ATPase with similarities to two-component metal transport systems. *Microbial pathogenesis* **24**, 133-143.

Camacho, L. R., Constant, P., Raynaud, C., Lanéelle, M.-A., Triccas, J. A., Gicquel, B., Daffé, M. & Guilhot, C. (2001). Analysis of the Phthiocerol Dimycocerosate Locus ofMycobacterium tuberculosis EVIDENCE THAT THIS LIPID IS INVOLVED IN THE CELL WALL PERMEABILITY BARRIER. *Journal of Biological Chemistry* **276**, 19845-19854.

Canueto-Quintero, J., Caballero-Granado, F. J., Herrero-Romero, M. & other authors (2003). Epidemiological, clinical, and prognostic differences between the diseases caused by Mycobacterium kansasii and Mycobacterium tuberculosis in patients infected with human immunodeficiency virus: a multicenter study. *Clinical infectious diseases* **37**, 584-590.

Card, G. L., Peterson, N. A., Smith, C. A., Rupp, B., Schick, B. M. & Baker, E. N. (2005). The crystal structure of Rv1347c, a putative antibiotic resistance protein from Mycobacterium tuberculosis, reveals a GCN5-related fold and suggests an alternative function in siderophore biosynthesis. *Journal of Biological Chemistry* **280**, 13978-13986.

Chan, E. D. & Iseman, M. D. (2013).Underlying host risk factors for nontuberculous mycobacterial lung disease. In Seminars in respiratory and critical care medicine, pp. 110-123: Thieme Medical Publishers.

Chavadi, S. S., Stirrett, K. L., Edupuganti, U. R. & other authors (2011). Mutational and phylogenetic analyses of the mycobacterial mbt gene cluster. *Journal of bacteriology* **193**, 5905-5913.

Chipperfield, J. R. & Ratledge, C. (2000). Salicylic acid is not a bacterial siderophore: a theoretical study. *Biometals* **13**, 165-168.

Christman, M. F., Storz, G. & Ames, B. N. (1989). OxyR, a positive regulator of hydrogen peroxide-inducible genes in Escherichia coli and Salmonella typhimurium, is homologous to a family of bacterial regulatory proteins. *Proceedings of the National Academy of Sciences* **86**, 3484-3488.

Cohavy, O., Harth, G., Horwitz, M., Eggena, M., Landers, C., Sutton, C., Targan, S. R. & Braun, J. (1999a). Identification of a novel mycobacterial histone H1 homologue (HupB) as an antigenic target of pANCA monoclonal antibody and serum immunoglobulin A from patients with Crohn's disease. *Infect Immun* **67**, 6510-6517.

Cohavy, O., Harth, G., Horwitz, M., Eggena, M., Landers, C., Sutton, C., Targan, S. R. & Braun, J. (1999b). Identification of a novel mycobacterial histone H1 homologue (HupB) as an

antigenic target of pANCA monoclonal antibody and serum immunoglobulin A from patients with Crohn's disease. *Infection and immunity* **67**, 6510-6517.

Cole, S., Eiglmeier, K., Parkhill, J. & other authors (2001). Massive gene decay in the leprosy bacillus. *Nature* **409**, 1007-1011.

Cole, S. T., Brosch, R., Parkhill, J. & other authors (1998). Deciphering the biology of Mycobacterium tuberculosis from the complete genome sequence. *Nature* **393**, 537-544.

Converse, S. E., Mougous, J. D., Leavell, M. D., Leary, J. A., Bertozzi, C. R. & Cox, J. S. (2003). MmpL8 is required for sulfolipid-1 biosynthesis and Mycobacterium tuberculosis virulence. *Proceedings of the National Academy of Sciences* **100**, 6121-6126.

Cooper, A. M., Dalton, D. K., Stewart, T. A., Griffin, J., Russell, D. & Orme, I. (1993). Disseminated tuberculosis in interferon gamma gene-disrupted mice. *The Journal of experimental medicine* **178**, 2243-2247.

Cooper, A. M., Magram, J., Ferrante, J. & Orme, I. M. (1997). Interleukin 12 (IL-12) is crucial to the development of protective immunity in mice intravenously infected with Mycobacterium tuberculosis. *The Journal of experimental medicine* **186**, 39-45.

Cooper, A. M., Segal, B. H., Frank, A. A., Holland, S. M. & Orme, I. M. (2000). Transient loss of resistance to pulmonary tuberculosis in p47 phox−/− mice. *Infection and immunity* **68**, 1231-1234.

Coros, A., Callahan, B., Battaglioli, E. & Derbyshire, K. M. (2008). The specialized secretory apparatus ESX-1 is essential for DNA transfer in Mycobacterium smegmatis. *Molecular microbiology* **69**, 794-808.

Cox, J. S., Chen, B., McNeil, M. & Jacobs, W. R. (1999). Complex lipid determines tissue-specific replication of Mycobacterium tuberculosis in mice. *Nature* **402**, 79-83.

Daffé, M., LACAVE, C., LANÉELLE, M. A. & LANÉELLE, G. (1987). Structure of the major triglycosyl phenol-phthiocerol of Mycobacterium tuberculosis (strain Canetti). *European Journal of Biochemistry* **167**, 155-160.

Daffé, M. & Draper, P. (1997). The envelope layers of mycobacteria with reference to their pathogenicity. *Advances in microbial physiology* **39**, 131-203.

Daffé, M. (2008). 1 The Global Architecture of the Mycobacterial Cell Envelope. In The mycobacterial cell envelope, pp. 3-11: American Society of Microbiology.

De Voss, J. J., Rutter, K., Schroeder, B. G. & Barry, C. E., 3rd (1999). Iron acquisition and metabolism by mycobacteria. *J Bacteriol* **181**, 4443-4451.

De Voss, J. J., Rutter, K., Schroeder, B. G., Su, H., Zhu, Y. & Barry, C. E. (2000). The salicylate-derived mycobactin siderophores of *Mycobacterium tuberculosis* are essential for growth in macrophages. *Proc Natl Acad Sci U S A* **97**, 1252-1257.

de Waal Malefyt, R., Abrams, J., Bennett, B., Figdor, C. G. & De Vries, J. E. (1991). Interleukin 10 (IL-10) inhibits cytokine synthesis by human monocytes: an autoregulatory role of IL-10 produced by monocytes. *The Journal of experimental medicine* **174**, 1209-1220.

Deretic, V., Philipp, W., Dhandayuthapani, S., Mudd, M., Curcic, R., Garbe, T., Heym, B., Via, L. & Cole, S. (1995). Mycobacterium tuberculosis is a natural mutant with an inactivated oxidative-stress regulatory gene: implications for sensitivity to isoniazid. *Molecular microbiology* **17**, 889-900.

Domenech, P., Reed, M. B., Dowd, C. S., Manca, C., Kaplan, G. & Barry, C. E. (2004). The role of MmpL8 in sulfatide biogenesis and virulence of Mycobacterium tuberculosis. *Journal of Biological Chemistry* **279**, 21257-21265.

Dover, L. G. & Ratledge, C. (1996). Identification of a 29 kDa protein in the envelope of Mycobacterium smegmatis as a putative ferri-exochelin receptor. *Microbiology* **142**, 1521-1530.

Drakesmith, H. & Prentice, A. M. (2012). Hepcidin and the iron-infection axis. *Science* **338**, 768-772.

Dubey, V. S., Sirakova, T. D. & Kolattukudy, P. (2002). Disruption of msl3 abolishes the synthesis of mycolipanoic and mycolipenic acids required for polyacyltrehalose synthesis in Mycobacterium tuberculosis H37Rv and causes cell aggregation. *Molecular microbiology* **45**, 1451-1459.

Dussurget, O., Rodriguez, M. & Smith, I. (1996). An ideR mutant of Mycobacterium smegmatis has derepressed siderophore production and an altered oxidative-stress response. *Molecular microbiology* **22**, 535-544.

Dussurget, O. & Smith, I. (1998). Interdependence of mycobacterial iron regulation, oxidative-stress response and isoniazid resistance. *Trends Microbiol* **6**, 354-358.

Dussurget, O., Timm, J., Gomez, M., Gold, B., Yu, S., Sabol, S. Z., Holmes, R. K., Jacobs, W. R., Jr. & Smith, I. (1999). Transcriptional control of the iron-responsive fxbA gene by the mycobacterial regulator IdeR. *J Bacteriol* **181**, 3402-3408.

Dussurget, O., Stewart, G., Neyrolles, O., Pescher, P., Young, D. & Marchal, G. (2001). Role of Mycobacterium tuberculosisCopper-Zinc Superoxide Dismutase. *Infection and immunity* **69**, 529-533.

Edwards, K. M., Cynamon, M. H., Voladri, R. K., Hager, C. C., DeSTEFANO, M. S., Tham, K. T., Lakey, D. L., Bochan, M. R. & Kernodle, D. S. (2001). Iron-cofactored superoxide dismutase inhibits host responses to Mycobacterium tuberculosis. *American journal of respiratory and critical care medicine* **164**, 2213-2219.

Ehlers, S. & Hölscher, C. (2005). DTH-Associated Pathology. *Topley and Wilson's Microbiology and Microbial Infections*.

Ehrt, S. & Schnappinger, D. (2009). Mycobacterial survival strategies in the phagosome: defence against host stresses. *Cellular microbiology* **11**, 1170-1178.

Fang, Z., Sampson, S. L., Warren, R. M., van Pittius, N. C. G. & Newton-Foot, M. (2015). Iron acquisition strategies in mycobacteria. *Tuberculosis* **95**, 123-130.

Feese, M. D., Ingason, B. P., Goranson-Siekierke, J., Holmes, R. K. & Hol, W. G. (2001). Crystal structure of the iron-dependent regulator from Mycobacterium tuberculosis at 2.0-Å resolution reveals the Src homology domain 3-like fold and metal binding function of the third domain. *Journal of Biological Chemistry* **276**, 5959-5966.

Fenton, H. (1894). LXXIII.—Oxidation of tartaric acid in presence of iron. *Journal of the Chemical Society, Transactions* **65**, 899-910.

Fenton, M. J. & Vermeulen, M. W. (1996). Immunopathology of tuberculosis: roles of macrophages and monocytes. *Infection and immunity* **64**, 683.

Finken, M., Kirschner, P., Meier, A., Wrede, A. & Böttger, E. C. (1993). Molecular basis of streptomycin resistance in Mycobacterium tuberculosis: alterations of the ribosomal protein S12 gene and point mutations within a functional 16S ribosomal RNA pseudoknot. *Molecular microbiology* **9**, 1239-1246.

Firmani, M. A. & Riley, L. W. (2002). Reactive nitrogen intermediates have a bacteriostatic effect on Mycobacterium tuberculosis in vitro. *Journal of clinical microbiology* **40**, 3162-3166.

Flynn, J. L., Chan, J., Triebold, K. J., Dalton, D. K., Stewart, T. A. & Bloom, B. R. (1993). An essential role for interferon gamma in resistance to Mycobacterium tuberculosis infection. *The Journal of experimental medicine* **178**, 2249-2254.

Flynn, J. L. & Chan, J. (2001). Immunology of tuberculosis. *Annual review of immunology* **19**, 93-129.

Francis, J., Madinaveitia, J., Macturk, H. & Snow, G. (1949). Isolation from acid-fast bacteria of a growth-factor for Mycobacterium johnei and of a precursor of phthiocol. *Nature* **163**, 365-365.

Frehel, C., Ryter, A., Rastogi, N. & David, H. (1986).The electron transparent zone in phagocytized Mycobacterium avium and other Mycobacteria Formation, persistence and role in bacterial survival. In Annales de l'Institut Pasteur/Microbiologie, pp. 239-257: Elsevier.

Fulton, S. A., Johnsen, J. M., Wolf, S. F., Sieburth, D. S. & Boom, W. H. (1996). Interleukin-12 production by human monocytes infected with Mycobacterium tuberculosis: role of phagocytosis. *Infection and immunity* **64**, 2523-2531.

Gaylord, H., Brennan, P., Young, D. & Buchanan, T. (1987). Most Mycobacterium leprae carbohydrate-reactive monoclonal antibodies are directed to lipoarabinomannan. *Infection and immunity* **55**, 2860-2863.

Gazzinelli, R. T., Oswald, I. P., James, S. L. & Sher, A. (1992). IL-10 inhibits parasite killing and nitrogen oxide production by IFN-gamma-activated macrophages. *The Journal of Immunology* **148**, 1792-1796.

George, K. M., Yuan, Y., Sherman, D. R. & Barry, C. E. (1995). The biosynthesis of cyclopropanated mycolic acids in Mycobacterium tuberculosis Identification and functional analysis of CMAS-2. *Journal of Biological Chemistry* **270**, 27292-27298.

Gerosa, F., Nisii, C., Righetti, S., Micciolo, R., Marchesini, M., Cazzadori, A. & Trinchieri, G. (1999). CD4+ T cell clones producing both interferon-γ and interleukin-10 predominate in bronchoalveolar lavages of active pulmonary tuberculosis patients. *Clinical Immunology* **92**, 224-234.

Giacomini, E., Iona, E., Ferroni, L., Miettinen, M., Fattorini, L., Orefici, G., Julkunen, I. & Coccia, E. M. (2001). Infection of Human Macrophages and Dendritic Cells with Mycobacterium tuberculosis Induces a Differential Cytokine Gene Expression That Modulates T Cell Response. *The Journal of Immunology* **166**, 7033-7041.

Gilleron, M., Stenger, S., Mazorra, Z. & other authors (2004). Diacylated sulfoglycolipids are novel mycobacterial antigens stimulating CD1-restricted T cells during infection with Mycobacterium tuberculosis. *The Journal of experimental medicine* **199**, 649-659.

Gilleron, M., Jackson, M., Nigou, J. & Puzo, G. (2008). 6 Structure, Biosynthesis, and Activities of the Phosphatidyl-myo-Inositol-Based Lipoglycans. In The mycobacterial cell envelope, pp. 75-105: American Society of Microbiology.

Girard, M. P., Fruth, U. & Kieny, M.-P. (2005). A review of vaccine research and development: tuberculosis. *Vaccine* **23**, 5725-5731.

Glickman, M. S. & Jacobs, W. R. (2001). Microbial pathogenesis of Mycobacterium tuberculosis: dawn of a discipline. *Cell* **104**, 477-485.

Gobin, J., Moore, C. H., Reeve, J. R., Jr., Wong, D. K., Gibson, B. W. & Horwitz, M. A. (1995a). Iron acquisition by Mycobacterium tuberculosis: isolation and characterization of a family of iron-binding exochelins. *Proc Natl Acad Sci U S A* **92**, 5189-5193.

Gobin, J., Moore, C. H., Reeve, J. R., Wong, D. K., Gibson, B. W. & Horwitz, M. A. (1995b). Iron acquisition by Mycobacterium tuberculosis: isolation and characterization of a family of iron-binding exochelins. *Proceedings of the National Academy of Sciences* **92**, 5189-5193.

Gobin, J. & Horwitz, M. A. (1996a). Exochelins of Mycobacterium tuberculosis remove iron from human iron-binding proteins and donate iron to mycobactins in the M. tuberculosis cell wall. *The Journal of experimental medicine* **183**, 1527-1532.

Gobin, J. & Horwitz, M. A. (1996b). Exochelins of Mycobacterium tuberculosis remove iron from human iron-binding proteins and donate iron to mycobactins in the M. tuberculosis cell wall. *J Exp Med* **183**, 1527-1532.

Goelz, S. E., Hamilton, S. R. & Vogelstein, B. (1985). Purification of DNA from formaldehyde fixed and paraffin embedded human tissue. *Biochemical and biophysical research communications* **130**, 118-126.

Gold, B., Rodriguez, G. M., Marras, S. A., Pentecost, M. & Smith, I. (2001). r. *Mol Microbiol* **42**, 851-865.

Goren, M. & Brennan, P. (1979). Mycobacterial lipids: chemistry and biologic activities. *Tuberculosis*, 63-193.

Goren, M. B., Brokl, O., Roller, P., Fales, H. M. & Das, B. C. (1976). Sulfatides of Mycobacterium tuberculosis: the structure of the principal sulfatide (SL-I). *Biochemistry* **15**, 2728-2735.

Griffiths, E. & Chart, H. (1999). Iron as a regulatory signal. *Iron and infection Wiley, Chichester, United Kingdom*, 213-253.

Guimarães, B. G., Souchon, H., Honoré, N., Saint-Joanis, B., Brosch, R., Shepard, W., Cole, S. T. & Alzari, P. M. (2005). Structure and mechanism of the alkyl hydroperoxidase AhpC, a key element of the Mycobacterium tuberculosis defense system against oxidative stress. *Journal of Biological Chemistry* **280**, 25735-25742.

Gupta, V., Gupta, R. K., Khare, G., Salunke, D. M. & Tyagi, A. K. (2009). Crystal structure of Bfr A from Mycobacterium tuberculosis: incorporation of selenomethionine results in cleavage and demetallation of haem. *PloS one* **4**, e8028.

Gutacker, M. M., Smoot, J. C., Migliaccio, C. A. L. & other authors (2002). Genome-wide analysis of synonymous single nucleotide polymorphisms in Mycobacterium tuberculosis complex organisms: resolution of genetic relationships among closely related microbial strains. *Genetics* **162**, 1533-1543.

Habermehl, K.-O. (2012). Rapid Methods and Automation in Microbiology and Immunology: Fourth International Symposium on Rapid Methods and Automation in Microbiology and Immunology, Berlin, June 7–10, 1984: Springer Science & Business Media.

Hall, R. M., Wheeler, P. R. & Ratledge, C. (1983). Exochelin-mediated Iron uptake into Mycobacterium leprae. *International Journal of Leprosy and Other Mycobacterial Diseases* **51**, 490-494.

Hall, R. M. & Ratledge, C. (1984). Mycobactins as chemotaxonomic characters for some rapidly growing mycobacteria. *Microbiology* **130**, 1883-1892.

Hall, R. M., Sritharan, M., Messenger, A. J. & Ratledge, C. (1987). Iron transport in Mycobacterium smegmatis: occurrence of iron-regulated envelope proteins as potential receptors for iron uptake. *J Gen Microbiol* **133**, 2107-2114.

Hanwell, M. D., Curtis, D. E., Lonie, D. C., Vandermeersch, T., Zurek, E. & Hutchison, G. R. (2012). Avogadro: an advanced semantic chemical editor, visualization, and analysis platform. *Journal of cheminformatics* **4**, 1.

Hasan, Z., Cliff, J. M., Dockrell, H. M., Jamil, B., Irfan, M., Ashraf, M. & Hussain, R. (2009). CCL2 responses to Mycobacterium tuberculosis are associated with disease severity in tuberculosis. *PloS one* **4**, e8459.

Heifets, L. B. (1994).Antimycobacterial drugs. In Seminars in respiratory infections, pp. 84-103.

Hernandez-Pando, R. & Rook, G. (1994). The role of TNF-alpha in T-cell-mediated inflammation depends on the Th1/Th2 cytokine balance. *Immunology* **82**, 591.

Heym, B., Zhang, Y., Poulet, S., Young, D. & Cole, S. (1993). Characterization of the katG gene encoding a catalase-peroxidase required for the isoniazid susceptibility of Mycobacterium tuberculosis. *Journal of bacteriology* **175**, 4255-4259.

Hickman, S. P., Chan, J. & Salgame, P. (2002). Mycobacterium tuberculosis induces differential cytokine production from dendritic cells and macrophages with divergent effects on naive T cell polarization. *The Journal of Immunology* **168**, 4636-4642.

Hobson, R. J., McBride, A. J., Kempsell, K. E. & Dale, J. W. (2002). Use of an arrayed promoter-probe library for the identification of macrophage-regulated genes in Mycobacterium tuberculosis. *Microbiology* **148**, 1571-1579.

Hoffmann, C., Leis, A., Niederweis, M., Plitzko, J. M. & Engelhardt, H. (2008). Disclosure of the mycobacterial outer membrane: cryo-electron tomography and vitreous sections reveal the lipid bilayer structure. *Proceedings of the National Academy of Sciences* **105**, 3963-3967.

Hoheisel, G., Izbicki, G., Roth, M., Chan, C., Leung, J., Reichenberger, F., Schauer, J. & Perruchoud, A. (1998). Compartmentalization of pro-inflammatory cytokines in tuberculous pleurisy. *Respiratory medicine* **92**, 14-17.

Howard, A. & Zwilling, B. (1999a). Reactivation of tuberculosis is associated with a shift from type 1 to type 2 cytokines. *Clinical and experimental immunology* **115**, 428.

Howard, A. & Zwilling, B. (1999b). Reactivation of tuberculosis is associated with a shift from type 1 to type 2 cytokines. *Clinical and experimental immunology* **115**, 428-434.

Hughes, A. L., Friedman, R. & Murray, M. B. (2002). Genomewide pattern of synonymous nucleotide substitution in two complete genomes of Mycobacterium tuberculosis.

Hunter, R. L., Venkataprasad, N. & Olsen, M. R. (2006). The role of trehalose dimycolate (cord factor) on morphology of virulent M. tuberculosis in vitro. *Tuberculosis* **86**, 349-356.

Hunter, S. W. & Brennan, P. (1990). Evidence for the presence of a phosphatidylinositol anchor on the lipoarabinomannan and lipomannan of Mycobacterium tuberculosis. *Journal of Biological Chemistry* **265**, 9272-9279.

Husseini, H. & Elberg, S. (1952). Cellular reactions to phthienoic acid and related branch ed-chain acids. *American review of tuberculosis* **65**, 655-672.

Jackson, M., Stadthagen, G. & Gicquel, B. (2007). Long-chain multiple methyl-branched fatty acid-containing lipids of Mycobacterium tuberculosis: biosynthesis, transport, regulation and biological activities. *Tuberculosis* **87**, 78-86.

Jain, M., Petzold, C. J., Schelle, M. W., Leavell, M. D., Mougous, J. D., Bertozzi, C. R., Leary, J. A. & Cox, J. S. (2007). Lipidomics reveals control of Mycobacterium tuberculosis virulence lipids via metabolic coupling. *Proceedings of the National Academy of Sciences* **104**, 5133-5138.

Jamil, B., Shahid, F., Hasan, Z., Nasir, N., Razzaki, T., Dawood, G. & Hussain, R. (2007). Interferonγ/IL10 ratio defines the disease severity in pulmonary and extra pulmonary tuberculosis. *Tuberculosis* **87**, 279-287.

Jankute, M., Cox, J. A., Harrison, J. & Besra, G. S. (2015). Assembly of the mycobacterial cell wall. *Annual review of microbiology* **69**, 405-423.

Johnson, M. M. & Odell, J. A. (2014). Nontuberculous mycobacterial pulmonary infections. *Journal of thoracic disease* **6**, 210-220.

Jones, C. M., Wells, R. M., Madduri, A. V., Renfrow, M. B., Ratledge, C., Moody, D. B. & Niederweis, M. (2014). Self-poisoning of Mycobacterium tuberculosis by interrupting siderophore recycling. *Proceedings of the National Academy of Sciences* **111**, 1945-1950.

Jones, D. T. & Cozzetto, D. (2015). DISOPRED3: precise disordered region predictions with annotated protein-binding activity. *Bioinformatics* **31**, 857-863.

Juffermans, N. P., Florquin, S., Camoglio, L., Verbon, A., Kolk, A. H., Speelman, P., Van Deventer, S. J. & Van der Poll, T. (2000). Interleukin-1 signaling is essential for host defense during murine pulmonary tuberculosis. *Journal of Infectious Diseases* **182**, 902-908.

Katsube, T., Matsumoto, S., Takatsuka, M. & other authors (2007). Control of cell wall assembly by a histone-like protein in Mycobacteria. *J Bacteriol* **189**, 8241-8249.

Keane, J., Balcewicz-Sablinska, M. K., Remold, H. G., Chupp, G. L., Meek, B. B., Fenton, M. J. & Kornfeld, H. (1997). Infection by Mycobacterium tuberculosis promotes human alveolar macrophage apoptosis. *Infection and immunity* **65**, 298-304.

Keating, L. A., Wheeler, P. R., Mansoor, H., Inwald, J. K., Dale, J., Hewinson, R. G. & Gordon, S. V. (2005). The pyruvate requirement of some members of the Mycobacterium tuberculosis complex is due to an inactive pyruvate kinase: implications for in vivo growth. *Molecular microbiology* **56**, 163-174.

Khare, G., Gupta, V., Nangpal, P., Gupta, R. K., Sauter, N. K. & Tyagi, A. K. (2011). Ferritin structure from Mycobacterium tuberculosis: comparative study with homologues identifies extended C-terminus involved in ferroxidase activity. *PloS one* **6**, e18570.

Kim, B.-J., Lee, S.-H., Lyu, M.-A. & other authors (1999). Identification of mycobacterial species by comparative sequence analysis of the RNA polymerase gene (rpoB). *Journal of Clinical Microbiology* **37**, 1714-1720.

Kochan, I. (1977). Role of Iron in the Regulation of Nutritional Immunity. In Bioinorganic Chemistry?II, pp. 55-77: AMERICAN CHEMICAL SOCIETY.

Kremer, L. & Besra, G. S. (2005). A waxy tale, by Mycobacterium tuberculosis. In Tuberculosis and the tubercle bacillus, pp. 287-305: American Society of Microbiology.

Krithika, R., Marathe, U., Saxena, P., Ansari, M. Z., Mohanty, D. & Gokhale, R. S. (2006). A genetic locus required for iron acquisition in Mycobacterium tuberculosis. *Proceedings of the National Academy of Sciences of the United States of America* **103**, 2069-2074.

Kumar, P., Schelle, M. W., Jain, M., Lin, F. L., Petzold, C. J., Leavell, M. D., Leary, J. A., Cox, J. S. & Bertozzi, C. R. (2007). PapA1 and PapA2 are acyltransferases essential for the biosynthesis of the Mycobacterium tuberculosis virulence factor sulfolipid-1. *Proceedings of the National Academy of Sciences* **104**, 11221-11226.

Kumar, S., Sardesai, A. A., Basu, D., Muniyappa, K. & Hasnain, S. E. (2010). DNA clasping by mycobacterial HU: the C-terminal region of HupB mediates increased specificity of DNA binding. *PloS one* **5**.

Kurthkoti, K., Tare, P., Paitchowdhury, R., Gowthami, V. N., Garcia, M. J., Colangeli, R., Chatterji, D., Nagaraja, V. & Rodriguez, G. M. (2015). The mycobacterial iron-dependent regulator IdeR induces ferritin (bfrB) by alleviating Lsr2 repression. *Molecular microbiology* **98**, 864-877.

Kusunose, E., ICHIHARA, K., Yojiro, N. & KUSUNOSE, M. (1976). Superoxide dismutase from Mycobacterium tuberculosis. *Journal of biochemistry* **80**, 1343-1352.

Ladel, C. H., Szalay, G., Riedel, D. & Kaufmann, S. (1997). Interleukin-12 secretion by Mycobacterium tuberculosis-infected macrophages. *Infection and immunity* **65**, 1936-1938.

Lane, S. J., Marshall, P. S., Upton, R. J. & Ratledge, C. (1998). Isolation and characterization of carboxymycobactins as the second extracellular siderophores in Mycobacterium smegmatis. *BioMetals* **11**, 13-20.

Larsen, C. G., Thomsen, M. K., Gesser, B. & other authors (1995). The delayed-type hypersensitivity reaction is dependent on IL-8. Inhibition of a tuberculin skin reaction by an anti-IL-8 monoclonal antibody. *The Journal of Immunology* **155**, 2151-2157.

Laskowski, R. A., MacArthur, M. W., Moss, D. S. & Thornton, J. M. (1993). PROCHECK: a program to check the stereochemical quality of protein structures. *Journal of applied crystallography* **26**, 283-291.

Laskowski, R. A. & Swindells, M. B. (2011). LigPlot+: multiple ligand–protein interaction diagrams for drug discovery. *Journal of chemical information and modeling* **51**, 2778-2786.

Law, K., Weiden, M., Harkin, T., Tchou-Wong, K., Chi, C. & Rom, W. N. (1996). Increased release of interleukin-1 beta, interleukin-6, and tumor necrosis factor-alpha by bronchoalveolar cells lavaged from involved sites in pulmonary tuberculosis. *American journal of respiratory and critical care medicine* **153**, 799-804.

Lee, P. P., Chan, K. W., Jiang, L. & other authors (2008). Susceptibility to mycobacterial infections in children with X-linked chronic granulomatous disease: a review of 17 patients living in a region endemic for tuberculosis. *The Pediatric infectious disease journal* **27**, 224-230.

Lehman, K. & Neumann, R. (1896). Atlas und grundriss der bakeriologie und lehrbuch der speziellen bakteriologischen diagnositk. *Teil II, München: Lehmann*.

Lei, B., Wei, C.-J. & Tu, S.-C. (2000). Action mechanism of antitubercular isoniazid Activation by Mycobacterium tuberculosis KatG, isolation, and characterization of InhA inhibitor. *Journal of Biological Chemistry* **275**, 2520-2526.

Lemassu, A., Ortalo-Magne, A., Bardou, F., Silve, G., Lanéelle, M.-A. & Daffé, M. (1996). Extracellular and surface-exposed polysaccharides of non-tuberculous mycobacteria. *Microbiology* **142**, 1513-1520.

Lewin, A., Baus, D., Kamal, E., Bon, F., Kunisch, R., Maurischat, S., Adonopoulou, M. & Eich, K. (2008). The mycobacterial DNA-binding protein 1 (MDP1) from Mycobacterium bovis BCG influences various growth characteristics. *BMC microbiology* **8**, 91.

Li, W., He, J., Xie, L., Chen, T. & Xie, J. (2013). Comparative genomic insights into the biosynthesis and regulation of mycobacterial siderophores. *Cellular Physiology and Biochemistry* **31**, 1-13.

Lima, V. M., Bonato, V. L., Lima, K. M. & other authors (2001). Role of trehalose dimycolate in recruitment of cells and modulation of production of cytokines and NO in tuberculosis. *Infection and immunity* **69**, 5305-5312.

Liu, J., Barry, C. E., Besra, G. S. & Nikaido, H. (1996). Mycolic acid structure determines the fluidity of the mycobacterial cell wall. *Journal of Biological Chemistry* **271**, 29545-29551.

Macedo, G. C., Bozzi, A., Weinreich, H. R., Bafica, A., Teixeira, H. C. & Oliveira, S. C. (2010). Human T cell and antibody-mediated responses to the Mycobacterium tuberculosis recombinant 85A, 85B, and ESAT-6 antigens. *Journal of Immunology Research* **2011**.

Mack, U., Migliori, G., Sester, M. & other authors (2009). LTBI: latent tuberculosis infection or lasting immune responses to M. tuberculosis? A TBNET consensus statement. *European Respiratory Journal* **33**, 956-973.

MacMicking, J. D., North, R. J., LaCourse, R., Mudgett, J. S., Shah, S. K. & Nathan, C. F. (1997). Identification of nitric oxide synthase as a protective locus against tuberculosis. *Proc Natl Acad Sci U S A* **94**, 5243-5248.

Mahapatra, S., Scherman, H., Brennan, P. J. & Crick, D. C. (2005). N Glycolylation of the nucleotide precursors of peptidoglycan biosynthesis of Mycobacterium spp. is altered by drug treatment. *Journal of bacteriology* **187**, 2341-2347.

Manca, C., Paul, S., Barry, C. E., Freedman, V. H. & Kaplan, G. (1999). Mycobacterium tuberculosis catalase and peroxidase activities and resistance to oxidative killing in human monocytes in vitro. *Infection and immunity* **67**, 74-79.

Martinon, F., Burns, K. & Tschopp, J. (2002). The inflammasome: a molecular platform triggering activation of inflammatory caspases and processing of proIL-β. *Molecular cell* **10**, 417-426.

Matsushima, K. & Oppenheim, J. J. (1989). Interleukin 8 and MCAF: novel inflammatory cytokines inducible by IL 1 and TNF. *Cytokine* **1**, 2-13.

McNeil, M., Daffe, M. & Brennan, P. (1991). Location of the mycolyl ester substituents in the cell walls of mycobacteria. *Journal of Biological Chemistry* **266**, 13217-13223.

Michelini-Norris, M. B., Blanchard, D. K., Pearson, C. A. & Djeu, J. Y. (1992). Differential release of interleukin (IL)-1α, IL-1β, and IL-6 from normal human monocytes stimulated with a virulent and an avirulent isogenic variant of Mycobacterium avium-intracellulare complex. *Journal of Infectious Diseases* **165**, 702-709.

Middlebrook, G. (1954). Isoniazid-resistance and catalase activity of tubercle bacilli; a preliminary report. *American Review of Tuberculosis* **69**, 471.

Middlebrook, G., Coleman, C. M. & Schaefer, W. B. (1959). Sulfolipid from virulent tubercle bacilli. *Proceedings of the National Academy of Sciences* **45**, 1801-1804.

Milano, A., Forti, F., Sala, C., Riccardi, G. & Ghisotti, D. (2001). Transcriptional Regulation of furAand katG upon Oxidative Stress inMycobacterium smegmatis. *Journal of bacteriology* **183**, 6801-6806.

Minnikin, D. E. (1982). Lipids: complex lipids, their chemistry, biosynthesis and roles. *The biology of the mycobacteria* **1**, 95-184.

Minnikin, D. E., Kremer, L., Dover, L. G. & Besra, G. S. (2002). The methyl-branched fortifications of Mycobacterium tuberculosis. *Chemistry & biology* **9**, 545-553.

Mitchison, D. (1985). The action of antituberculosis drugs in short-course chemotherapy. *Tubercle* **66**, 219-225.

Mohan, V. P., Scanga, C. A., Yu, K., Scott, H. M., Tanaka, K. E., Tsang, E., Tsai, M. C., Flynn, J. L. & Chan, J. (2001). Effects of tumor necrosis factor alpha on host immune response in chronic persistent tuberculosis: possible role for limiting pathology. *Infection and immunity* **69**, 1847-1855.

Morgan, M., Kalantri, S., Flores, L. & Pai, M. (2005). A commercial line probe assay for the rapid detection of rifampicin resistance in Mycobacterium tuberculosis: a systematic review and meta-analysis. *BMC infectious Diseases* **5**, 1.

Mori, T., Sakatani, M., Yamagishi, F. & other authors (2004). Specific detection of tuberculosis infection: an interferon-γ–based assay using new antigens. *American journal of respiratory and critical care medicine* **170**, 59-64.

Möst, J., Neumayer, H. P. & Dierich, M. P. (1990). Cytokine-induced generation of multinucleated giant cells in vitro requires interferon-γ and expression of LFA-1. *European journal of immunology* **20**, 1661-1667.

Muñoz, M., Lanéelle, M.-A., Luquin, M., Torrelles, J., Julián, E., Ausina, V. & Daffé, M. (1997). Occurrence of an antigenic triacyl trehalose in clinical isolates and reference strains of Mycobacterium tuberculosis. *FEMS microbiology letters* **157**, 251-259.

Nagabhushanam, V., Solache, A., Ting, L.-M., Escaron, C. J., Zhang, J. Y. & Ernst, J. D. (2003). Innate Inhibition of Adaptive Immunity: Mycobacterium tuberculosis-Induced IL-6 Inhibits Macrophage Responses to IFN-γ. *The Journal of Immunology* **171**, 4750-4757.

Nathan, C. & Shiloh, M. U. (2000). Reactive oxygen and nitrogen intermediates in the relationship between mammalian hosts and microbial pathogens. *Proceedings of the National Academy of Sciences* **97**, 8841-8848.

Nathan, C. (2002). Inducible nitric oxide synthase in the tuberculous human lung. *American journal of respiratory and critical care medicine* **166**, 130-131.

Nathan, C. & Ehrt, S. (2004). Nitric oxide in tuberculosis. *Tuberculosis, 2nd ed Lippincott, Williams & Wilkins, Philadelphia, PA*, 215-235.

Netea, M. G., Kullberg, B. J., Verschueren, I. & Van der Meer, J. W. (2000). Interleukin-18 induces production of proinflammatory cytokines in mice: no intermediate role for the cytokines of the tumor necrosis factor family and interleukin-1β. *European journal of immunology* **30**, 3057-3060.

Ng, V. H., Cox, J. S., Sousa, A. O., MacMicking, J. D. & McKinney, J. D. (2004). Role of KatG catalase-peroxidase in mycobacterial pathogenesis: countering the phagocyte oxidative burst. *Mol Microbiol* **52**, 1291-1302.

Noll, H. & Block, H. (1953). A Toxic Lipid Component of the Tubercle Bacillus (" Cord Factor"). II. Occurrence in Chloroform Extracts of Young and Older Bacterial Cultures. *American Review of Tuberculosis and Pulmonary Diseases* **67**, 828-852.

Noll, H., Bloch, H., Asselineau, J. & Lederer, E. (1956). The chemical structure of the cord factor of Mycobacterium tuberculosis. *Biochimica et biophysica acta* **20**, 299-309.

Notredame, C., Higgins, D. G. & Heringa, J. (2000). T-Coffee: A novel method for fast and accurate multiple sequence alignment. *Journal of molecular biology* **302**, 205-217.

O'Boyle, N. M., Banck, M., James, C. A., Morley, C., Vandermeersch, T. & Hutchison, G. R. (2011). Open Babel: An open chemical toolbox. *Journal of cheminformatics* **3**, 1.

O'Neill, L. A. & Greene, C. (1998). Signal transduction pathways activated by the IL-1 receptor family: ancient signaling machinery in mammals, insects, and plants. *Journal of Leukocyte Biology* **63**, 650-657.

Ojha, A., Anand, M., Bhatt, A., Kremer, L., Jacobs, W. R. & Hatfull, G. F. (2005). GroEL1: a dedicated chaperone involved in mycolic acid biosynthesis during biofilm formation in mycobacteria. *Cell* **123**, 861-873.

Ojha, A. K., Trivelli, X., Guerardel, Y., Kremer, L. & Hatfull, G. F. (2010). Enzymatic hydrolysis of trehalose dimycolate releases free mycolic acids during mycobacterial growth in biofilms. *Journal of Biological Chemistry* **285**, 17380-17389.

Ortalo-Magne, A., Dupont, M.-A., Lemassu, A., Andersen, A. B., Gounon, P. & Mamadou, D. (1995). Molecular composition of the outermost capsular material of the tubercle bacillus. *Microbiology* **141**, 1609-1620.

Ortalo-Magne, A., Lemassu, A., Laneelle, M.-A., Bardou, F., Silve, G., Gounon, P., Marchal, G. & Daffé, M. (1996). Identification of the surface-exposed lipids on the cell envelopes of Mycobacterium tuberculosis and other mycobacterial species. *Journal of bacteriology* **178**, 456-461.

Othieno, C., Hirsch, C. S., Hamilton, B. D., Wilkinson, K., Ellner, J. J. & Toossi, Z. (1999). Interaction of Mycobacterium tuberculosis-induced transforming growth factor β1 and interleukin-10. *Infection and immunity* **67**, 5730-5735.

Ottenhoff, T. H., Kumararatne, D. & Casanova, J.-L. (1998). Novel human immunodeficiencies reveal the essential role of type-1 cytokines in immunity to intracellular bacteria. *Immunology today* **19**, 491-494.

Ottenhoff, T. H., Verreck, F. A., Lichtenauer-Kaligis, E. G., Hoeve, M. A., Sanal, O. & van Dissel, J. T. (2002). Genetics, cytokines and human infectious disease: lessons from weakly pathogenic mycobacteria and salmonellae. *Nature genetics* **32**, 97-105.

Pacelli, R., Wink, D. A., Cook, J. A., Krishna, M. C., DeGraff, W., Friedman, N., Tsokos, M., Samuni, A. & Mitchell, J. B. (1995). Nitric oxide potentiates hydrogen peroxide-induced killing of Escherichia coli. *The Journal of experimental medicine* **182**, 1469-1479.

Pandey, R. & Rodriguez, G. M. (2012). A ferritin mutant of Mycobacterium tuberculosis is highly susceptible to killing by antibiotics and is unable to establish a chronic infection in mice. *Infection and immunity* **80**, 3650-3659.

Pandey, R. & Rodriguez, G. M. (2013). IdeR is required for iron homeostasis and virulence in Mycobacterium tuberculosis. *Molecular microbiology* **91**, 98-109.

Pandey, S. D., Choudhury, M. & Sritharan, M. (2014a). Transcriptional regulation of Mycobacterium tuberculosis hupB gene expression. *Microbiology* **160**, 1637-1647.

Pandey, S. D., Choudhury, M., Yousuf, S., Wheeler, P. R., Gordon, S. V., Ranjan, A. & Sritharan, M. (2014b). Iron-regulated protein HupB of Mycobacterium tuberculosis positively regulates siderophore biosynthesis and is essential for growth in macrophages. *Journal of bacteriology* **196**, 1853-1865.

Pavelka, M. (2000). Genetics of mycobacterial metabolism. *Molecular genetics of mycobacteria* **14**, 221-234.

Perez, R. L., Roman, J., Roser, S., Little, C., Olsen, M., Indrigo, J., Hunter, R. L. & Actor, J. K. (2000). Cytokine message and protein expression during lung granuloma formation and resolution induced by the mycobacterial cord factor trehalose-6, 6'-dimycolate. *Journal of Interferon & Cytokine Research* **20**, 795-804.

Pessolani, M., Smith, D. R., Rivoire, B., McCormick, J., Hefta, S. A., Cole, S. T. & Brennan, P. J. (1994). Purification, characterization, gene sequence, and significance of a bacterioferritin from Mycobacterium leprae. *The Journal of experimental medicine* **180**, 319-327.

Pethe, K., Alonso, S., Biet, F., Delogu, G., Brennan, M. J., Locht, C. & Menozzi, F. D. (2001). The heparin-binding haemagglutinin of M. tuberculosis is required for extrapulmonary dissemination. *Nature* **412**, 190-194.

Pethe, K., Bifani, P., Drobecq, H., Sergheraert, C., Debrie, A.-S., Locht, C. & Menozzi, F. D. (2002). Mycobacterial heparin-binding hemagglutinin and laminin-binding protein share antigenic methyllysines that confer resistance to proteolysis. *Proceedings of the National Academy of Sciences* **99**, 10759-10764.

Piddington, D. L., Fang, F. C., Laessig, T., Cooper, A. M., Orme, I. M. & Buchmeier, N. A. (2001). Cu, Zn superoxide dismutase of Mycobacterium tuberculosis contributes to survival in activated macrophages that are generating an oxidative burst. *Infection and immunity* **69**, 4980-4987.

Pitarque, S., Larrouy-Maumus, G., Payré, B., Jackson, M., Puzo, G. & Nigou, J. (2008). The immunomodulatory lipoglycans, lipoarabinomannan and lipomannan, are exposed at the mycobacterial cell surface. *Tuberculosis* **88**, 560-565.

Pohl, E., Holmes, R. K. & Hol, W. G. (1999). Crystal structure of the iron-dependent regulator (IdeR) from Mycobacterium tuberculosis shows both metal binding sites fully occupied. *Journal of molecular biology* **285**, 1145-1156.

Posey, J. E. & Gherardini, F. C. (2000). Lack of a role for iron in the Lyme disease pathogen. *Science* **288**, 1651-1653.

Powrie, F. & Coffman, R. (1993). Inhibition of cell-mediated immunity by IL4 and IL10. *Research in immunology* **144**, 639-643.

Prabhakar, S., Annapurna, P. S., Jain, N. K., Dey, A. B., Tyagi, J. S. & Prasad, H. K. (1998). Identification of an immunogenic histone-like protein (HLPMt) of Mycobacterium tuberculosis. *Tuber Lung Dis* **79**, 43-53.

Prabhakar, S., Mishra, A., Singhal, A., Katoch, V., Thakral, S., Tyagi, J. & Prasad, H. (2004). Use of the hupB gene encoding a histone-like protein of Mycobacterium tuberculosis as a target for detection and differentiation of M. tuberculosis and M. bovis. *Journal of clinical microbiology* **42**, 2724-2732.

Priya, V. H. S., Anuradha, B., Gaddam, S. L., Hasnain, S. E., Murthy, K. & Valluri, V. L. (2009). In vitro levels of interleukin 10 (IL-10) and IL-12 in response to a recombinant 32-kilodalton antigen of Mycobacterium bovis BCG after treatment for tuberculosis. *Clinical and Vaccine Immunology* **16**, 111-115.

Puren, A. J., Fantuzzi, G., Gu, Y., Su, M. & Dinarello, C. A. (1998). Interleukin-18 (IFNgamma-inducing factor) induces IL-8 and IL-1beta via TNFalpha production from non-CD14+ human blood mononuclear cells. *Journal of Clinical Investigation* **101**, 711.

Pym, A. S., Domenech, P., Honoré, N., Song, J., Deretic, V. & Cole, S. T. (2001). Regulation of catalase–peroxidase (KatG) expression, isoniazid sensitivity and virulence by furA of Mycobacterium tuberculosis. *Molecular microbiology* **40**, 879-889.

Quadri, L. E., Sello, J., Keating, T. A., Weinreb, P. H. & Walsh, C. T. (1998). Identification of a Mycobacterium tuberculosis gene cluster encoding the biosynthetic enzymes for assembly of the virulence-conferring siderophore mycobactin. *Chem Biol* **5**, 631-645.

Ratledge, C. & Ewing, M. (1996). The occurrence of carboxymycobactin, the siderophore of pathogenic mycobacteria, as a second extracellular siderophore in Mycobacterium smegmatis. *Microbiology* **142 (Pt 8)**, 2207-2212.

Ratledge, C. & Dover, L. G. (2000). Iron metabolism in pathogenic bacteria. *Annu Rev Microbiol* **54**, 881-941.

Ratledge, C. (2004). Iron, mycobacteria and tuberculosis. *Tuberculosis (Edinb)* **84**, 110-130.

Raymond, J. B., Mahapatra, S., Crick, D. C. & Pavelka, M. S. (2005). Identification of the namH gene, encoding the hydroxylase responsible for the N-glycolylation of the mycobacterial peptidoglycan. *Journal of Biological Chemistry* **280**, 326-333.

Reddy, P. V., Puri, R. V., Khera, A. & Tyagi, A. K. (2012). Iron storage proteins are essential for the survival and pathogenesis of Mycobacterium tuberculosis in THP-1 macrophages and the guinea pig model of infection. *Journal of bacteriology* **194**, 567-575.

Reed, M. B., Domenech, P., Manca, C., Su, H., Barczak, A. K., Kreiswirth, B. N., Kaplan, G. & Barry, C. E. (2004). A glycolipid of hypervirulent tuberculosis strains that inhibits the innate immune response. *Nature* **431**, 84-87.

Rodrigues, L. C., Pereira, S. M., Cunha, S. S. & other authors (2005). Effect of BCG revaccination on incidence of tuberculosis in school-aged children in Brazil: the BCG-REVAC cluster-randomised trial. *The Lancet* **366**, 1290-1295.

Rodriguez, G. M., Voskuil, M. I., Gold, B., Schoolnik, G. K. & Smith, I. (2002). ideR, an essential gene in Mycobacterium tuberculosis: role of IdeR in iron-dependent gene expression, iron metabolism, and oxidative stress response. *Infection and immunity* **70**, 3371-3381.

Rodriguez, G. M. & Smith, I. (2003). Mechanisms of iron regulation in mycobacteria: role in physiology and virulence. *Molecular microbiology* **47**, 1485-1494.

Rodriguez, G. M. & Smith, I. (2006). Identification of an ABC transporter required for iron acquisition and virulence in Mycobacterium tuberculosis. *Journal of bacteriology* **188**, 424-430.

Rohner, P., Ninet, B., Metral, C., Emler, S. & Auckenthaler, R. (1997). Evaluation of the MB/BacT system and comparison to the BACTEC 460 system and solid media for isolation of mycobacteria from clinical specimens. *Journal of clinical microbiology* **35**, 3127-3131.

Rousseau, C., Turner, O. C., Rush, E. & other authors (2003). Sulfolipid deficiency does not affect the virulence of Mycobacterium tuberculosis H37Rv in mice and guinea pigs. *Infection and immunity* **71**, 4684-4690.

Rousseau, C., Winter, N., Pivert, E., Bordat, Y., Neyrolles, O., Avé, P., Huerre, M., Gicquel, B. & Jackson, M. (2004). Production of phthiocerol dimycocerosates protects Mycobacterium tuberculosis from the cidal activity of reactive nitrogen intermediates produced by macrophages and modulates the early immune response to infection. *Cellular microbiology* **6**, 277-287.

Ryndak, M. B., Wang, S., Smith, I. & Rodriguez, G. M. (2010a). The Mycobacterium tuberculosis high-affinity iron importer, IrtA, contains an FAD-binding domain. *J Bacteriol* **192**, 861-869.

Ryndak, M. B., Wang, S., Smith, I. & Rodriguez, G. M. (2010b). The Mycobacterium tuberculosis high-affinity iron importer, IrtA, contains an FAD-binding domain. *Journal of bacteriology* **192**, 861-869.

Ryter, A., Frehel, C., Rastogi, N. & David, H. (1983). Macrophage interaction with mycobacteria including M. leprae. *Acta leprologica* **2**, 211-226.

Saavedra, R., Segura, E., Leyva, R., Esparza, L. A. & López-Marín, L. M. (2001). Mycobacterial di-O-acyl-trehalose inhibits mitogen-and antigen-induced proliferation of murine T cells in vitro. *Clinical and diagnostic laboratory immunology* **8**, 1081-1088.

Sahiratmadja, E., Alisjahbana, B., de Boer, T. & other authors (2007). Dynamic Changes in Pro- and Anti-Inflammatory Cytokine Profiles and Gamma Interferon Receptor Signaling Integrity Correlate with Tuberculosis Disease Activity and Response to Curative Treatment. *Infection and Immunity* **75**, 820-829.

Sakamoto, K. (2012). The pathology of Mycobacterium tuberculosis infection. *Veterinary Pathology Online* **49**, 423-439.

Sala, C., Forti, F., Di Florio, E., Canneva, F., Milano, A., Riccardi, G. & Ghisotti, D. (2003). Mycobacterium tuberculosis FurA autoregulates its own expression. *Journal of bacteriology* **185**, 5357-5362.

Sambandan, D., Dao, D. N., Weinrick, B. C. & other authors (2013). Keto-mycolic acid-dependent pellicle formation confers tolerance to drug-sensitive Mycobacterium tuberculosis. *MBio* **4**, e00222-00213.

Sambrook, J., Fritsch, E. F. & Maniatis, T. (1989). Molecular cloning: Cold spring harbor laboratory press New York.

Sánchez, F. O., Rodríguez, J. I., Agudelo, G. & García, L. F. (1994). Immune responsiveness and lymphokine production in patients with tuberculosis and healthy controls. *Infection and Immunity* **62**, 5673-5678.

Sani, M., Houben, E. N., Geurtsen, J. & other authors (2010). Direct visualization by cryo-EM of the mycobacterial capsular layer: a labile structure containing ESX-1-secreted proteins. *PLoS Pathog* **6**, e1000794.

Saraiva, M. & O'Garra, A. (2010). The regulation of IL-10 production by immune cells. *Nature Reviews Immunology* **10**, 170-181.

Saran, M., Beck-Speier, I., Fellerhoff, B. & Bauer, G. (1999). Phagocytic killing of microorganisms by radical processes: consequences of the reaction of hydroxyl radicals with chloride yielding chlorine atoms. *Free Radical Biology and Medicine* **26**, 482-490.

Sasindran, S. J. & Torrelles, J. B. (2011). Mycobacterium tuberculosis infection and inflammation: what is beneficial for the host and for the bacterium? *Frontiers in microbiology* **2**, 2.

Saunders, B. M. & Cooper, A. M. (2000). Restraining mycobacteria: role of granulomas in mycobacterial infections. *Immunology and cell biology* **78**, 334-341.

Saunders, B. M., Frank, A. A., Orme, I. M. & Cooper, A. M. (2000). Interleukin-6 Induces Early Gamma Interferon Production in the Infected Lung but Is Not Required for Generation of Specific Immunity to Mycobacterium tuberculosisInfection. *Infection and immunity* **68**, 3322-3326.

Schägger, H. & Von Jagow, G. (1987). Tricine-sodium dodecyl sulfate-polyacrylamide gel electrophoresis for the separation of proteins in the range from 1 to 100 kDa. *Analytical biochemistry* **166**, 368-379.

Schindler, R., Mancilla, J., Endres, S., Ghorbani, R., Clark, S. & Dinarello, C. (1990). Correlations and interactions in the production of interleukin-6 (IL-6), IL-1, and tumor necrosis factor (TNF) in human blood mononuclear cells: IL-6 suppresses IL-1 and TNF. *Blood* **75**, 40-47.

Schleifer, K. H. & Kandler, O. (1972). Peptidoglycan types of bacterial cell walls and their taxonomic implications. *Bacteriological reviews* **36**, 407.

Schmitt, M. P., Predich, M., Doukhan, L., Smith, I. & Holmes, R. K. (1995). Characterization of an iron-dependent regulatory protein (IdeR) of Mycobacterium tuberculosis as a functional homolog of the diphtheria toxin repressor (DtxR) from Corynebacterium diphtheriae. *Infection and immunity* **63**, 4284-4289.

Serafini, A., Boldrin, F., Palù, G. & Manganelli, R. (2009). Characterization of a Mycobacterium tuberculosis ESX-3 conditional mutant: essentiality and rescue by iron and zinc. *Journal of bacteriology* **191**, 6340-6344.

Sharadamma, N., Khan, K., Kumar, S., Neelakanteshwar Patil, K., Hasnain, S. E. & Muniyappa, K. (2011). Synergy between the N-terminal and C-terminal domains of Mycobacterium tuberculosis HupB is essential for high-affinity binding, DNA supercoiling and inhibition of RecA-promoted strand exchange. *FEBS Journal* **278**, 3447-3462.

Sharma, S. & Mohan, A. (2004). Extrapulmonary tuberculosis. *Indian Journal of Medical Research* **120**, 316-353.

Sharman, G., Williams, D., Ewing, D. & Ratledge, C. (1995a). Isolation, purification and structure of exochelin MS, the extracellular siderophore from Mycobacterium smegmatis. *Biochem J* **305**, 187-196.

Sharman, G. J., Williams, D. H., Ewing, D. F. & Ratledge, C. (1995b). Determination of the structure of exochelin MN, the extracellular siderophore from Mycobacterium neoaurum. *Chemistry & biology* **2**, 553-561.

Shaw, T. C., Thomas, L. H. & Friedland, J. S. (2000). REGULATION OF IL-10 SECRETION AFTER PHAGOCYTOSIS OF< i> MYCOBACTERIUM TUBERCULOSIS</i> BY HUMAN MONOCYTIC CELLS. *Cytokine* **12**, 483-486.

Sherman, D. R. & Mdluli, K. (1996). Compensatory ahpC gene expression in isoniazid-resistant Mycobacterium tuberculosis. *Science* **272**, 1641.

Shimoji, Y., Ng, V., Matsumura, K., Fischetti, V. A. & Rambukkana, A. (1999). A 21-kDa surface protein of Mycobacterium leprae binds peripheral nerve laminin-2 and mediates Schwann cell invasion. *Proc Natl Acad Sci U S A* **96**, 9857-9862.

Shiratsuchi, H., Johnson, J. L. & Ellner, J. J. (1991). Bidirectional effects of cytokines on the growth of Mycobacterium avium within human monocytes. *The Journal of Immunology* **146**, 3165-3170.

Siegrist, M. S., Unnikrishnan, M., McConnell, M. J., Borowsky, M., Cheng, T.-Y., Siddiqi, N., Fortune, S. M., Moody, D. B. & Rubin, E. J. (2009). Mycobacterial Esx-3 is required for mycobactin-mediated iron acquisition. *Proceedings of the National Academy of Sciences* **106**, 18792-18797.

Siegrist, M. S., Steigedal, M., Ahmad, R., Mehra, A., Dragset, M. S., Schuster, B. M., Philips, J. A., Carr, S. A. & Rubin, E. J. (2014). Mycobacterial Esx-3 requires multiple components for iron acquisition. *MBio* **5**, e01073-01014.

Simeone, R., Constant, P., Malaga, W., Guilhot, C., Daffe, M. & Chalut, C. (2007). Molecular dissection of the biosynthetic relationship between phthiocerol and phthiodiolone dimycocerosates and their critical role in the virulence and permeability of Mycobacterium tuberculosis. *Febs Journal* **274**, 1957-1969.

Sinha, S., Arora, S., Kosalai, K., Namane, A., Pym, A. S. & Cole, S. T. (2002). Proteome analysis of the plasma membrane of Mycobacterium tuberculosis. *Comparative and functional genomics* **3**, 470-483.

Sivakolundu, S., Mannela, U. D., Jain, S., Srikantam, A., Peri, S., Pandey, S. D. & Sritharan, M. (2013). Serum iron profile and ELISA-based detection of antibodies against the iron-regulated protein HupB of Mycobacterium tuberculosis in TB patients and household contacts in Hyderabad (Andhra Pradesh), India. *Trans R Soc Trop Med Hyg* **107**, 43-50.

Slayden, R. A. & Barry, C. E. (2001). Analysis of the lipids of Mycobacterium tuberculosis. *Mycobacterium tuberculosis Protocols*, 229-245.

Smith, I. (2003). Mycobacterium tuberculosis pathogenesis and molecular determinants of virulence. *Clinical microbiology reviews* **16**, 463-496.

Snow, G. A. (1970). Mycobactins: iron-chelating growth factors from mycobacteria. *Bacteriol Rev* **34**, 99-125.

Soares de Lima, C., Zulianello, L., Marques, M. A. & other authors (2005). Mapping the laminin-binding and adhesive domain of the cell surface-associated Hlp/LBP protein from Mycobacterium leprae. *Microbes and infection / Institut Pasteur* **7**, 1097-1109.

Somoskovi, A., Parsons, L. M. & Salfinger, M. (2001). The molecular basis of resistance to isoniazid, rifampin, and pyrazinamide in Mycobacterium tuberculosis. *Respiratory research* **2**, 1.

Soto, M. E., Ávila-Casado, M. D. C., Huesca-Gómez, C. & other authors (2012). Detection of IS6110 and HupB gene sequences of Mycobacterium tuberculosis and bovis in the aortic tissue of patients with Takayasu's arteritis. *BMC infectious diseases* **12**, 194.

Soysal, A. & Bakir, M. (2011). T-SPOT. TB assay usage in adults and children. *Expert review of molecular diagnostics* **11**, 643-660.

Spigelman, M. & Gillespie, S. (2006). Tuberculosis drug development pipeline: progress and hope. *The Lancet* **367**, 945-947.

Springer, B., Master, S., Sander, P. & other authors (2001). Silencing of Oxidative Stress Response in Mycobacterium tuberculosis: Expression Patterns of ahpC in Virulent and Avirulent Strains and Effect ofahpC Inactivation. *Infection and immunity* **69**, 5967-5973.

Sritharan, M. & Ratledge, C. (1989). Co-ordinated expression of the components of iron transport (mycobactin, exochelin and envelope proteins) in Mycobacterium neoaurum. *FEMS Microbiol Lett* **51**, 183-185.

Sritharan, M. & Ratledge, C. (1990). Iron-regulated envelope proteins of mycobacteria grown in vitro and their occurrence in Mycobacterium avium and Mycobacterium leprae grown in vivo. *Biol Met* **2**, 203-208.

Sritharan, M. (2000). Iron as a candidate in virulence and pathogenesis in mycobacteria and other microorganisms. *World Journal of Microbiology and Biotechnology* **16**, 769-780.

Sritharan, M., Yeruva, V. C., Sivasailappan, S. C. & Duggirala, S. (2006). Iron enhances the susceptibility of pathogenic mycobacteria to isoniazid, an antitubercular drug. *World Journal of Microbiology and Biotechnology* **22**, 1357-1364.

Sritharan, M. (2016). Iron homeostasis in Mycobacterium tuberculosis: mechanistic insights into siderophore-mediated iron uptake. *Journal of Bacteriology*, JB. 00359-00316.

Sritharan, N., Choudhury, M., Sivakolundu, S., Chaurasia, R., Chouhan, N., Rao, P. & Sritharan, M. (2014). Highly immunoreactive antibodies against the rHup-F2 fragment (aa 63–161) of the iron-regulated HupB protein of Mycobacterium tuberculosis and its potential for the serodiagnosis of extrapulmonary and recurrent tuberculosis. *European Journal of Clinical Microbiology & Infectious Diseases*, 1-8.

Sritharan, N., Choudhury, M., Sivakolundu, S., Chaurasia, R., Chouhan, N., Rao, P. & Sritharan, M. (2015). Highly immunoreactive antibodies against the rHup-F2 fragment (aa 63–161) of the iron-regulated HupB protein of Mycobacterium tuberculosis and its potential for the serodiagnosis of extrapulmonary and recurrent tuberculosis. *European Journal of Clinical Microbiology & Infectious Diseases* **34**, 33-40.

Stephenson, M. C. & Ratledge, C. (1979). Iron transport in Mycobacterium smegmatis: uptake of iron from ferriexochelin. *Microbiology* **110**, 193-202.

Stewart, G. R., Robertson, B. D. & Young, D. B. (2003). Tuberculosis: a problem with persistence. *Nature Reviews Microbiology* **1**, 97-105.

Stodola, F., Lesuk, A. & Anderson, R. (1938). The chemistry of the lipids of tubercle bacilli liv. The isolation and properties of mycolic acid. *Journal of Biological Chemistry* **126**, 505-513.

Stuehr, D. J. & Marletta, M. A. (1985). Mammalian nitrate biosynthesis: mouse macrophages produce nitrite and nitrate in response to Escherichia coli lipopolysaccharide. *Proceedings of the National Academy of Sciences* **82**, 7738-7742.

Surcel, H., Troye-Blomberg, M., Paulie, S., Andersson, G., Moreno, C., Pasvol, G. & Ivanyi, J. (1994). Th1/Th2 profiles in tuberculosis, based on the proliferation and cytokine response of blood lymphocytes to mycobacterial antigens. *Immunology* **81**, 171.

Takatsuka, M., Osada-Oka, M., Satoh, E. F. & other authors (2011). A histone-like protein of mycobacteria possesses ferritin superfamily protein-like activity and protects against DNA damage by Fenton reaction. *PloS one* **6**, e20985.

Takayama, K. & Kilburn, J. O. (1989). Inhibition of synthesis of arabinogalactan by ethambutol in Mycobacterium smegmatis. *Antimicrobial agents and chemotherapy* **33**, 1493-1499.

Takayama, K., Wang, C. & Besra, G. S. (2005). Pathway to synthesis and processing of mycolic acids in Mycobacterium tuberculosis. *Clinical microbiology reviews* **18**, 81-101.

Tamura, K., Peterson, D., Peterson, N., Stecher, G., Nei, M. & Kumar, S. (2011). MEGA5: molecular evolutionary genetics analysis using maximum likelihood, evolutionary distance, and maximum parsimony methods. *Molecular biology and evolution* **28**, 2731-2739.

Thorpe, T. C., Wilson, M., Turner, J., DiGuiseppi, J., Willert, M., Mirrett, S. & Reller, L. (1990). BacT/Alert: an automated colorimetric microbial detection system. *Journal of clinical microbiology* **28**, 1608-1612.

Toossi, Z., Gogate, P., Shiratsuchi, H., Young, T. & Ellner, J. J. (1995). Enhanced production of TGF-beta by blood monocytes from patients with active tuberculosis and

presence of TGF-beta in tuberculous granulomatous lung lesions. *The journal of Immunology* **154**, 465-473.

Toossi, Z. & Ellner, J. J. (1998). The role of TGFβ in the pathogenesis of human tuberculosis. *Clinical immunology and immunopathology* **87**, 107-114.

Torrea, G., Van de Perre, P., Ouedraogo, M. & other authors (2005). PCR-based detection of the Mycobacterium tuberculosis complex in urine of HIV-infected and uninfected pulmonary and extrapulmonary tuberculosis patients in Burkina Faso. *Journal of medical microbiology* **54**, 39-44.

Torres, M., Herrera, T., Villareal, H., Rich, E. A. & Sada, E. (1998). Cytokine Profiles for Peripheral Blood Lymphocytes from Patients with Active Pulmonary Tuberculosis and Healthy Household Contacts in Response to the 30-Kilodalton Antigen of Mycobacterium tuberculosis. *Infection and Immunity* **66**, 176-180.

Tortoli, E., Cichero, P., Piersimoni, C., Simonetti, M. T., Gesu, G. & Nista, D. (1999). Use of BACTEC MGIT 960 for recovery of mycobacteria from clinical specimens: multicenter study. *Journal of Clinical Microbiology* **37**, 3578-3582.

Tortoli, E. (2003). Impact of genotypic studies on mycobacterial taxonomy: the new mycobacteria of the 1990s. *Clinical microbiology reviews* **16**, 319-354.

Touchette, M. H., Holsclaw, C. M., Previti, M. L., Solomon, V. C., Leary, J. A., Bertozzi, C. R. & Seeliger, J. C. (2015). The rv1184c locus encodes Chp2, an acyltransferase in Mycobacterium tuberculosis polyacyltrehalose lipid biosynthesis. *Journal of bacteriology* **197**, 201-210.

Towbin, H., Staehelin, T. & Gordon, J. (1979). Electrophoretic transfer of proteins from polyacrylamide gels to nitrocellulose sheets: procedure and some applications. *Proceedings of the National Academy of Sciences* **76**, 4350-4354.

Trunz, B. B., Fine, P. & Dye, C. (2006). Effect of BCG vaccination on childhood tuberculous meningitis and miliary tuberculosis worldwide: a meta-analysis and assessment of cost-effectiveness. *The Lancet* **367**, 1173-1180.

van Crevel, R., Karyadi, E., Preyers, F., Leenders, M., Kullberg, B.-J., Nelwan, R. H. & van der Meer, J. W. (2000). Increased production of interleukin 4 by CD4+ and CD8+ T cells from patients with tuberculosis is related to the presence of pulmonary cavities. *Journal of Infectious Diseases* **181**, 1194-1197.

Van Crevel, R., Ottenhoff, T. H. & van der Meer, J. W. (2002). Innate immunity to Mycobacterium tuberculosis. *Clinical microbiology reviews* **15**, 294-309.

van Soolingen, D., De Haas, P. E., Hermans, P. W. & Van Embden, J. D. (1994). DNA fingerprinting of Mycobacterium tuberculosis. *Methods in enzymology* **235**, 196-205.

Vankayalapati, R. R., Wizel, B., Weis, S. E., Samten, B., Girard, W. M. & Barnes, P. F. (2000). Production of interleukin-18 in human tuberculosis. *Journal of Infectious Diseases* **182**, 234-239.

Voskuil, M. I., Schnappinger, D., Visconti, K. C., Harrell, M. I., Dolganov, G. M., Sherman, D. R. & Schoolnik, G. K. (2003). Inhibition of respiration by nitric oxide induces a Mycobacterium tuberculosis dormancy program. *The Journal of experimental medicine* **198**, 705-713.

Ward, J. R., West, P. W., Ariaans, M. P., Parker, L. C., Francis, S. E., Crossman, D. C., Sabroe, I. & Wilson, H. L. (2010). Temporal interleukin-1β secretion from primary human peripheral blood monocytes by P2X7-independent and P2X7-dependent mechanisms. *Journal of Biological Chemistry* **285**, 23147-23158.

Wayne, L. G. & Diaz, G. A. (1982). Serological, Taxonomic, and Kinetic Studies of the T and M Classes of Mycobacterial Catalase. *International Journal of Systematic Bacteriology* **32**, 296-304.

Wayne, L. G. & Diaz, G. A. (1988). Detection of a novel catalase in extracts of Mycobacterium avium and Mycobacterium intracellulare. *Infection and immunity* **56**, 936-941.

Weininger, D. (1988). SMILES, a chemical language and information system. 1. Introduction to methodology and encoding rules. *Journal of chemical information and computer sciences* **28**, 31-36.

Wells, R. M., Jones, C. M., Xi, Z. & other authors (2013). Discovery of a siderophore export system essential for virulence of Mycobacterium tuberculosis. *PLoS Pathog* **9**, e1003120.

Westendorp, R. G., Langermans, J. A., Huizinga, T. W., Elouali, A. H., Verweij, C. L., Boomsma, D. I. & Vandenbrouke, J. P. (1997). Genetic influence on cytokine production and fatal meningococcal disease. *The Lancet* **349**, 170-173.

WHO (2015). Global tuberculosis report 2015: World Health Organization.

Wong, D. K., Lee, B. Y., Horwitz, M. A. & Gibson, B. W. (1999). Identification of fur, aconitase, and other proteins expressed by Mycobacterium tuberculosis under conditions of low and high concentrations of iron by combined two-dimensional gel electrophoresis and mass spectrometry. *Infect Immun* **67**, 327-336.

Yamada, H., Mizumo, S., Horai, R., Iwakura, Y. & Sugawara, I. (2000). Protective Role of Interleukin-1 in Mycobacterial Infection in IL-1 α/β Double-Knockout Mice. *Laboratory investigation* **80**, 759-767.

Yang, C.-S., Yuk, J.-M. & Jo, E.-K. (2009). The role of nitric oxide in mycobacterial infections. *Immune network* **9**, 46-52.

Yeruva, C. V. (2012). Iron limitation in Mycobacterium tuberculosis: studies on iron-regulated envelope proteins & catalase-peroxidases.

Yeruva, V. C., Sundaram, C. A. & Sritharan, M. (2005). Effect of iron concentration on the expression and activity of catalase-peroxidases in mycobacteria. *Indian journal of biochemistry & biophysics* **42**, 28-33.

Yeruva, V. C., Duggirala, S., Lakshmi, V., Kolarich, D., Altmann, F. & Sritharan, M. (2006). Identification and characterization of a major cell wall-associated iron-regulated envelope protein (Irep-28) in Mycobacterium tuberculosis. *Clinical and vaccine immunology : CVI* **13**, 1137-1142.

Yuan, Y., Lee, R. E., Besra, G. S., Belisle, J. T. & Barry, C. (1995). Identification of a gene involved in the biosynthesis of cyclopropanated mycolic acids in Mycobacterium tuberculosis. *Proceedings of the National Academy of Sciences* **92**, 6630-6634.

Zahrt, T. C., Song, J., Siple, J. & Deretic, V. (2001). Mycobacterial FurA is a negative regulator of catalase–peroxidase gene katG. *Molecular microbiology* **39**, 1174-1185.

Zahrt, T. C. & Deretic, V. (2002). Reactive nitrogen and oxygen intermediates and bacterial defenses: unusual adaptations in Mycobacterium tuberculosis. *Antioxidants and Redox Signaling* **4**, 141-159.

Zhang, M., Lin, Y., Iyer, D. V., Gong, J., Abrams, J. S. & Barnes, P. F. (1995a). T-cell cytokine responses in human infection with Mycobacterium tuberculosis. *Infection and immunity* **63**, 3231-3234.

Zhang, Y., Heym, B., Allen, B., Young, D. & Cole, S. (1992). The catalase-peroxidase gene and isoniazid resistance of Mycobacterium tuberculosis. *Nature* **358**, 591-593.

Zhang, Y., Broser, M., Cohen, H., Bodkin, M., Law, K., Reibman, J. & Rom, W. N. (1995b). Enhanced interleukin-8 release and gene expression in macrophages after exposure to Mycobacterium tuberculosis and its components. *Journal of Clinical Investigation* **95**, 586.

Zhang, Y. (2008). I-TASSER server for protein 3D structure prediction. *BMC bioinformatics* **9**, 1.

Zhu, W., Arceneaux, J. E., Beggs, M. L., Byers, B. R., Eisenach, K. D. & Lundrigan, M. D. (1998). Exochelin genes in Mycobacterium smegmatis: identification of an ABC transporter and two non-ribosomal peptide synthetase genes. *Molecular microbiology* **29**, 629-639.

Zuber, B., Chami, M., Houssin, C., Dubochet, J., Griffiths, G. & Daffé, M. (2008). Direct visualization of the outer membrane of mycobacteria and corynebacteria in their native state. *Journal of bacteriology* **190**, 5672-5680.